Detection of Cell-Surface Antigens Using Antibody-Conjugated Fluorospheres (ACF): Application for Six-Color Immunofluorescence

BioTechniques 21:498-503 (September 1996)

Andrew J. Beavis and Kenneth J. Pennline[1]
The Hospital for Special Surgery, New York, NY and [1]Schering-Plough Research Institute, Kenilworth, NJ, USA

ABSTRACT

Antibody-conjugated fluorospheres (ACF) were used to phenotype murine leukocytes by flow cytometric analysis. Multicolor immunofluoresence (beyond simultaneous 4-color analysis) is limited by the availability of specific antibody–fluorochrome conjugates and even further restricted by the spectral emission overlap of many of the fluorochromes when used in combination. Fluorospheres possessing unique excitation/emission spectra can provide much needed versatility to existing protocols of multicolor fluorescence. SKY BLUE (647 nm excitation, 730 nm emission) fluorospheres conjugated to CD11b monoclonal antibody were used in combination with the monoclonal antibodies IAd-FITC, L3T4 (CD4)-PE, LYT2 (CD8)-APC, THY1.2 (CD90)-biotin and B220 (CD45R)-RED613 for the simultaneous detection of six distinct cell-surface antigens in a mixed cell population. All fluorescence signals were resolved, and comparison of results from five-, six- and single-color samples indicated that the percentages of cells positive for specific surface antigens were equivalent.

INTRODUCTION

Flow cytometry provides a rapid method to phenotype and characterize subpopulations of cells for a variety of research and clinical applications. There is a wide range of fluorochrome-conjugated monoclonal antibodies and fluorescent probes that are available for the analysis of numerous antigens that define cell type and function in many diverse applications including the clinical diagnoses of disease states (10,12), bone marrow progenitor cell isolation (11), ion flux measurements (14,17), nucleic acid quantitation (16), cell migration (2) and metabolic activation (1). These fluorescent reagents exhibit a variety of excitation and emission maxima, which allows the selection of a combination of fluorochromes to complement the optical configuration of individual flow cytometers for the purpose of multicolor flow cytometric analyses. The selection of fluorochromes that can be used for multicolor flow cytometry is limited by several factors including the excitation wavelengths available, optical filters, the number and configuration of optical detectors and the availability of the appropriate fluorochrome conjugates.

Fluorescent particles provide a versatile alternative to the more conventional fluorochrome–antibody or fluorochrome–ligand/receptor systems for the detection of cellular antigens. These uniform particles are available with a wide range of excitation and emission wavelengths and typically display a bright, homogeneous fluorescence signal. Fluorescent particles have been used for instrumentation calibration (15), cell-surface antigen detection (7,8), cell migration (19) and quantitation of phagocytic cell function (4,5,9). Furthermore, monoclonal antibodies can be conjugated to the fluorescent particles and then subsequently used in combination with other direct antibody conjugates or with indirect reagents such as biotin/streptavidin systems.

This report illustrates the use of SKY BLUE fluorospheres (emission at 730 nm) for the detection of cell-surface antigens by flow cytometry. We describe an optical configuration used to resolve and optimize the fluorescence signal of SKY BLUE in a multicolor immunofluorescence protocol and demonstrate the use of antibody-conjugated fluorospheres (ACF) with standard immunofluorescence reagents in a new protocol that allows the simultaneous detection of six cell-surface antigens on murine leukocytes. SKY BLUE-CD11b ACF identified the macrophages, while the five remaining fluorescence signals were used to detect Class II (IA), THY1.2 (CD90, T cell), L3T4 (CD4, helper/inducer T cell), LYT2 (CD8a, cytotoxic/suppressor T cell) and B220 (CD45R, B cell) as described previously (3). All experiments, including simultaneous six-color immunofluorescence, were performed using commercially available reagents on a FACS Vantage™ cell sorter with minor instrument modifications and without the use of cross-laser compensation.

MATERIALS AND METHODS

Spleen Cell Preparation

The method for preparing single-cell suspensions from mouse spleen has been described previously (3). Spleen cells were harvested, washed and resuspended to a concentration of 1×10^7 cells/mL.

Fluorospheres and Fluorescent Reagents

The SKY BLUE fluorospheres (0.45 and 2.08 µm in diameter) were purchased from Spherotech (Libertyville, IL, USA). The monoclonal antibodies L3T4-PE and THY1.2-Biotin were obtained from Becton Dickinson Immunocytometry Systems (B.D.I.S.) (San Jose, CA, USA); IAd-FITC, LYT2-APC and Fc-Block were from Pharmingen (San Diego, CA, USA); B220-RED613 was from Life Technologies (Gaithersburg, MD, USA) and the purified CD11b was from Devaron, (Dayton, NJ, USA). The streptavidin-Cascade Blue® (CB) was purchased from Molecular Probes (Eugene, OR, USA).

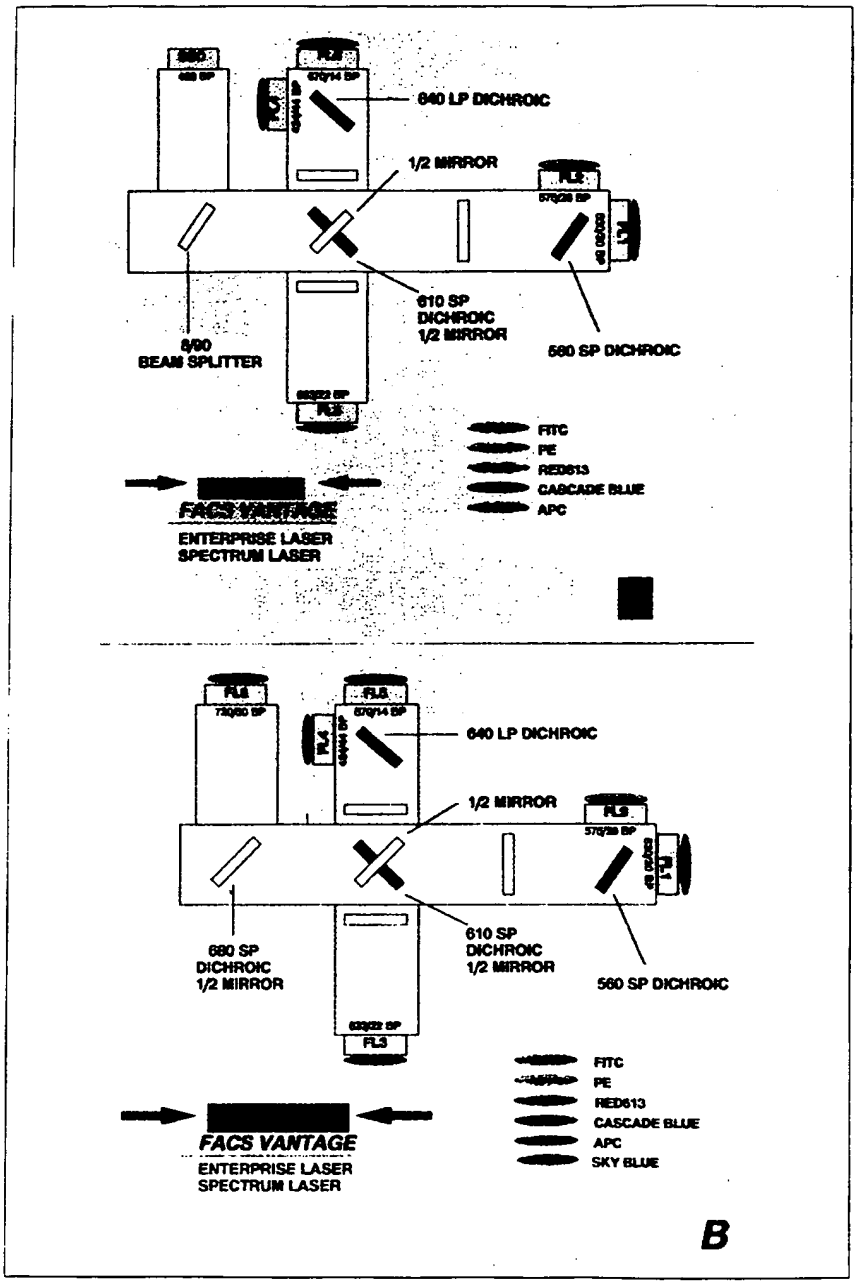

Figure 1. Diagrammatic representation of the optical configuration of the FACS Vantage for collection of seven parameters. A: Standard configuration for collection of FSC (FSC diode not shown), SSC and five-color immunofluorescence. B: Custom optical configuration for collection of FSC (FSC diode not shown), and six-color immunofluorescence. The SSC optics (8/90 beam splitter and 488 BP) were replaced with a 680 SPDi (1/2 mirror) and a 730/30 BP for collection of SKY BLUE as the sixth fluorescence parameter.

Flow Cytometric Analysis of the SKY BLUE Fluorospheres

The instrumentation used in these studies was a dual-laser, triple-beam FACS Vantage flow cytometer (B.D.I.S.) equipped with a Coherent Enterprise laser (300 mW at 488 nm; 60 mW at 351–364 nm), a Coherent Spectrum laser tuned to 45 mW at 647 nm and a seventh detector option for five-color fluorescence measurements (3). The 680 shortpass dichroic (SPDi), 465/30 bandpass (BP) and 730/30 BP optical filters were purchased from Omega Optical (Brattleboro, VT, USA), and the red-sensitive photomultiplier tube (PMT) R-1477 was obtained from Hamamatsu (Bridgewater, NJ, USA). The SKY BLUE fluorospheres were excited with the 647-nm line from the Spectrum laser and collected with a 730/30 BP filter. Unlabeled, FITC- and PE-labeled beads (CaliBRITE™ kit, B.D.I.S.) were mixed with aliquots of either SKY BLUE fluorospheres or SKY BLUE and APC beads (Flow Cytometry Standards Corporation, San Juan, PR, USA) and analyzed for fluorescence. The fluorescence signals from the FITC (FL1) and PE (FL2) CaliBRITE beads were separated with a 560 SPDi and collected with 530/30 and 575/26 BP filters, respectively. SKY BLUE and APC fluorescence signals were separated with a 680 SPDi and collected as the FL4 and FL5 parameters, respectively.

Conjugation of the Fluorospheres with Monoclonal Antibodies

The fluorospheres were conjugated to monoclonal antibodies by passive adsorption. Briefly, 300 µL of 2.08 µm SKY BLUE fluorospheres (1% wt/vol)

were added to 100 µL of CD11b (1 mg/mL) and 1.6 mL phosphate buffer (0.1 M, pH 7.0); 250 µL of 0.45-µm SKY BLUE fluorospheres (1% wt/vol) were added to 200 µL of CD11b (1 mg/mL) and 1.55 mL phosphate buffer. The fluorosphere–antibody mixtures were vortex mixed and incubated for 60 min at room temperature (rt). After centrifugation at 3000× *g* for 15 min, the ACF were washed 2× in 4 mL of phosphate-buffered saline (PBS) and incubated as above in 2 mL PBS containing 10% fetal bovine serum (FBS). After this time, the ACF were washed 2× in PBS, resuspended in 4 mL of PBS (0.25% wt/vol) solution and stored at 4°C in the dark.

Six-Color Immunofluorescence

SKY BLUE ACF were also used for the simultaneous detection of six cell-surface antigens by six-color immunofluorescence. Cells were stained with the following monoclonal antibodies as single-color controls, a five-color sample (without ACF) and as a six-color sample: IAd-FITC (10 µL of 1:10 dilution), L3T4-PE (4 µL), THY1.2-Biotin (4 µL), LYT2-APC (10 µL) and B220-RED613 (10 µL of a 1:25 dilution). After all volumes were equalized with PBS-FCS, the cells were incubated for 30 min at 4°C. Subsequently, these cells were washed, incubated with streptavidin-CB (10 µL of a 1:10 dilution) and/or CD11b-SKY BLUE (50 µL) for 30 min, washed and fixed in 1% paraformaldehyde. Isotypic control antibodies, streptavidin-CB or serum-adsorbed SKY BLUE particles were added as nonspecific binding controls.

Instrument Settings

For six-color immunofluorescence analysis, the SKY BLUE fluorescence signal was collected instead of side scatter (SSC) by replacing the 8/90 beam splitter, the 488/10 BP and the SSC PMT IP28A with a 680 SPDi (1/2 mirror), a 730/30 BP (FL6) and a red-sensitive PMT, respectively. The 488-nm line from the Enterprise laser was the primary beam, with threshold trigger set on forward scatter, and the 351–364 nm beam (from the Enterprise) and the 647 nm beam (from the Spectrum) coincident as secondary beams with a 15-µs time delay. The primary laser fluorescence signals were separated using a 610 SPDi and a 560 SPDi and collected with a 630/22 BP (FL3 RED613), a 575/26 BP (FL2 PE) and a 530/30 BP (FL1 FITC). The secondary laser fluorescence signals were separated with a 640 LPDi and collected with a 424/44 BP (FL4 CB) and a 670/14 BP (FL5 APC). Fluorescence signals were collected in logarithmic mode with pulse processing on.

Data Analysis

For each sample, 50 000 events were collected in listmode using LYSYS™ II or CELLQUEST and analyzed with CELLQUEST and ATTRACTORS (B.D.I.S.). Cells were gated on a histogram of forward scatter (FSC) and from a 2-parameter dot plot of FSC vs. SKY BLUE (FL6).

RESULTS

Analysis of SKY BLUE Fluorospheres by Flow Cytometry

Flow cytometric analysis of unconjugated SKY BLUE fluorospheres demonstrated that the fluorescence emission signal (730 nm) was resolved from those of the FITC and PE CaliBRITE beads. In addition, the fluorescence signals of the SKY BLUE fluorospheres (collected as FL4) and APC alignment beads (collected as FL5) were clearly resolved with the 680 SPDi, with compensation settings of FL4 -%FL5 = 39.8% and FL5 -%FL4 = 25.6% (not shown).

Use of SKY BLUE ACF for Six-Color Immunofluorescence

To perform six-color immunofluorescence analysis, the SKY BLUE fluorescence signal, designated as FL6, was collected in place of the SSC parameter (Figure 1). The 8/90 beam splitter was replaced with a 680 SPDi (1/2 mirror), which reflected the SKY BLUE signal and transmitted the APC (FL5) and CB (FL4) signals. Light-scatter analysis indicated that CD11b ACF(+) cells exhibited an increase in the SSC (granularity) parameter. Examination by light microscopy indicated that variable numbers of fluorospheres were attached to the surface of cells (not shown). These cells also exhibited a heterogeneous pattern of fluorescence, which supports the light microscopy findings. In order to ensure that the ACF signal was true fluorescence and not the result of increased laser scatter described above, a mixture of 2.08-µm SKY BLUE fluorospheres and 6.6-µm CaliBRITE beads was analyzed. CaliBRITE beads were identi-

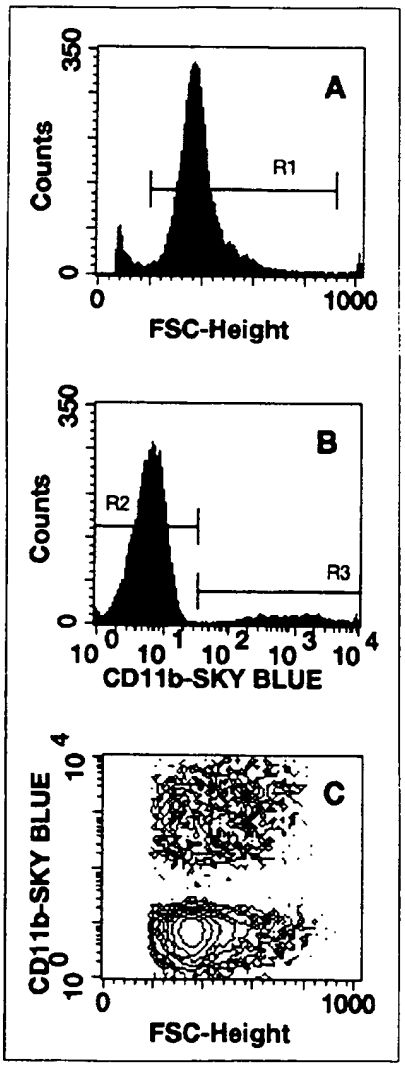

Figure 2. Identification of macrophages in a murine spleen cell sample with CD11b-SKY BLUE ACF. Murine spleen cells were stained with monoclonal antibodies specific for six distinct cell-surface antigens and analyzed on a FACS Vantage as described. A: Single parameter histogram of FSC. B: Single parameter histogram of spleen cells stained with CD11b-SKY BLUE (gated on FSC, R1) showingCD11b(-) (R2) and CD11b(+) cells (R3). C: Two-dimensional contour plot of FSC vs. SKY BLUE (FL6) showing CD11b-SKY BLUE(+) cells (gated on FSC, R1).

fied by their greater FSC and the SKY BLUE particles were resolved from CaliBRITE beads on the basis of FL6 fluorescence (not shown).

In six-color analysis, macrophages were identified in a spleen cell preparation using CD11b-SKY BLUE ACF. Leukocytes gated on FSC were shown to contain 6.6% CD11b(+) cells by a single-parameter histogram of FL6 and from a 2-dimensional dotplot of FSC vs. FL6 (Figure 2). Comparison of results from single-color, five-color and six-color analyses indicated that the percentages of cells expressing THY-1.2, L3T4, LYT2, B220 and IAd (class II major histocompatibility complex [MHC] antigen) were similar (differing by only 2%–6% in all cases). ATTRACTORS analysis software was used to show the clear resolution of SKY BLUE from the other five fluorescence signals. The CD11b(+) and CD-11b(-) cells were identified from a plot of FSC vs. FL6, and their positions on 2-dimensional dot plots can be seen in Figure 3A. The fluorescence from the SKY BLUE-positive cells was also detected above background fluorescence in FL1, FL4 and FL5 channels. However, gating on CD11b-SKY BLUE(-) cells eliminated this overlapping population and thus allowed quantitation of the various lymphocyte subpopulations (Figure 3B). Analysis of the CD11b-ACF(+) cells indicated that there was minimal contamination by B220 (9%) or THY1.2 (3%) positive cells (0.6% and 0.2% of total cells, respectively; Figure 3A).

DISCUSSION

In multicolor flow cytometric analysis, the ability to spectrally resolve the fluorescence signals limits the number of combinations of fluorochromes that may be used simultaneously. Recently, we described a simultaneous five-color protocol that utilized Cascade Blue and APC (excited with UV and 647-nm laser lines with emissions at 425 nm and 670 nm, respectively) which were well resolved from FITC, PE and RED613 signals (3). An extension of this protocol would require a sixth fluorochrome that could be excited with one of the available laser lines and be spectrally resolved from the other fluorescence signals. Six-color immunofluorescence has been proposed previously (18), and the problems associated with such a protocol have been addressed (13). Based on this information and our own experience (3), there were two important considerations for selecting the reagent for the sixth color. First, it was realized that the range of the fluorescence emission spectrum for the five initial fluorochromes was somewhat "congested", and the use of

other commercially available dyes would result in significant spectral overlap. Second, it was necessary that the configuration of the sixth fluorochrome be in the form of a direct conjugate or a unique ligand/ligand indirect system, since the protocol already included one two-step biotin/streptavidin system (CB) and the use of a secondary antibody could produce problems with cross-reactivity.

Fluorescent microspheres have been used previously to characterize surface antigen expression and cellular functions (4,5,7–9). Historically, these microspheres were used in place of FITC, PE, etc., because the emission maxima were similar to these dyes. More recently, fluorescent particles have been produced with emission wavelengths that are distinct from the more frequently used fluorochromes. The surface chemistry of these fluorescent polystyrene spheres allows for the passive adsorption of monoclonal antibodies, which can then be used as direct conjugate reagents in immunofluorescence assays. The potential use of these conjugates increases the versatility of monoclonal antibodies that are available only in purified form or conjugated to a limited number of fluorochromes. The application of these highly fluorescent microspheres may be particularly important for the detection of low-density cell-surface antigens or for use with monoclonal antibodies having low affinity towards cell-surface antigens.

This report describes the use of SKY BLUE fluorospheres whose fluorescence signal was shown to be resolved from that of FITC-, PE- and APC-labeled beads. The resolution of fluorescence emission signals from SKY BLUE and APC is an important finding, since it demonstrates that the 647-nm line from the Spectrum laser, as shown here (or a 633-nm line from the HeNe), can now be used to collect two fluorescence parameters simultaneously.

The CD11b-ACF(+) cells exhibited some heterogeneity in fluorescence, which indicated that the binding of ACF was variable. This heterogeneity in fluorescence was due to different numbers of ACF binding to cells, as seen by microscopy, and the discrete fluorescence intensity of emission for each fluorophore. However, the variable binding did not affect the specificity of CD11b-ACF, which was confirmed by multicolor immunofluorescence. Results from light-scatter

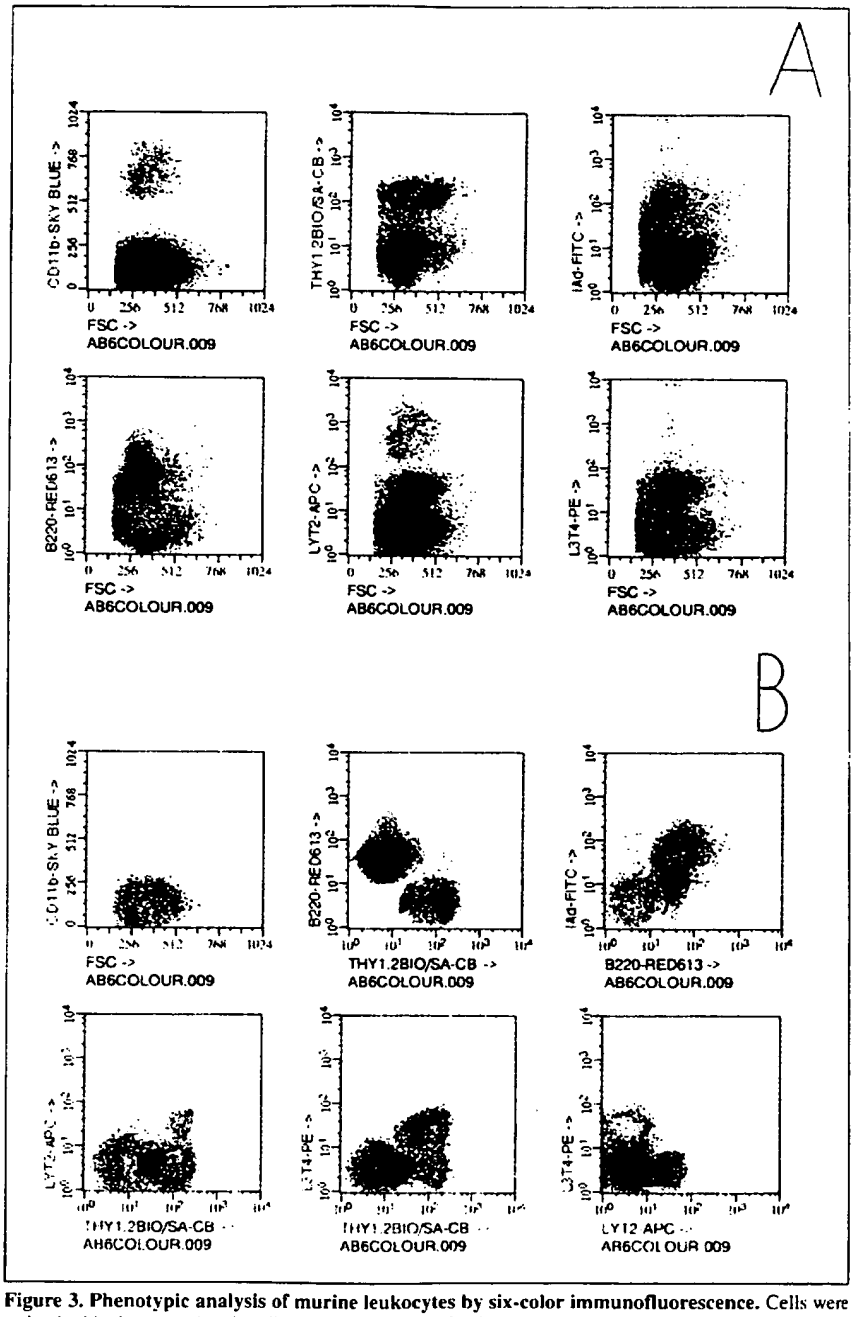

Figure 3. Phenotypic analysis of murine leukocytes by six-color immunofluorescence. Cells were stained with six monoclonal antibodies and analyzed for fluorescence. The listmode data was analyzed using ATTRACTORS (B.D.I.S.), whereby the specific phenotype of a subpopulation is gated and assigned a color. Each subpopulation may be identified on any two-dimensional dotplot by the position of the colored dots. A: Resolution of SKY BLUE (FL6) from the other five fluorescence signals: CD11b(-) = RED; CD11b(+) = BLUE and phenotypic analysis of the CD11b(+) subpopulation of splenocytes: CD11b(+)/THY1.2(−) = YELLOW; CD11b(+)/B220(+) = GREEN. B: Phenotypic analysis of the CD11b(-) cells: THY1.2(+)/B220(-)/L3T4(-)/LYT2(+)/IA(-) = PINK; THY1.2(+)/B220(-)/L3T4(+)/LYT2(-)/IA(-) = LIGHT BLUE; THY1.2(-)/B220(+)/L3T4(-)/LYT2(-)/IA(-) = RED; THY1.2(-)/B220(+)/L3T4(-)/LYT2(-)/IA(+) = GREEN; THY1.2(+)/B220(+)/L3T4(-)/LYT2(-)/IA(+) = ORANGE; and THY1.2(-)/B220(-)/L3T4(+)/LYT2(-)/IA(+,-) = YELLOW.

analysis indicated that ACF(+) cells exhibited an increase in SSC. This effect most likely is a direct result of surface-bound ACF increasing the amount of orthogonal light scatter. However, it should be noted that the increased SSC is not sufficient to resolve ACF(+) cells, as it is in the case of immunogold staining (6), nor is it responsible for ACF fluorescence. The latter was demonstrated by studies to identify a FL6 signal in the analysis of SKY BLUE fluorospheres and larger CaliBRITE beads. Both microspheres exhibited similar SSC profiles, but only the SKY BLUE particles exhibited positive FL6 fluorescence. This was further confirmed using CD11b-ACFs.

In the six-color protocol, the SKY BLUE-ACF (CD11b) signal was collected as FL6 in the SSC position. The SKY BLUE-ACF (+) cells (macrophages) were then excluded by gating, allowing for the analysis of T- and B-cell surface antigens on CD11b(-) cells alone. This procedure provides an accurate method to eliminate the macrophage cell population using a phenotypic gate rather than light-scatter properties alone and also conserves a parameter that could be used for the analysis of leukocytes. The spectral overlap of the SKY BLUE signal with FITC, CB (minimal excitation by 488 and UV) and APC may prevent the use of this fluorosphere for the positive selection of cells. However, preliminary evidence suggests that this spectral overlap can be minimized by using smaller microspheres that emit a lower fluorescence intensity. On the other hand, these fluorospheres can clearly be used for positive phenotypic analysis with various combinations of fluorochromes including PE, RED613 and CB.

In summary, we have successfully used a combination of conventional fluorochrome-conjugated monoclonal antibodies and antibody-conjugated fluorescent microspheres to measure six different cell-surface antigens simultaneously on murine spleen cells by six-color immunofluorescence. Only minor instrument modifications were required and included a simple set of custom optics designed for resolution and collection of six fluorescence signals without cross-laser compensation. Presently, we are investigating the use of the fluorescent microspheres in other flow cytometric protocols such as in situ hybridization and intracellular protein determination. Continued advancements in the acquisition of multicolor immunofluorescence data and in the ability to compensate combinations of fluorescence signals generated from different lasers will undoubtedly facilitate the use of a wide range of fluorochromes and fluorescent probes in current and future applications of flow cytometry.

ACKNOWLEDGMENTS

We would like to thank Mr. Jerome Zawadski and Mr. Samuel Witherspoon for their helpful comments during this study.

REFERENCES

1. **Bass, D.A., J.W. Parce, L.R. DeChatelet, P. Szejda, M.C. Seeds and M. Thomas.** 1993. Flow cytometric studies of oxidative product formation by neutrophils: a graded response to membrane stimulation. J. Immunol. *130*: 1910-1917.
2. **Beavis, A.J. and K.J. Pennline.** 1994. Tracking of murine spleen cells in vivo: detection of PKH26-labeled cells in the pancreas of non-obese diabeteic (NOD) mice. J. Immunol. Methods *170*:57-65.
3. **Beavis, A.J. and K.J. Pennline.** 1994. Simultaneous measurement of five cell surface antigens by five-colour immunofluorescence. Cytometry *15*:371-376.
4. **Bender, J.G., K.L. Unverzagt, P.B. Maples, Y. Mehrotra, J. Mellon, D.E. Van Epps and C.C. Stewart.** 1992. Functional characterization of mouse granulocytes and macrophages produced in vitro from bone marrow progenitors stimulated with interleukin 3 (IL-3) or granulocyte-macrophage colony-stimulating factor (GM-CSF). Exp. Hematol. *20*:1135-1140.
5. **Blair, O.C., R. Carbone and A.C. Sartorelli.** 1986. Differentiation of HL-60 promyelocytic leukemia cells: simultaneous determination of phagocytic activity and cell cycle distribution by flow cytometry. Cytometry *7*:171-177.
6. **Bohmer, R.M. and N.J.C. King.** 1984. Flow cytometric analysis of immunogold cell surface label. Cytometry *5*:543-546.
7. **Cosio, F.G., S. Xiao-Ping, D.J. Birmingham, M. Van Aman and L.A. Herbert.** 1990. Evaluation of the mechanisms responsible for the reduction in erythrocyte complement receptors when immune complexes form in vivo in primates. J. Immunol. *145*:4198-4206.
8. **Cosio, F.G., S. Xiao-Ping and L.A. Hebert.** 1990. Immune complexes bind preferentially to specific subpopulations of human erythrocytes. Clin. Immunol. Immunopathol. *55*:337-354.
9. **Fredrickson, A.G., C. Hatzis and F. Srienc.** 1992. A statistical analysis of flow cytometric determinations of phagocytosis rates. Cytometry *13*:423-431.
10. **Gale, H.B. and K. Henry.** 1992. Measuring percent lymphocytes by flow cytometry to calculate absolute lymphocyte subset counts for HIV+ specimens. Cytometry *13*:175-181.
11. **Huang, S. and L.W. Terstappen.** 1992. Formation of haematopoietic microenvironment and haematopoietic stem cells from single human bone marrow stem cells. Nature *360*:745-749.
12. **Ichikawa, Y., H. Shimizu, M. Yoshida and S. Arimori.** 1990. Activation of T cell subsets in the peripheral blood of patients with Sjogren's syndrome. Multicolor flow cytometric analysis. Arthritis Rheum. *33*:1674-1681.
13. **Lanier, L.L. and D.J. Recktenwald.** 1991. Multicolor immunofluorescence and flow cytometry, p. 192-199. Methods: A Companion to Methods in Enzymology, Vol. 2(3). Academic Press, New York.
14. **Minta, A., J.P.Y. Kao and R.Y. Tsien.** 1989. Fluorescent indicators for cytosolic calcium based on rhodamine and fluorescein chromaphores. J. Biol. Chem. *264*:8171-8178.
15. **Pallis, M., A. Robins and R. Powell.** 1993. Quantitative analysis of lymphocyte CD11a using standardized flow cytometry. Scand. J. Immunol. *38*:559-564.
16. **Pennline, K.J., F. Pellerito-Bessette, S.P. Umland, M.I. Siegel and S.R. Smith.** 1992. Detection of in vivo-induced IL-1 mRNA in murine cells by flow cytrometry and fluorescent in situ hybridization (FISH). Cytokine Res. *11*:65-71.
17. **Rabinovitch, P.S., C.H. June, A. Grossman and J.A. Ledbetter.** 1986. Heterogeneity among T-cells in intracellular free calcium responses after mitogen stimulation with PHA or anti-CD3. Simultaneous use of INDO-1 and immunofluorescence with flow cytometry. J. Immunol. *137*:952-961.
18. **Recktenwald, D., B. Prezelin, C.H. Chen and J. Kimura.** 1990. Biological pigments as fluorescent labels for cytometry, p. 106-111. *In* G.C. Salzman (Ed.), New Technologies in Cytometry and Molecular Biology, Vol. 1206. SPIE.
19. **Technau, U. and T.W. Holstein.** 1992. Cell sorting during the regeneration of Hydra from reaggregated cells. Dev. Biol. *151*:117-127.

Received 7 July 1995; accepted 13 February 1996.

Address correspondence to:

Kenneth J. Pennline
Schering-Plough Research Institute
Department of Immunology
2015 Galloping Hill Road
Kenilworth, NJ 07033, USA
Internet: kenneth.pennline@spcorp.com

Cytometry 36:36–45 (1999)

Nine Color Eleven Parameter Immunophenotyping Using Three Laser Flow Cytometry

Martin Bigos,* Nicole Baumgarth, Gina C. Jager, Ometa C. Herman, Thomas Nozaki, Richard T. Stovel, David R. Parks, and Leonard A. Herzenberg

Department of Genetics, Stanford University School of Medicine, Stanford, California

Received 26 June 1998; Revision Received 17 December 1998; Accepted 22 December 1998

Background: This study describes a three laser flow cytometer, reagents, and software used to simultaneously evaluate nine distinct fluorescent parameters on one cell sample. We compare the quality of data obtained with (1) full software compensation and (2) the use of partial spectral compensation of selected pairs of parameters in analog hardware, in combination with final software compensation. An application characterizing low frequency murine B cell subpopulations is given.

Methods: The fluorochromes used are: fluorescein (FITC), phycoerythrin (PE), Cy5PE and Cy7PE, excited at 488 nm by an argon laser; Texas Red (TR), allophycocyanin (APC), and Cy7APC excited at 595 nm by a pumped dye laser; and cascade blue (CB) and cascade yellow (CY) excited at 407 nm by a violet-enhanced krypton laser. Custom additions to commercial electronics and an extended optical bench allow the measurement of these nine parameters plus forward and side scatter light signals.

Results: We find the use of partial analog compensation reduces the variation in the background staining levels introduced by the compensation process. Novel B cell populations with frequencies below 1% are characterized.

Conclusions: Nine color flow cytometry is capable of providing measurements with high information content. The choice of reagent-dye combinations and the ability to compensate in multi-parameter measurement space are crucial to obtaining satisfactory results. Cytometry 36:36–45, 1999. © 1999 Wiley-Liss, Inc.

Key terms: B lymphocytes; FACS; flow cytometry; multiparameter compensation

The introduction of cascade blue (CB) and cascade yellow (CY) (Molecular Probes, Inc., Eugene, OR) as violet-excited fluorochromes (2), and the use of Cy7 energy transfer conjugates with the phycobiliproteins phycoerythrin (Cy7PE) and allophycocyanin (Cy7APC) (13) has extended the number of useful fluorescence measurement parameters for immunophenotyping to nine. The use of eight of these simultaneously was demonstrated previously (2,12). We have now extended the instrumentation described therein to allow all nine of these fluorescent labels to be evaluated on each cell.

Capable instrumentation is only one aspect of performing complex multiparameter experiments. Two other, and equally important, aspects are reagent-dye selection and data analysis tools. In Roederer et al. (12) data were presented on two of the issues of reagent-dye selection: relative dye "brightness" and spectral interactions. Relative dye "brightness" is the ability of that dye to separate stained populations from background. Three different methods were presented to quantitate this attribute. Based on those results, the authors concluded that Cy5PE and APC are the two "brightest" dyes, followed by PE; TR and FITC are roughly equivalent, and CB and CY somewhat "duller" than the other dyes. The usefulness of these dyes, however, is also affected by their spectral interaction and the expression levels of the markers under investigation. In this report, we demonstrate how these aspects can be considered in the design of a set of reagent-dye combinations that identifies various murine splenic B-cell populations by incorporating all nine available fluorochromes.

Correcting for the spectral overlap between two dyes excited by the same laser to provide corrected estimates of the amount of signal produced by each dye was first introduced by Loken et al. (10). This system used subtraction of linear voltage pulses from the linear preamplification system of the electronics to implement the correction. Critical to this process is the requirement that the pulses produced by the electronic detection system (photomultiplier tube and current-to-voltage amplifier) for each dye are matched in shape and timing. Because flow instrumentation then and now uses the pulse height produced by the detection system as the measurement of the signal intensity, discrepancies of shape between subtracted pulses, which should yield a low or zero-level

Grant sponsor: NIH; Grant number: CA42509.

*Correspondence to: Martin Bigos, Beckman Center B007, Stanford University, Stanford, CA 94305-5318.

E-mail: bigos@stanford.edu

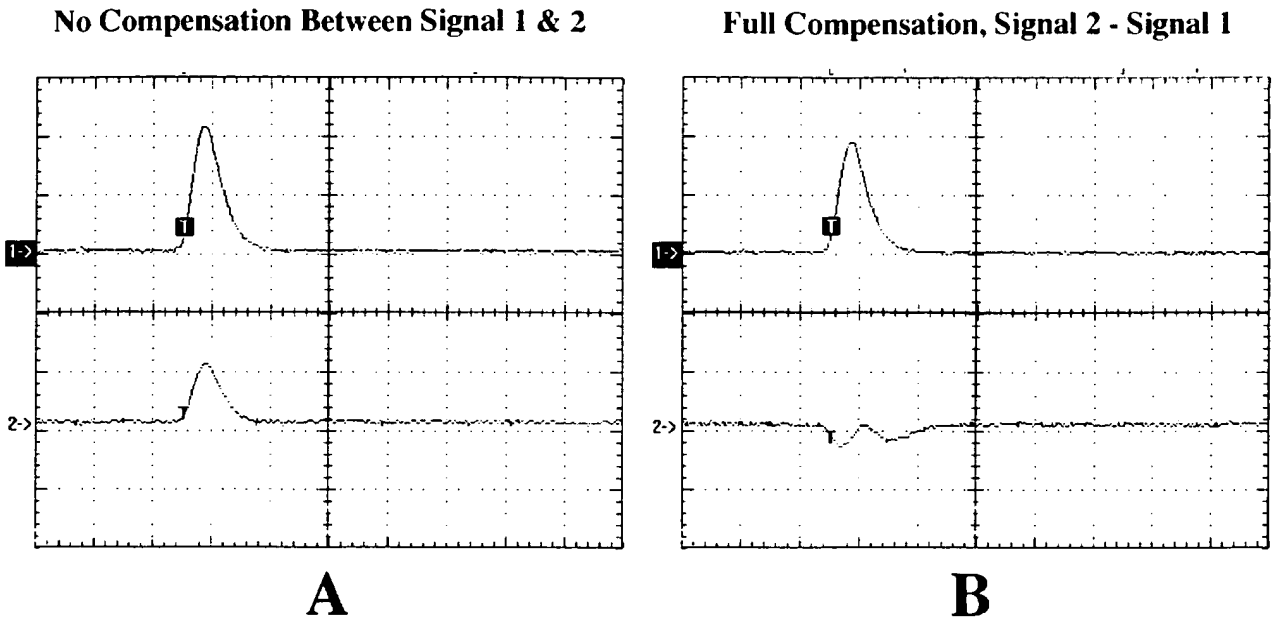

FIG. 1. Analog Pulse Subtraction. A and B are voltage pulses from the preamplifiers on the flow cytometer described in this paper generated by Rainbow Beads (Spherotech, Inc. Libertyville, IL). They are captured on a Textronix TDS 420 oscilloscope using Wavestar software (Textronix, Inc. Beaverton OR). Trace 1 shows the fluorescein signal, trace 2 shows the PE signal. The horizontal scale in both panels is 2 μsec. A: Vertical scale is 2 V, and no compensation is applied. B: Compensation has been used to subtract fluorescein from PE with the result shown as trace 2 (vertical scale 100 mv).

signal, will have residual peak(s) that do not correspond to the desired measurement (see Fig. 1). This error will tend to increase the variation of compensated signals, limiting the ability to measure low level signals above the autofluorescence background. This process of electronic peak subtraction is called analog compensation.

Mathematically, analog compensation can be modeled as a linear transformation of the "signal" vector space into the "dye" vector space, where the axes in that space represent the measurements of each dye alone. This model can easily be extended to any number of measurement parameters and implemented in software to correct flow data (as computer list mode files) for the spectral overlaps of more than two dyes; this was first mentioned by Roederer and Murphy (14) and further elaborated upon in Bagwell and Adams (3). The computations require that the list mode data be converted from log signal levels (which is used for the measurement of most immunofluorescence data) back to the linear domain to apply the model, then the results reconverted back to the log domain. However, a log amp is not a perfect device; our investigations (data not shown) have found that errors of ±5% are typical of log amp designs for flow cytometers, with the errors generally increasing at the bottom and top of the scale. Moreover, in most staining situations, the "negative" population signal is a mixture of cellular autofluorescence and non-specific staining. Thus, calculation errors and incomplete matching to the software model of the data deteriorates digitally compensated data.

Just as the software model can be extended as described above, the analog hardware can also be elaborated to correct more than two measurements. For multi-laser multi-fluorochrome configurations, a design that included delay lines to synchronize the pulses from the differently timed laser crossings and a large subtractive network to implement the myriad interactions among different dyes (see Table 1A) could be constructed. However, such a scheme has engineering difficulty meeting the requirement of matching pulse shapes and aligning them precisely in time, and would be difficult to expand as more measurement parameters are added.

Conceptually simpler would be to move the software model into the electronics by digitizing "on the fly" the linear pulses or peak heights of each event and processing them to obtain compensated log data that are then collected for analysis and/or used for sorting. Although modern microprocessors can easily handle the computation load, the engineering requirements in terms of bandwith and dynamic range of a system to digitize the linear signals have not yet been adequately met.

In this paper, we investigate a compromise system that uses analog compensation to partially compensate significant same laser spectral overlaps, followed by post-hoc software (digital) compensation. Using partial analog compensation minimizes the calculation errors of post-hoc software compensation while bringing the major same-laser spectral overlaps to a low level. By not attempting to fully compensate with analog electronics, the bias introduced by mismatched peak shapes is avoided. Applying software compensation to these signals minimizes the effects of calculation errors since the values subtracted are significantly smaller (see Table 1B) than those used for

Table 1
*Typical Spectral Spillover Matrices for Software Compensation**

Source	Measurement Parameter								
	FITC	PE	Cy5PE	TR	APC	Cy7APC	Cy7PE	CB	CY
A. Without partial analog compensation									
FITC	—	0.28	0.04	0	0	0	0.01	0	0.02
PE	0.02	—	0.18	0.03	0	0	0.02	0	0.02
Cy5PE	0	0.03	—	0.01	0.10	0.02	0.15	0	0
TR	0	0	0.01	—	0.12	0.02	0	0	0
APC	0	0	0.07	0.14	—	0.10	0.01	0	0
Cy7APC	0	0	0.05	0.25	0.68	—	0.14	0	0
Cy7PE	0	0.03	0.01	0	0	0.03	—	0	0
CB	0	0	0	0	0	0	0	—	0.07
CY	0.06	0.04	0.02	0	0	0	0.01	0.01	—
B. With partial analog compensation									
FITC	—	0	0	0	0	0	0	0	0.02
PE	0	—	0.03	0.03	0	0	0.01	0	0.02
Cy5PE	0	0.01	—	0	0.10	0.02	0.09	0	0
TR	0	0	0.01	—	0.02	0.01	0	0	0
APC	0	0	0.07	0.02	—	0.04	0	0	0
Cy7APC	0	0	0.05	0.17	0.57	—	0.14	0	0
Cy7PE	0	0.03	0	0	0	0.02	—	0	0
CB	0	0	0	0	0	0	0	—	0.01
CY	0.06	0.02	0.02	0	0	0	0.01	0	—

*A is with no analog compensation; B is with partial analog compensation as described in the text. For each row a sample singly stained with the source fluorochrome is run. The positive staining cells are selected and the median in each measurement channel calculated. Each row element is the ratio of the median in that measurement channel to the median in the source channel (spillover into source channel is not relevant and indicated by a dash). The inverse of this matrix, normalized so the position of the source medians remains constant, is the matrix used to calculate compensated parameters. The highlighted cells represent spillover values greater than 5%, which have been reduced by the use of partial analog compensation. Cross laser spillovers, in general, are not changed by the analog compensation used here.

pure digital compensation. In this study we show that this results in cleaner measurements on selected parameters than using software compensation alone.

However, there is at least one limitation in the compensation process that applies equally to all of the above possible methods: the quality of the underlying measurements itself. Compensation cannot decrease the variation in the original signals. Thus, in a log-log presentation of compensated data, visually the spread of a stained population relative to a spillover channel will generally be greater than the spread of the unstained cells. Moreover, the amount of light gathered for the measurements is an underlying determinant of how much the original variation may increase. In the red emission regions, the overall amount of light converted into electrical signals (photoelectrons) is lower that in the shorter wavelengths. Even though the staining intensity on the red-emitting parameters in general has a better signal/background ratio compared to the shorter wavelength-emitting dye, the absolute intensity is, in general, lower. This results in a greater uncertainty of measuring these signals, both in the primary measurement channels and channels with spectral overlap. In several cases, this is the limiting factor in how well compensation can be done independent of the method chosen. In the context of our study, while the use of partial analog followed by digital compensation results in a measurable decrease in the variation of the compensated signal compared to using digital compensation alone, the underlying variation in some measurement parameters due to the limited light available for the measurements obscures any advantage gained.

Data collection and analysis tools used for multiparameter experiments can help or hinder the process. Full annotation of data sets, including information regarding dye color, reagent, cell type, and any special conditions associated with the particular sample, is particularly useful for multiparameter analysis. A tool for constructing protocols, with which an entire cytometer run can be delineated in advance has been described previously (11) and has aided greatly in the management of complex multiparameter experiments. Furthermore, it is important to have analysis tools that can manage complex subset analysis, visualize data sets in different forms, and be able to handle large multiparameter data sets. A software program, FlowJo®, commercially available from Tree Star, Inc. (San Carlos, CA), has been designed over the past few years by our laboratory to fulfill these criteria.

We demonstrate here that with this system of hardware, software, and reagent system, nine fluorometric parameters can be used simultaneously, along with forward and side light scatters, for state of the art immunophenotyping. The data quality achieved is sufficient to characterize populations with both high and low (<1%) frequencies.

MATERIALS AND METHODS

Antibody Reagents

FITC-labeled monoclonal antibodies (mAbs) anti-CD21/CD35 (7G6), PE-labeled anti-CD24 (30F1), Cy5PE labeled

anti-CD3 (145-2C11), anti-CD5 (5.7) and anti-B220 (RB3-6B2), and purified, unconjugated anti-CD1 (3C11) were obtained from Pharmingen (San Diego, CA). Streptavidin-TR was obtained from Vector (Burlingame, CA). The following anti-murine mAbs were obtained by purifying serum-free tissue culture supernatants from hybridomas using protein G (Pharmacia, Piscataway, NJ) affinity chromatography: anti-B220 (RB3-6B2); anti-CD3 (145-2C11); anti-CD4 (G.K. 1.5); anti-CD8 (56.7.1); anti-F4/80 antigen (F4/80); anti-IgD (1126); anti-IgM (331); anti-CD43 (S7). The purified antibodies were conjugated to the following fluorochromes: CB: anti-CD3, anti-CD4, anti-CD8, anti-IgM, anti-B220, anti-F4/80; CY: anti-B220, anti-CD8; APC: anti-CD43, anti-IgM, anti-B220; Cy7APC: anti-IgM, anti-IgD; Cy7PE: anti-IgD; biotin: anti-CD1; PE: anti-CD5. Conditions of conjugations were exactly as described previously (6, 7, 12). Optimal staining concentrations were determined separately for each antibody-conjugate by titration on appropriate primary cells.

As controls for partial analog compensation individual samples of murine spleen cells were stained separately using each fluorochrome. To achieve optimal brightness some samples were stained with two or three antibodies conjugated to the same fluorochrome: FITC: anti-B220 and anti-IgM; PE: anti-IgM, anti-IgD and anti-B220; Cy5-PE: anti-B220; TR: anti-IgM, anti-IgD; APC: anti-IgM, anti-B220; Cy7APC: anti-IgM, anti-IgD; Cy7PE: anti-IgD; CB: anti-B220, anti-IgM; CY: anti-CD8. Partial analog compensation settings were chosen so that the spillover of the positively staining compensation control was reduced by at least half, when possible, without driving any related signals onto the measurement axes.

Murine spleen cells stained with anti-CD5 PE or TR and anti-CD3 Cy5PE were used to illustrate the visual comparison of partial analog compensation vs. no analog compensation.

Cell Staining and Analysis

Eight- to twelve-week-old BALB/c mice were taken from our breeding colony at the Research Animal Facility at Stanford University. Mice were sacrificed by cervical dislocation and single cell suspensions from spleens were obtained by gently disrupting the tissue between two glass-slides. Erythrocytes were lysed in ACK (9) buffer and remaining cells were resuspended at 2.5 x 10^7/ml in staining medium (deficient RPMI, 3% newborn calf serum, 1 mM EDTA, 20 μM azide). IgFcγR-receptors were blocked by incubating cells for 15 min on ice with the anti-FcγRII/III mAb 2.4.G2 (Pharmingen, San Diego, CA). For cell staining, equal volumes of (blocked) cells and antibody-cocktails, containing each antibody at its optimized concentration, were incubated in 96-well round-bottom plates on ice for 20 min. Cells were washed twice with staining medium and streptavidin-TR was added for a further 15 min on ice. Cells were washed twice, resuspended in staining medium containing propidium iodide at a final concentration of 0.25 μg/ml, and analyzed immediately. Data were collected by FACS-Desk (11) and analyzed using FlowJo® software (Tree Star, San Carlos, CA). In order to facilitate the elucidation of potentially small subpopulations, 100,000 events per sample were collected.

Cytometry Hardware

The hybrid flow cytometer, combining a modified FACStarPlus® optical bench (Becton Dickinson, San Jose CA) with MoFlo® (Cytomation, Inc., Fort Collins, CO) and custom electronics, has been described in detail (12). Figure 2 is revised from Roederer et al. (12) to show the nine color detector configuration. The 407-nm emission arm was modified by adding a beam splitter and emission filter for CY, and by reversing the position of the CB detector and the (formerly spare and now) CY detector.

The overall layout of the electronics was left unchanged from Roederer et al. (12) and is not reproduced here. However, three modifications were made to different parts of the system. First, the MoFlo® electronics console was upgraded by the manufacturer to use a 32-word data frame. This makes it possible to add ADC boards (now 6 in the console) to process eleven measurement parameters (two light scatter signals and nine colors). Second, some of our custom electronics were changed. In particular, the preamplifiers were replaced with a set of computer-controlled compensating preamplifiers, and the preamplifiers are connected to non-rectifying logarithmic amplifiers (8) whose outputs feed linear inputs of the MoFlo® electronics. This allows pair-wise analog compensation between the following fluorochromes: FITC and PE, PE and Cy5PE, PE and Cy7PE, Cy5PE and Cy7PE, TR and APC, APC and Cy7APC, and CB and CY. Third, minor modifications were made to our instrument control and monitoring software to accommodate the above hardware changes.

RESULTS

Reagents

All direct antibody conjugates can be used to stain cells simultaneously. However, we observed that a high concentration of CB or CY can lead to unspecific binding of the other violet-light excited fluorochrome to the stained cells, resulting in false double-positive staining. To avoid this problem, we currently use only one of the two violet-light excited flurochromes conjugated during the first staining step and stain with the other reagent in a second step, if applicable, together with the streptavidin conjugate.

Compensation Between 407-nm and 488-nm Excited Parameters

Both FITC and PE are slightly excited by the 407-nm laser line, and CY is slightly excited by the 488-nm laser line. Thus, FITC and PE show a small but measurable spillover into the CY measurement channel and CY has a similar spillover into the FITC and PE measurement channels (see Table 1A). CB and CY also have small spectral overlaps with each other in this configuration. Digital compensation is effective at removing this low level of specral overlap (data not shown), while the combination of partial analog compensation and post-hoc software

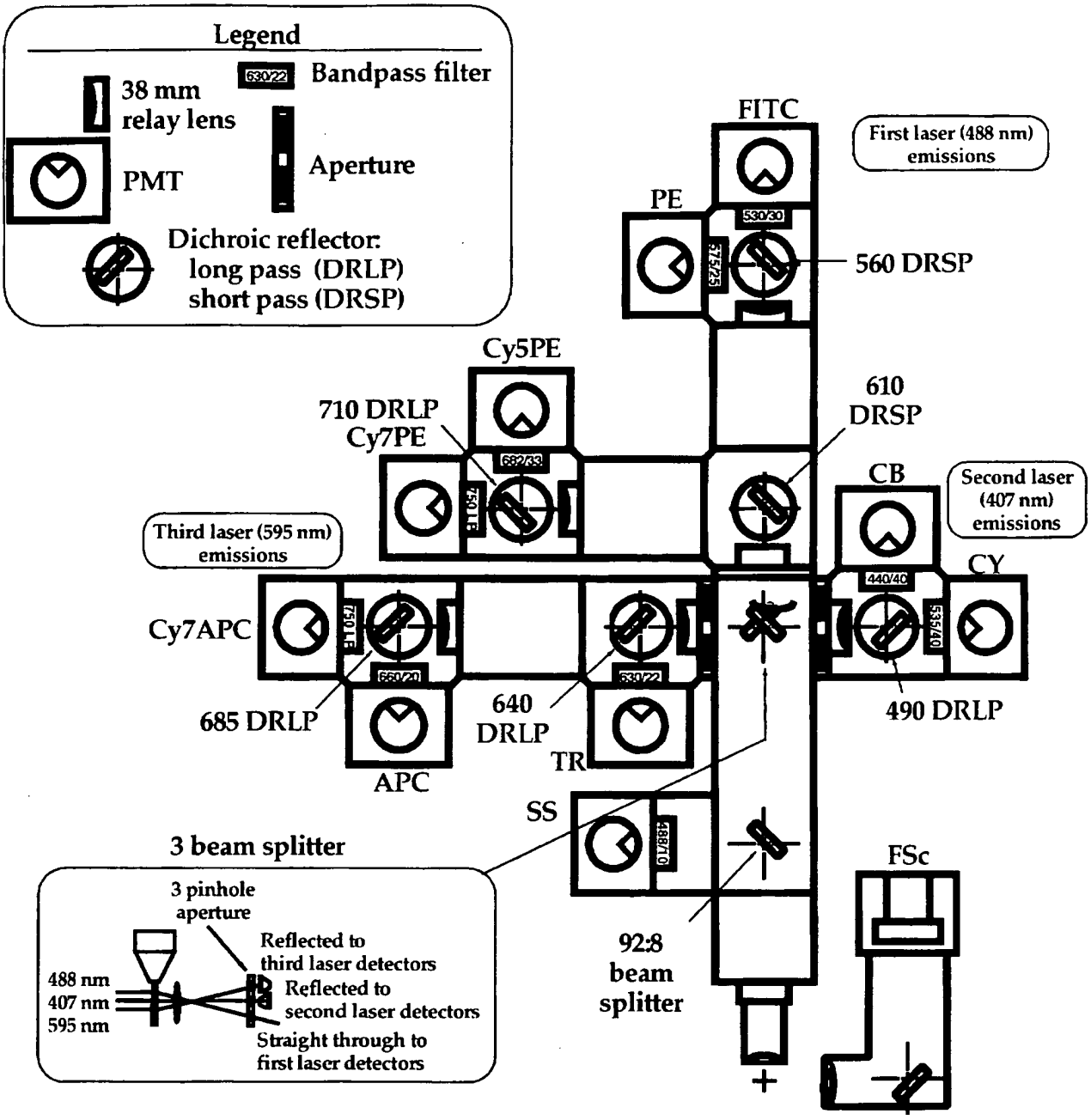

FIG. 2. Optical Layout and Filters for Nine Color Measurements. This block diagram shows the optical layout on the modified FACStarPlus® bench that is in use for nine color eleven parameter measurements. Relay lenses are used on the extended pathways to refocus the emission onto the PMT detectors. Filters and beam splitters that are not standard Becton Dickinson parts were obtained from either Chroma Technology Corp, Brattleboro VT, or Omega Optical, Brattleboro, VT. Note the change in position of the CB detector when CY is added, compared to Figure 2 in Roederer et al. (12).

compensation is effective at removing the overlap of CB into CY (see Table 2 and Fig. 3).

Using Partial Analog Compensation

We next determined whether the use of partial analog compensation can improve the compensation results. Poor compensation will result in a broader range of the compensated signal on a spillover channel. That is, a poor signal, compared to a better one, will simultaneously have more events on the reagent axis as well as events further off the axis. Thus, compensated signals with lower introduced variation will allow one to better discriminate low-level staining from negative events in multicolor measurements.

Table 2
Typical Effects of Partial Analog Compensation on Signal Measurement[a]

Measurement	Spectral spillover (no analog comp.)	Spectral spillover (partial analog comp.)	Light level on spillover channel (cv) (%)	Reduction in variation on spillover channel (%)
FITC → PE	0.29	0.01	5.5	15
PE → Cy5PE	0.18	0.03	9.3	18
Cy5PE → Cy7PE	0.15	0.09	9.6	15
TR → APC	0.12	0.02	15	15
APC → TR	0.14	0.02	14	8
APC → Cy7APC	0.10	0.04	21	7
Cy7APC → APC	0.68	0.57	29	0
CB → CY	0.07	0.01	7.1	11

[a]The compensation controls were run with no analog compensation and partial analog compensation as described. Forward and side light scatter gates were set to eliminate dead cells and debris. The spectral spillover columns are copied from Table 1. The "Reduction in variation on spillover" resulting from partial analog compensation is measured on the spillover channel, calculated using the difference between the 75th and 50th percentiles of the gated cells in the samples described, without and with the use of partial analog compensation. The "light level on spillover" is the CV of a narrow slice around the median of positively staining cells calculated on the spillover channel.

A common statistical metric for comparing the range of a measurement is the difference between a high and low percentile, say the 75th and 25th percentiles. However, this metric will not be usable here because half or more of the events of the unstained population are at lowest measurable signal level (i.e., "on the axis"). To avoid this artifact, we choose the somewhat ad-hoc metric of the difference between the 75th and 50th percentiles on the spillover parameters.. This allows us to numerically compare the variation in the two methods of compensation.

The boxes highlighted in Table 1A show the same laser spectral overlaps that are significant and can be reduced using partial analog compensation, as shown in the corresponding spectral overlaps in Table 1B. Table 2 list these results from Table 1 and the computed changes along with our ad-hoc metric. Also listed is the coefficient of variation (CV) on the spillover channel of a uniform population of positively staining cells on the source channel. This number reflects the uncertainty of measurements due to statistical variation (photon statistics) on both the source and spillover channels, with more uncertainty resulting in a larger value.

Table 2 shows that partial analog compensation followed by digital compensation results in reduction of the variation of signal in the spillover channel compared to using digital compensation alone. This improvement is correlated, with one exception, with the light level estimates provided. There is less relation to the original size of the spillover or the amount of spillover reduction provided by analog compensation, as long as both are non-trivial. We are not sure why the 4th row of this table (TR-APC) does not fit this pattern, and plan to investigate this further.

Figure 3 shows the underlying data sets for Table 2 displayed as contour maps. The horizontal lines help visualize the reduction in variation by showing a decrease in the extreme values of the stained populations. Plots corresponding to the last two rows of Table 2 are not shown; there is no variation change in Cy7APC-stained population as measured on APC, and the variation changes for CB-stained populations do not noticeably affect the extreme values of them.

Application to Immunophenotyping of Murine Splenic B-Cells

To identify potentially novel B-cell subsets in the spleen, 9-color staining cocktails were devised that included a series of surface markers that are known to stain B-cell subpopulations. Figure 4 shows the analysis of one such cocktail on one cell sample. After live cell gating by Forward Scatter-Side Scatter profile and propidium iodide exclusion (data not shown), cells were selected for their expression of the pan-B cell marker B220. To exclude the small number of T-cells that express this marker, and to exclude macrophages that might interfere with the analysis, cells were also stained with several anti-T-cell markers (anti CD3, anti-CD4, anti-CD8) and the macrophages marker F4/80.

Non-T-cells expressing B220 were then separated into IgM^{low} IgD^{hi} and IgM^{hi} IgD^{low} B cells. The majority of IgD^{hi} IgM^{low} cells (gate E, Fig. 4A) expressed all characteristics of follicular B cells: $CD21^{int.}$ $CD43^{-}$ $CD1^{low}$ $CD24^{low}$ $CD5^{-}$. However, like the cells within gates A and D, a subpopulation of cells expressed high levels of CD1 (shown as expression levels above indicated bar in plot), consistent with a previous report that demonstrated that a subset of follicular B cells expressed high levels of CD1 (1).

Analysis of CD43 and CD21 revealed three subpopulation among the IgM^{hi} IgD^{low} cells: $CD21^{-}CD43^{-}$ (gate B) $CD21^{int.}$ $CD43^{-}$ (gate A) and $CD21^{hi}$ $CD43^{-}$ (gate C). Cells within gate B were characterized as a homogeneous population of $CD24^{hi}$, $CD1^{low}$ and $CD5^{-}$ cells, consistent with their being immature B-cells (1,5). Cells in gate C also appeared homogenous, expressing the following phenotype: $CD1^{hi}$ $CD24^{int.}$ $CD5^{-}$. This phenotype is associated with marginal zone B-cells (1). The majority of cells within gate A was $CD24^{int.}$ $CD1^{low}$ and $CD5^{+}$. Therefore, the phenotype of this cell population is that of B-1 cells, representing about 0.3% of all events acquired. The

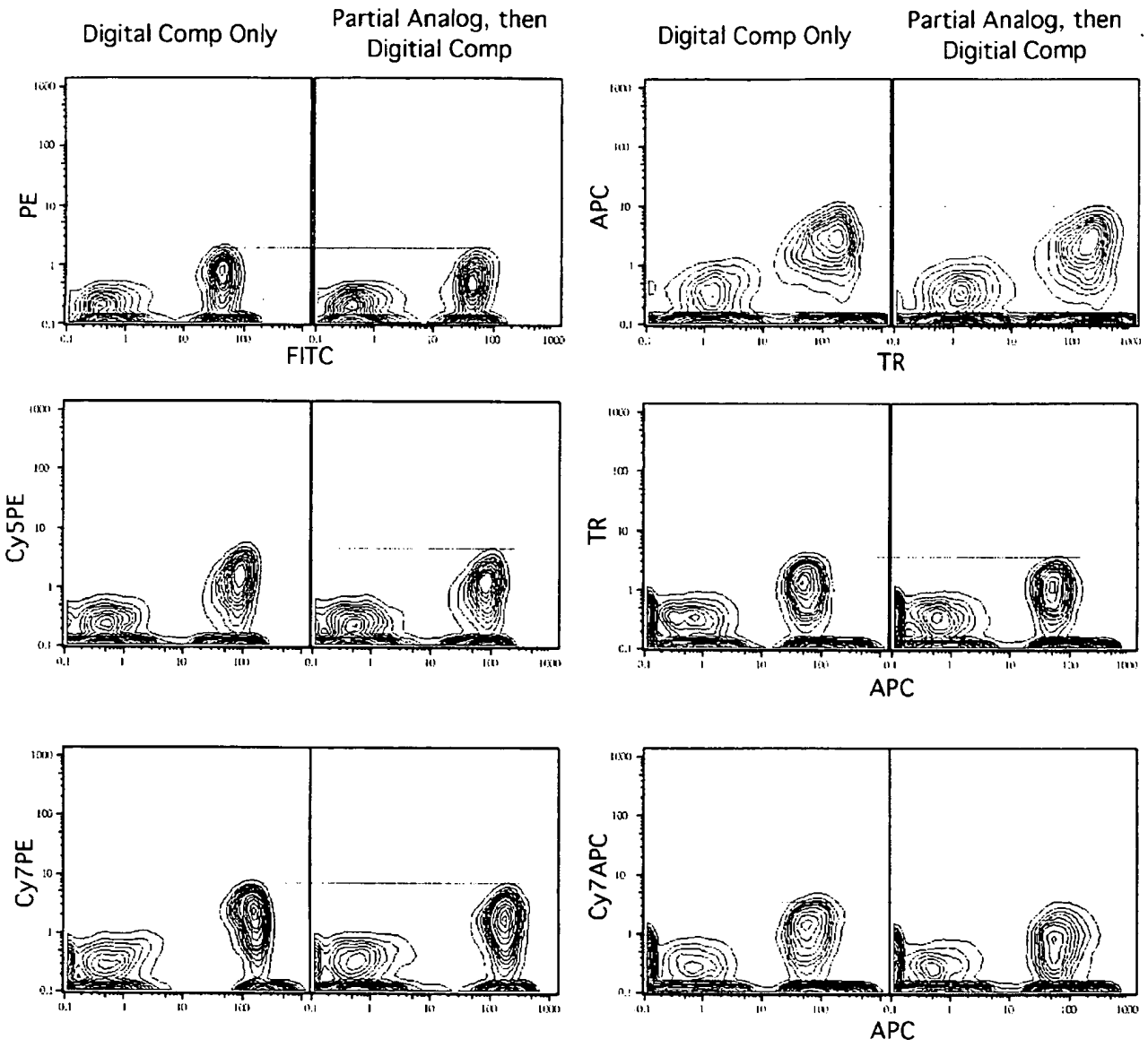

FIG. 3. Typical influence of compensation on data quality. Spleen cells from BALB/c mice were stained were stained as compensation controls as described in the text. Forward and side light scatter gates were set to eliminate dead cells and debris. The six pairs of contour plots (5% probability contours) correspond to the first six lines in Table 2. In each pair the left plot is generated using software (digital) compensation only, and the right plot is generated from data to which analog compensation was applied, followed by software compensation. The horizontal line on each pair is drawn at the lowest contour level of the positivily stained population in the right plot.

hallmark of B-1 cells is their expression of CD5 and CD43, which is believed to be restricted to this subset (1,5).

Interestingly, a second $CD5^+$ B cell population was identified which also expressed high levels of CD43, but belonged within the IgM^{low} IgD^{hi} B cell subset (D), associated with follicular B cells. Cells within gate D were similar to the B-1 cells in their expression of CD43 and CD21, however, they expressed less CD24 than B-1 cells, as measured by their mean fluorescent intensities (MFI) of 7.9 vs. 14.2. Furthermore, they also expressed lower levels of CD5 (MFI 11 vs. 22, respectively). This population of cells with the phenotype IgD^{hi} IgM^{low} $CD43^+$ $CD24^{int.}$ $CD1^{low}$ $CD5^+$ represents 0.6% of cells within the original sample, and does not correspond to any previously published B-cell subpopulation.

To confirm that this population was not artificially created by the gates set to separate IgM^{hi} IgD^{low} and IgM^{hi} IgD^{low} cells, we determined the expression of IgM vs. IgD on $B220^+$ $CD43^+$ and $B220^+$ $CD43^-$ cells. As shown in Figure 5, $B220^-$ $CD21^{int.}$ $CD43^+$ cells are heterogeneous in their expression of IgM and IgD. In comparison to the $CD43^-$ cells, a higher relative frequency of $CD43^+$ cells expresses IgM^{hi} IgD^{low}, presumably B-1 cells. However, a significant number of cells in this gate expresses IgM^{low}

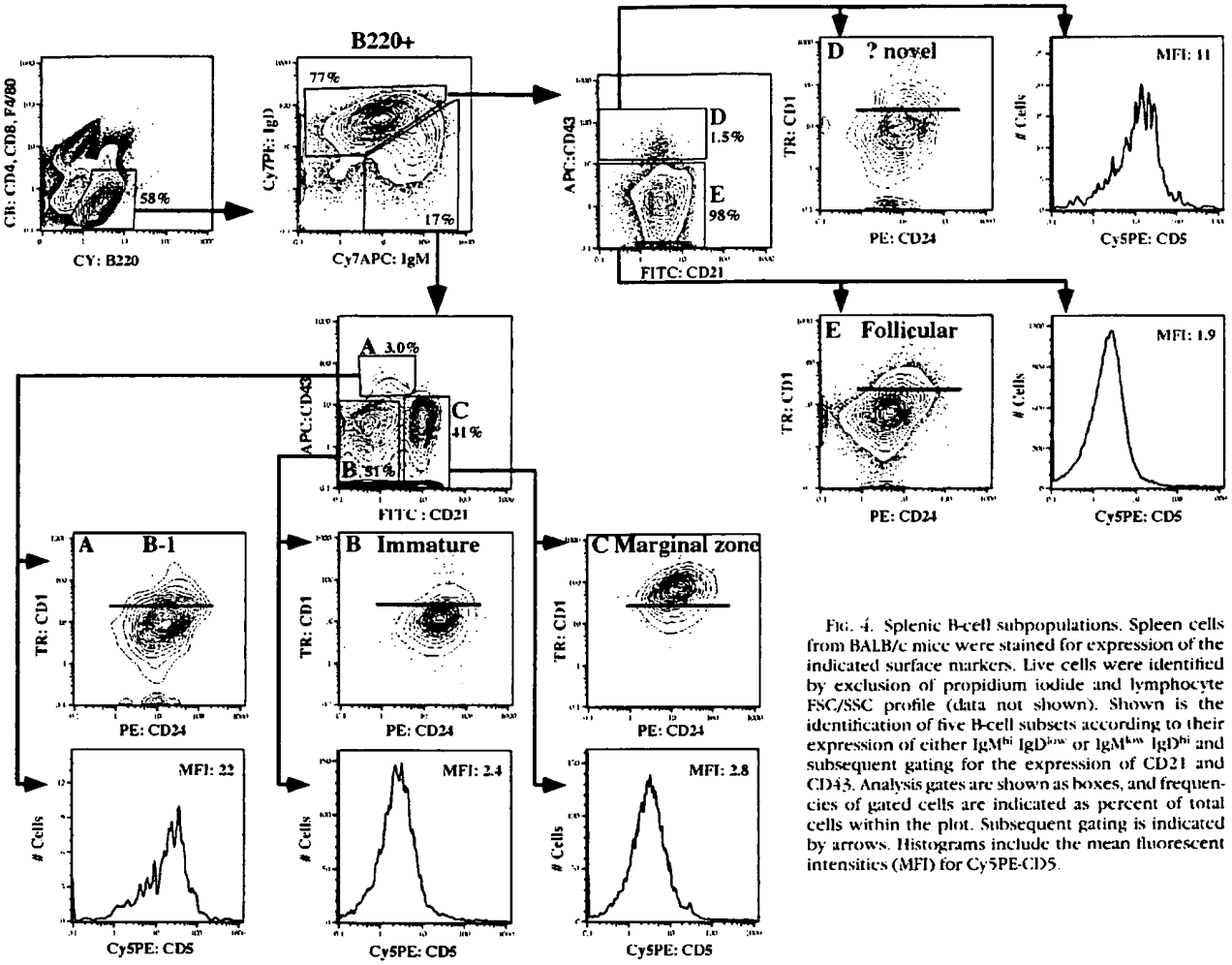

FIG. 4. Splenic B-cell subpopulations. Spleen cells from BALB/c mice were stained for expression of the indicated surface markers. Live cells were identified by exclusion of propidium iodide and lymphocyte FSC/SSC profile (data not shown). Shown is the identification of five B-cell subsets according to their expression of either IgM^{hi} IgD^{low} or IgM^{low} IgD^{hi} and subsequent gating for the expression of CD21 and CD43. Analysis gates are shown as boxes, and frequencies of gated cells are indicated as percent of total cells within the plot. Subsequent gating is indicated by arrows. Histograms include the mean fluorescent intensities (MFI) for Cy5PE-CD5.

IgD^{hi}, therefore constituting the second population of $CD43^+$ cells, identified as $CD5^+$ conventional B-cells.

Therefore, we identified, using nine distinct conjugates on one sample, five discrete B-cell subpopulations, at least three of which showed further heterogeneity with regard to their expression of CD1 and CD24.

DISCUSSION

We demonstrate in this report the feasibility of using nine dyes along with two light scatter signals for immunophenotype analysis. Using antibodies conjugated to four different fluorochromes excited at 488 nm, three excited at 595 nm, and two excited at 407 nm, we further demonstrate the unprecedented capabilities of this flow cytometric assay by identifying with a single data collection a total of five distinct murine B-cell subpopulations in the spleen of normal mice, one of which has not been described before.

For the simultaneous analysis of multiple cell surface markers, careful choice of the dyes to be used with each antibody is critical. The first consideration is whether a certain marker is expressed at high or low levels on the cells of interest. A suitable candidate dye should be chosen based on (1) dye "brightness" and (2) spectral interactions. Spectral interactions have to be considered, as spectral overlap and the compensation process can degrade the measurement, especially when the signal size, overlaps, and amount of adjustments required are large. For example, CD5 is expressed highly on T-cells, but is expressed at low levels on certain B-cell subsets. Very few conjugates will resolve these cells from the background. "Bright" dyes in our system are Cy5PE and APC. Considerable overlap exists between APC and Cy7APC, and other dyes such as Cy5PE and TR also interfere with the APC measurement. As a result of these overlaps, the APC negative cells have a relatively broad distribution, which potentially can make the resolution of dimly staining populations difficult. In contrast, less spillover into the Cy5PE channel was observed, and Cy5PE proved to be a useful dye in our configuration for measuring the low expression of CD5 on certain B cell subsets. Thus, for the analysis of a novel surface marker for which the particular characteristics in expression levels are not clear, it is important to choose stains and combination of stains that

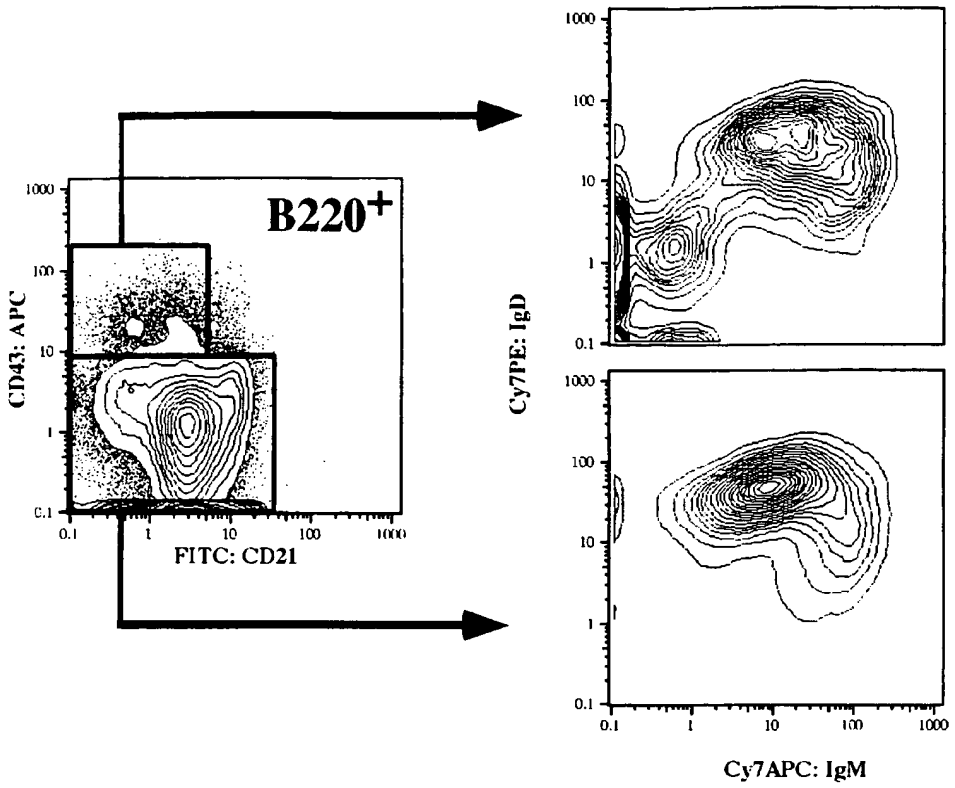

FIG. 5. CD43 expressing B cells are heterogeneous. B220$^+$CD3 CD4$^-$CD8 F4/80$^-$ cells obtained as shown in Figure 4 were gated as indicated into CD43$^+$ and CD43$^-$ cells and analyzed for their expression of IgM and IgD. Shown are 5% probability contour plots.

have minimal influence on the channels in which the markers of interest are measured.

At the other end of the "brightness" spectrum are the dyes CB and CY. These dyes produce a relatively small signal in relation to typical autofluorescence background, so that antibody conjugates have to be chosen that identify markers that are expressed uniformly at relatively high levels on cell subsets. An example is given in Figure 4, in which distinct B- and T-cell markers were chosen for use with the Krypton laser excited dyes. On the other hand, these dyes have very little measurement overlap from other fluorochromes, so that even low frequency populations of cells can be identified distinctively with these dyes.

In the case of FITC, the overlap from the other dyes range from small to negligible. Even though FITC is only a moderately "bright" dye, it is useful for distinguishing even relative small differences in the expression levels of a given cell surface marker. An example for this is provided in Figure 4, in which the expression of the complement receptor CD21 is studied on B-cells. As shown, the expression levels of this marker vary only about 10- to 20-fold among the different B-cell subsets, however, good separation was achieved and enabled the identification of three B-cell subsets among the IgM^{hi} IgD^{low} cells.

The usefulness of some dyes can be further increased by using a biotin-avidin system. In the example shown in Figure 4, "bright" CD1 staining was achieved using biotin-CD1 together with Streptavidin-TR.

In the process of making these choices, it is important to confirm the staining patterns for each of the reagent-dye combinations by measuring the marker of interest in the presence and absence of each of the other stains in the antibody cocktail. When compensation is applied, ideally the expression levels, as measured by mean fluorescent intensity of the populations of interest, should be identical in the presence or absence of each of the other reagents. For certain dye combinations, such as APC and Cy7APC, this is very difficult to achieve. When a population with high expression levels is stained with a conjugate using one of these dyes, the background levels measured for the other reagent most often will also increase somewhat. Carrying out the control measurements described above will facilitate the distinction of weak positive staining from background.

It is also important to note that the figures of merit for dye brightness given in Roederer et al. (12), upon which the above considerations are based, are not absolute, but relative both to the dyes and the instrument. Optical and flow geometry, the level of the background on various measurement parameters, and excitation conditions can have a strong effect on the ordering of the various dyes For example, among the three 488 nm excited dyes, FITC, PE, and Cy5PE, PE is the "brightest" on a FACScan® (Becton Dickinson, San Jose, CA) by the three criteria used in Roederer et al. (12) (data not shown), while Cy5PE is the "brightest" on our jet-in-air sorter. Thus, until appropriate inter-instrument standards and calibrations exist, one

should evaluate the dyes in use in their own particular configuration before making final determinations regarding their "brightness."

Partial analog compensation followed by digital compensation in post-hoc software, reduces the variation of cell distributions than software compensation used alone. Visually this can result in small improvements in the separation of subpopulations depending upon the reagent-dye combinations used. However, the improvement is not great enough to overcome unsuitable reagent combinations or the inherent variation due to low light (i.e., photoelectron) levels on some measurement parameters, hence the process of reagent choice described above must be carefully carried out for satisfactory results.

After a certain staining combination has been established and the staining patterns verified with the appropriate controls, the introduction of one new marker in a tested reagent combination becomes easy. It is then that the power of multicolor analysis becomes apparent. The expression levels of the new marker among the previously identified cell subpopulations can be determined within one sample. In the example shown in Figure 4A, a novel B cell subpopulation was identified not by introducing a novel marker, but by the ability to apply simultaneously a number of known surface makers. Expression of CD5 and CD43 was thought to be restricted to B-1 cells, which comprise only a small fraction of the B cells in the spleen of adult mice and are thought to represent a separate B-cell lineage from follicular B-cells (15). However, the data shown here suggest that a small percentage of B-cells, which show all the hallmarks of follicular B-cells, namely their expression of IgM^{low} IgD^{hi} $CD21^{int}$ $CD24^{int}$ $CD1^{low}$, can also express these two markers. Further differences between conventional CD5-expressing B-cells and B-1 cells were seen with regard to the levels of CD5 that are expressed by these different cells. The finding of conventional CD5-expressing B-cells is in agreement with earlier in vitro studies that demonstrated that conventional B-cells can express CD5 under certain stimulation conditions (4). Further work is needed to confirm the origin of the two CD5 expressing B-cell populations in the spleens of normal mice, to determine whether they indeed belong to separate B-cell lineages.

Although our hardware involved considerable in-house development, at least one manufacturer (Cytomation, Inc.) can supply a system with similar multicolor measurement capability, although without analog compensation. We expect the other major manufacturers, as they introduce new systems and retrofit their old ones, to provide similar capability for making these simultaneous measurements. Flow cytometric measurements on cells are used not only for phenotypic analysis, but also for various functional studies, such as Ca^{++}-flux analysis, activation marker expression, gene expression, and the identification of type and frequency of cytokines produced by a given cell population. The development of multicolor flow cytometric systems, such as the one described in this study, provides the tools for combining complex functional and phenotypic measurements on heterogeneous cell populations for their analysis immediately ex vivo. The system described here can, therefore, enhance the quality and the feasibility of many cell biological studies.

ACKNOWLEDGMENTS

We thank the reviewers for their careful reading and helpful comments, which have improved the presentation of this paper.

LITERATURE CITED

1. Amano M, Baumgarth N, Dick M, Herzenberg LA, Herzenberg LA. CD1 expression defines subsets of follicular and marginal zone B cells in the spleen: B2m-dependent and independent forms. J Immunol 1998;161:1710–1717.
2. Anderson MT, Baumgarth N, Haugland RP, Gerstein RM, Tjioe IT, Herzenberg LA, Herzenberg LA. Pairs of violet-light excited fluorochromes for flow cytometric analysis. Cytometry 1998;33:435–444.
3. Bagwell CB, Adams EG. Fluorescence spectral overlap compensation for any number of flow cytometry parameters. Ann NY Acad Sci 1993;677:167–184.
4. Bandyopadhyay RS, Teutsch MR, Wortis HH. Activation of B-cells by sIgM cross-linking induces accumulation of CD5 mRNA. Curr Top Microbiol Immunol 1995;194:219–228.
5. Best CG, Kemp JD, Waldschmidt TJ. Murine B-cell subsets defined by CD23. In: Methods: a companion to methods in enzymology. San Diego: Academic Press, Inc.; 1995. p 3–10.
6. Hardy RR. Purification and characterization of monoclonal antibodies. In: Weir DM, editor. Handbook of experimental immunology. Oxford: Blackwell Scientific Publications; 1986. p 13.11.
7. Hardy RR. Purification and coupling of fluorescent proteins for use in flow cytometry. In: Weir DM, editor. Handbook of experimental immunology. Oxford: Blackwell Scientific Publications; 1986. p 31.31.
8. Hiebert RD, Sweet RG. Electronics for flow cytometers and sorters. In: Van Dilla M, editor. Flow cytometry: instrumentation and data analysis. London: Academic Press; 1985. p 129–161.
9. Lalor PA, Stall AM, Adams S, Herzenberg LA. Permanent alteration of the murine Ly-1 B repertoire due to selective depletion of Ly-1 B cells in neonatal animals. Eur J Immunol 1989;19:501–506.
10. Loken MR, Parks DR, Herzenberg LA. Two-color immunofluorescence using a flourescence-activated cell sorter. J Hist Cytol 1977;25:899–907.
11. Moore WA, Kautz RA: Data analysis in flow cytometry. In: Weir DM, Herzenberg LA, Blackwell CM, Herzenberg LA, editors. Handbook of experimental immunology, 4 ed. Edinburgh: Blackwell Scientific Publications; 1986. p 30.31–30.11.
12. Roederer M, DeRosa S, Gerstein R, Anderson MT, Bigos M, Stovel RT, Nozaki T, Parks DR, Herzenberg LA, Herzenberg LA. 8 color, 10-parameter flow cytometry to elucidate complex leukocyte heterogeneity. Cytometry 1997;29:328–339.
13. Roederer M, Kantor AB, Parks DR, Herzenberg LA. Cy7PE and Cy7APC: bright new probes for immunofluorescence. Cytometry 1996;24:191–197.
14. Roederer M, Murphy R. Cell-by-cell autofluorescence correction for low signal-to-noise systems: application to epidermal growth factor endocytosis by 3T3 fibroblasts. Cytometry 1986;7:558–565.
15. Wells SM, Kantor AB, Stall AM. CD43 (S7) expression identifies peripheral B cell subsets. J Immunol 1994;153:5503–5515.

Cytometry 39:96-107 (2000)

Four-Color Multiparameter DNA Flow Cytometric Method to Study Phenotypic Intratumor Heterogeneity in Cervical Cancer

Willem E. Corver,[1]* Louise A. Koopman,[1] Jan van der Aa,[2] Mira Regensburg,[3] Gert Jan Fleuren,[1] and Cees J. Cornelisse[1]

[1]Department of Pathology, Leiden University Medical Center, Leiden, The Netherlands
[2]Becton Dickinson, Immunocytometry Systems, Erembodegem, Belgium
[3]Leiden Cytology Pathology Laboratory, Leiden, The Netherlands

Received 28 June 1999; Revision Received 29 September 1999; Accepted 30 September 1999

Background: Multiparameter DNA flow cytometry using a one-laser bench-top flow cytometer has been restricted to three different colors. The two laser FACSCalibur has recently been introduced, allowing four-color analysis. Therefore, we optimized and extended our three-color method (Corver et al., 1994, Corver et al. 1996) to a four-color analysis of phenotypic intra-tumor heterogeneity using a bench-top flow cytometer.

Methods: First, the effect of a range of different propidium iodide (PI) and TO-PRO-3 iodide (TP3) concentrations on the coefficient of variation (CV) of the DNA histograms was measured using paraformaldehyde-fixed lysolecithin-permeabilized peripheral blood lymphocytes (PBLs) and SiHa and HeLa cervical cancer cells. Second, labeling freshly isolated cervical cancers from solid tumors was optimized with a mixture of anti-keratin antibodies. Third, the FACSCalibur hardware was modified, thereby allowing the simultaneous measurement of allophycocyanin (APC) fluorescence (FL4) in combination with FL3 pulse processing (FL3-W vs. FL3-A). The optimized procedure was then applied to cell suspensions from four different human cervical cancers to study phenotypic intratumor heterogeneity. Cell suspensions were simultaneously stained for DNA (PI, fluorescence) and three cellular antigens: (a) the epithelial cell-adhesion molecule (Ep-CAM; APC fluorescence), (b) keratin (R-phycoerythrin [RPE] fluorescence) to identify the epithelial fraction, and (c) vimentin (fluorescein-isothiocyanate [FITC] fluorescence) to label stromal cells.

Results: Overall, PI produced better CVs than did TP3. The optimal concentration of PI was 50-100 μM for all cells tested. Average CVs were 1.76% (PBL), 3.16% (HeLa), and 2.50% (SiHa). Optimal TP3 concentrations were 0.25-2.0 μM. Average CVs were 2.58% (PBL), 5.16% (HeLa), and 3.96% (SiHa). Inter- or intra-DNA stem line heterogeneity of Ep-CAM expression was observed in the keratin-positive fractions. Vimentin-positive, keratin-negative cells were restricted to the DNA diploid fraction.

Conclusions: PI is a superior DNA stain to TP3 when using intact normal PBL and human cancer cells. Four-color high-resolution multiparameter DNA flow cytometry allows the identification of intratumor subpopulations using PI as DNA stain and FITC, RPE, and APC as reporter molecules. The FACSCalibur bench-top flow cytometer can be used for this purpose, allowing the application of this technique in clinical laboratories. Cytometry 39: 96-107, 2000. © 2000 Wiley-Liss, Inc.

Key terms: cervical cancer; Ep-CAM; keratin; vimentin; tumor heterogeneity; multiparameter; flow cytometry; DNA ploidy

Multiparameter DNA flow cytometry (FCM) is a powerful tool for analyzing intratumor heterogeneity (1-3) of human solid tumors. Compared with standard immunohistochemistry, FCM has several advantages for studying intratumor heterogeneity, despite the fact that cells cannot be visually examined. Multiple cellular protein expression can be measured simultaneously in thousands of cells in combination with DNA ploidy analysis. Moreover, tumor subpopulations identified by differential protein marker expression and DNA ploidy can be flow sorted for subsequent molecular genetic characterization (4,5).

Until now, a maximum of three parameters (DNA and two cellular proteins) could be measured on a bench-top single-laser flow cytometer (FACScan). The use of anti-keratin monoclonal antibodies (mAbs) enables the identi-

Part of this work was presented at the 11th Heidelberg Cytometry Symposium, Heidelberg, 22-24 October 1998.

*Correspondence to: Willem E. Corver, Department of Pathology, Leiden University Medical Center, P.O. Box 9600, Building 1, L1-Q, 2300 RC, Leiden, The Netherlands.
E-mail: W.E.Corver@Pathology.MedFac.LeidenUniv.nl

Table 1
*Monoclonal Antibodies Used to Study Phenotypic Intratumor Heterogeneity of Ep-CAM Expression**

mAb	Antigen	IgG subclass	Reporter molecule	Reference
CL80	"Pan-keratin"	IgG1	RPE	22
AE1/AE3	"Pan-keratin"	IgG1	RPE	23
MNF116	Keratins 4, 6, 8, 17, 19	IgG1	RPE	24
6B10	Keratin 4	IgG1	RPE	25
OV-TL 12/30	Keratin 7	IgG1	RPE	26
M20	Keratin 8	IgG1	RPE	27
DE-K10	Keratin 10	IgG1	RPE	28
KS-1A3	Keratin 13	IgG1	RPE	29
M9	Keratin 18	IgG1	RPE	30
BA17	Keratin 19	IgG1	RPE	31
V9	Vimentin	IgG2b	FITC	18
323/A3	Ep-CAM	IgG2a	APC	15

*APC, allophycocyanin; Ep-CAM, epithelial cell-adhesion molecule; FITC, fluorescein-isothiocyanate; mAb, monoclonal antibody; RPE, R-phycoerythrin. The anti-keratin mAbs were mixed in order the labeling of all epithelial cells present in squamous cell carcinomas, adenocarcinomas, and adenosquamouscarcinomas of the uterine cervix. The other mAbs used in this study for staining Ep-CAM and vimentin, differ in mouse IgG isotype, which allowed the simultaneous labeling of three cellular antigens with an indirect staining technique.

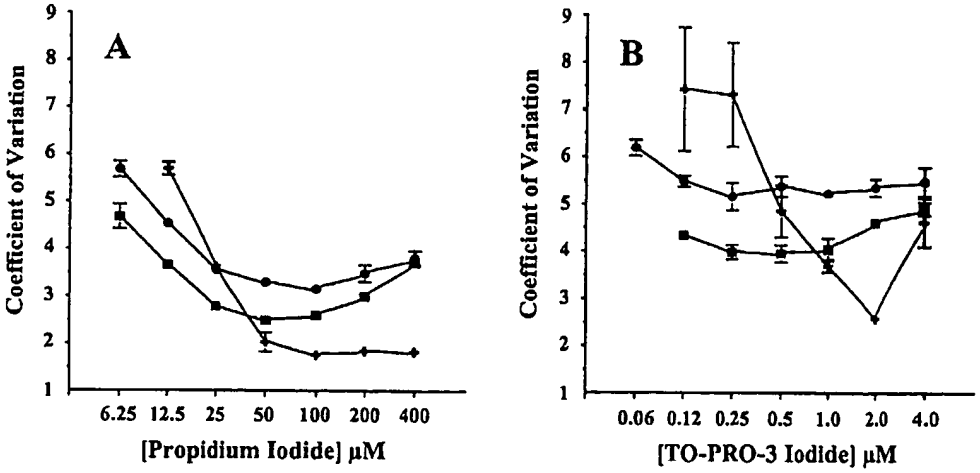

FIG. 1. Coefficient of variation (CV) of the DNA histograms as a function of DNA dye concentrations. Human peripheral blood lymphocytes (PBLs) and cells from human cervical carcinoma cell lines were fixed, permeabilized, and stained by different TO-PRO-3 iodide (TP3) and propidium iodide (PI) concentrations. TP3 fluorescence was measured using the FL4. ModFit 5.2 (Verity Software House) was used for DNA histogram analysis. The results from one complete experiment are shown. A: CVs of PBL (+) and HeLa (circles) and SiHa (squares) cells stained with PI. B: CVs of PBL (+) and HeLa (circles) and SiHa (squares) cells stained with TP3. Note that the CVs of the PBL more strongly depend on the TP3 concentration than those of HeLa and SiHa.

fication of carcinoma cells in cell suspensions from solid tumors. Simultaneously, these cells can be stained for a second cellular protein, e.g., p53 (6,7), the epithelial cell adhesion molecule (Ep-CAM), erbB2 (2), or epidermal growth factor receptor (EGFR) (3), and DNA. Fluorescein-isothiocyanate (FITC) and R-phycoerythrin (RPE) are frequently used as fluorescent reporter molecules for cellular proteins, and DNA is stained with propidium iodide (PI). However, mAbs must be carefully selected based on mouse IgG subclass differences to allow correct indirect staining for multiple cellular proteins. Directly conjugated mAbs for multiparameter DNA FCM of human solid tumors are still not readily available.

Recently, the FACSCalibur flow cytometer was introduced; it can be equipped, next to a standard 15-mW 488-nm argon-ion laser, with a 12-mW diode laser emitting at 635 nm. This model allows TO-PRO-3 iodide (TP3), a recently developed DNA stain with an excitation optimum of 642 nm (8), to be used as an alternative to PI for multiparameter DNA measurements (9). This method opens the possibility to measure four colors simultaneously by using a standard bench-top flow cytometer, e.g., FITC, RPE, RPE-Cy5 and TP3 or FITC, RPE, allophycocyanin (APC) and PI. The usefulness of TP3 as a DNA stain for multiparameter DNA studies on clinical samples has been demonstrated (10,11). An advantage of the use of TP3 compared with PI is the minimal cross-talk into green (FL1), orange (FL2), and deep red (FL3) fluorescence detectors because of a time delay between TP3 fluorescence and fluorescence signals from dyes excited by the 488-nm laser line. However, for the study of intratumor heterogeneity by multiparameter DNA FCM and

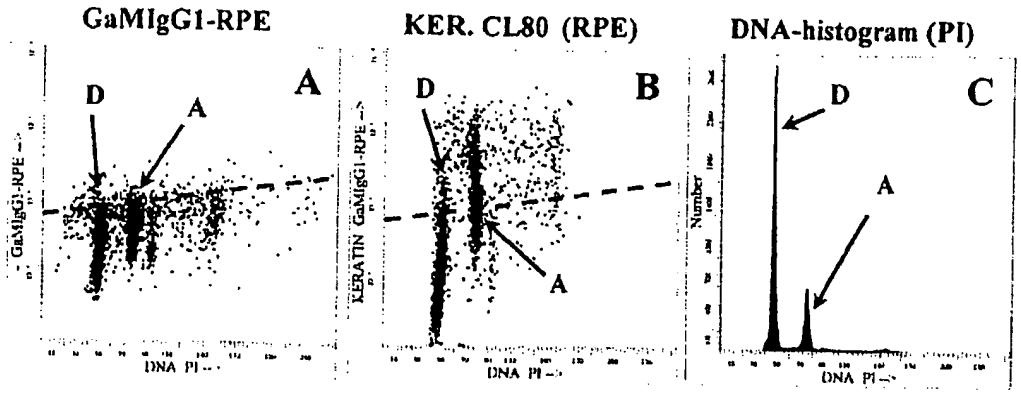

FIG. 2. "Pan-keratin" marker CL80 identifies only part of the tumor cells in the DNA aneuploid fraction. Cells isolated from a cervical cancer were stained for keratin by CL80 (R-phycoerythrin, RPE) and DNA (propidium iodide) and analyzed for keratin expression by dual-parameter flow cytometry. A: Background fluorescence of the GaMIgG1-RPE control. B: Partial staining of the DNA aneuploid (A) fraction by the pan-keratin marker CL80. C: Corresponding DNA histogram with a DNA diploid (D) and a DNA aneuploid (A) fraction (DNA index = 1.55).

flow sorting, narrow coefficients of variation (CVs) of the DNA peaks are required. This is a necessity in cases with multiple DNA stem lines or a stem line with a DNA index (DI) close to 1.0. Thus, first we compared PI and TP3 to be used as DNA stain for four-color multiparameter studies on a two-laser FACSCalibur. A range of different PI and TP3 concentrations was used to stain the DNA of paraformaldehyde-fixed lysolecithin permeabilized (1) human peripheral blood lymphocytes (PBLs) and the human cervical cell lines HeLa and SiHa.

Second, to study phenotypic intratumor heterogeneity in cervical cancer, a mixture of anti-keratin mAbs was composed to identify the complete epithelial fraction irrespective of the different cervical tumor types. This was done because keratin expression pattern of cervical carcinomas differs strongly across squamous cell carcinomas, adenocarcinomas, and adenosquamouscarcinomas and can be very complex (12). Pilot studies demonstrated that the so-called pan-keratin markers failed to label the complete epithelial fraction in cervical carcinomas as measured by FCM.

Because the standard equipped FACSCalibur does not allow the simultaneous measurement of APC fluorescence (FL4-H) and PI pulse processing (FL3-A vs. FL3-W), we developed a simple modification of the FACSCalibur hardware to allow these kinds of measurements.

Third, the optimized four-color staining protocol was applied to cervical carcinoma cell suspensions to study phenotypic intratumor heterogeneity of the epithelial cellular adhesion molecule (Ep-CAM) (13), a tumor-associated antigen that is highly expressed on many human solid tumors (14) including cervical cancer (15).

We show that tumor-associated cell surface molecules (e.g., Ep-CAM, APC fluorescence) can be measured simultaneously with the intermediate filaments vimentin (FITC fluorescence) and keratin (RPE fluorescence) and that high resolution of DNA histograms is preserved when using PI as the DNA stain. With the same protocol, we could demonstrate the presence of discrete tumor subpopulations differing in Ep-CAM expression, keratin expression, and DNA content in cervical cancers.

MATERIALS AND METHODS

Cell Lines

Human cervical carcinoma cell lines HeLa and SiHa were obtained from the American Type Culture Collection (Atlanta, GA). Both cell lines were cultured and maintained in standard Dulbecco's minimum essential medium (DMEM; GibcoBRL, Paisley, Scotland, UK) containing 10% heat-inactivated fetal calf serum (FCS; GibcoBRL) under 5.0% CO_2 condition and 95% humidified air. Culture media were supplemented with 2 mM L-glutamine (Flow Laboratories, Irvine, Scotland, UK), 50 mg/l streptomycin, and 50 IU/ml penicillin (Flow Laboratories). The monolayer cells were harvested using Hank's balanced salt solution (Sigma Diagnostics, St. Louis, MO) buffered 5 mM ethylene-diaminetetraacetic acid/025% trypsin (Flow Laboratories), as described in detail previously (16). Human PBLs were obtained from a healthy donor.

DNA Staining Titration Experiments

Freshly isolated human PBLs and HeLa and SiHa cervical cancer cells were washed twice with cold phosphate buffered saline (PBS). One million cells per test tube were fixed with freshly prepared phosphate buffered 1.0% paraformaldehyde (Merck, Darmstadt, Germany) containing 160 μg/ml of lysolecithin (from egg yolk; Sigma) for permeabilization, added drop-wise under constant swirling (1). After 5 min, the reaction was blocked by adding 1.0 ml PBS/1% bovine serum albumin (BSA; PBA). Cells were then spun down and washed once with 1.0 ml PBA. DNA staining solutions were prepared in PBA containing 0.1% RNase (Sigma) and various concentrations of TP3 (Molecular Probes, Eugene, OR), ranging from 0.06 μM to 4.0 μM, or containing various concentrations of PI (Calbiochem, San Diego, CA), ranging from 6 μM to 400 μM, respectively. Each dye concentration was evaluated in

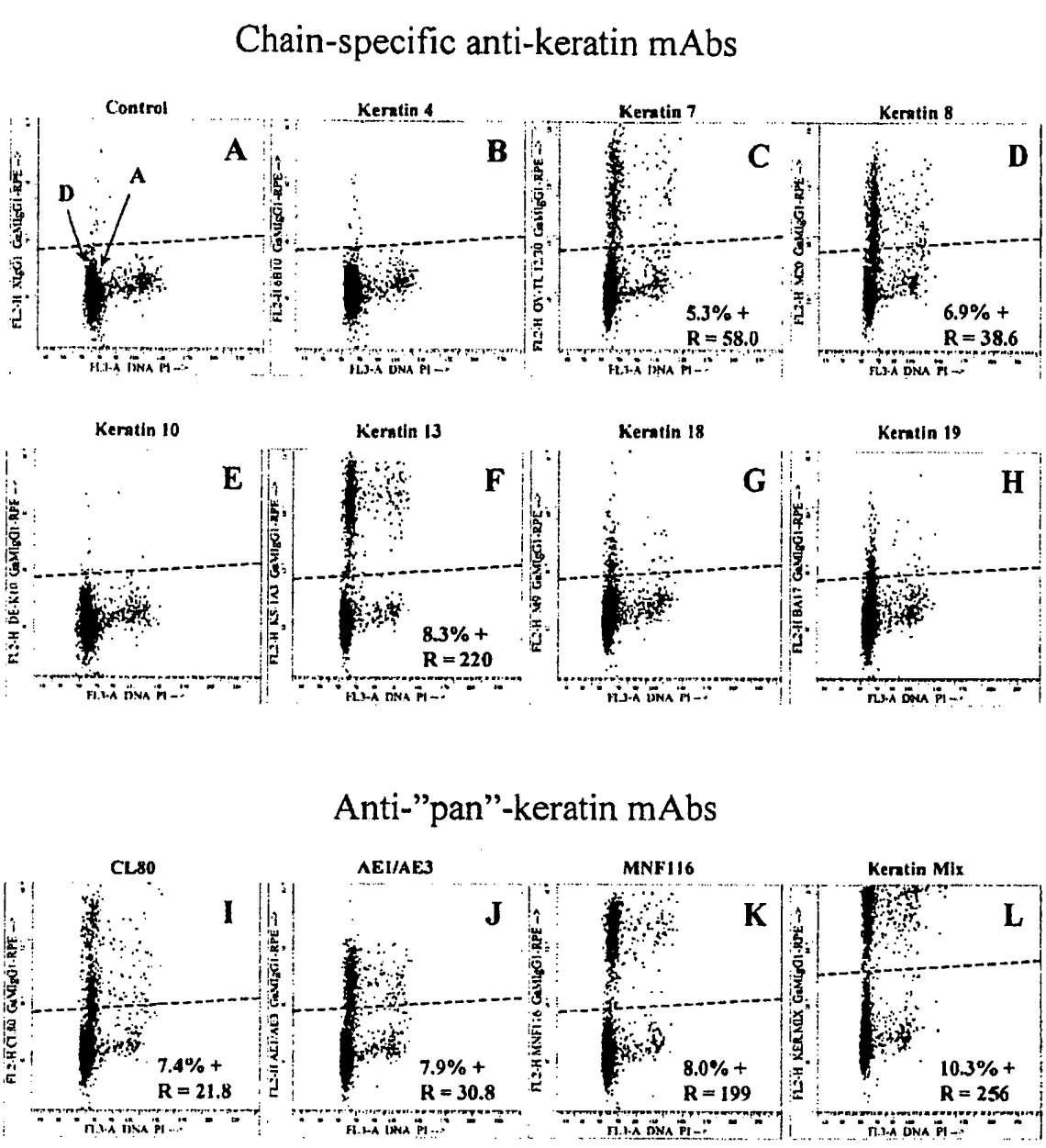

FIG. 3. Optimization of labeling cervical cancers by a mixture of anti-keratin monoclonal antibodies (mAbs). Cervical cancer cells were stained for keratin (R-phycoerythrin fluorescence) by using chain-specific anti-keratin mAbs, anti-"pan-keratin" mAbs, or a mixture of different anti-keratin mAbs (Table 1) and DNA (propidium iodide). Samples were analyzed on a FACSCalibur. The highest percentage of keratin-positive cells and the highest signal-to-noise ratio (R) were obtained by using a mixture of anti-keratin mAbs (L), compared with the control (A), the use of a mAb against keratin 7 (C), keratin 8 (D), keratin 13 (F), and pan-keratin markers CL80 (I), AE1/AE3 (J), and MNF116 (K). A weak signal was obtained with a mAb directed against keratin 18 (G) or keratin 19 (H). Keratin 10-positive cells and keratin 4-positive cells could not be detected (B,E).

triplicate by using the same cell batch. Cells were incubated with 0.5 ml DNA staining solution for 30 min at 37°C to activate the RNase and stored overnight at 4°C before flow cytometric analysis.

Solid Tumors

Four fresh cervical tumors obtained from the Clinical Pathology Department of the Leiden University Medical Center were used for this study. Adipose and necrotic tissues were removed. Samples were cut in fragments of approximately 1-2 mm^3 and incubated at 37°C for 1-2 h in 10 ml DMEM (GibcoBRL) per 1.0 g tissue, without FCS, containing 0.5 mg/ml collagenase II (Sigma) and 0.002% DNA I (Sigma) (17). Suspensions were then passed over a nylon sieve with a 100-μM pore size (Verseidag-Industrietextilien GmbH, Kempen, Germany). The cell suspen-

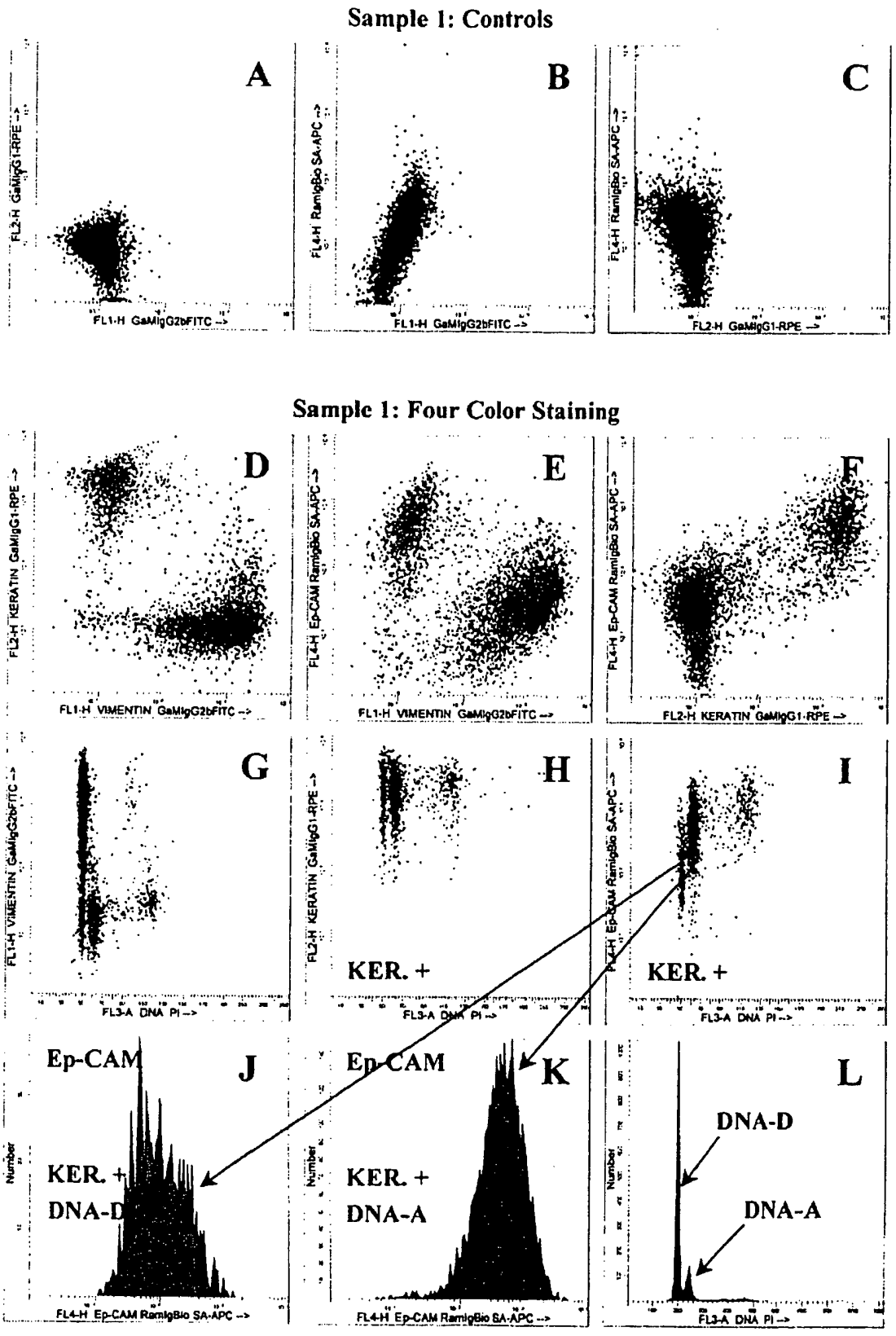
Sample 1: Controls
A
FL2-H GaMIgG1-RPE -->
FL1-H GaMIgG2bFITC -->
B
FL4-H RamIgBio SA-APC -->
FL1-H GaMIgG2bFITC -->
C
FL4-H RamIgBio SA-APC -->
FL2-H GaMIgG1-RPE -->
Sample 1: Four Color Staining
D
FL2-H KERATIN GaMIgG1-RPE -->
FL1-H VIMENTIN GaMIgG2bFITC -->
E
FL4-H Ep-CAM RamIgBio SA-APC -->
FL1-H VIMENTIN GaMIgG2bFITC -->
F
FL4-H Ep-CAM RamIgBio SA-APC -->
FL2-H KERATIN GaMIgG1-RPE -->
G
FL1-H VIMENTIN GaMIgG2bFITC -->
FL3-A DNA PI -->
H
FL2-H KERATIN GaMIgG1-RPE -->
KER. +
FL3-A DNA PI -->
I
FL4-H Ep-CAM RamIgBio SA-APC -->
KER. +
FL3-A DNA PI -->
Ep-CAM
J
Number
KER. +
DNA-D
FL4-H Ep-CAM RamIgBio SA-APC -->
Ep-CAM
K
Number
KER. +
DNA-A
FL4-H Ep-CAM RamIgBio SA-APC -->
L
DNA-D
DNA-A
Number
FL3-A DNA PI -->

FIGURE 4

sions were kept on ice. FCS was added, to a final concentration of 10%, to block proteolytic activity. The total percentage of viable and dead cells was obtained by using the trypan blue exclusion method. Average yield was 42 × 10^6 cells/g tissue. Average viability was higher than 87%.

Cells were pelleted and resuspended in standard DMEM containing 10% FSC, 10% dimethylsulfoxide and stored in liquid nitrogen until flow cytometric analysis.

Monoclonal Antibodies

A mixture of anti-keratin mAbs was composed for staining the epithelial fraction of dispersed cervical carcinomas (Table 1). Clones 80, 6B10, M20, M9, and V9 (producing mAbs directed against keratin [pan-keratin marker], keratin 4, keratin 8, keratin 18, and vimentin, respectively) were established at the Department of Pathology, Leiden University Medical Center, The Netherlands (18,19). Hybridoma cells were cultured and maintained in standard medium. The culture supernatants, diluted 1:5, were used for staining. Clones MNF116, DE-K10, OV-TL 12/30, and BA17 were kindly provided by DAKO A/S (Glostrup, Denmark). Clone KS-1A3 was obtained from Sigma Diagnostics. Clones AE1 and AE3 were obtained premixed from Boehringer Diagnostica (Mannheim, Germany). Centocor Europe (Leiden, The Netherlands) kindly provided clone 323/A3, directed against Ep-CAM as the purified antibody. All dilutions were made in PBS containing 1% BSA (Sigma Diagnostics).

Four-Color Immunofluorescent Staining

Tumor cells were thawed, washed twice with cold PBA, and stained for surface antigens as follows. One million cells were incubated for 30 min on ice with 100 μl of diluted mAbs. Cells were then washed twice with 1.0 ml cold PBA (500*g*, 5 min, 4°C). After washing, cells were incubated for 30 min on ice with 100 μl of a biotinylated rabbit anti-mouse Ig polyclonal secondary reagent (DAKO) diluted 1:100. Cells were washed twice, followed by an incubation with 100 μl of Streptavidin-APC, diluted 1:200 (Molecular Probes). After 30 min on ice, cells were washed twice with 1.0 ml of cold PBS alone. Cells were subsequently fixed and permeabilized, as described above, using 1.0 % paraformaldehyde (Merck) containing 160 μg/ml of lysolecithin (Sigma). After 5 min on ice, 1.0 ml PBA was added. Cells were spun down at 500*g* for 5 min. Cells were then incubated for 30 min on ice with 125 μl of a mixture composed of anti-keratin mAbs (IgG1; Table 1) and anti-vimentin mAbs (IgG2b). After incubation, cells were washed twice with cold PBA and incubated with 100 μl of a mixture composed of goat $F(ab')_2$ anti-mouse IgG1-RPE and goat $F(ab')_2$ anti-mouse IgG2b-FITC polyclonal antibodies, both diluted 1:200 in PBA (Southern Biotechnology Associates, Birmingham, AL). DNA was stained by using 100 μM PI, as described above.

Flow Cytometry

For each measurement, data from 10,000–20,000 events were collected with a standard FACSCalibur (Becton Dickinson Immunocytometry Systems, San Jose, CA) flow cytometer, equipped with a 15-mW argon-ion laser (488 nm) and 12-mW diode laser (635 nm). FITC (FL1, BP 530/30 nm), RPE (FL2, BP 585/42 nm), and APC fluorescence (FL4, BP 661/16 nm) measurements were collected in the logarithmic mode. PI and TP3 fluorescence measurements were collected in the linear mode by using a 670-nm LP filter (FL3) and the 661/16 BP filter (FL4), respectively.

A standard equipped FACSCalibur does not allow the simultaneous use of the FL3-A versus FL3-W pulse processor in combination with APC fluorescence measurements. Therefore, FACSCalibur hardware was modified to allow the use of the FL3-A versus FL3-W pulse processor in combination with FITC, RPE, and APC fluorescence measurements. A detailed description is given in the Appendix (Fig. 8).

Data were analyzed with WinList 3.0 and ModFit 5.2 software (Verity Software House, Inc., Topsham, ME). N-color compensation was used for postacquisition spectral cross-talk correction.

RESULTS

Effect of PI and TP3 Concentrations on CVs

DNA histogram resolution was compared between three cell lines stained with a range of different PI or TP3 concentrations, respectively.

Nonstimulated human PBLs and proliferating HeLa (40% S phase) and SiHa (10% S phase) cervical carcinoma cells were stained in triplicate. Figure 1 shows the average CVs. For all three cell lines, the lowest CVs were obtained when using PI. Optimal PI concentrations were 50–100 μM for HeLa and SiHa cells; for PBL, the optimal concentration was 100–400 μM.

For TP3, the CVs of HeLa and SiHa cells appeared to be less dependent on the dye concentration. The optimal dye concentration was 0.25–2.0 μM. A narrow optimal concentration range was found for PBL. CVs obtained at optimal PI concentrations were significantly lower than those obtained at optimal TP3 concentrations. The complete experiment was repeated once, producing similar results.

FIG. 4. Measurement of epithelial cell-adhesion molecule (Ep-CAM) expression (allophycocyanin, APC) of a freshly isolated cervical carcinoma cell suspension containing normal stromal cells and cancer cells. A–C: Levels of background fluorescence from goat anti-mouse controls (see Materials and Methods). A: FL1, green fluorescence, versus FL2, orange fluorescence. B: FL1, green fluorescence, versus FL4, red fluorescence. C: FL2, orange fluorescence, versus FL4, red fluorescence. Tumor subpopulations can be clearly identified based on cell lineage-specific protein expression. D: Vimentin (FL1, fluorescein-isothiocyanate [FITC]) versus keratin (FL2, R-phycoerythrin [RPE]). E: Vimentin (FL1, FITC) versus Ep-CAM (FL4, APC). F: Keratin (FL2, RPE) versus Ep-CAM (FL4, APC). G: Note that the vimentin-positive, keratin-negative cells are restricted to the DNA diploid fraction. H: Keratin-positive, vimentin-negative cells can be clearly identified in the DNA diploid and in the DNA aneuploid fraction after gating on the keratin-positive fraction. I: The Ep-CAM expression (FL4, APC) of the keratin-positive DNA aneuploid fraction (J) is higher than the Ep-CAM expression of the keratin-positive DNA diploid fraction (K). L: DNA histogram of the total population.

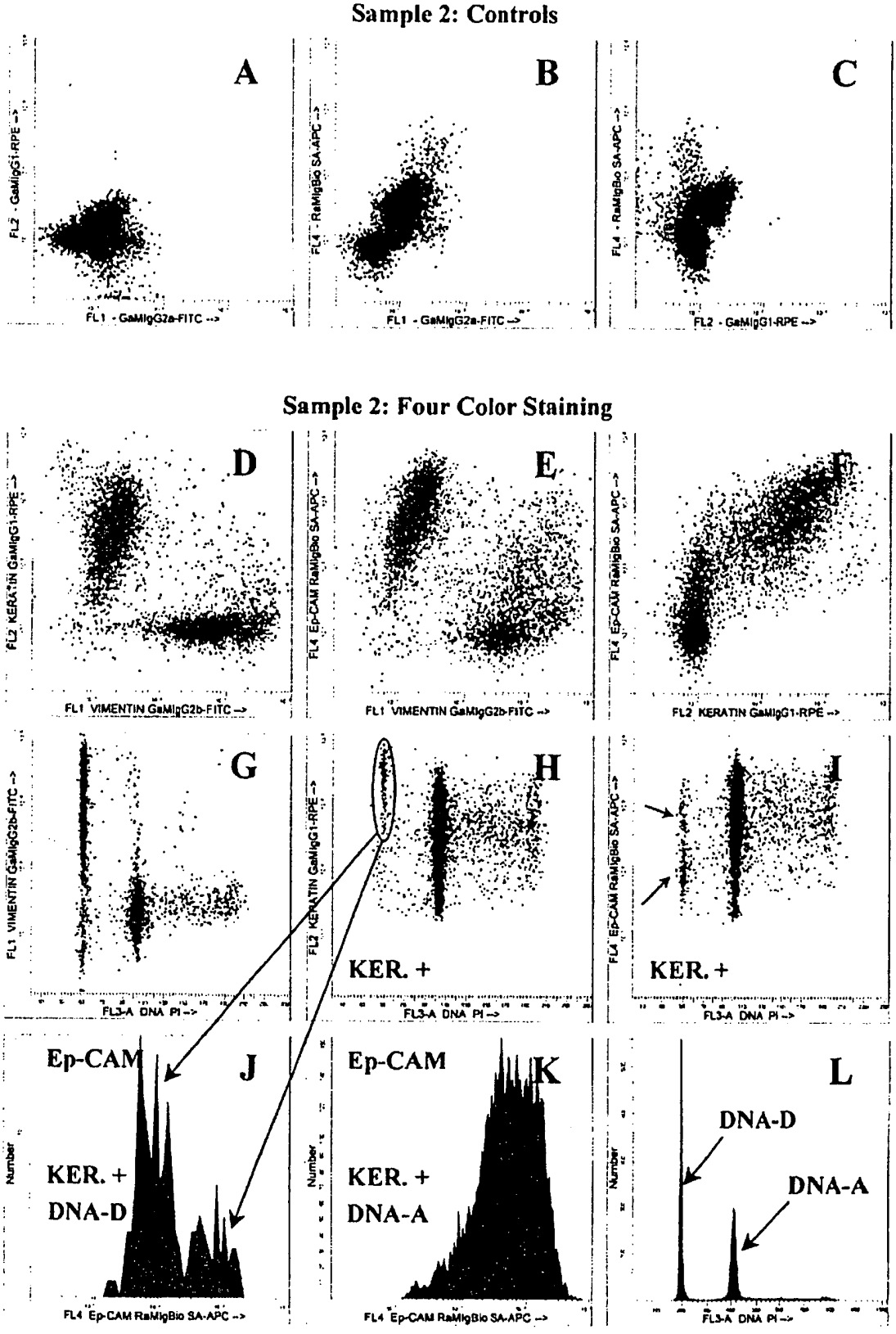
Sample 2: Controls
A
B
C
FL2 - GaMIgG1-RPE -->
FL1 - GaMIgG2a-FITC -->
FL4 - RaMIgBio SA-APC -->
Sample 2: Four Color Staining
D
E
F
FL2 KERATIN GaMIgG1-RPE -->
FL1 VIMENTIN GaMIgG2b-FITC -->
FL4 Ep-CAM RaMIgBio SA-APC -->
G
H
I
FL1 VIMENTIN GaMIgG2b-FITC -->
FL2 KERATIN GaMIgG1-RPE -->
FL3-A DNA PI -->
KER. +
J
K
L
Ep-CAM
KER. +
DNA-D
DNA-A
Number
FL4 Ep-CAM RaMIgBio SA-APC -->
FL3-A DNA PI -->

FIGURE 5

Optimization of Keratin Staining of Cervical Cancers

Figure 2 shows a DNA aneuploid tumor with a DI of 1.55. A majority of the DNA aneuploid cells is positive for keratin compared with the control. However, DNA aneuploid cells with a low or negative keratin expression can also be observed. This was also found for other cervical carcinomas stained with the same combination. Thus, experiments were performed to optimize the staining of epithelial cells by mAbs directed against various types of keratins. Figure 3 shows a cervical carcinoma with a minor DNA aneuploid fraction. Epithelial cells can be identified by several mAbs directed against keratin subtypes 7, 8, 13, 18, and 19 (Fig. 3C,D,F,G,H, respectively). Monoclonal antibody KS-1A3, directed against keratin 13, produced the best results when compared with the other keratin-subtype-specific mAbs (Fig. 3F). However, the highest fluorescence signal, as estimated by the ratio between positive and negative stained cells, and the highest percentage of keratin-positive cells (10.3%) were obtained with a mixture of anti-keratin mAbs (Table 1, Fig. 3L). Single mAbs with broad keratin specificity (CL80, AE1/AE3, and MNF116; Fig. 3I–K) produced less satisfactorily results. Cells expressing keratin 4 (6B10) or keratin 10 (DE-K10) were not detected in this case (Fig. 3B,E, respectively). Therefore, the mixture of anti-keratin mAbs was used for all further experiments.

Four-Color Multiparameter DNA FCM to Study Phenotypic Intratumor

Sample 1 is from a cervical carcinoma showing one DNA aneuploid stem line with a DI of 1.22 (Fig. 4L). Two cell populations from different cell lineages can be clearly identified on the basis of vimentin expression (mesenchymal cells, FL1 parameter, FITC fluorescence) and keratin expression (epithelial cells, FL2 parameter, RPE fluorescence; Fig. 4D) compared with the corresponding control (Fig. 4A). The vimentin-positive cells are completely restricted to the DNA diploid fraction (Fig. 4G). This allows the use of the vimentin-positive, keratin-negative fraction (mesenchymal cells) as patient-specific intrinsic DNA diploid reference cells.

The keratin-positive cells are also positive for Ep-CAM, as shown by Figure 4E,F, compared with the corresponding control (Fig. 4B,C). In contrast to the vimentin-positive fraction, keratin-positive cells can be identified in the DNA aneuploid fraction and the DNA diploid fraction (Fig. 4H). The Ep-CAM expression of the DNA aneuploid keratin-positive fraction is higher than that of the keratin-positive DNA diploid fraction (Fig. 4I). The majority of the vimentin-positive cells is also weakly positive for Ep-CAM but at a much lower level than the keratin-positive fraction (Fig. 4E).

Sample 2 (Fig. 5) shows a clear DNA aneuploid stem line, with a DI of 2.08. The staining of three cellular proteins is compatible with low CVs (DNA diploid = 2.24 and DNA aneuploid = 2.62; Fig. 5L). Keratin expression and vimentin expression readily identifies the epithelial and mesenchymal cell populations (Fig. 5D) as opposed to the corresponding control (Fig. 5A). Keratin-positive cells clearly express Ep-CAM protein molecules on the cell surface (Fig. 5E). Strikingly, DNA diploid cells can be identified with a higher keratin expression compared with that of the DNA aneuploid fraction (Fig. 5H). Two subpopulations can be distinguished within this keratin-positive DNA diploid fraction, which differ markedly in Ep-CAM expression (intra-DNA stem line heterogeneity; Fig. 5I,J, see arrows). The Ep-CAM expression of the keratin-positive DNA aneuploid fraction shows a more continuos variation (Fig. 5K).

Furthermore, heterogeneity of Ep-CAM expression was studied in two additional DNA aneuploid cervical cancers (samples 3 and 4). Figure 6 shows the inter-DNA stem line heterogeneity of Ep-CAM expression found in sample 3. One major (A1, DI = 1.15) and one minor (A2, DI = 1.28) DNA aneuploid stem line can be identified (Fig. 6C,F) as positive for Ep-CAM as opposed to the control (Fig. 6B). The second DNA aneuploid stem line (A2) shows a relatively higher expression of Ep-CAM than the first DNA aneuploid stem line (A1; Fig. 6E).

Figure 7 shows (sample 4) a second example of intra-DNA stem line heterogeneity of Ep-CAM expression. Two populations can be identified in the keratin-positive DNA aneuploid fraction (DI = 1.47; Fig. 7D,E): one population being clearly positive for Ep-CAM and one negative for Ep-Cam, with a relative fluorescence intensity similar to that of the control (Fig. 7A,B). Samples 3 and 4 were also simultaneously stained for vimentin. Results were comparable to the results obtained with samples 1 and 2 (data not shown).

FIG. 5. Second example of a cervical carcinoma stained for epithelial cell-adhesion molecule (Ep-CAM) expression analyzed by four-color multiparameter DNA flow cytometry. A–C: Levels of background fluorescence from goat anti-mouse controls (see Materials and Methods). A: FL1, green fluorescence, versus FL2, orange fluorescence. B: FL1, green fluorescence, versus FL4, red fluorescence. C: FL2, orange fluorescence, versus FL4, red fluorescence. Tumor subpopulations can be clearly identified based on cell lineage–specific protein expression. D: Vimentin (FL1, fluorescein-isothiocyanate [FITC]) versus keratin (FL2, R-phycoerythrin [RPE]). E: Vimentin (FL1, FITC) versus Ep-CAM (FL4, allophycocyanin [APC]). F: Keratin (FL2, RPE) versus Ep-CAM (FL4, APC). G: Vimentin-positive, keratin-negative cells are restricted to the DNA diploid fraction. H: Keratin-positive, vimentin-negative cells can be clearly identified in the DNA diploid and in the DNA aneuploid fraction after gating on the keratin-positive fraction. Note that the level of keratin expression of the DNA diploid keratin-positive cells is higher than that of the DNA aneuploid keratin-positive cells. I: The DNA diploid keratin-positive fraction shows two subpopulations differing in Ep-CAM expression (FL4, APC; J). K: The majority of cells of the DNA aneuploid keratin-positive fraction has a high Ep-CAM expression. L: DNA histogram of the total population. Note the high resolution of this DNA histogram.

DISCUSSION

We have demonstrated the potentialities of a newly developed four-colour staining procedure for the flow cytometric detection of tumor cell subpopulations in primary cervical carcinomas. Our results show that the simultaneous measurement of three different cellular proteins is compatible with high-resolution DNA ploidy measurements. The availability of DNA content as a fourth parameter proved to be essential for discriminating tumor

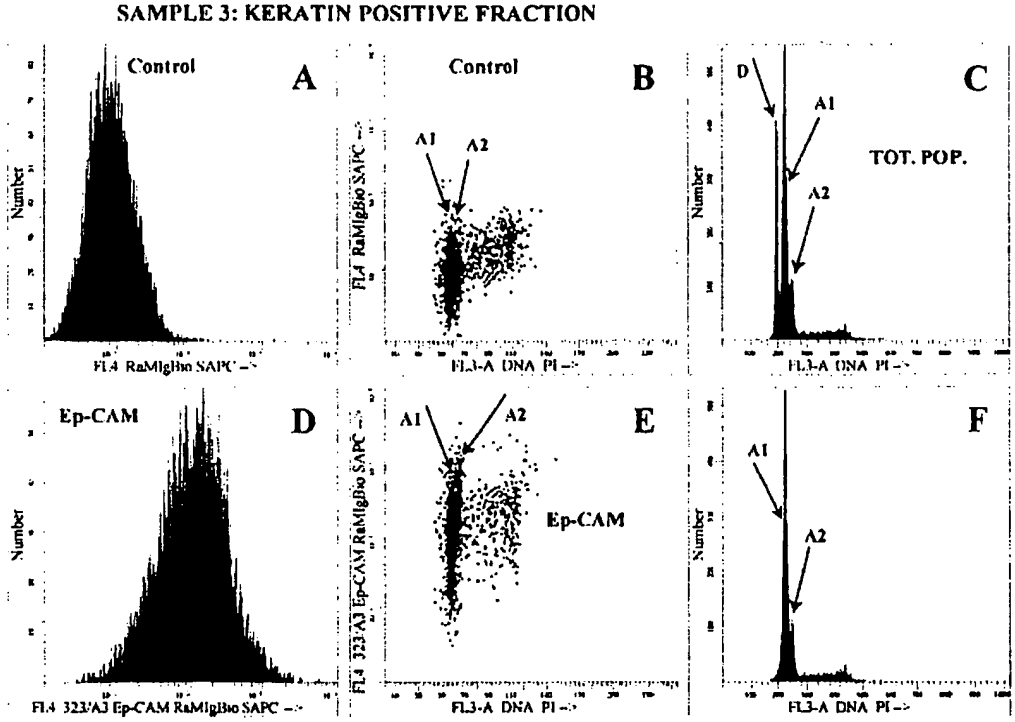

FIG. 6. Inter-DNA stem line heterogeneity of epithelial cell-adhesion molecule (Ep-CAM) expression analyzed by four-color multiparameter DNA flow cytometry (sample 3). A–B: Level of background fluorescence of the keratin-positive fraction. Note the two closely related DNA aneuploid stem lines with comparable background fluorescence (FL4). C: DNA histogram of the total population. D–E: Relative Ep-CAM expression of the total keratin-positive DNA aneuploid fraction. The second DNA aneuploid stem line (A2) has a higher Ep-CAM expression than the first DNA aneuploid fraction (A1). This tumor subpopulation cannot be identified in the single-parameter distribution of Ep-CAM expression (D). F: DNA histogram of the keratin-positive fraction. Cells were simultaneously stained for vimentin (fluorescein-isothiocyanate fluorescence, data not shown).

cell subpopulations that would have not have been identified on the basis of protein expression alone. Previously we showed that optimal DNA histogram resolution could be obtained by using a mixture of PI and TP3 as DNA stains (7). However, this combined use of PI and TP3 is not possible on a blue-red dual-laser flow cytometer required for four-color DNA-protein analysis. Although TP3 shows minimal spectral cross-talk into green (FL1), orange (FL2), and deep red (FL3) fluorescence detectors, we found that use of PI resulted in superior DNA histogram resolution. A similar difference in DNA histogram resolution between PI and TP3 was observed by Hirons et al. (8) using ethanol-fixed cells. This result may be due to steric properties of TP3, which hinder DNA binding, and the amount of bound dye may be sensitive to small differences in chromatin compactness. We found that the use of a mixture of anti-keratin mAbs with a broad anti-keratin specificity is superior in labeling the epithelial fraction of dispersed cervical carcinomas. This was in contrast to pan-keratin mAbs or the single use of chain-specific anti-keratin mAbs (Table 1), which failed to stain the entire epithelial cell fraction of cervical carcinomas. Pilot studies clearly demonstrated that the so-called pan-keratin markers, mAbs with a broad specificity for keratin as studied by immunohistochemistry and immunoblotting, were not able to label the complete epithelial fraction of cell suspensions obtained from dispersed cervical carcinomas (Figs. 2, 3). This could be clearly demonstrated with DNA aneuploid tumors stained for keratin using CL80. The DNA aneuploid fraction showed a very broad distribution of keratin fluorescence intensities levels (Fig. 2) with lowest signals comparable to those from negative controls. Single use of mAb MNF116, specific for keratins 5, 6, 8, 17, and probably 19, also failed in labeling the complete epithelial fraction of most tumors evaluated. The inability to stain all epithelial cells by these pan-keratin markers is probably caused by the complex and heterogeneous keratin expression patterns in different types of cervical carcinomas (12). Furthermore, differences in the accessibility of keratin epitopes between immunohistochemistry and flow cytometry could play a role. For immunohistochemistry, tissue sections are prepared in such a way that intermediate filaments are easily accessible for mAbs.

Multiparameter FCM requires intact cells. We applied a short fixation/permeabilization procedure using 1.0% paraformaldehyde and lysolecithin (1). Keratin filaments are probably present in their native form after fixation and permeabilization, thereby masking certain epitopes essential for immunorecognition. The use of 100% methanol instead of paraformaldehyde/lysolecithin did not result in an increase of the percentage of keratin-positive cells (data not shown). Others have used a mAb solely directed

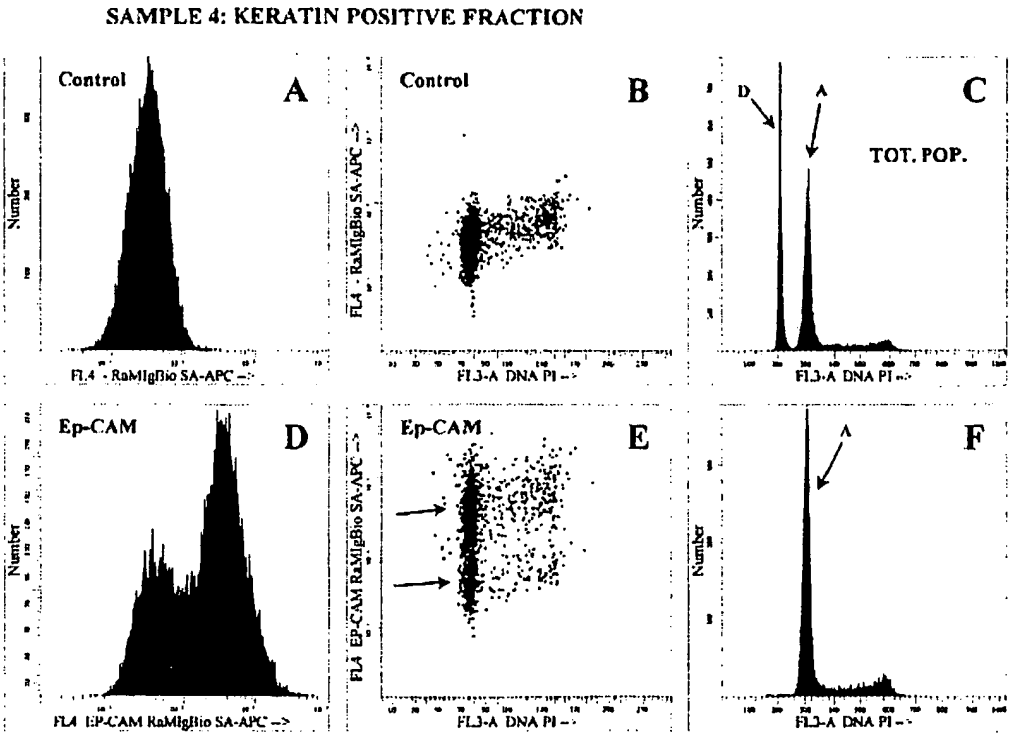

FIG. 7. Intra-DNA stem line heterogeneity of epithelial cell-adhesion molecule (Ep-CAM) expression analyzed by four-color multiparameter DNA flow cytometry. A–B: Level of background fluorescence of the keratin-positive (DNA aneuploid) fraction. C: DNA histogram of the total population. D–E: Relative Ep-CAM expression of the total keratin-positive DNA aneuploid fraction. Note that the DNA aneuploid can be subdivided into an Ep-CAM-positive and an Ep-CAM-negative population. F: DNA histogram of the keratin-positive fraction. Cells were also stained for vimentin (data not shown).

against keratins 5, 6, and 18 to stain the epithelial fraction of cervical carcinomas (20). In one case only, 50% of the epithelial cells were stained using this mAb, which was confirmed by FCM. These findings are in contrast to our observations. Part of this discrepancy may be explained by the use of the secondary reagent in combination with high concentrations of PI (100 μM). We used an RPE-conjugated secondary reagent instead of an FITC-conjugated reagent. Detection threshold of RPE fluorescence in the presence of PI is elevated compared with the simultaneous use of FITC and PI (1). This hinders a good discrimination between dimly keratin-positive cells and keratin-negative cells.

DNA aneuploid cells were clearly positive for keratin after applying the mixture of anti-keratin mAbs (Table 1) to the samples in all other cases. This also allowed a good separation between DNA diploid keratin-positive cells and DNA diploid keratin-negative cells. Remarkably, in the second case (Fig. 5), the keratin expression of DNA diploid keratin-positive cells was more intense than that of the DNA aneuploid cells. This observation may indicate differentiation differences between DNA diploid keratin-positive cells and DNA aneuploid keratin-positive cells within the same tumor. These findings are supported by differences in Ep-CAM expression between DNA diploid keratin-positive cells and DNA aneuploid keratin-positive cells or inter-DNA aneuploid keratin-positive stem lines (Fig. 6). It has been shown that increased Ep-CAM expression is associated with proliferation (15). Strikingly, the DNA diploid keratin-positive fraction of the second case also showed two minor subpopulations clearly varying in Ep-CAM expression. Intra-DNA stem line heterogeneity was also observed for another DNA aneuploid tumor (Fig. 7).

These examples demonstrate the potentials of multiparameter DNA FCM for studying intratumor heterogeneity at the phenotypic level. Furthermore, by using anti-vimentin mAbs, which are directed against intermediate filaments present in cells from a mesenchymal origin, we were able to identify the DNA diploid fraction of these carcinomas. Keratin-negative, vimentin-positive cells were restricted to the DNA diploid fraction. Thus, the use of anti-vimentin mAbs might be an alternative for the more widely accepted anti-CD45 mAbs to identify normal leukocytes that can serve as a patient-specific intrinsic DNA reference (21). The use of anti-vimentin mAbs has another advantage in that cross-reactivity of mAbs directed against epithelial-associated protein molecules with cells from a nonepithelial origin can be monitored. Some vimentin-positive cells exhibit Ep-CAM reactivity, a known feature of this mAb when applied for FCM (S.O. Warnaar, personal communication). Even for carcinomas expressing vimentin, the vimentin-positive, keratin-negative cell frac-

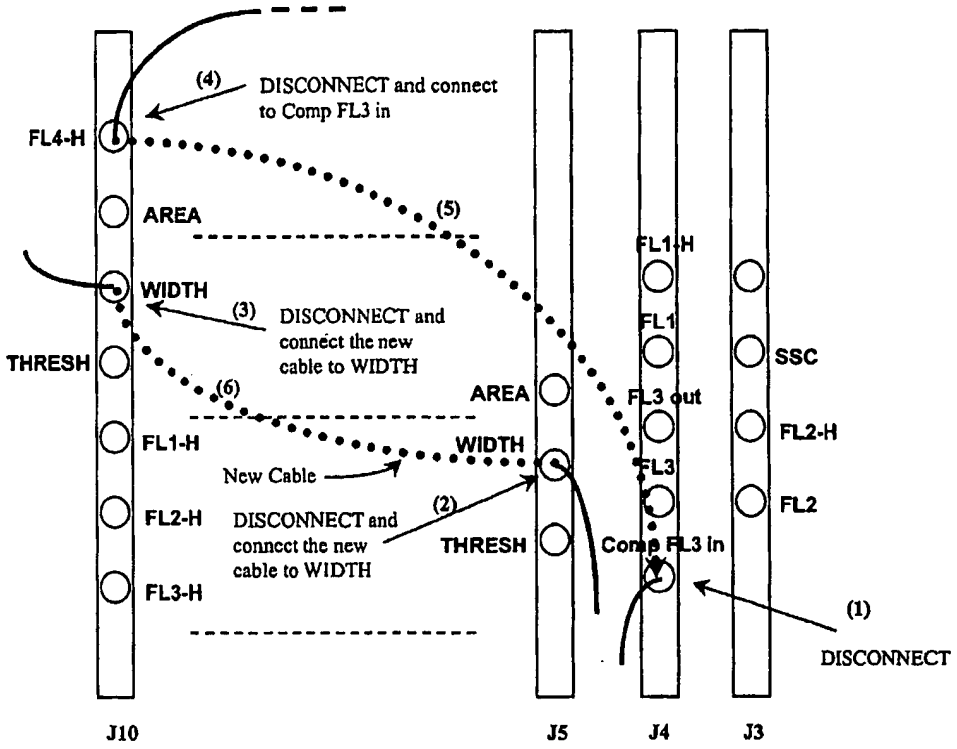

FIG. 8. FACSCalibur hardware adjustment for simultaneous measurement of allophycocyanin fluorescence (FL4) and FL3A/W pulse processing (see Appendix for a detailed description).

tion can be used for identification of the DNA diploid reference peak.

A limiting factor for these kinds of studies is the paucity of directly conjugated high-quality mAbs suitable for multiparameter FCM studies of human solid tumors. This greatly limits multiparameter FCM of human solid tumors because staining for multiple cellular proteins requires selection of mAbs differing in IgG subclass. Furthermore, anti-mouse IgG subclass-specific secondary reagents must be used, and these reagents must be IgG subclass specific. Nonetheless, we could use an anti-mouse Ig biotinylated secondary reagent for cell surface staining before fixation and permeabilization; at the same time, intermediate filaments keratin and vimentin were stained after fixation and permeabilization using mAbs differing in IgG subclass and applying subclass-specific secondary reagents. No significant cross-reactivity was observed when using proper controls. The use of paraformaldehyde, a known protein cross-linker, probably inactivates the remaining binding sites of this anti-mouse Ig secondary reagent. This anti-mouse Ig reagent does not bind newly added mAbs after fixation and permeabilization for staining intermediate filaments.

We have demonstrated that three different cellular proteins in combination with high-resolution DNA FCM can be simultaneously analyzed using the FACSCalibur benchtop flow cytometer. By this technique, we were able to identify neoplastic subpopulations based on protein expression and DNA content. The vimentin-positive, keratin-negative cell fraction could be used as a patient-specific DNA diploid intrinsic reference. Flow sorting of tumor subpopulations based on protein expression and DNA content in combination with molecular biology may further elucidate possible genetic mechanisms underlying intratumor heterogeneity (4,5).

ACKNOWLEDGMENTS

We thank Steve M. Saarinen from DAKO A/S, Glostrup, Denmark, for kindly providing anti-keratin antibodies.

LITERATURE CITED

1. Corver WE, Cornelisse CJ, Fleuren GJ. Simultaneous measurement of two cellular antigens and DNA using fluorescein-isothiocyanate, R-phycoerythrin, and propidium iodide on a standard FACScan. Cytometry 1994;15:117-128.
2. Corver WE, Bonsing BA, Abeln ECA, Vlak-Theil PM, Cornelisse CJ, Fleuren GJ. One tube triple staining method for the flow cytometric analysis of DNA ploidy and phenotypic heterogeneity of human solid tumors using single laser excitation. Cytometry 1996;25:358-366.
3. Brockhoff G, Endl E, Minuth W, Hofstädter F, Knüchel R. Options of flow cytometric three-colour DNA measurements to quantitate EGFR in subpopulations of human bladder cancer. Anal Cell Pathol 1996; 11:55-70.
4. Li BDL, Harlow SP, Budnick RM, Sheedy DL, Stewart CC. Detection of HER-2/*neu* oncogene amplification in flow cytometry-sorted breast ductal cells by competitive polymerase chain reaction. Cancer 1994; 73:2771-2778.
5. Abeln ECA, Corver WE, Kuipers-Dijkshoorn NJ, Fleuren GJ, Cornelisse CJ. Molecular genetic analysis of flow-sorted ovarian tumour cells: improved detection of loss of heterozygosity. Br J Cancer 1994;70: 255-262.
6. Bonsing BA, Corver WE, Gorsira MCB, van Vliet M, Oud PS, Cornelisse CJ, Fleuren GJ. Specificity of seven monoclonal antibodies against p53 evaluated with Western blotting, immunohistochemistry, confocal laser scanning microscopy and flow cytometry. Cytometry 1997;28: 11-24.

7. Corver WE, Fleuren GJ, Cornelisse CJ. Improved single laser measurement of two cellular antigens and DNA-ploidy by the combined use of propidium iodide and TO-PRO-3 iodide. Cytometry 1997;28:329-336.
8. Hirons GT, Fawcett JJ, Crissman HA. TOTO and YOYO: new very bright fluorochromes for DNA content analyses by flow cytometry. Cytometry 1994;15:129-140.
9. Doornbos RMP, De Grooth BG, Kraan YM, Van Der Poel CJ, Greve J. Visible diode lasers can be used for flow cytometric immunofluorescence and DNA analysis. Cytometry 1994;15:267-271.
10. Glade CP, Botermans RJG, Van Erp PEJ, Van de Kerkhof PCM. The dynamics of the response of normal skin to single and multiple epicutaneous leukotriene B4 applications analysed by by three-colour flow cytometry. Acta Derm Venereol (Stockh) 1995;75:437-441.
11. Glade CP, Van Erp PEJ, Van de Kerkhof PCM. Epidermal cell DNA content and intermediate filaments keratin 10 and vimentin after treatment of psoriasis with calcipotriol cream once daily, twice daily and in combination with clobetasone 17-butyrate cream or betamethasone 17-valerate cream: a comparative flow cytometric study. Br J Dermatol 1996;135:379-384.
12. Smedts F, Ramaekers F, Troyanovsky S, Pruszczynski M, Link M, Lane B, Leigh I, Schijf C, Vooijs P. Keratin expression in cervical cancer. Am J Pathol 1992;141:497-511.
13. Litvinov SV, Velders MP, Bakker HAM, Fleuren GJ, Warnaar SO. Ep-CAM: a human epithelial antigen is a homophilic cell-cell adhesion molecule. J Cell Biol 1994;125:437-446.
14. Moldenhauer G, Momburg F, Möller P, Schwartz R, Hämmerling GJ. Epithelium-specific surface glycoprotein of Mr 34,000 is a widely distributed human carcinoma marker. Br J Cancer 1987;56:714-721.
15. Litvinov SV, Van Driel W, Van Rhijn CM, Bakker HAM, Van Krieken H, Fleuren GJ, Warnaar SO. Expression of Ep-CAM in cervical squamous epithelia correlates with an increased proliferation and the disappearance of markers for terminal differentiation. Am J Pathol 1996;148:865-875.
16. Corver WE, Cornelisse CJ, Hermans J, Fleuren GJ. Limited loss of nine tumor-associated surface antigenic determinants after tryptic cell dissociation. Cytometry 1995;19:267-272.
17. Ensley JF, Maciorowski Z, Pietraszkiewicz H, Klemic G, KuKuruga M, Sapareto S, Corbett T, Crissman J. Solid tumor preparation for flow cytometry using a standard murine model. Cytometry 1987;8:479-487.
18. Van Muijen GNP, Ruiter DJ, Warnaar SO. Coexpression of intermediate filament polypeptides in human fetal and adult tissues. Lab Invest 1987;57:359-369.
19. Van Muijen GNP, Warnaar SO, Ponec M. Differentiation-related changes of cytokeratin expression in cultured keratinocytes and in fetal, newborn, and adult epidermis. Exp Cell Res 1987;171:331-345.
20. Kimmig R, Kapsner T, Speisberg H, Untch M, Hepp H. DNA cell-cycle analysis of cervical cancer by flow cytometry using simultaneous cytokeratin labelling for identification of tumour cells. J Cancer Res Clin Oncol 1995;121:107-114.
21. Zarbo RJ, Visscher D, Crissman JD. Two-color multiparametric method for flow cytometric DNA analysis of carcinomas using staining for cytokeratin and leukocyte-common antigen. Anal Quant Cytol Histol 1989;11:391-402.
22. Van Muijen GNP, Ruiter DJ, Ponec M, Huiskens-van der Mey C, Warnaar SO. Monoclonal antibodies with different specificities against cytokeratin. Am J Pathol 1984;114:9-17.
23. Ulich TR, Liao SY, Layfield L, Romansky S, Cheng L, Lewin KJ. Endocrine and tumor differentiation markers in poorly differentiated small-cell carcinoids of the cervix and vagina. Arch Pathol Lab Med 1986;110:1054-1057.
24. Prieto VG, Lugo J, McNutt NS. Intermediate- and low-molecular-weight keratin detection with the monoclonal antibody MNF116. An immunohistochemical study on 232 paraffin-embedded cutaneous lesions. J Cutan Pathol 1996;23:234-241.
25. Van Muijen GNP, Ruiter DJ, Franke WW, Achtstätter T, Haasnoot WHB, Ponec M, Warnaar SO. Cell type heterogeneity of cytokeratin expression in complex epithelia and carcinomas as demonstrated by monoclonal antibodies specific for cytokeratins nos. 4 and 13. Exp Cell Res 1986;162:97-113.
26. Wauters CC, Smedts F, Gerrits LG, Bosman FT, Ramaekers FC. Keratins 7 and 20 as diagnostic markers of carcinomas metastatic to the ovary. Hum Pathol 1995;26:852-855.
27. Schaafsma HE, Ramaekers FC, van Muijen GN, Ooms EC, Ruiter DJ. Distribution of cytokeratin polypeptides in epithelia of the adult human urinary tract. Histochemistry 1989;91:151-159.
28. Ivanyi D, Ansink A, Groeneveld E, Hageman PC, Mooi WJ, Heintz AP. New monoclonal antibodies recognizing epidermal differentiation-associated keratins in formalin-fixed, paraffin-embedded tissue. Keratin 10 expression in carcinoma of the vulva. J Pathol 1989;159:7-12.
29. Levy R, Czernobilsky B, Geiger B. Subtyping of epithelial cells of normal and metaplastic human uterine cervix, using polypeptide-specific cytokeratin antibodies. Differentiation 1988;39:185-196.
30. Broers JL, Ramaekers FC, Rot MK, Oostendorp T, Huysmans A, van Muijen GN, Wagenaar SS, Vooijs GP. Cytokeratins in different types of human lung cancer as monitored by chain-specific monoclonal antibodies. Cancer Res 1988;48:3221-3229.
31. Perkins W, Campbell I, Leigh IM, MacKie RM. Keratin expression in normal skin and epidermal neoplasms demonstrated by a panel of monoclonal antibodies. J Cutan Pathol 1992;19:476-482.

APPENDIX

The FACSCalibur hood is opened, and the following wires are disconnected from the main boards (Fig. 8): (**step 1**) disconnect "Comp FL3 in J-200" of main board J4, (**step 2**) disconnect "ADC Width" of main board J5, (**step 3**) disconnect "Width" of main board J10, (**step 4**) disconnect "FL4-H" of main board J10 and connect it to "Comp FL3 in J-200" of main board J4, and connect the "Width" of main board J10 (**step 5**) with a new electrical wire to the "ADC Width" of main board J5 (**step 6**). Switch off the red diode laser to change the FL3-W gain (P7). FL3-W instrument settings will be maintained if the red diode laser is turned on again but P7 (FL3-W) is inactive (gray) in the "Detectors/Amps" window. Note that the detectors of P5 and P7 have been interchanged (P5 = FL4 and P7 = FL3). The modes of P5 and P7, in the "Detectors/Amps" window, must be "Log" and "Lin," and the P5 and P7 parameter labels must be changed into FL4-H and FL3-W, respectively.

Peripheral Blood CD34+ Cells Differ From Bone Marrow CD34+ Cells in Thy-1 Expression and Cell Cycle Status in Nonhuman Primates Mobilized or Not Mobilized With Granulocyte Colony-Stimulating Factor and/or Stem Cell Factor

By R.E. Donahue, M.R. Kirby, M.E. Metzger, B.A. Agricola, S.E. Sellers, and H.M. Cullis

Granulocyte colony-stimulating factor (G-CSF) and stem cell factor (SCF) have been shown to stimulate the circulation of hematopoietic progenitor cells in both mice and nonhuman primates. We evaluated the immunophenotype and cell cycle status of CD34+ cells isolated from the bone marrow (BM) and leukapheresis product of cytokine-mobilized nonhuman primates. CD34+ cells were isolated from rhesus macaques that had received no cytokine therapy, 100 μg/kg/d G-CSF, 200 μg/kg/d SCF, or a combination of both 100 μg/kg/d G-CSF and 200 μg/kg/d SCF as a subcutaneous injection for 5 days. BM was aspirated before (day 0) and on the last day (day 5) of cytokine administration. On days 4 and 5, peripheral blood (PB) mononuclear cells were collected using a novel method of leukapheresis. Threefold more PB mononuclear cells were collected from animals receiving G-CSF alone or G-CSF and SCF than from animals that had received either SCF alone or no cytokine therapy. CD34+ cells were positively selected using an immunoadsorptive system from the BM, PB, and/or leukapheresis product. Threefold and 10-fold more CD34+ cells were isolated from the leukapheresis product of animals receiving G-CSF or G-CSF and SCF, respectively, than from animals receiving no cytokine therapy or SCF alone. The isolated CD34+ cells were immunophenotyped using CD34-allophycocyanin, CD38-fluorescein isothiocyanate, and Thy-1-phycoerythrin. These cells were later stained with 4',6-diamidino-2-phenylindole for simultaneous DNA analysis and immunophenotyping. BM-derived CD34+ cells did not differ significantly in cell cycle status and Thy-1 or CD38 phenotype before or after G-CSF and/or SCF administration. Similarly, CD34+ cells isolated from the leukapheresis product did not differ significantly in immunophenotype or cell cycle status before or after G-CSF and/or SCF administration. However, there were consistent differences in both immunophenotype and cell cycle status between BM- and PB-derived CD34+ cells. CD34+ cells isolated from the PB consistently had a smaller percentage of cells in the S+G2/M phase of the cell cycle and had a higher percentage of cells expressing Thy-1 than did CD34+ cells isolated from the BM. A greater proportion of PB-derived CD34+ cells were in the S+G2/M phase of the cell cycle after culture in media supplemented with interleukin-6 and SCF. However, culturing decreased the proportion of CD34+ cells expressing Thy-1.

THE IDENTIFICATION AND characterization of CD34+ hematopoietic stem cells from peripheral blood (PB) and bone marrow (BM) is of both clinical and biological interest. Initially identified by a monoclonal antibody (MoAb) raised against a human erythroleukemia cell line, KG-1a,[1] CD34 has been identified as a ligand for L-selectin[2] and has been found to be expressed by vascular endothelium[3] and virtually all hematopoietic progenitor cells detected by in vitro assays.[4] Antibodies that recognize CD34 have frequently been used for hematopoietic stem cell enrichment. Approximately 0.2% of normal PB mononuclear cells (PBMNCs) and 1% to 4% of human BM cells express CD34.[5] With chemotherapy and/or hematopoietic growth factor mobilization, the number of circulating CD34+ cells increases. The percentage of CD34+ cells in the leukapheresis product of patients receiving chemotherapy alone, the cytokine granulocyte colony-stimulating factor (G-CSF) alone, or the combination of chemotherapy and G-CSF is approximately 0.6%, 0.4%, and 2%, respectively.[6,7] Investigators have shown that hematopoietic growth factors, such as interleukin-3 (IL-3), G-CSF, granulocyte/macrophage CSF, and stem cell factor (SCF) can effectively increase the absolute number of circulating progenitor and CD34+ cells.[8-17] This increase in circulating CD34+ cell number has allowed clinicians to obtain sufficient quantities of CD34+ cells from the PB of mobilized donors so as to be able to perform transplants. Mobilized PB cells in human patients have proven quite effective in accelerating reconstitution after myeloablative therapies.[8-11] Cytokine-mobilized PB cells have also been capable of contributing to the hematopoietic reconstitution of myeloablated mice,[12-14] dogs,[15] and primates.[16,17] The combination of G-CSF and SCF has proven to be quite effective in mobilizing PB progenitor cells capable of hastening engraftment of irradiated animals.[12-17] The combination of G-CSF and SCF was superior to G-CSF alone in mobilizing PB progenitor cells and reconstituting baboons treated with a single dose of 1,070 cGy total body irradiation.[17]

Multiparameter flow cytometry and cell cycle analysis has shown that human CD34+ cells can be subdivided into a number of distinct cell populations.[18] Two cell surface antigens that have been used to subdivide CD34+ cells have been CD38 and Thy-1. Human cells that express CD34, but not CD38, appear to give rise to primitive hematopoietic colonies that can be replated up to five sequential generations.[19] Similarly, human CD34+ cells that coexpress Thy-1 have been shown in vitro to initiate long-term hematopoiesis.[20] In preclinical studies, human fetal CD34+Thy-1+ BM cells have been shown to engraft human thymus transplanted in severe combined immunodeficiency (SCID) mice.[21] In addition, CD34+Thy-1+ cells from human umbilical cord blood have been shown to have functional properties of prim-

From the Hematology Branch, National Heart, Lung, and Blood Institute, National Institutes of Health, Bethesda, MD; and the Fenwal Division, Baxter Healthcare, Deerfield, IL.

Submitted April 18, 1995; accepted September 29, 1995.

*Presented in abstract form at the Thirty-Sixth Annual Meeting of the American Society of Hematology held in Nashville, TN from December 2-6, 1994 (*Blood *84:273a, 1995 [abstr, suppl]).*

Address reprint requests to Robert E. Donahue, VMD, Hematology Branch, National Heart, Lung, and Blood Institute, 5 Research Ct, Rockville, MD 20850.

The publication costs of this article were defrayed in part by page charge payment. This article must therefore be hereby marked "advertisement" in accordance with 18 U.S.C. section 1734 solely to indicate this fact.

0006-4971/96/8704-0032$3.00/0

itive hematopoietic progenitor cells,[22] and $CD34^+Thy\text{-}1^+Lin^-$ isolated from the PB of cancer patients mobilized after chemotherapy plus granulocyte-macrophage CSF or G-CSF possess long-term hematopoietic activity both in vitro (using a 7-week cobblestone area-forming assay) and in vivo (using a SCID-hu mouse model).[23] CD38 appears to function as an adenosine 5'-diphosphate ribosyl cyclase,[24] whereas the function of Thy-1 remains unknown.[20] It has been speculated that Thy-1 may mediate a negative signal that results in the inhibition of primitive cell proliferation.[20] The expression of Thy-1 and CD38 on rhesus macaque $CD34^+$ cells has not been well characterized, although the cross-reactivity of some MoAbs directed against human antigens has been evaluated in nonhuman primates.

There is an interest in determining the in vitro and in vivo cell cycle status of subpopulations of $CD34^+$ cells isolated from the BM and PB to improve our ability to expand quiescent hematopoietic stem cells and use viral vectors that require cell cycling for viral integration. Recently, cell cycle differences have been identified in BM $CD34^+$ subsets. The $CD34^+CD38hi$ subset appeared to have had more cells in the S and G2/M than did the $CD34^+CD38lo$ subset.[25] After 2 days in cytokine-supplemented culture, the $CD34^+CD38lo$ cells showed increased numbers of cells in the S and G2/M phases.[25] In another study, the combination of IL-3 and SCF was found to increase the percentage of BM-isolated $CD34^+$ cells to enter cycle.[26] Because nonhuman primates have been used to evaluate cytokine, transplantation, and gene therapy protocols before human clinical trials, we were interested in examining the immunophenotype and cell cycle status of BM and PB $CD34^+$ cells derived from rhesus macaques that were either mobilized or not mobilized with high doses of G-CSF and/or SCF.

MATERIALS AND METHODS

Animals. The young adult rhesus macaques (*Macaca mulatta*) that were used in these studies were serologically negative for simian T-cell lymphotrophic virus, simian immunodeficiency virus, and simian AIDS-related type D virus. Animals with blood type B were selected and had an indwelling central catheter established. Experimental animals were quarantined and housed in accordance with the guidelines set by the Committee on Care and Use of Laboratory Animals of the Institute of Laboratory Animal Resources, National Research Council (Committee on Care and Use of Laboratory Animals, DHHS Public #NIH85-23, Revised 1985) and the policies set by the Veterinary Research Program of the National Institutes of Health (NIH; Bethesda, MD). The protocols evaluated were approved by the Animal Care and Use Committee of the National Heart, Lung, and Blood Institute.

Cytokine administration. Rhesus macaques received no cytokines, 100 μg/kg/d recombinant human G-CSF, 200 μg/kg/d recombinant human pegylated SCF, or a combination of both 100 μg/kg/d G-CSF and 200 μg/kg/d SCF (all provided by Amgen, Inc, Thousand Oaks, CA) as a subcutaneous injection for 5 days. Growth factor doses were based on previous studies.[16,17] Purified material was stored at 4°C until used. All cytokines for this study were pyrogen-free.

Rhesus leukapheresis procedure. To collect PBMNCs by leukapheresis from donors weighing less than 5 kg, modifications were made to the fluid path of a CS3000 *Plus* Blood Cell Separator (Baxter Healthcare Corp, Fenwal Division, Deerfield IL) to lower the extracorporeal volume requirement to 132 mL (see Fig 1). Collection was accomplished using a small S25A separation chamber and a shunt chamber (Fenwal no. 710700027) in the place of a collection chamber. A standard apheresis kit (Fenwal no. 4R2210) was installed in the CS3000. After autoprime, the roller clamps to the acid citrate dextrose-NIH formulation (ACD-A), saline, and vent prime lines were closed to prevent hemodiluting the donor when using halt/irrigate. The return line was modified by tightly rolling and taping a 150-mL transfer pack (Fenwal no. 4R2001) and sterile-docking a male luer to the shortened outlet line. A blood component recipient set with a 170-μm filter and drip chamber (Fenwal no. 4C2100) was spiked into the modified 150-mL transfer pack and connected to the packed red blood cell line using a needle lock device (Fenwal no. 2C7831). The blood component recipient set was connected to a 20- to 18-gauge Angiocath placed in the saphenous vein of the donor. Hemostats were placed both on the standard, unused, return line and the inlet for the ACD line present on the draw line. The apheresis kit was primed with autologous blood that had been collected in citrate phosphate dextrose plus adsol 2 to 3 weeks before the leukapheresis procedure. The donor received a dose of 100 U/kg heparin immediately before the procedure. The inlet line was connected to an indwelling 6.6 French catheter placed in the right atrium of the heart. Blood was processed at the rate of 12 mL/min in automatic mode for a total of 2.5 times the animal's calculated blood volume. At the completion of the procedure, the product was collected and 5 mL of ACD was added. The remaining cells were salvaged and either were used to prime the CS3000 for future leukapheresis procedures or were directly reinfused into the animal. PBMNCs were collected by leukapheresis on day 4 and day 5 of cytokine administration. These days were selected based on evidence in rhesus macaques (data not shown) and in baboons[16] that circulating progenitor numbers had increased by these time points. The number of PBMNCs processed during the leukapheresis procedure was calculated by averaging the number of mononuclear cells in the complete blood cell count of samples taken immediately before, in the middle of, and at the end of the leukapheresis procedure, and then multiplying this average by the volume of blood processed. Cell counts were performed on a Coulter Model S5 electronic cell counter (Hialeah, FL) or on a Cell-Dyn3500 automated hematology analyzer (Abbott Laboratories, Abbott Park, IL). The number of PBMNCs processed for each cytokine mobilization group was evaluated, and the mean and standard error of the mean (SEM) was then determined. The number of PBMNCs collected as the product was based on the complete blood cell count of the leukapheresis product multiplied by the total percentage of lymphocytes and monocytes within the product and the volume of the leukapheresis product. The PBMNCs for each cytokine mobilization group was evaluated, and the mean and standard of deviation (SD) was then determined. The PBMNCs collected from the leukapheresis products on day 4 and day 5 were processed and analyzed as independent samples.

BM collection. Before the administration of hematopoietic growth factors (day 0), 30 mL of heparinized BM was surgically harvested from one femur. Additional BM was harvested immediately before the second leukapheresis procedure (day 5) from the alternate femur. After BM harvest, the animal received a course of buprenorphine (0.1 to 0.3 mg/kg intramuscularly) for 3 days to alleviate any bone pain that may have been associated with the harvest.

Immunoselection of $CD34^+$ cells. $CD34^+$ cells from the BM and PB leukapheresis product were recovered by positive immunoselection using the Ceprate LC-34-Biotin Kit (CellPro, Inc) according to the manufacturers instructions. An accurate determination of $CD34^+$ cell yield after immunoselection was not determined, in part, because of the rarity of $CD34^+$ cells in both the BM and leukapheresis product. No apparent difference was observed when comparing the immunophenotype of immunoselected $CD34^+$ cells and $CD34^+$ cells that were analyzed from the original blood sample. Cytospin prepara-

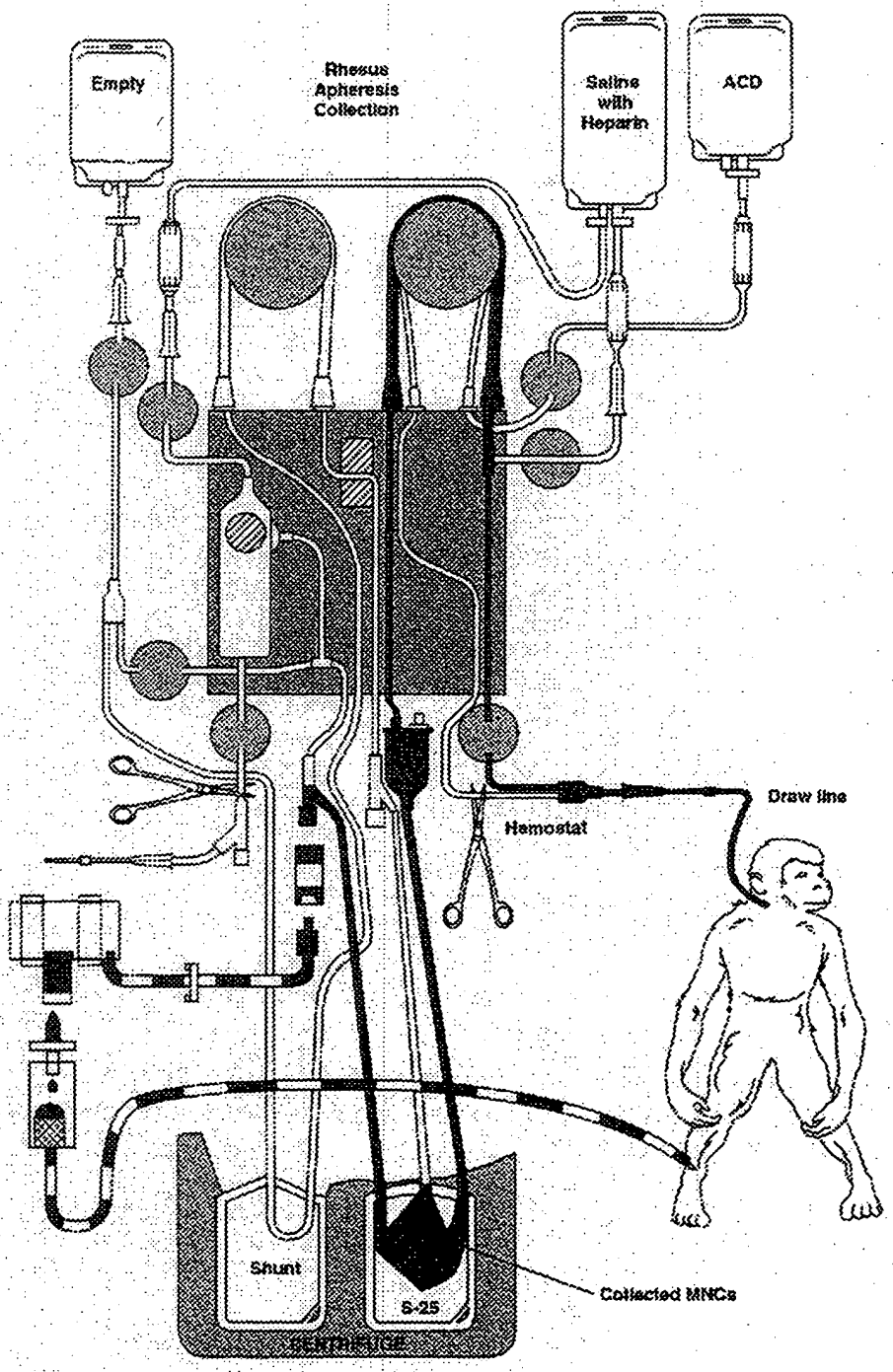

Fig 1. A diagram of the rhesus apheresis procedure is shown. Red denotes the red blood cell pathway; yellow, the pathway of plasma; and blue, the area where the leukapheresis product was collected.

tions of the cells were prepared to document cellular morphology. Separate immunoselections were performed on each leukapheresis product collected on day 4 and day 5. The $CD34^+$ cells collected on each day were stained and analyzed independently.

Culture of immunoselected $CD34^+$ cells. $CD34^+$ cells were immunoselected from the leukapheresis product of animals mobilized with SCF and G-CSF and were cultured in suspension for 3.5 days in Dulbecco's modified Eagle's medium (Biofluids, Rockville, MD) plus 15% fetal calf serum (Hyclone Laboratories, Inc., Logan, UT) supplemented with 50 ng/mL of IL-6 and 100 ng/mL of SCF (both cytokines provided by Amgen, Inc).

Immunophenotyping of CD34 cells from BM and PB. The BM and PB leukapheresis $CD34^+$ cells that were positively selected using the CellPro immunoadsorption system were immunophenotyped with CD34-allophycocyanin (APC) to evaluate CD34 purity and were also immunophenotyped with CD38-fluorescein isothiocyanate (FITC) and Thy-1-phycoerythrin (PE) to identify $CD34^+CD38^-$ and $CD34^+$ Thy-1 subpopulations. The CD34 MoAb used (clone 563) was a gift from Dr G. Gaudernack (Institution of Transplantation Immunology, Rikshospitalet, The National Hospital, Oslo, Norway). Clone 563 is a murine IgG1 that recognizes a different CD34 epitope from that of the CellPro CD34 MoAb clone (clone

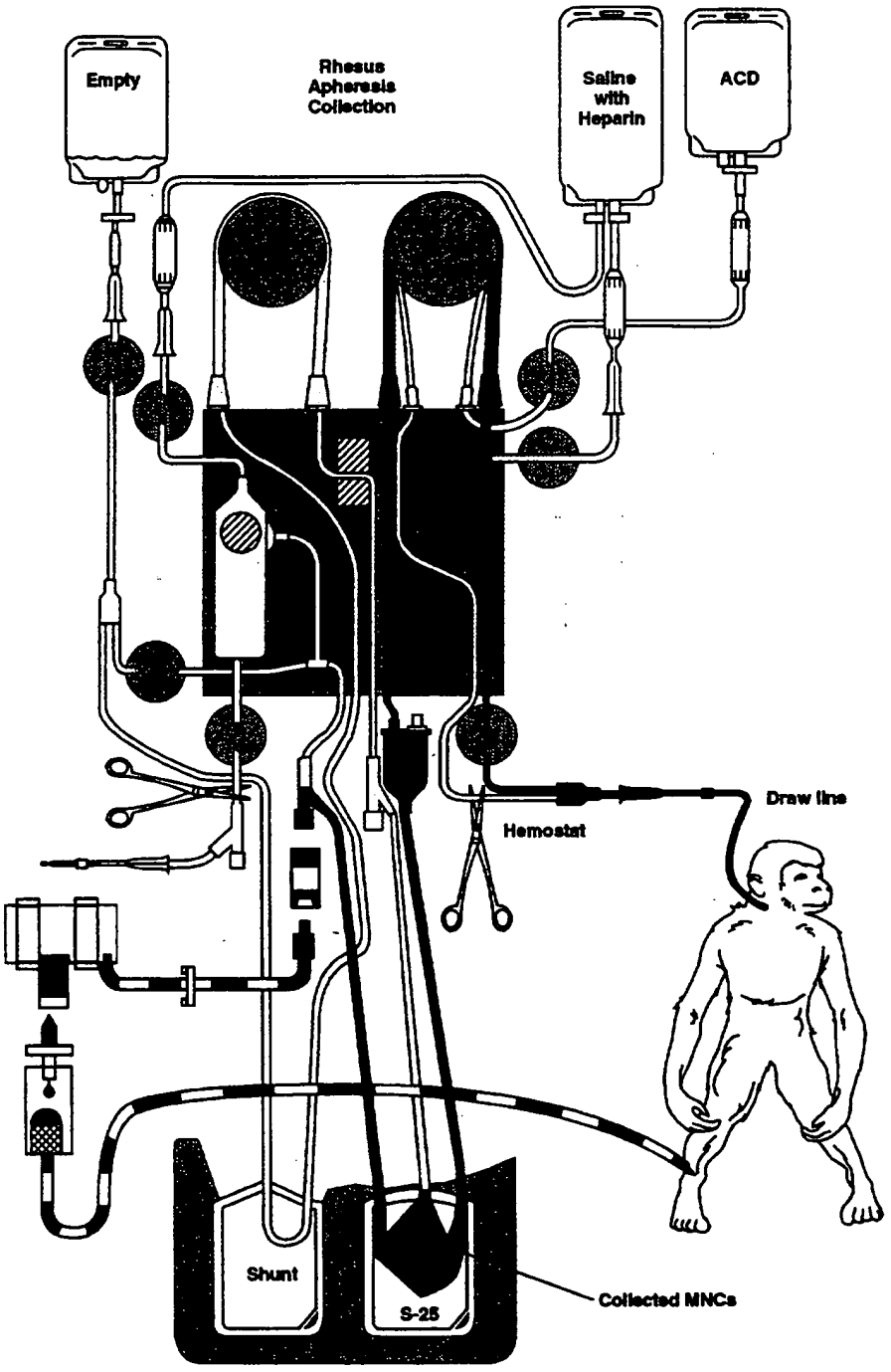

Fig 1. A diagram of the rhesus apheresis procedure is shown. Red denotes the red blood cell pathway; yellow, the pathway of plasma; and blue, the area where the leukapheresis product was collected.

tions of the cells were prepared to document cellular morphology. Separate immunoselections were performed on each leukapheresis product collected on day 4 and day 5. The $CD34^+$ cells collected on each day were stained and analyzed independently.

Culture of immunoselected $CD34^+$ cells. $CD34^+$ cells were immunoselected from the leukapheresis product of animals mobilized with SCF and G-CSF and were cultured in suspension for 3.5 days in Dulbecco's modified Eagle's medium (Biofluids, Rockville, MD) plus 15% fetal calf serum (Hyclone Laboratories, Inc, Logan, UT) supplemented with 50 ng/mL of IL-6 and 100 ng/mL of SCF (both cytokines provided by Amgen, Inc).

Immunophenotyping of CD34 cells from BM and PB. The BM and PB leukapheresis $CD34^+$ cells that were positively selected using the CellPro immunoadsorption system were immunophenotyped with CD34-allophycocyanin (APC) to evaluate CD34 purity and were also immunophenotyped with CD38-fluorescein isothiocyanate (FITC) and Thy-1–phycoerythrin (PE) to identify $CD34^+CD38$ and $CD34^+$Thy-1 subpopulations. The CD34 MoAb used (clone 563) was a gift from Dr G. Gaudernack (Institution of Transplantation Immunology, Rikshospitalet, The National Hospital, Oslo, Norway). Clone 563 is a murine IgG1 that recognizes a different CD34 epitope from that of the CellPro CD34 MoAb clone (clone

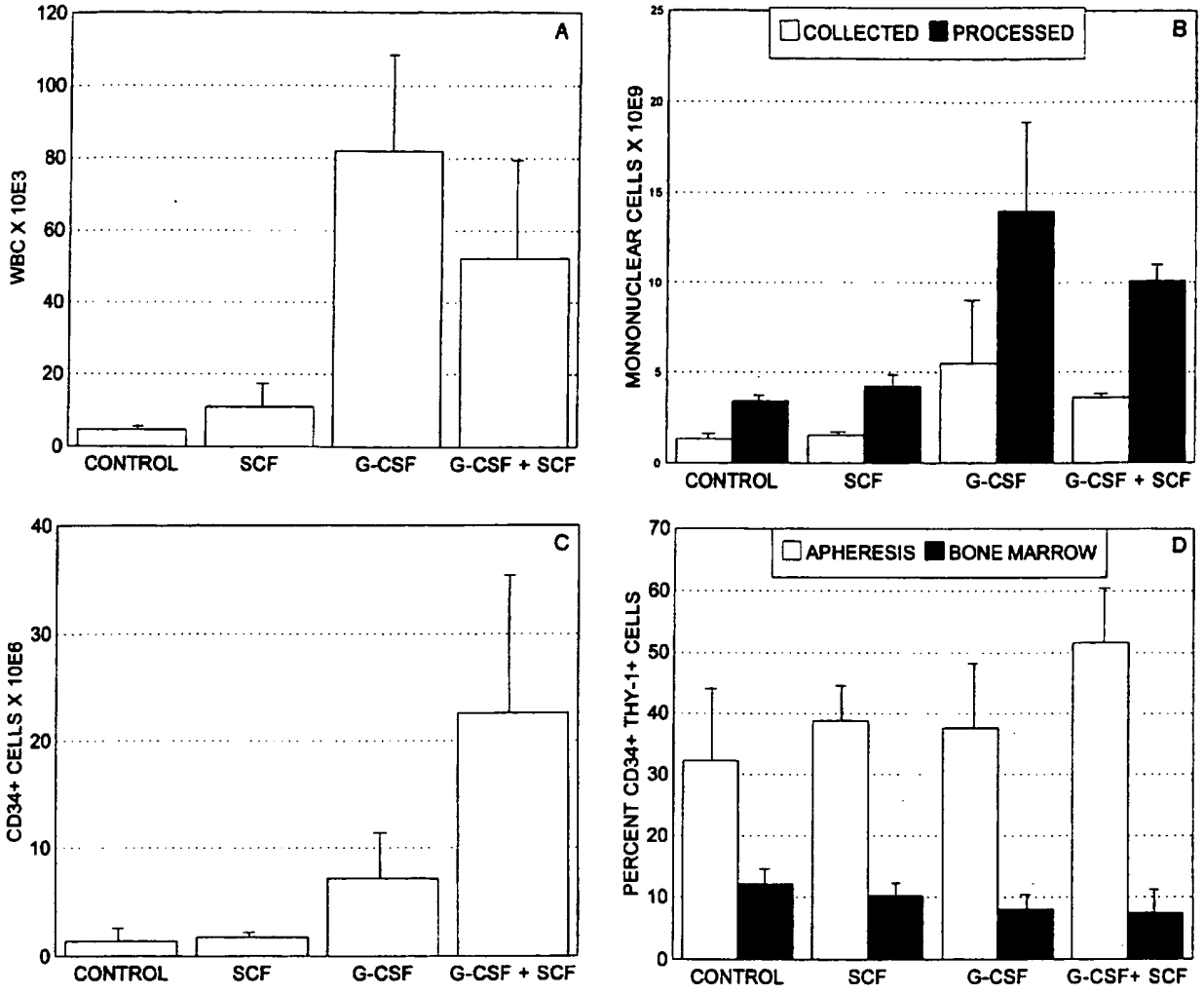

Fig 2. (A) Cytokine mobilization of WBC into PB. The average (SD) circulating WBC/μL of blood from animals that had received a 4- and 5-day subcutaneous course of either no cytokines (n = 6), 200 μg/kg/d SCF (n = 6), 100 μg/kg/d of G-CSF (n = 6), or the combination of SCF and G-CSF (n = 11) before leukapheresis. (B) Total number of mononuclear cells processed and collected from PB by leukapheresis. The average (SEM) number of mononuclear cells processed through the CS3000 *Plus* Cell Separator and the average (SD) number (SD) of PBMNCs collected in the leukapheresis product from animals that received either no cytokines (n = 6), SCF (n = 6), G-CSF (n = 6), or the combination of SCF and G-CSF (n = 11). (C) Absolute number of CD34+ cells obtained after immunoselection from the leukapheresis product. The average (SD) absolute number of CD34+ cells immunoselected from the leukapheresis product from animals that received either no cytokines (n = 6), SCF (n = 5), G-CSF (n = 6), or the combination of SCF and G-CSF (n = 6). (D) The percentage of Thy-1 expressing CD34+ immunoselected cells from the leukapheresis product or BM. The average (SD) percentage of CD34+ cells that express Thy-1 from (1) the leukapheresis product of animals that received a 4- and 5-day subcutaneous course of either no cytokines (n = 6), SCF (n = 5), G-CSF (n = 6), or the combination of SCF and G-CSF (n = 6); or (2) the BM of animals that received either no cytokines (n = 6), SCF (n = 6), G-CSF (n = 6), or the combination of SCF and G-CSF (n = 5).

12.8) used in the immunoselection. Most antihuman CD34 MoAbs either do not cross react with rhesus macaque CD34+ cells or recognize the same epitope as that of the antibody used in the immunoselection. Fortunately, immunoselection for rhesus CD34+ cells with clone 12.8 did not interfere with subsequent CD34 staining with clone 563. For immunophenotyping, the CD34 clone 563 was directly conjugated to APC by Molecular Probes, Inc (Eugene, OR). The CD38-FITC MoAb used was the OKT10 clone (Ortho Diagnostics, Raritan, NJ). The Thy-1–PE clone used was a gift from Dr P. Lansdorp (Terry Fox Laboratories Vancouver, British Columbia, Canada). To evaluate adhesion proteins CD29-FITC and CDw49d-FITC antibodies were obtained from AMAC, Inc (Westbrook, ME).

Cells were incubated in the MoAbs or isotype controls for 30 minutes on ice and then washed 2 times with phosphate-buffered saline (PBS) containing 1% bovine serum albumin. Fc receptors were blocked by preincubating the cells for 5 minutes in 10% human AB serum (Advanced Biotechnologies Inc, Columbia, MD) without washing before the addition of MoAbs. Cells were fixed in 1% paraformaldehyde in PBS and stored at 4°C. All tubes were first run to analyze for immunophenotyping patterns of CD34-APC, CD38-FITC, and Thy-1–PE before the cells were processed for DNA analysis. The remaining cells were then processed for DNA analysis using a nuclear DNA staining procedure[27] that was modified for intact cells. The DNA-staining procedure involved taking a 300-μL aliquot of cells and slowly adding 700 μL of −20°C cold 100% ethanol to yield a final concentration of 70% ethanol. The cells were

put on dry ice for 5 to 10 minutes, and then 3 mL of cold PBS plus 1% fetal calf serum with 0.01 μmol/L 4',6-diamidino-2-phenylindole (DAPI; Molecular Probes) was added and tubes were gently mixed and centrifuged for 10 minutes at 1,000 rpm. The supernatant was removed leaving approximately 200 μL of liquid, and the cells were gently mixed. Cells were allowed to stain in the DAPI solution for at least 1 hour or overnight before analysis on the Coulter Elite flow cytometer (Hialeah, FL).

Flow cytometry data for FITC, PE, APC, DAPI, forward scatter and side scatter was collected in listmode. The DAPI fluorescence was measured as both linear-integrated and linear-peak signals and FITC, PE, and APC were collected as logarithmic signals. Cell doublets were excluded by gating using either DAPI-peak versus DAPI-integrated signals or using DAPI-peak versus ratio of DAPI-peak/-integrated signals. The pre-DNA processing immunophenotyping was compared with post-DNA immunophenotyping to assure that fluorescence of FITC, PE, and APC did not change. The $CD34^+Thy\text{-}1^+$ populations were then gated, and DNA histograms for this population were created and imported into the Multicycle software package by Phoenix Flow Systems (San Diego, CA) for DNA curve-fitting and statistical analysis of the G0/G1, S, and G2/M phases of the cell cycle. These results were tabulated, means and SDs determined, and, where stated, statistical analysis performed using the Student's *t*-test of the differences between two means.

The absolute number of $CD34^+Thy\text{-}1^+$ cells/mL of either BM or leukapheresis product was calculated by multiplying the percentage of $CD34^+$ cells that were $Thy\text{-}1^+$ by the absolute number of $CD34^+$ cells collected, and dividing this number by the volume of either BM or leukapheresis product collected for each animal. These numbers were then averaged based on group, and an SD was determined.

RESULTS

Rhesus apheresis of cytokine-mobilized PB cells. The effectiveness of different human cytokines to mobilize the release of rhesus leukocytes from BM into the PB was evaluated. White blood cell (WBC) counts measured immediately before leukapheresis (Fig 2A) show that G-CSF alone and the combination of G-CSF and SCF both increased the WBC count significantly above the levels achieved with SCF alone or with no cytokine therapy. The WBC average (SD) measured for the control group without cytokines was 4.7 (0.7) $\times 10^3/\mu L$ (n = 6); for those treated with SCF alone, the WBC count was 11.0 (7.1) $\times 10^3/\mu L$ (n = 6); for those treated with G-CSF alone, the WBC count was 82.0 (30.2) $\times 10^3/\mu L$ (n = 6); and for those treated with the combination of G-CSF and SCF, the WBC count was 61.6 (19.3) $\times 10^3/\mu L$ (n = 6). No significant difference in WBC count was observed between G-CSF–mobilized and G-CSF– and SCF-mobilized animals at day 4 and day 5. This is consistent with a similar study in baboons in which, at these early time points, there was little difference in WBC count between the two groups.[16] The relative effectiveness of G-CSF or the combination of G-CSF and SCF to increase mobilized PB cells was also observed in both the PBMNC fraction processed and collected (Fig 2B). The average (SD) PBMNCs collected after leukapheresis was 1.3 (0.3) $\times 10^9$ PBMNCs (n = 6) for the control group, 1.5 (0.2) $\times 10^9$ PBMNCs (n = 6) for the SCF alone group, 5.5 (3.5) $\times 10^9$ PBMNCs (n = 6) for the G-CSF alone group, and 3.6 (2.1) $\times 10^9$ PBMNCs (n = 11) for the SCF and G-CSF group (Fig 2B). The average collection efficiency for PBMNCs using the CS3000 was 40.4% (12.5%) (n = 24), with no apparent difference in efficiency between mobilized and nonmobilized donors.

$CD34^+$ cell mobilization and recovery. $CD34^+$ cells were positively selected from the leukapheresis product or BM, and the purities of the recovered $CD34^+$ cells were evaluated. Purities after immunoselection for $CD34^+$ cells were consistently better for BM than for the leukapheresis product. Immunoselected $CD34^+$ cells from mobilized and nonmobilized BM had CD34 purities averaging 88.7% (7.4%) (n = 23). Leukapheresis products processed using the same immunoadsorptive system had CD34 purities averaging 60.9% (21.8%) (n = 23). Cytokine mobilization with G-CSF and SCF clearly increased the absolute number of $CD34^+$ cells recovered from the leukapheresis product following the CD34 immunoselection (Fig 2C). The absolute number of $CD34^+$ cells was greater from the leukapheresis products obtained from animals mobilized with the combination of G-CSF and SCF (2.3 [1.3] $\times 10^7$ $CD34^+$ cells; n = 6) than the leukapheresis products obtained from animals mobilized with G-CSF alone (0.7 [0.4] $\times 10^7$ $CD34^+$ cells; n = 6; see Fig 2C). Still fewer $CD34^+$ cells were collected from leukapheresis products obtained from animals mobilized with SCF alone (0.2 [0.1] $\times 10^7$ $CD34^+$ cells; n = 5) and from nonmobilized animals (0.1 [0.1] $\times 10^7$ $CD34^+$ cells; n = 6; see Fig 2C). Leukapheresis products from day 4 and day 5 yielded similar numbers of $CD34^+$ cells. The absolute number of $CD34^+$ cells collected per milliliter of BM was 2.7 (1.3) $\times 10^5$ (n = 12), 7.3 (1.7) $\times 10^5$ (n = 3), 4.3 (1.3) $\times 10^5$ (n = 3), and 5.7 (3.3) $\times 10^5$ (n = 3) for the nonmobilized, SCF-mobilized, G-CSF–mobilized, and SCF plus G-CSF–mobilized animals, respectively. The absolute number of $CD34^+$ cells collected per milliliter of leukapheresis product was 0.4 (0.4) $\times 10^5$ (n = 6), 0.4 (0.2) $\times 10^5$ (n = 5), 1.8 (1.2) $\times 10^5$ (n = 6), and 5.8 (3.5) $\times 10^5$ (n = 6) for the nonmobilized, SCF-mobilized, G-CSF–mobilized,

Fig 3. G-CSF and SCF mobilized $CD34^+$ cells immunoselected from a rhesus macaque, RQ826. $CD34^+$ cells were immunoselected from rhesus macaque (RQ826) (A) premobilization BM, (B) postmobilization BM, or (C) leukapheresis product postmobilization with G-CSF and SCF for 5 days. Immunophenotypic analysis using CD34-APC, CD38-FITC, and Thy-1–PE was performed on the cells gated on size and granularity (outlined in green). The $CD34^+Thy\text{-}1^+$ cells were gated and color backgated (delineated in red). The cell cycle analysis shown was performed on the gated $CD34^+Thy\text{-}1^+$ cells.

Fig 5. DNA cell cycle analysis of BM, PB, leukapheresis product, and postculture leukapheresis product $CD34^+Thy\text{-}1^+$ cells from a G-CSF and SCF-mobilized rhesus macaque, RQ1111. Immunophenotypic analysis and DNA cycle analysis of $CD34^+$ cells immunoselected from BM, PB, and the leukapheresis product of a rhesus macaque (RQ1111) mobilized with SCF and G-CSF. Some of the leukapheresis product immunoselected $CD34^+$ cells were cultured in 50 μg/mL of IL-6 and 100 μg/mL of SCF for 3.5 days and also analyzed for immunophenotype and DNA cell cycle. The $CD34^+Thy\text{-}1^+$ cells were gated (delineated in red), and cell cycle analysis was performed on these gated $CD34^+Thy\text{-}1^+$ cells. Cells that are $CD34^-Thy\text{-}1^+$ are primate granulocytes.

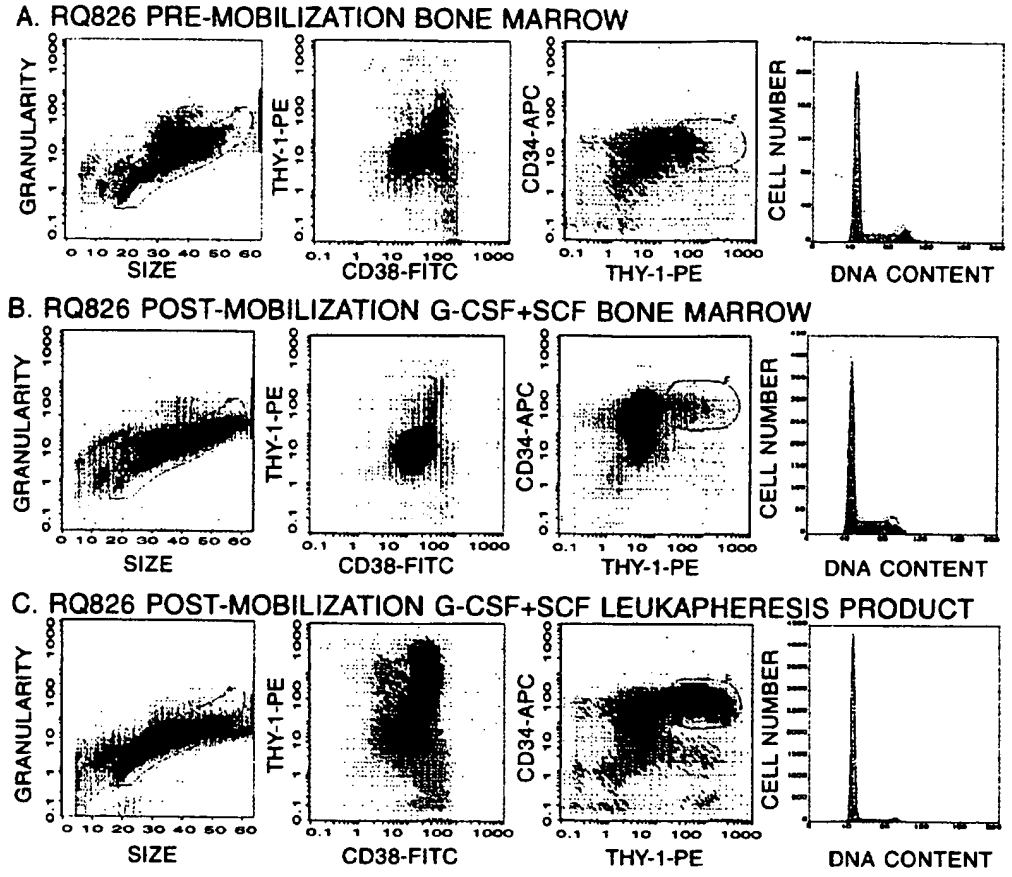
A. RQ826 PRE-MOBILIZATION BONE MARROW
GRANULARITY
SIZE
THY-1-PE
CD38-FITC
CD34-APC
THY-1-PE
CELL NUMBER
DNA CONTENT
B. RQ826 POST-MOBILIZATION G-CSF+SCF BONE MARROW
GRANULARITY
SIZE
THY-1-PE
CD38-FITC
CD34-APC
THY-1-PE
CELL NUMBER
DNA CONTENT
C. RQ826 POST-MOBILIZATION G-CSF+SCF LEUKAPHERESIS PRODUCT
GRANULARITY
SIZE
THY-1-PE
CD38-FITC
CD34-APC
THY-1-PE
CELL NUMBER
DNA CONTENT

Fig 3.

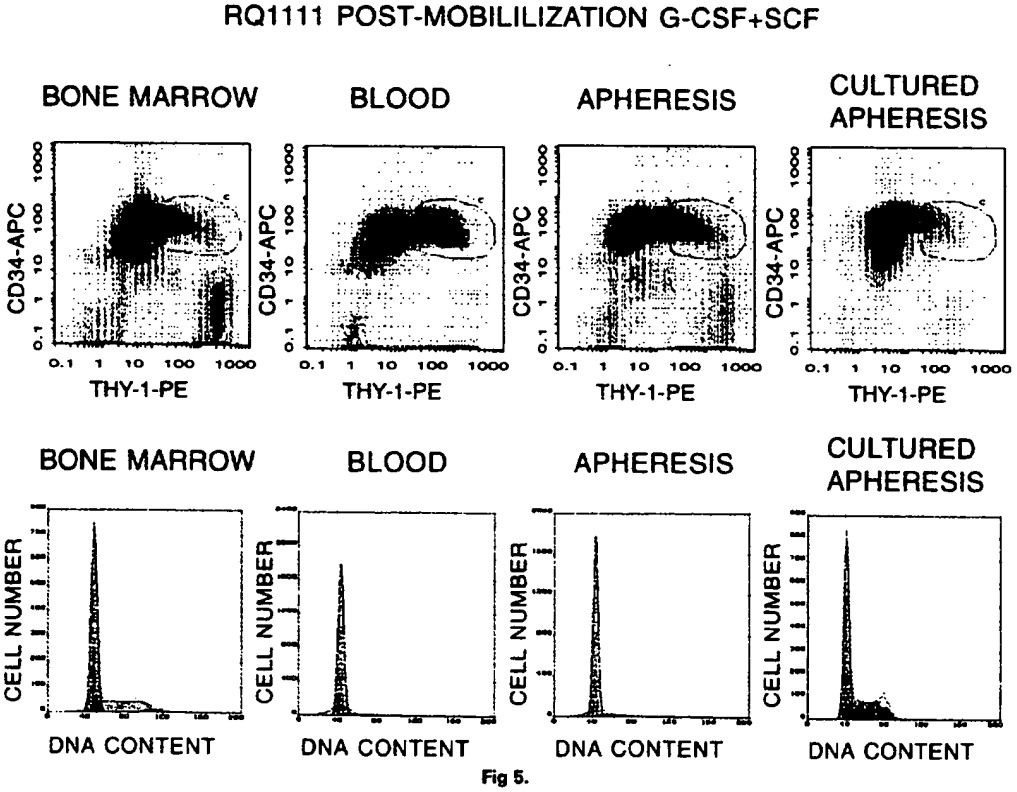
RQ1111 POST-MOBILILIZATION G-CSF+SCF
BONE MARROW
BLOOD
APHERESIS
CULTURED APHERESIS
CD34-APC
THY-1-PE
BONE MARROW
BLOOD
APHERESIS
CULTURED APHERESIS
CELL NUMBER
DNA CONTENT

Fig 5.

and SCF plus G-CSF–mobilized animals, respectively. For the BM, the absolute number of $CD34^+$ cells collected using the Ceprate LC-34-Biotin column represented 1.6% (0.5%) (n = 12), 2.0% (0.8%) (n = 3), 0.4% (0.2%) (n = 3), and 1.0% (0.4%) (n = 3) of the mononuclear cells collected after ficoll-hypaque separation for the nonmobilized, SCF-mobilized, G-CSF–mobilized, and G-CSF plus SCF-mobilized animals, respectively. For the leukapheresis product, the absolute number of $CD34^+$ cells represented 0.09% (0.08%) (n = 6), 0.16% (0.14%) (n = 5), 0.07% (0.04%) (n = 6), and 0.24% (0.18%) (n = 6) of the mononuclear cells collected after ficoll-hypaque separation for the nonmobilized, SCF-mobilized, G-CSF–mobilized, and G-CSF plus SCF-mobilized animals, respectively.

Phenotypic analysis. BM and PB $CD34^+$ cells obtained with or without cytokine mobilization were examined for differences in Thy-1 and CD38 expression. All $CD34^+$ cells expressed some level of Thy-1. A subpopulation of $CD34^+$ cells expressed higher levels of Thy-1 and was designated as Thy-1^+ (Fig 3). $CD34^+$ cells obtained from PB had a greater proportion of cells expressing higher levels of Thy-1 than did $CD34^+$ cells obtained from BM, independent of cytokine mobilization. $CD34^+$ cells isolated from the BM of nontreated animals were 12.1% (2.4%) Thy-1^+ (n = 6). The percentage of BM $CD34^+$ cells expressing Thy-1 at higher levels remained constant whether the animals were treated with SCF (10.3% [1.9%]; n = 6), G-CSF (8.1% [1.4%]; n = 6), or the combination of SCF and G-CSF (7.6% [2.8%]; n = 5; see Fig 2D). In contrast to the BM, circulating $CD34^+$ cells isolated from the leukapheresis product had a greater proportion of $CD34^+$ cells expressing higher levels of Thy-1 than did BM ($P < .01$). This difference between PB and BM was independent of whether an animal had received a cytokine or not (Fig 2D). Circulating $CD34^+$ cells were 32.2% (11.7%) Thy-1^+ from nonmobilized animals (n = 6), 38.8% (5.6%) Thy-1^+ from animals treated with SCF (n = 5), 37.6% (10.3%) Thy-1^+ from animals treated with G-CSF (n = 6), and 51.6% (8.7%) Thy-1^+ from animals treated with the combination of SCF and G-CSF (n = 6; see Fig 2D). The absolute number of $CD34^+$Thy-1^+ cells collected per milliliter of BM was 2.8 (1.5) $\times 10^4$ (n = 12), 8.0 (2.0) $\times 10^4$ (n = 3), 3.7 (0.7) $\times 10^4$ (n = 3), and 5.3 (4.3) $\times 10^4$ for the nonmobilized, SCF-mobilized, G-CSF–mobilized, and SCF plus G-CSF–mobilized animals, respectively. The absolute number of $CD34^+$Thy-1^+ cells collected per milliliter of leukapheresis product was 0.8 (5.5) $\times 10^4$ (n = 6), 1.8 (0.5) $\times 10^4$ (n = 5), 7.2 (6.5) $\times 10^4$ (n = 6), and 30.0 (21.5) $\times 10^4$ for the nonmobilized, SCF-mobilized, G-CSF–mobilized, and SCF plus G-CSF–mobilized animals, respectively. Interestingly, the cellular distribution of Thy-1 appears to be different between rhesus macaques and humans. Unlike human granulocytes, which are negative for Thy-1, granulocytes isolated from rhesus macaques strongly express Thy-1. Two populations of $CD34^+$Thy-1^+ cells were identified (Fig 3) based on their CD38 expression, CD38-bright and CD38-dim. Using the OKT10 clone, we have been unable to identify a $CD34^+CD38^-$ cell population in rhesus BM or leukapheresis product. For animal RQ826, 84% of the backgated $CD34^+$Thy-1^+ BM cells were CD38-bright before cytokine mobilization, 77% of the BM $CD34^+$Thy-1^+ cells were CD38-bright after G-CSF and SCF administration, and 90% of the mobilized PB G-CSF and SCF $CD34^+$Thy-1^+ cells were CD38-bright (Fig 3). The population of cells seen in Fig 3 that were dimly staining for CD34 and Thy-1 were small in size and expressed low levels of CD38.

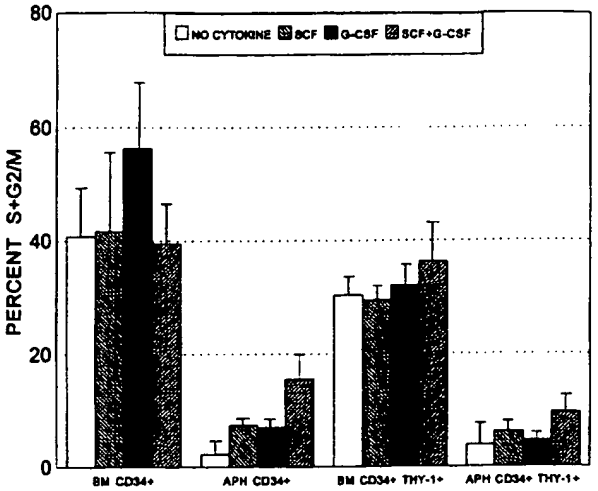

Fig 4. Cell cycle analysis of cytokine-mobilized immunoselected $CD34^+$ cells from BM or the leukapheresis product. Percentage of cells in S+G2/M for cells gated on $CD34^+$ or $CD34^+$Thy-1^+ immunophenotyping. The average (SD) percentage of $CD34^+$ or $CD34^+$Thy-1^+ cells in S+G2/M was determined for BM from animals that received either no cytokines (n = 14), SCF (n = 3), G-CSF (n = 3), or the combination of SCF and G-CSF (n = 7), and the leukapheresis product from animals that received either no cytokines (n = 6), SCF (n = 6), G-CSF (n = 6), or the combination of SCF and G-CSF (n = 11).

Because there were differences in Thy-1 expression between BM and PB, we were also interested in determining whether there were phenotypic differences in the expression of adhesion proteins between circulating PB- and BM-derived $CD34^+$ cells. In particular, we evaluated the expression of the integrin $\alpha 4\ \beta 1$ on $CD34^+$ cells. This adhesion protein has been shown to play a role in hematopoietic stem cell and microenvironment interactions.[28] $CD34^+$ cells isolated from the BM and leukapheresis product were no different in CD29 (the integrin $\beta 1$ chain) and CDw49d (the VLA-$\alpha 4$ chain) expression (data not shown).

Cell cycle analysis. After the initial immunophenotyping, the immunoselected $CD34^+$ cells were stained with DAPI for simultaneous DNA analysis and immunophenotyping. An example of an animal mobilized with the combination of G-CSF and SCF and analyzed for CD34, CD38, and Thy-1 expression and DNA cell cycle status is shown in Fig 3. As shown in Fig 3 and summarized in Fig 4, circulating PB $CD34^+$ cells and $CD34^+$ Thy-1^+ cells have fewer cells cycling in S+G2/M than their BM-derived counterparts ($P < .01$). For example, after cytokine therapy with G-CSF and SCF, 36.3% (6.8%) of the $CD34^+$Thy-1^+ BM cells were in S+G2/M (n = 7), whereas only 9.6% (3.2%) of the PB-circulating $CD34^+$Thy-1^+cells were in S+G2/M (n = 11; see Fig 4). The difference in cell cycle status observed between either PB and BM $CD34^+$ cells or $CD34^+$ Thy-1^+

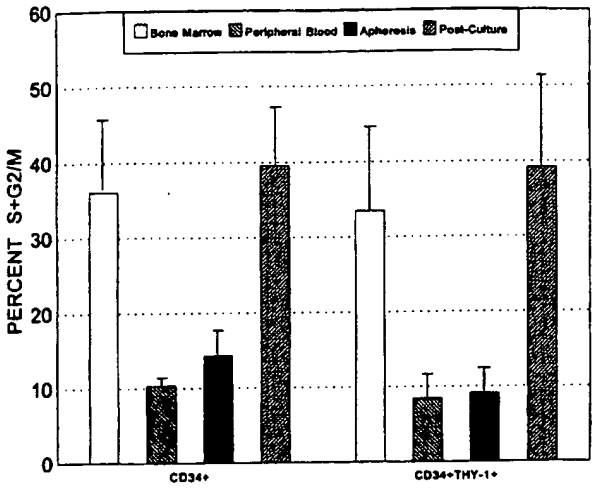

Fig 6. Comparison of BM, PB, leukapheresis product, and postculture leukapheresis product CD34+ cells and CD34+Thy-1+ cells. The average (SD) percentage of CD34+ or CD34+Thy-1+ cells in S+G2/M for BM (n = 5), PB (n = 4), leukapheresis product (n = 5), and after culture of the CD34+ cells isolated from the leukapheresis product in 50 μg/mL of IL-6 and 100 μg/mL of SCF for 3.5 days (n = 4).

cells was independent of cytokine mobilization. Similar to the G-CSF and SCF mobilization example, differences in cell cycle status between PB and BM CD34+ cells or CD34+ Thy-1+ cells were observed without cytokine treatment, with G-CSF treatment alone, or with SCF treatment alone. Administration of cytokines did not significantly alter the cell cycle profiles observed in premobilization and postmobilization BM. However, there was a slight increase in the percentage of cycling PB CD34+ cells observed with SCF+G-CSF mobilization, but this increase was not statistically significant for the data set. As one might expect, small CD34+ cells were not in the S + G2/M phases of the cell cycle.

One potential explanation for the differences observed in Thy-1 expression and cell cycle status between BM-derived and leukapheresis-derived CD34+ cells was that the leukapheresis procedure itself may have selected for nondividing cells of this particular phenotype. Counterflow centrifugation is commonly used as a method for isolating cells in different phases of the cell cycle. To evaluate this possibility further, G-CSF and SCF-mobilized CD34+ cells were immunoselected both from the PB and the leukapheresis product and compared. No significant differences in phenotype or in cell cycle status were observed between CD34+ cells immunoselected directly from the PB versus the leukapheresis PBMNC product (Figs 5 and 6).

To evaluate whether a greater percentage of PB CD34+ cells would be in cycle after culture, immunoselected PB CD34+ cells were placed in culture for 3.5 days in media supplemented with SCF and IL-6. Over the 3.5 days, the cells increased 1.6-fold (0.5-fold) in number (n = 4). After culture, the cell cycle status and immunophenotype were reevaluated. The phenotype of the circulating CD34+ cells was altered after culture, with a substantial loss in the percentage of CD34+Thy-1+ cells (Fig 5). In addition, both the CD34+ cells and the CD34+Thy-1+ subset following culture had a greater percentage of cells in S+G2/M from a baseline value of 14.3% (3.7%) and 9.1% (3.3%) to postculture values of 39.6% (7.9%) and 39.2% (12.3%) for CD34+ cells and CD34+ Thy-1+ cells, respectively (Fig 6).

DISCUSSION

No alterations in phenotype were observed for either the BM or PBMNC CD34+ cells with cytokine mobilization. The proportions of cells expressing CD34, Thy-1, and CD38 all remained fairly constant. What did change was the absolute number of CD34+ cells immunoselected from the leukapheresis product. Despite comparable numbers of PBMNCs being collected from animals receiving G-CSF alone and the combination of G-CSF and SCF, greater numbers of CD34+ cells were collected from animals immobilized with the combination of G-CSF and SCF. This observation may explain why there was a significant difference in WBC count between G-CSF–mobilized and G-CSF and SCF-mobilized baboons after approximately 1 week of cytokine therapy.[16]

The immunoselected CD34+ cells obtained from the PB, BM, and leukapheresis product were characterized for purity and for CD38 and Thy-1 expression. Unlike human CD34+ cells, which have a distinct CD38− subset,[18] rhesus macaque CD34+ cells express CD38 on all CD34+ cells. The absence of a CD34+CD38− population of cells in rhesus macaques, however, does not prevent multilineage reconstitution of rhesus macaques after BM transplantation, because immunoselected CD34+ cells from rhesus macaques have previously been shown to contribute to multilineage hematopoietic reconstitution.[29]

The distribution of Thy-1 on rhesus macaque CD34+ cells collected from the leukapheresis product and BM are quite similar to that observed for human CD34+ cells. Human CD34+ cells isolated from the BM and the leukapheresis product of cancer patients treated with cytotoxic chemotherapy and hematopoietic growth factors have been found to differ in Thy-1 expression.[23,30] These immunophenotypic differences between PB- and BM-derived CD34+ cells may account for the accelerated hematopoietic engraftment observed in patients receiving mobilized PB when compared with that for those receiving BM.[8-11] An increase in the absolute number of CD34+ cells and CD34+Thy-1+ cells collected by leukapheresis was observed with either G-CSF or the combination of G-CSF and SCF therapy. Thus, the increased frequency of Thy-1+ cells in the circulation may be caused by either a failure of a subpopulation of BM CD34+ cells to migrate into the circulation or a predilection for CD34+Thy-1+ cells to circulate.

In addition to differences between BM and PB CD34+ cell immunophenotype, there was a consistent difference between the cell cycle status of PB and BM CD34+ cells. The percentage of noncycling CD34+ cells was consistently higher for the PB or leukapheresis product than that for the BM. Preliminary results suggest that human PB CD34+ cells may also have fewer cells in S-phase under steady state conditions and after mobilization with chemotherapy and cytokines than CD34+ cells isolated from BM.[31] Both observations are consistent with earlier studies that found that circulating granulopoietic[32] and erythropoietic[33] progenitor

cells were more resistant to ^{3}H-thymidine suicide, and a more recent study that found that PB progenitor cells mobilized by G-CSF and other cytokines were resistant to ^{3}H-thymidine suicide.[34] All these results suggest that there is a selective difference in cell cycle status between CD34$^+$ cells found in the circulation and CD34$^+$ cells found within the BM, despite the presence of high levels of circulating hematopoietic growth factors. Potential reasons for this difference are that noncycling CD34$^+$ cells may have a lower affinity for binding to the hematopoietic microenvironment than do cycling CD34$^+$ cells and, therefore, would have a greater tendency to circulate, or that, for CD34$^+$ cells to cycle, adherence to the BM stroma is required. No phenotypic difference in $\alpha 4\beta 1$ expression, however, was observed between PB CD34$^+$ cells and their BM counterpart. However, differences in $\alpha 4\beta 1$ function or in the expression of other adhesion molecules, such as lymphocyte function-associated antigen-1, between BM-derived and circulating CD34$^+$ cells were not precluded.[35]

Failure to cycle when exposed to a combination of hematopoietic growth factors has been used as a criteria for identifying primitive, hematopoietic stem cells. Recent examples include retention of the membrane label PKH26 on a subset of CD34$^+$ cells when cultured in serum-free medium supplemented with IL-3, IL-6, SCF, and erythropoietin[36] and resistance of a subset of CD34$^+$ cells to the antimetabolite 5-fluorouracil when stimulated with IL-3 and SCF.[37] Although IL-3 was not used in our study, G-CSF and the combination of G-CSF and SCF have been used in mice, dogs, nonhuman primates, and humans to mobilize progenitors that contain BM repopulating cells.[10,12-17] This suggests that mobilized CD34$^+$ cells contain a population of primitive cells that are not in cycle in the presence of G-CSF and SCF and have the capacity to repopulate the BM of a myeloablated host. Because cellular replication is required for efficient retroviral infection,[38] it would appear that immunoselected CD34$^+$ cells from the leukapheresis product would be more difficult to transduce than BM. However, this does not appear to be the case in that immunoselected CD34$^+$ cells from the leukapheresis product could be induced to proliferate in suspension culture, and in that the absolute number of CD34$^+$ cells that were collected per milliliter of the leukapheresis product from the SCF and G-CSF–mobilized animals was greater than that collected from BM. These observations are consistent with murine studies that have shown that retrovirus transduction efficiency was higher for PB from splenectomized mice mobilized with G-CSF and SCF than for BM from mice treated with 5-fluorouracil,[39] and that the culturing of murine BM cells in IL-3, IL-6, and SCF enhances retroviral transduction efficiencies in murine hematopoietic cells.[40]

The leukapheresis procedure developed has permitted the collection of large numbers of PB leukocytes from 3- to 5-kg donors without the need for exposing the donor to allogeneic blood products in priming the instrument. This prevents allosensitization before myelosuppression, thus minimizing the opportunity for developing antibodies to erythrocyte, leukocyte, and platelet antigens and subsequent destruction of transfused blood products because of antibody formation. In addition, this leukapheresis procedure has permitted the collection of large quantities of other PB cells, such as lymphocytes and/or monocytes, for further study. Evaluation of cytokine-mobilized PB and BM stem cells from 3- to 5-kg donors may have application in pediatric and veterinary medicine in which cell transfusion, cell therapy, and genetic therapy are practiced. Future studies may examine why there is a predilection for noncycling CD34$^+$ cells to circulate in the PB and may further delineate the role of the subpopulations of CD34$^+$ cells in hematopoiesis.

ACKNOWLEDGMENT

The authors are indebted to Mr B. Thompson and Mr E. West for their assistance in caring for the animals; Mr C. Carter and his associates in the Department of Transfusion Medicine in the Clinical Center for their help on this project; Dr S. Feldman and his staff in the Laboratory of Animal Medicine and Surgery (NHLBI) for placing and removing the central line catheters; and Dr P. Rabinovitch (University of Washington, Seattle, WA) and Dr K. Becker (Phoenix Flow Systems, Inc, San Diego, CA) for their help in the interpretation of the DNA cell cycle analysis data. We would also like to thank Dr G. Gaudernack (The National Hospital, Oslo, Norway) for supplying the CD34 MoAb, clone 563; Dr P. Lansdorp (Terry Fox Laboratory, Vancouver, Canada) for supplying the Thy-1 antibody, clone 5E10, directly conjugated to PE; and Amgen, Inc for supplying all the hematopoietic growth factors used in these studies.

REFERENCES

1. Civin CI, Strauss LC, Brovall C, Fackler MJ, Schwartz JF, Shaper JH: Antigenic analysis of hematopoiesis. III. A hematopoietic progenitor cell surface antigen defined by a monoclonal antibody raised against KG-1a cells. J Immunol 133:157, 1984

2. Baumhueter S, Singer M, Henzel W, Hemmerich S, Renz M, Rosen S, Lasky LA: Binding of L-selectin to the vascular sialomucin CD34. Science 262:436, 1993

3. Fina L, Molgaatd HV, Robertson D, Bradley NJ, Monoghan P, Delia E, Sutherland DR, Baker MA, Greaves MF: Expression of the CD34 gene in vascular endothelial cells. Blood 75:2417, 1990

4. Andrews RG, Singer JW, Bernstein ID: Human hematopoietic precursors in long-term culture: Single CD34$^+$ cells that lack detectable T cell, B cell, and myeloid cell antigens produce multiple colony-forming cells when cultured with marrow stromal cells. J Exp Med 172:355, 1990

5. Bender JG, Unverzagt KL, Walker DE, Lee W, Van Epps DE, Smith DH, Stewart CC, To LB: Identification and comparison of CD34-positive cells and their subpopulations from normal peripheral blood and bone marrow using multicolor flow cytometry. Blood 77:2591, 1991

6. Bender JG, Unverzagt K: Flow cytometric analysis of peripheral blood stem cells. J Hematother 2:421, 1993

7. Bender JG, Unverzagt K, Walker DE, Lee W, Smith S, Williams S, Van Epps DE: Phenotypic analysis and characterization of CD34$^+$ cells from normal human bone marrow, cord blood, peripheral blood, and mobilized peripheral blood from patients undergoing autologous stem cell transplantation. Clin Immunol Immunopathol 70:10, 1994

8. Kessinger A, Armitage JO, Smith DM, Landmark JD, Bierman PJ, Weisenburger DD: High-dose therapy and autologous peripheral blood stem cell transplantation for patients with lymphoma. Blood 74:1260, 1989

9. Gianni AM, Siena S, Bregni M, Tarella C, Stern A, Bonadonna G: Granulocyte-macrophage colony-stimulating factor to harvest circulating haematopoietic stem cells for autotransplantation. Lancet 2:580, 1989

10. Sheridan WP, Begley CG, Juttner CA, Szer J, To LB, Maher D, McGrath KM, Morstyn G, Fox RM: Effect of peripheral-blood

progenitor cells mobilized by filgrastim (G-CSF) on platelet recovery after high-dose chemotherapy. Lancet 339:640, 1992

11. Brugger W, Bross K, Frisch J, Dern P, Weber B, Mertelsmann R, Kanz L: Mobilization of peripheral blood progenitor cells by sequential administration of interleukin-3 and granulocyte-macrophage colony-stimulating factor following polychemotherapy with etoposide, ifosfamide, and cisplatin. Blood 79:1193, 1992

12. McNiece IK, Briddell RA, Hartley CA, Andrews RG: The role of stem cell factor in mobilization of peripheral blood progenitor cells: Synergy with G-CSF. Stem Cells 11:83, 1993

13. McNiece IK, Briddell RA, Hartley CA, Smith KA, Andrews RG: Stem cell factor enhances *in vivo* effects of granulocyte colony stimulating factor for stimulating mobilization of peripheral blood progenitor cells. Stem Cells 11:36, 1993

14. Bodine DM, Seidel NE, Gale MS, Nienhuis AW, Orlic D: Efficient retrovirus transduction of mouse pluripotent hematopoietic stem cells mobilized into the peripheral blood by treatment with granulocyte colony-stimulating factor and stem cell factor. Blood 84:1482, 1994

15. de Revel T, Appelbaum FR, Storb R, Schuening F, Nash R, Deeg J, McNiece I, Andrews R, Graham T: Effects of granulocyte colony-stimulating factor and stem cell factor, alone and in combination, on the mobilization of peripheral blood cells that engraft lethally irradiated dogs. Blood 83:3795, 1994

16. Andrews RG, Briddell RA, Knitter GH, Opie T, Bronsden M, Myerson D, Appelbaum FR, McNiece IK: In vivo synergy between recombinant human stem cell factor and recombinant human granulocyte colony-stimulating factor in baboons: Enhanced circulation of progenitor cells. Blood 84:800, 1994

17. Andrews RG, Briddell RA, Knitter GH, Rowley SD, Appelbaum FR, McNiece IK: Rapid engraftment by peripheral blood progenitor cells mobilized by recombinant human stem cell factor and recombinant human granulocyte colony-stimulating factor in nonhuman primates. Blood 85:15, 1995

18. Terstappen LWMM, Gandour D, Huang S, Lund-Johansen F, Manion K, Nguyen M, Mickaels R, Olweus J, Topker S: Assessment of hematopoietic cell differentiation by multidimensional flow cytometry. J Hematother 2:431, 1993

19. Terstappen LWMM, Huang S, Safford M, Lansdorp PM, Loken MR: Sequential generations of hematopoietic colonies derived from single nonlineage-committed $CD34^+38^-$ progenitor cells. Blood 77:1218, 1991

20. Craig W, Kay R, Cutler RL, Lansdorp PM: Expression of Thy-1 on human hematopoietic progenitor cells. J Exp Med 177:1331, 1993

21. Baum CM, Weissman IL, Tsukamoto AS, Buckle AM, Peault B: Isolation of a candidate human hematopoietic stem-cell population. Proc Natl Acad Sci USA 89:2804, 1992

22. Mayani H, Lansdorp PM: Thy-1 expression is linked to functional properties of primitive hematopoietic progenitor cells from human umbilical cord blood. Blood 83:2410, 1994

23. Murray L, Chen B, Galy A, Chen S, Tushinski R, Uchida N, Negrin R, Tricot G, Jagannath S, Vesole D, Barlogie B, Hoffman R, Tsukamoto A: Enrichment of human hematopoietic stem cell activity in the $CD34^+Thy\text{-}1^+Lin^-$ subpopulation from mobilized peripheral blood. Blood 85:368, 1995

24. Howard M, Grimaldi JC, Bazan JF, Lund FE, Santos-Argumedo L, Parkhouse RME, Walseth TF, Lee HC: Formation and hydrolysis of cyclic ADP-ribose catalyzed by lymphocyte antigen CD38. Science 262:1056, 1993

25. Reems JA, Torok-Storb B: Cell cycle and functional differences between $CD34^+/CD38^{hi}$ and $CD34^+/38^{lo}$ human marrow cells after in vitro cytokine exposure. Blood 85:1480, 1995

26. Gore SD, Amin S, Weng L-J, Civin CI: Steel factor supports the cycling of isolated human $CD34^+$ cells in the absence of other growth factors. Exp Hematol 23:413, 1995

27. Otto F: DAPI staining of fixed cells for high-resolution flow cytometry of nuclear DNA, in Darzynkiewicz Z, Crissman HA (eds): Methods in Cell Biology, vol 33 Flow Cytometry. San Diego, CA, Academic, 1990, p 105

28. Williams DA, Rios M, Stephens C, Patel V: Fibronectin and VLA-4 in haematopoietic stem cell-microenvironment interactions. Nature 352:438, 1991

29. Bodine DM, Moritz T, Donahue RE, Luskey BD, Kessler SW, Martin DIK, Orkin SH, Nienhuis AW, Williams DA: Long-term in vivo expression of a murine adenosine deaminase gene in rhesus monkey hematopoietic cells of multiple lineages after retroviral mediated gene transfer into $CD34^+$ bone marrow cells. Blood 82:1975, 1993

30. Haas R, Möhle R, Pförsich M, Fruehauf S, Witt B, Goldschmidt H, Hunstein W: Blood-derived autografts collected during granulocyte colony-stimulating factor-enhanced recovery are enriched with early $Thy\text{-}1^+$ hematopoietic progenitor cells. Blood 85:1936, 1995

31. Danova M, Rosti V, Mazzini G, Locatelli F, Comoli P, Riccardi A, Cazzola M, Ascari E: Proliferative activity of bone marrow versus peripheral blood CD34-positive cells on steady state and following chemotherapy plus G-CSF. Blood 84:23a, 1994 (abstr, suppl 1)

32. Tebbi K, Rubin S, Cowan DH, McCulloch EA: A comparison of granulopoiesis in culture from blood and bone marrow cells of nonleukemic individuals and patients with acute leukemia. Blood 48:235, 1976

33. Ogawa M, Grush OC, O'Dell RF, Hara H, MacEchern MD: Circulating erythropoietic precursors assessed in culture: Characterization in normal men and patients with hemoglobinopathies. Blood 50:1081, 1977

34. Roberts AW, Metcalf D: Noncycling state of peripheral blood progenitor cells mobilized by granulocyte colony-stimulating factor and other cytokines. Blood 86:1600, 1995

35. Möhle R, Haas R, Hunstein W: Expression of adhesion molecules and c-kit on $CD34^+$ hematopoietic progenitor cells: Comparison of cytokine-mobilized blood stem cells with normal bone marrow and peripheral blood. J Hematother 2:483, 1993

36. Lansdorp PM, Dragowska W, Mayani H: Ontogeny-related changes in proliferative potential of human hematopoietic cells. J Exp Med 178:787, 1993

37. Berardi AC, Wang A, Levine JD, Lopez P, Scadden DT: Functional isolation and characterization of human hematopoietic stem cells. Science 267:104, 1995

38. Miller DG, Adam MA, Miller AD: Gene transfer by retrovirus vectors occurs only in cells that are actively replicating at the time of infection. Mol Cell Biol 10:4239, 1990

39. Bodine DM, Seidel NE, Gale MS, Nienhuis AW, Orlic D: Efficient retrovirus transduction of mouse pluripotent hematopoietic stem cells mobilized into the peripheral blood by treatment with granulocyte colony-stimulating factor and stem cell factor. Blood 84:1482, 1994

40. Luskey BD, Rosenblatt M, Zsebo K, Williams DA: Stem cell factor, interleukin-3, and interleukin-6 promote retroviral-mediated gene transfer into murine hematopoietic stem cells. Blood 80:396, 1992

Cytometry 15:267–271 (1994)

BRIEF REPORT

Visible Diode Lasers can be Used for Flow Cytometric Immunofluorescence and DNA Analysis

Richard M.P. Doornbos, Bart G. De Grooth,[1] Yvonne M. Kraan, Carel J. Van Der Poel,[2] and Jan Greve

Applied Optics Group, Faculty of Applied Physics, University of Twente, Enschede, The Netherlands

Received for publication June 22, 1993; accepted October 11, 1993

This report describes a feasibility study concerning the use of a visible diode laser for two important fluorescence applications in a flow cytometer. With a 3 mW 635 nm diode laser, we performed immunofluorescence measurements using the fluorophore allophycocyanin (APC). We have measured CD8 positive lymphocytes with a two-step labeling procedure and the resulting histograms showed good separation between the negative cells and the dim and the bright fluorescent subpopulations. As a second fluorescence application, we chose DNA analysis with the recently developed DNA/RNA stains TOTO-3 and TO-PRO-3. In our setup TO-PRO-3 yielded the best results with a CV of 3.4%. Our results indicate that a few milliwatts of 635 nm light from a visible diode laser is sufficient to do single color immunofluorescence measurements with allophycocyanin and DNA analysis with TO-PRO-3. The major advantages of using a diode laser in a flow cytometer are the small size, the low price, the high efficiency, and the long lifetime. © 1994 Wiley-Liss, Inc.

Key terms: Miniaturization, instrumentation, DNA/RNA staining, allophycocyanin, APC, TOTO-3, TO-PRO-3, CD8, flow cytometry

Since its introduction in flow cytometry (3), fluorescence detection has proven to be a very sensitive and versatile technique. Specific stains for DNA, RNA, and other cellular constituents (e.g., mitochondria) and functional stains for detection of Ca^{2+}, pH, and membrane potential are now well developed. Combined with the monoclonal antibody labeling technique, a very sensitive and specific research tool is available for flow cytometry. Most fluorescent dyes used for these purposes are excitable with UV, blue, or green light, which means that argon-ion or krypton gas lasers have to be used. The major disadvantages of these lasers are well known: they are very expensive, bulky, inefficient, noisy, need considerable cooling, require regular maintenance, and have a limited lifetime.

Another laser, the helium-neon (He-Ne) gas laser, is not often used even though for a number of important applications good results can be obtained with it (8,10,11). The major drawback is the fact that very few red-excitable dyes (excitation maximum above 600 nm) are commercially available (C-phycocyanin (CPC), allophycocyanin (APC), and indodicarbocyanin (Cy-5)), and only single color measurements can be done.

Recent developments in the field of solid state physics have led to the production of visible diode lasers with a power of a few to tens of milliwatts (depending on the exact wavelength). We have already shown that diode lasers yield good results for scattering measurements in a flow cytometer (4). Now we have investigated whether diode lasers are worthy substitutes for He-Ne lasers in flow cytometric applications. In other words, can the currently available diode laser now also

[1]Address reprint requests to B.G. De Grooth, Applied Optics Group, Faculty of Applied Physics, University of Twente, P.O. Box 217, 7500 AE Enschede, The Netherlands.

[2]C.J. Van Der Poel is now at the Philips Optoelectronics Centre Philips Research Labs, P.O. Box 80000, 5600 JA Eindhoven, The Netherlands.

be used for fluorescence measurements? We have tested this for two common flow cytometric applications: first, immunofluorescence measurements using the dye allophycocyanin (APC) coupled to a monoclonal antibody, and second, DNA analysis by using the DNA stains TOTO-3 and TO-PRO-3 (benzothiazolium-4-quinolinium dimer and monomer iodide, respectively).

MATERIALS AND METHODS

The visible diode laser we used was the Philips CQL 840/D (Philips, Eindhoven, The Netherlands), a ridge structure InGaAlP-based laser with a maximum optical output power of 3 mW at 635 nm. This single mode laser emits the light highly divergent; it has a 6° far-field angle (FWHM) parallel to the junction and a 35° angle perpendicular to the junction. The laser is mounted in a SOT 148D case (size: 9 mm in diameter, 5 mm in height) together with a photodiode to monitor the output power. We have mounted this laser into a small aluminum cylinder (25 mm diameter) in order to cool it passively to room temperature. The diode laser driver we used was a voltage stabilized power supply (E-018–0.6/D, Delta Elektronika, Zierikzee, The Netherlands) in series with a 150 Ω resistor (inserted to limit the current).

The optical setup (see Fig. 1) contains the diode laser and a compact disk (CD) lens (RP 036 equivalent, Philips), which collects the highly divergent emitted light and creates a collimated beam. In order to eliminate spontaneous emission we have used a 640 nm shortpass interference filter (35–5420, Ealing, Watford, England) in the excitation beam. In the case of immunofluorescence measurements, a spherical lens (80 mm focal length) was used to focus the light in the flow cell, yielding a spot of ~78 μm by 14 μm. Due to the elliptical emission profile of the laser, an elliptical spot is obtained, which has its long axis horizontally. With a sheath flow velocity of ~2.5 m/s, this results in an illumination time of ~5 μs. For DNA analysis a highly uniform illumination profile is needed, so we used (instead of one spherical lens) a 200 mm and a 100 mm cylindrical lens to create a focus of ~200 μm by 30 μm. The forward scattered light is detected with a negatively biased photodiode (PIN 10 D, United Detector Technology, Santa Monica, CA). Fluorescence is collected on one side of the quartz cuvette with a 1.2 NA gel-immersion objective and detected with a head-on photomultiplier (R 1104, Hamamatsu, Hamamatsu City, Japan). The rectangular cuvette has a flow channel of 160 μm by 400 μm, which allows the use of high numerical aperture objectives in the orthogonal direction. Two 3 mm color glass filters (RG 665, Schott, Mainz, Germany) block the scattered laser light. These filters gave enough suppression at the laser wavelength (more than 10^{-6}) and although the cutoff was 30 nm above the laser wavelength, transmission of APC fluorescence was calculated to be still about 40%. On the opposite side of the flow cell, a 0.4 NA CD lens collects the orthogonally scattered light and focuses it on a side-on photomultiplier (R 928, Hamamatsu).

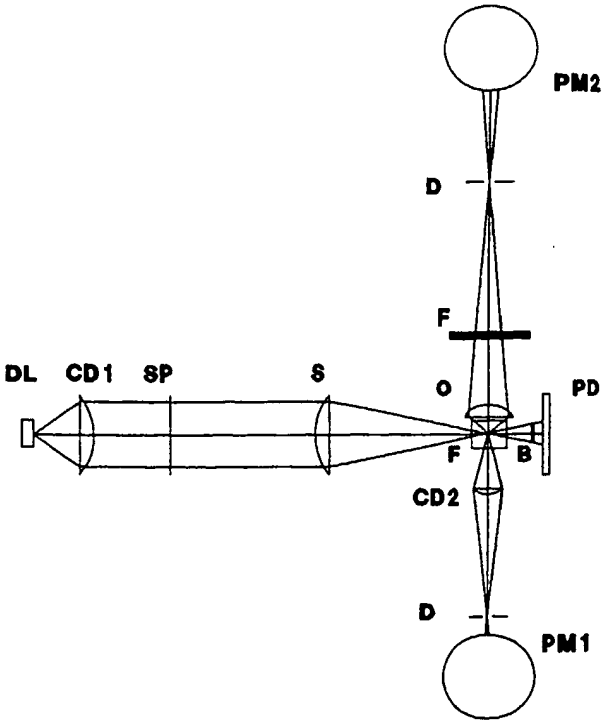

FIG. 1. Setup of the flow cytometer used for immunofluorescence measurements using a visible diode laser. Note that fluorescence and scattering is detected on opposite sides of the flow cell. DL, diode laser; CD1, CD2, Compact Disk player lenses; SP, 640 nm short pass filter; S, spherical lens; F, flow cell; O, objective; B, beam stop; PD, photodiode; F, 665 nm long pass filter; D, diaphragm; PM1, PM2, photomultipliers.

Signals are processed using a conventional peak detection system and a 12-bit analog-to-digital converter (2). The acquired data are stored and analyzed with a PC (1).

The immunofluorescence labeling procedure is as follows: human lymphocytes of a healthy donor were isolated by density centrifugation over Percoll (1.077 g/dm^3) and labeled with antihuman CD8-biotin conjugate (Beckton-Dickinson, San Jose, CA). The second labeling step is performed with streptavidin-APC conjugate (Molecular Probes, Eugene, OR).

The DNA staining procedure: 10^6 K562 cells (an erythroblast cell line) in 1 ml RPMI were washed and suspended in 0.2 ml PBS, 1 ml Modified Vindelov's PI solution (9) without PI (0.01 M Tris pH = 8, 1 mM NaCl, 0.1% NP-40, 0.07% RNAse) was added to the cells and incubated for at least 10 min on ice. The cells were washed once and stained with 100 μl TOTO-3 iodide (10 μM in PBS) or 300 μl TO-PRO-3 iodide (10 μM in PBS) (Molecular Probes) and incubated for 30 min at room temperature and in the dark.

Allophycocyanin calibration beads (8 μm) were ob-

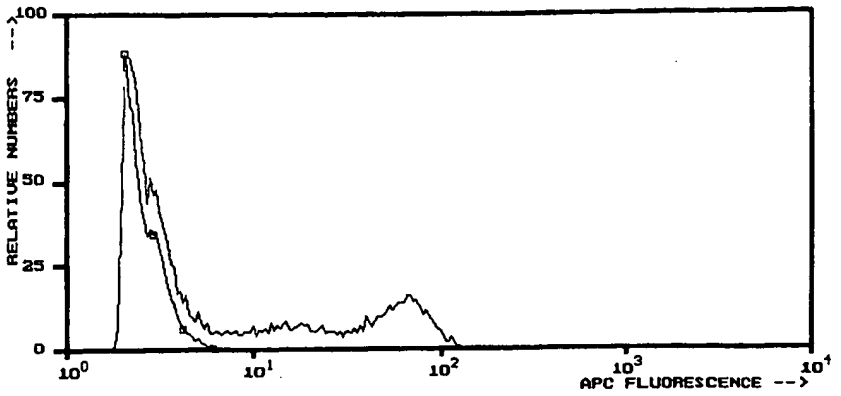

FIG. 2. Histogram of fluorescence signals obtained from (13,182) lymphocytes incubated with CD8-biotin/streptavidin-APC with the diode laser-based flow cytometer. The negative control is indicated with the rectangles.

tained from Flow Cytometry Standards Corporation (cat. 901, NC).

RESULTS

The specified power of 3 mW was obtained at a laser current of ~75 mA; this current strongly depends on the ambient temperature. After the warming up period of 30 min, output power fluctuations were negligible during 1-h experiments. High frequency noise (≥ 1 kHz) is very low and determined by the quality of the laser driver; in our case the noise and ripple was ~0.02%. When operated at maximum power, the temperature of the metal block was increased by one or two degrees.

In Figure 2 we show the results of an immunofluorescence measurement of human lymphocytes indirectly labeled with APC. The histogram clearly shows three subpopulations of cells: the bright positive cells (cytotoxic T cells), the dim fluorescent subpopulation (mostly NK cells), and the negative cells. The histograms of control cells (which are only incubated with streptavidin-APC) and untreated cells overlapped with that of the negative subpopulation (see Fig. 2), the nonspecific labeling can therefore be considered negligible.

In Figure 3 results are shown of measurements for different laser powers. This figure indicates that the histogram peaks of the logarithmically measured fluorescence intensity increase logarithmically with the increase of the power. It can be seen also that even with optical powers of only about 1.5 mW, adequate separation between the dim positive and negative cells can be obtained.

We found that the diode laser also emits some light of longer wavelengths than the specified wavelength, probably resulting from spontaneous (LED) emission. Scatter of this light by the cells can increase background in a fluorescence measurement. In order to eliminate this, we have inserted a short pass filter (cut off wavelength 640 nm) in the excitation beam. For very low fluorescence signals this filter proved to be necessary.

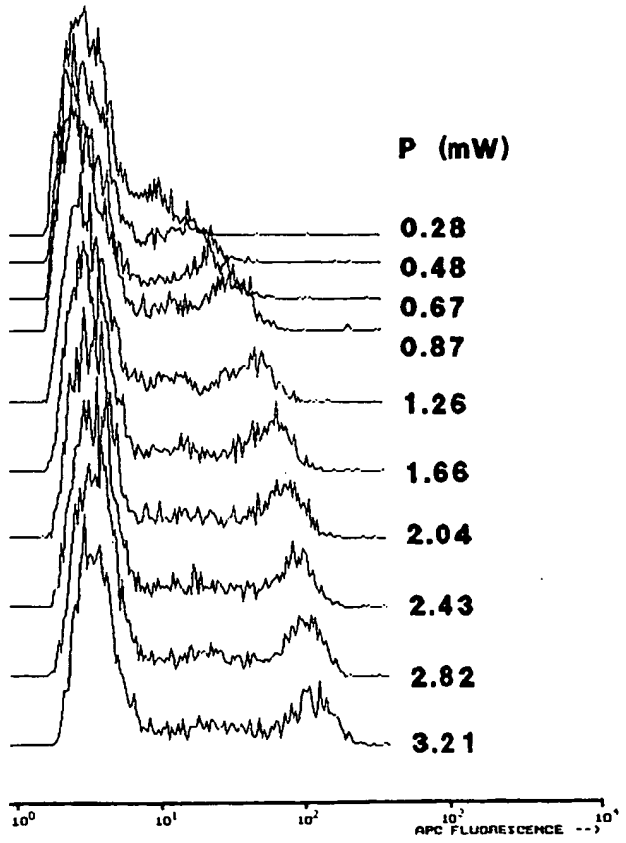

FIG. 3. Histograms of (~4,096) CD8-biotin/streptavidin-APC incubated lymphocytes obtained with different optical powers (indicated on the righthand side).

In order to evaluate the use of a diode laser for DNA analysis, we had to improve the uniformity of the illumination profile. We replaced the focusing lens by two cylindrical lenses, which resulted in a larger and more uniform focus. With the described setup we measured

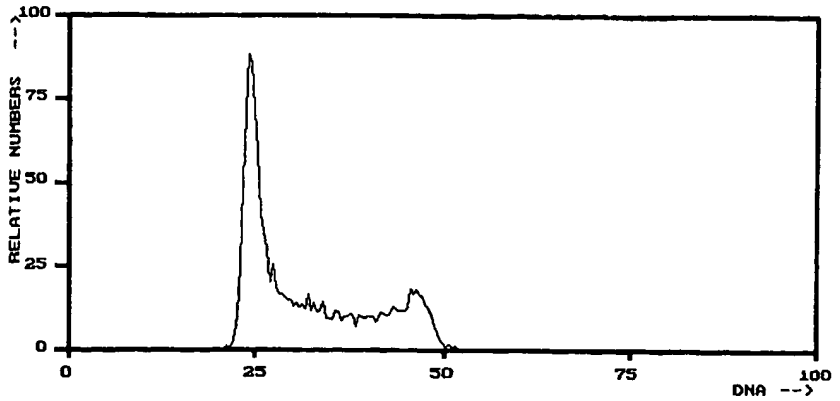

FIG. 4. Flow cytometric DNA histogram of (9,645) K562 cells stained with TO-PRO-3 using the 635 nm diode laser as light source. The CV of the diploid cell population is 3.4%.

DNA histograms of TO-PRO-3 stained K562 cells; in Figure 4 a typical example is shown. Similar results were obtained with TOTO-3 for the same cell type and experimental conditions. Also, other cell types (human NK, Epstein-Barr virus transfected human B cells, mouse L1210 cells) yielded good DNA histograms. We observed that the TO-PRO-3 fluorescence intensity is on the average 30–50% higher than that of TOTO-3. Also, the CVs of TO-PRO-3 histograms are in our measurements better than the CVs of TOTO-3 histograms, namely, ~3.4% compared to 4.1%.

In experiments to determine the optimal staining procedure, we obtained maximum fluorescence signals when ~100 μl TOTO-3 solution and 300 μl TO-PRO-3 solution was applied to 10^6 K562 cells/ml. Above 300 μl TO-PRO-3, the fluorescence intensity saturated and remained stable, whereas the TOTO-3 fluorescence displayed a decrease when the applied amount exceeded 100 μl.

The fluorescence intensity of TO-PRO-3 stained K562 cells is ~20 times higher than that of the CD8-positive lymphocytes. The intensity of APC calibration beads lies in between these two and is ~6.5 times less than that of the TO-PRO-3 stained cells.

DISCUSSION

Earlier attempts to measure immunofluorescence, using a 5 mW 670 nm diode laser for excitation of Ultralite 720 (Ultralite Corporation, no longer available) and a 0.6 NA objective, were unsuccessful (4). However, in this study we show that by using highly efficient fluorescence detection with an 1.2 NA objective and a 3 mW 635 nm diode laser, it is possible to perform immunofluorescence measurements and DNA analysis.

The results in Figure 2 indicate that a diode laser can be used for single-color immunofluorescence measurements. The measurement of CD8 labeled lymphocytes has about the same quality as measurements of FITC labeled cells measured in a routine flow cytometer. The signal of the negative cells lies in the order of a few photoelectrons per cell and probably originates from autofluorescence.

A critical inspection of our setup shows that still some improvements can be made. First, only 60% of the excitation beam is transmitted by the short pass filter; this can easily be increased to 90%, e.g., by using a line filter centered at 635 nm. Second, only 40% of the APC fluorescence is transmitted by the long pass filters. This fraction can also be enlarged by using optimized filters. Third, our photomultiplier has a low quantum efficiency at 660 nm (~3%), whereas a photomultiplier with a GaAs photocathode (e.g., the Hamamatsu R636) can have efficiencies at 660 nm as high as 13%. Altogether, these improvements would increase the signals roughly by a factor of 10.

As a second test, we chose the measurement of DNA with the recently developed dyes TOTO-3 and TO-PRO-3. These dyes are reported to have a high fluorescence intensity and a high enhancement of the fluorescence when bound to DNA (or RNA) (6). Both stains could be used to measure DNA histograms, but with TO-PRO-3 we have obtained the best results (CV = 3.4%). At this stage it is not clear yet if the CV is determined by the instrument, the dye, or the staining procedure. It should be noted that the measured intensities are of such a low level that photon noise could also be the determining factor for the CV. The G0/G1 peak of the DNA histogram corresponds roughly with 1,000 photoelectrons, resulting in a theoretical CV of 3%. We have not found flow cytometric DNA measurements using these dyes in the literature.

In principle, optimal fluorescence detection in an orthogonal setup requires a vertical polarization (7). In our setup we used the different emission angles of the diode laser to create an elliptical spot with a horizontal polarization. By inserting a half-wave retarder, which rotates the polarization 90°, we observed marginal differences in the fluorescence signal. This was probably caused by the fact that the loss of light due to the trans-

mission factor of the retarder (~80% transmission) was compensated by more efficient detection. Furthermore, the high numerical aperture makes the detection less critically dependent on incident polarization (compare 5).

The output power of the diode laser strongly depends on the temperature. In our experiments we did not use a stabilization circuit, so these fluctuations were noticeable, but during 1-h experiments, no adjustments were necessary. For practical purposes, however, we advise a power-controlled laser driver and a simple Peltier element-based temperature stabilization unit.

The advantages of diode lasers are remarkable. Diode lasers are inexpensive (~$150), very small, efficient, have a long lifetime, and can be modulated at frequencies up to 1 GHz. At present the power is still low compared to argon-ion lasers, but it is enough for immunofluorescence. A second disadvantage is the fact that the laser emission is astigmatic, but this can be corrected for by relatively simple optics. The fact that diode lasers can easily be modulated with frequencies up to 1 GHz indicates that they can be used for fluorescence lifetime experiments (12). We can also imagine a system consisting of two diode lasers with different wavelengths, which are chopped out of phase, that can separate two fluorophores with different excitation spectra but overlapping emission spectra.

The main problem is the limited availability and exploitation of red-excitable dyes. We therefore stress the need for more red-excitable dyes to enable development of dual-color or even three-color immunofluorescence measurements.

Currently, a large effort is being put into the development of diode lasers with shorter wavelengths, so we expect a bright future for these lasers in flow cytometry.

CONCLUSIONS

We have shown that a 3 mW 635 nm diode laser can be used for two-step immunofluorescence measurements with streptavidin-APC as a secondary label, yielding good separation between negative, dim positive and bright positive subpopulations. Also, DNA analysis using TOTO-3 and TO-PRO-3 can readily be done with a visible diode laser.

LITERATURE CITED

1. Bakker Schut TC, Doornbos RMP, De Grooth BG: Analysis: Software for Graphical Analysis of Multidimensional Flow Cytometric List Mode Data (accepted for publication in Computers and Biomedical Research).
2. Bakker Schut TC, Florians A, Van Der Werf KO, De Grooth BG: Flow Cytometry Data Processing and Data Acquisition with a Personal Computer Using an RTI-800 Multifunction A/D I/O Board (accepted for publication in Review of Scientific Instruments).
3. Dittrich W, Göhde W: Impulsfluorometrie bei Einzelzellenin Suspensionen. Z. Naturforsch 24b:360–361, 1969.
4. Doornbos RMP, Hennink EJ, Putman CAJ, De Grooth BG, Greve J: White blood cell differentiation using a solid state flow cytometer. Cytometry 14:589–594, 1993.
5. Eisert WG, Beisker W: Epi-Illumination optical design for fluorescence polarization measurements. Biophys J 31:97–112, 1980.
6. Haughland RP: Handbook of Fluorescent Probes and Research Chemicals, 5th ed. Molecular Probes, Eugene (OR), 1992.
7. Kerker M, Van Dilla MA, Brunsting A, Kratohvil JP, Hsu P, Wang DS, Gray JW, and Langlois RG: Is the central dogma of flow cytometry True: That fluorescence intensity is proportional to cellular dye content. Cytometry 3:71–78, 1982.
8. Loken MR, Keij JF, Kelley KA: Comparison of helium-neon and dye lasers for the excitation of allophycocyanin. Cytometry 8:96–100, 1987.
9. Robinson JP (ed): Handbook of Flow Cytometry Methods. Wiley/Liss, New York, 1993.
10. Shapiro HM, Glazer AN, Christenson L, Williams JM, Strom TB: Immunofluorescence measurement in a flow cytometer using low-power helium-neon laser excitation. Cytometry 4:276–279, 1983.
11. Shapiro HM, Stephens S: Flow cytometry of DNA content using oxazine 750 or related laser dyes with 633 nm excitation. Cytometry 7:107–110, 1986.
12. Steinkamp JA, Martin JC, Crissman HA: Phase-sensitive flow-cytometer. Cytometry Supplement 6:20, 1993.

Cytometry 24:214–225 (1996)

A Strategy for Multiple Immunophenotyping by Image Cytometry: Model Studies Using Latex Microbeads Labeled With Seven Streptavidin-Bound Fluorochromes

André Gothot, Jean-Claude Grosdent, and Jean-Michel Paulus
Laboratory of Hematology, Hôpital du Sart-Tilman and University of Liège, Liège, Belgium

Received for publication October 11, 1995; accepted February 19, 1996

Multiple immunophenotyping is aimed at identifying several cell populations in a single labeling procedure by their ability to bind combinations of specific labeled antibodies. The present work demonstrates the simultaneous discrimination by using image cytometry of aminomethylcoumarin acetate (AMCA), Lucifer yellow (LY), fluorescein isothiocyanate (FITC), R-phycoerythrin (PE), PE-Texas red tandem (Red613), peridinin-chlorophyll protein (PerCP), and allophycocyanin (APC), which were all bound to latex beads as streptavidin-conjugated fluorochromes. This has been the result of a step-by-step optimization of the several factors affecting the sensitivity and specificity of multiple immunofluorescence analysis. First, 14 streptavidin-conjugated fluorochromes were evaluated by using spectrofluorometry. A primary selection was then made of ten spectrally separable dyes that could be evaluated by using image cytometry. These dyes were bound to latex particles, and specific filter combinations were assembled to minimize crosstalk between fluorophores while preserving sufficient fluorescence intensity and counting statistics. Potential probe associations were then assessed by measuring the emissions of all fluorochromes that were detected by each filter combination. The resulting crosstalk matrix served as the basic tool both for final selection of the optimal filter combination and for dye set (composed, in this case, of the seven fluorochromes described above) and for mathematical correction of residual spectral overlap. Next, an image cytometry system was adapted to collect seven images of matched brightness with the selected combination of excitation/emission filters and dichroic mirrors. Finally, seven-parameter synthetic images were generated by digital image processing. © 1996 Wiley-Liss, Inc.

Key terms: Multiple immunophenotyping, image cytometry, multicomponent analysis, spectral compensation

Multiple fluorescence immunophenotyping allows the determination of several target antigens on individual cells by using fluorochrome-labeled antibodies. Thus far, double and triple immunophenotyping has been used extensively, for instance, to characterize hemopoietic precursor subpopulations (9,11,17,18,36) and to investigate aberrant antigen combinations expressed by leukemic blasts (5). Recent works have demonstrated the feasibility of discriminating four (13,18,19,22,23,32,33) or five (4,8,27,38) fluorescence signals by using flow or image cytometry. However, to detect rare or complex phenotypes, there is still a need to devise methods for the discrimination of greater numbers of probes bound to individual cells. The development of multiple immunophenotyping has benefitted from the availability of monoclonal antibodies that bind to precursor subpopulations (7,28), from the introduction of sets of fluorochromes spanning a wide region of the light spectrum (see references in Table 1), and from recent studies on the theory and application of multiparameter imaging (3,8,12,33,38). Moreover, further improvements of such procedures can be provided by technological advances in fluorescence microscopy and digital image processing.

Our initial motivation in developing multiple immunophenotyping color analysis has been to help classify early hemopoietic precursors and progenitors and to de-

Supported by grants from the FNRS (3.4562.85 and 3.4502.86), the Loterie Nationale Belge, Télévie (7.4545.92), the Fonds de la Recherche of the University of Liège, and the Oeuvre Belge du Cancer.

A.G. and J.M.P. are Aspirant and Director of Research, respectively, at the Fonds National de la Recherche Scientifique (FNRS), Brussels, Belgium.

Address reprints requests to Jean-Michel Paulus, Laboratory of Hematology, Hôpital du Sart-Tilman, 4000 Liège, Belgium.

termine their pathways of development. Because an informative phenotype of hemopoietic precursors should ideally specify both the lineage specificity and the stage of maturation, we estimated that the simultaneous detection of six to eight antigens would be required to enumerate uncommitted stem cells and progenitors committed to the granulomonocytic, erythrocytic, thrombocytic, and lymphocytic lineages. In leukemia diagnosis, multiple immunophenotyping could be exploited to improve the detection of aberrant antigenic phenotypes expressed by leukemic blasts.

A major problem in multicolor fluorescence applications is spectral overlap. Because of the broad excitation and/or emission spectra of available fluorochromes, the optimal emission band of each dye generally collects the light emitted by more than one component of the labeling cocktail. This fraction of the emission of a given fluorochrome, which is collected through an adjacent filter set, is termed spectral overlap. When more than four dyes are mixed, spectral overlap has to be corrected by mathematical rather than electronic compensation (3,30). However, the accuracy of spectral correction based on multicomponent analysis depends on many factors, such as the fluorescence spectra of individual components, the selected excitation/emission bands, as well as a number of optical and electronic variables (24). Therefore, a thorough and exhaustive examination of these variables is needed. In this paper, 14 streptavidin-conjugated fluorochromes were first evaluated by spectrofluorometry. From this evaluation, an initial set of ten spectrally separable dyes and filter combinations were chosen. These dyes were then bound to latex particles, and the various parameters influencing the accuracy of multiple immunophenotyping were assessed by measuring the emission of all dyes in each filter combination. The resulting crosstalk matrix served as the basic tool for final selection of the optimal probe and filter associations, for development of the image cytometry set up, and for correction of residual spectral overlap. The present study illustrates the application of this strategy to the discrimination of seven protein-conjugated dyes bound to latex particles.

MATERIALS AND METHODS

Fluorescent Conjugates and Microbeads

Because fluorescence immunophenotyping measures the emission of protein-bound fluorochromes, all of the model studies described below used streptavidin (SA)-fluorochrome conjugates rather than free dyes. SA-conjugates of Cascade blue (CB), Lucifer yellow (LY), Bodipy, fluorescein isothiocyanate (FITC), R-phycoerythrin (PE), Texas red (TxR), and allophycocyanine (APC) were obtained from Molecular Probes (Eugene, OR). SA-conjugates of tandem labels of PE and TxR (Red613) and PE and Cy5 (Red670) were purchased from Gibco BRL (Grand Island, NY). Peridinin-chlorophyll-protein complex conjugated to SA (PerCP) was from Becton-Dickinson (Mountain View, CA); aminomethylcoumarin acetate-SA (AMCA), cyanin 3-SA (Cy3), and cyanin 5-SA (Cy5) were from Jackson Immunoresearch (West Grove, PA). C-phycocyanin-SA (CPC) was purchased from Sigma (St. Louis, MO) (Table 1).

Table 1
Spectrofluorometric Data of 14 Dyes Evaluated for Multiple Labeling

Fluorochrome[a]	Excitation max. (nm)	Emission max. (nm)	References
AMCA	345	450	2,16,40
CB	379	420	40
LY	424	533	6,35
FITC	493	531	26
Bodipy	500	513	14
PE	563	576	10,21
Cy3	554	571	31
Red613	565	613	39
TxR	593	614	37
PerCP	493	675	1
Red670	540	666	39
APC	653	660	10,21
CPC	629	643	10,21
Cy5	658	668	31

[a]All fluorescence measurements were performed on solutions of streptavidin-conjugated fluorochromes. For fluorochrome abbreviations, see Materials and Methods.

To simulate cell surfaces labeled with fluorescent antibodies, Accuscan synthetic microbeads (Sigma), which have surfaces linked covalently with goat antimouse immunoglobulin (IgG), were used as model particles. Their mean diameter, as measured by image cytometry, was 10.61 μm with a coefficient of variation (CV) of 4.8%, and their mean cross-sectional area was 88.61 μm^2 with a CV of 9.8%. They were sequentially incubated with mouse biotinylated IgG (Molecular Probes) at various concentrations for 1 h at 4°C and with SA-conjugated fluorochromes for 30 min at 4°C.

Spectrofluorometry

Excitation and emission spectra were obtained in an LS 50 Perkin Elmer spectrofluorometer. Fluorescence measurements were performed on solutions of streptavidin-conjugated dyes diluted in phosphate-buffered saline (PBS) containing 0.2% bovine serum albumin (BSA). Emission spectra were corrected for the spectral characteristics of source, monochromators, and photomultipliers of the spectrofluorometer according to the procedure recommended by the manufacturer. Briefly, correction factors between 400 and 630 nm were obtained by comparing the emission spectrum of quinine sulphate, which was used as standard compound, with its corrected spectrum. Assuming that the wavelength-dependent efficiency of the detection system remained constant above 630 nm, a monotonous correction using the 630 nm correction factor was applied between 630 and 800 nm.

Fluorescence Microscopy

The microscope instrumentation is shown in Figure 1. An Axiovert 135 inverted microscope (Zeiss, Ober-

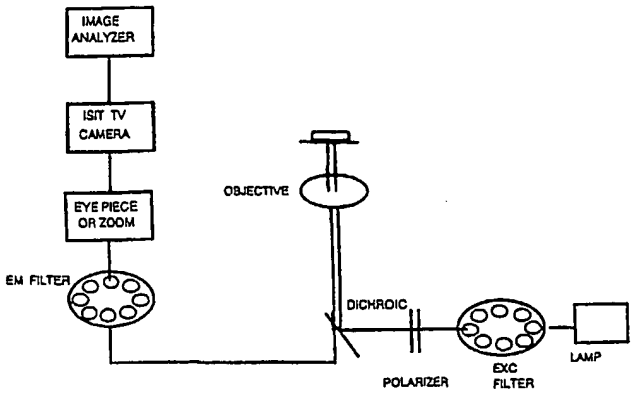

FIG. 1. Schematic representation of the image cytometry setup. Note that the same lenses serve as both objective and condenser.

kochen, Federal Republic of Germany) was equipped with a 100 W high-pressure mercury lamp. A 75 W Xenon lamp was mounted on a second port on the same microscope. It was not used in this study, because its intensity did not match that of the mercury lamp, except in the 450–540 nm range (34), where, however, the mercury lamp provided sufficient excitation for FITC, PE, Red613, and PerCP. Latex particles were suspended in a drop of saline solution and examined on a 0.17-μm-thick Hamax slide (Biotest, Brussels, Belgium). A ×40 oil NA 1.3 Plan Neofluar objective obtained from Zeiss was used in all experiments together with a ×1.0 camera ocular lens. High numerical aperture maximized light gathering of fluorescence emission and signal-to-noise ratio while minimizing the influence of out-of-focus sources (15). A set of two computer-controlled polarizing filters that could be rotated between each image collection was used to modulate lamp output. Excitation and emission filters were placed on two eight-position wheels that could be motorized independently under program control, making it possible to select a large number of relevant excitation/emission combinations. Four dichroic mirrors were adjusted on a Zeiss motorized slide, using an autocollimator to eliminate image shift resulting from inaccurate mirror positioning. All filters and dichroic mirrors were purchased from Omega Optical (Brattleboro, VT).

A Dage-MTI ISIT camera (Michigan City, IN), which is known to be sensitive to an illumination level of 5×10^4 lux, was used. Digital images were obtained at a resolution of 512 × 512 pixels at eight bits/pixel, providing 256 gray levels. One pixel corresponded to 16 μm in the image plane.

Image Processing

Image collection. The images were processed and analyzed with an IBAS 2000 image analyzer (Kontron, Eching, Federal Republic of Germany). This system uses a 486/66 MHz computer with 16 MB RAM and an MIAP 2 array processor with a 16 MB video memory and a real TV video board. The software was IBAS release 2.5. Sets of fluorescent images of the same field were collected sequentially with appropriate pairs of excitation/emission filters. To compensate for variations in brightness due to different dye efficiencies, the excitation intensity was adjusted for each image by the two rotating polarizing filters. After each image collection, a shutter in the excitation light path was closed to minimize dye bleaching. Sequence of illumination was used for all preparations, beginning with the longest wavelength at 660 nm and ending with the ultraviolet (UV) excitation at 365 nm. For each preparation, the voltage was adjusted to the highest value that gave no saturation in the brightest image (generally, the PE image) and was kept fixed for all sequential acquisitions of the same field in order to avoid image rotation. The black level was not removed electronically. An additional brightfield transmitted image was used for segmentation and as alignment reference. All images were recorded by averaging 100 frames for a total exposure time of about 4 s. Images were stored on disk for further analysis.

Selection and alignment of objects. The segmentation of objects from background was achieved by an interactive thresholding procedure, which was performed on the brightfield image. A CLOSE operation connected incomplete outlines. Particles that were too small or dirt particles were removed on the basis of their size (less than 30 pixels). Attached spots were separated by a THINBIN procedure, which was used to erode object outlines. Objects were then filled. Detected objects were displayed as binary masks and were identified. An automatic step was used to discard objects touching the edge of the image frame and, finally, to check the objects to be quantified. Because the available emission filters did not have strictly parallel faces, object shifts occurred at the different excitation/emission combinations. Therefore, sequential images of the same field were realigned interactively with the brightfield mask as reference.

Image restoration. The following corrections were performed on each image to ensure accurate fluorescence quantification. For shading correction, a set of reference images (one per filter set) was acquired that consisted of a drop of saline solution placed onto a Hamax slide. Each image was divided, pixel to pixel, by its reference and was multiplied by the mean gray level of the latter. Background correction was made by subtracting the modal value of the first peak of the gray level histogram obtained after shading correction. This value was considered to be a valid estimate of the field background, because it was unlikely to be influenced by cellular halos and impurities. The mean gray level originating from light reflected by the surface of unlabeled beads was also subtracted.

Image display and printing. The images shown in Figure 4 were obtained by converting the red, green, and blue images into .TIFF format and by exporting them to Photoshop software (Adobe, Mountain View, CA) for display on a PC screen and graphical sublimation printing. Following automatic compression, the images were stored on Bernouilli cassettes.

RESULTS

Development of Seven-Dye Immunophenotyping

Primary selection of probes and filter sets. Multiple immunophenotyping required careful fluorochrome selection. A spectrofluorometric evaluation of 14 dyes was first performed to identify a combination of dyes that could be spectrally resolved (Fig. 2, Table 1). When two probes were found to display approximately the same excitation and emission spectra, the less readily available probe was discarded: For this reason, FITC, PE, and APC were chosen in place of Bodipy, Cy3, and CPC, respectively. TxR gave a weak signal compared with its tandem with PE (Red613) and also was discarded. For the other pairs of spectrally close dyes (i.e., AMCA/CB and Red670/PerCP), selection could not be made from spectrofluorometric analyzes, and these had to be compared under image cytometry (see below).

Appropriate pairs of excitation and emission filters were selected to optimize excitation and light collection while minimizing the crosstalk between fluorophores (Table 2). Excitation filters for AMCA/CB and LY were set to match mercury emission lines at 365 and 405 nm, respectively; a single filter at 485 nm was sufficient for excitation of FITC, PE, Red613, Red670, and PerCP, even though excitation of PE and PE tandems by the 546 nm line of the mercury lamp resulted in a greater signal-to-noise ratio than at 485 nm (34). APC excitation was set at 590 nm, slightly below its absorption maximum, in an attempt to reduce overlap with Cy5. Finally, Cy5 excitation was placed at 660 nm. Emission filters were set near the emission maxima of their respective dyes, except for Cy5, which was measured above 700 nm to facilitate spectral resolution from APC.

Determination of crosstalk matrix by digital imaging cytometry. Microbeads labeled with saturating concentrations of the different conjugated dyes were used. Emission intensities of all fluorochromes were recorded under eight filter combinations, which are listed in Table 2. From these data, the crosstalk matrix of Table 3 was obtained. The columns indicate the fluorescence intensities recorded for each fluorochrome with the different filter sets; inversely, the rows record all dye emissions occurring through each of the filter combinations. This matrix, as shown below, served as the basic tool for both final dye selection and correction of spectral overlap.

Final selection of probes and filter sets. The matrix provided clear criteria with which to achieve a definitive dye selection. CB and AMCA could be both used as UV-excited dyes. Other investigators have reported the superiority of CB over AMCA in terms of quantum yield and resolution (40). However, with the 410/530 nm LY set, CB, AMCA, and LY had emission intensities of 8, 3, and 47 units, respectively, indicating that AMCA was resolved better than CB in the configuration used, whereas both dyes gave near identical emission efficiency with the 365/425 nm set.

In the near UV region, LY has an interesting spectrum. It has approximately the same emission as FITC at 530 nm, but its absorption band is located at the lower wavelength of 410 nm. Although it has a rather weak efficiency (4.7% of PE; see Table 3), LY excitation is ideally placed between that of AMCA and FITC. Therefore, LY was included in the fluorochrome combination.

In the group of 485 nm-excitable dyes, the most commonly used (FITC and PE) are easy to separate for two-color immunofluorescence. Additional probes (i.e., Red613, Red670, and PerCP) that were introduced initially for three- and four-color flow cytometry along with FITC and PE were evaluated in image cytometry. Although there is considerable overlap between the emissions of PE and Red613, the high signals provided by these two dyes allowed their spectral discrimination. PerCP was preferred to Red670, because its narrower emission spectrum facilitated its spectral discrimination from PE and Red613.

Among red-emitting dyes, APC and CY5 were compared in image cytometry. Cy5 has a greater proportion of its emission above 700 nm than APC, but these two dyes could not be resolved spectrally when they were used simultaneously. This was due to the fact that too many dyes (i.e., PE, Red613, PerCP, APC, and Cy5) were detected with the 590/660 nm filter set, and this led to a spectral compensation that was too complex. The solution implemented was to measure APC fluorescence with the 660/LP700 nm filter set, which was designed initially for Cy5, and to discard Cy5 from the probe combination. The spectra of the seven-dye combination that was selected with their respective excitation/emission filters are depicted in the left part of Figure 2.

Modulation of image intensity. Because of the limited dynamic range of the ISIT camera and also because better discrimination can be expected if all images have comparable brightness, it was necessary to modulate the source intensity with two rotating polarizing filters positioned in front of the mercury lamp. The source intensity could be reduced up to 100-fold by turning the planes of polarization from parallel to perpendicular (Table 4). The polarizing filters could be rotated between each image collection, making it possible to adapt the lamp output to each dye. The bright signals, especially those of PE, Red613, and PerCP, were attenuated, while the weaker signals of LY and APC were relatively amplified. Further amplification of AMCA and LY emissions would have been useful, but this option was limited by the high background in the UV region due to the strong intensities of the 365 and 405 nm lines of the mercury lamp and the insufficient blocking of the filters outside the mercury lines. Spectral overlap values recorded with relative amplification were consequently increased, whereas the other ones were attenuated. Therefore, a second spectral crosstalk matrix was acquired by using output modulation. All subsequent recordings using spectral overlap correction coefficients derived from this second matrix were performed under the same conditions of illumination adjustment (Table 4).

Automatic spectral compensation. A set of linear equations describing the mathematical relationships be-

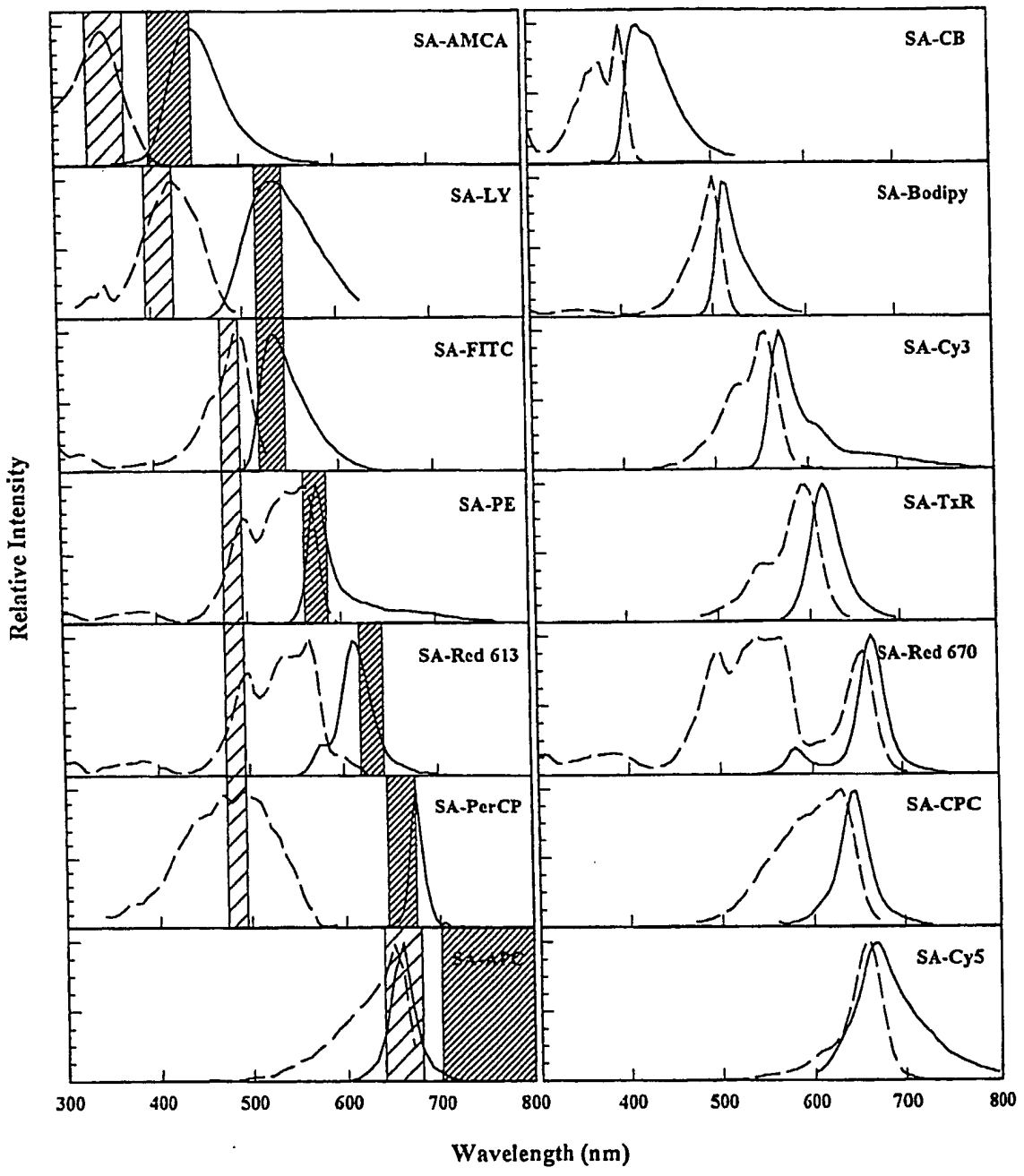

FIG. 2. Excitation (dashed line) and emission (solid line) spectra of 14 streptavidin-conjugated fluorochromes. Excitation/emission bandpasses are indicated by light and heavy hatching, respectively, for the seven dyes that were finally selected for multifluorescence imaging.

tween all dye emissions was derived from the spectral crosstalk matrix (see Appendix). The equations were introduced into the image restoration program following the shading and background correction steps. The resolution of these equations was applied numerically to the mean gray level within each data region to yield the corrected value of each object. Pixelwise combinations were also computed by using the COMBINE procedure of the IBAS software to display corrected images.

Evaluation of Seven-Dye Immunophenotyping

Fluorochrome fading. Compared with free output, the interposition of two polarizers in parallel directions reduced the source intensity to about 50%, which was useful to reduce dye fading. Rates of fading produced with this baseline output in all cases were less that 10% during the 4-s exposure used. These were further slowed down by output modulation, except for the APC channel.

Table 2
Filter Sets Designed for Initial Evaluation of Spectral Overlaps in the Ten-Dye Set[a]

	Wavelengths (nm)				
	Excitation			Emission	
Fluorescent probe	Center	Bandpass[b]	Dichroic (50%)[c]	Center	Bandpass
AMCA/CB	355	40	400	425	45
LY	405	10	510	530	30
FITC	485	22	510	530	30
PE	485	22	510	575	25
Red613	485	22	510	630	23
PerCP/Red670	485	22	510	660	32
APC[d]	590	45	620	660	32
Cy5/APC[d]	660	40	690	700	LP[e]

[a]All filters were interference filters from Omega Optical Inc., Brattleboro, VT. For fluorescent probe abbreviations, see Materials and Methods.
[b]Total bandpass at half maximum transmittance.
[c]Wavelength of half maximum transmittance.
[d]APC fluorescence was finally recorded with a 660/LP700 filter set in place of the 590/660 filter set (see text).
[e]This is a long-pass filter.

Table 3
Spectral Crosstalk Matrix for Initial Evaluation of the Ten-Dye and Filter Set[a]

	Mean emission intensity (arbitrary units)									
Filter sets (nm)[b]	CB	AMCA	LY	FITC	PE	Red613	PerCP	Red670	APC	Cy5
365/425	107	100	8							
410/530	8	3	47	16						
485/530			6	176	11					
485/575				43	1,000	102		40		
485/630					225	347		31		
485/660					75	162	416	556	5	
590/660					102	234	32	724	154	29
660/LP700[c]							14	52	39	40

[a]Ten dyes were measured in eight channels to evaluate their potential spectral resolution. All data are from streptavidin-conjugated fluorochromes bound to latex microbeads at saturation (for fluorochrome abbreviations, see Materials and Methods). Fluorescence intensities are expressed in arbitrary units relative to a value of 1,000 attributed to the fluorescence of PE at 575 nm. Columns indicate the fluorescence intensities of each probe recorded in all channels; rows record all dye emissions occurring through particular filter sets.
[b]Filter sets are indicated by the center wavelengths of excitation and emission bandpasses.
[c]This is a long-pass filter.

which was recorded without additional source attenuation. Fading was reversible in part during the period following exposure, when the beam was shifted out from the preparation. Another way to reduce the influence of fading on spectral crosstalk values was to use the same sequence of illumination, beginning with the lowest energy at 660 nm and ending with the highest one at 365 nm.

Precision and linearity of spectral compensation. Microbead suspensions coated with different concentrations of biotinylated IgG1 were labeled with the various dyes to obtain wide ranges of fluorescence intensities. They were visualized sequentially with each one of the filter combinations (Table 2). For each fluorochrome microbead, emissions measured with its own filter set were plotted against the emissions obtained with the other filter sets. An example of the spectral contaminations of PE-labeled beads is shown in Figure 3. The slopes of these curves indicate the percentage crosstalk of PE in other relevant emission filters, i.e., 630 nm for Red613 and 660 nm for PerCP/Red670. Similar measures were made for all possible dye and filter combinations. Accurate quantitative measurement of fluorescence intensities was checked by the stability of these crosstalk values when measured on a number of different fields. The CV of such repeated measurements was less than 6% for percentage crosstalk values above 10 and less than 9% for values between 3 and 10. The independence of spectral crosstalk from emission intensity values was ascertained by the linearity of these curves (correlation coefficient >0.90 in all cases). The accuracy of background and

Table 4
Spectral Crosstalk Matrix for the Selected Filter and Seven-Dye Set[a]

Filter sets (nm)[b]	Lamp output (adjustment factor)[c]	Mean emission intensity (arbitrary units) AMCA	LY	FITC	PE	Red613	PerCP	APC
365/425	0.46	46.6 (100)	3.6 (6)					
410/530	1.26	4.2 (9)	58.7 (100)	20.6 (17)				
485/530	0.70		4.3 (7)	123.3 (100)	8.1 (8)			
485/575	0.10			4.3 (3)	100 (100)	10.2 (8)		
485/630	0.35				78.9 (79)	121.5 (100)		
485/660	0.30				22.6 (23)	48.7 (40)	124.9 (100)	4 (1)
660/LP700[d]	2.90						40.4 (32)	111.7 (100)

[a]Data are from latex microbeads labeled at saturation with seven streptavidin-conjugated fluorochromes selected for multiparameter image cytometry (for fluorochrome abbreviations, see Materials and Methods). Spectral crosstalk values were measured under adaptation of lamp output to the brightness of each dye. Fluorescence intensities are expressed in arbitrary units relative to a value of 100 attributed to the fluorescence of PE at 575 nm. Columns indicate the fluorescence intensities of each probe recorded in all channels; rows record all dye emissions occurring through each of the filter sets. Figures in parentheses indicate percentage crosstalk values of each dye.
[b]Filter sets are indicated by the center wavelengths of excitation and emission bandpasses.
[c]Compared with data in Table 3, lamp output was multiplied by the factors indicated for each channel.
[d]This is a long-pass filter.

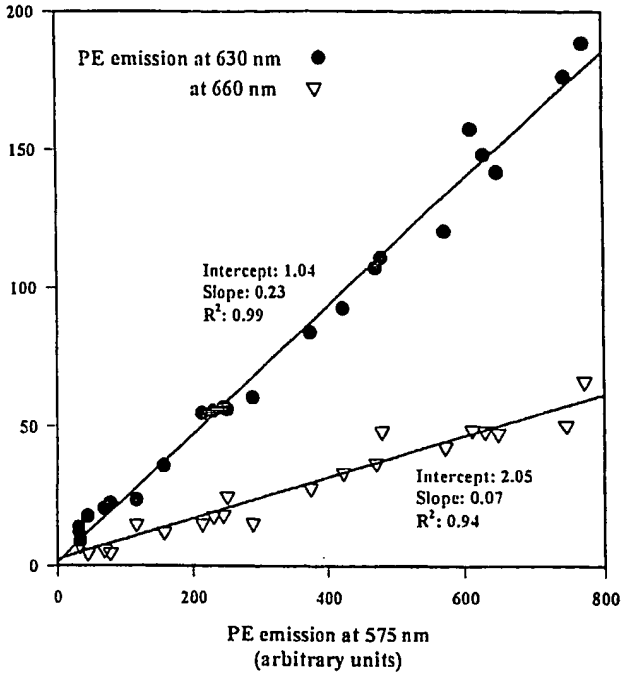

FIG. 3. Emission intensities of streptavidin-conjugated R-phycoerythrin (PE) bound to latex microbeads under three different filter sets. Latex particles were labeled with PE under various concentrations of biotinylated immunoglobulin (IgG)1 in order to obtain a wide range of fluorescence intensities. Excitation was at 485 nm in each case. Overlapping PE emissions in the PE-Texas red tandem Red613 and peridinin-chlorophyll-protein (PerCP) channels at 630 and 660 nm, respectively, are plotted vs. PE emission at 575 nm. Each point represents the mean gray level (in arbitrary units) of a single particle. The slopes of these curves correspond to the crosstalk values 225 and 75 listed in Table 3.

shading corrections was established by the intercept of the regression lines with the axis origin.

Accuracy of spectral compensation. To verify that correction of spectral overlap did not cause some particles to be classified erroneously as positive or negative, two series of experiments were made. First, each of seven bead suspensions was labeled with one different dye; then, all seven suspensions were mixed (Fig. 4A). The statistics of positive and negative objects, which are listed in Table 5, demonstrate the ability of the image cytometry system to detect accurately seven distinct probes in one field and to correct spectral contaminations originating from any of these probes. The legend to Figure 4A illustrates how the algorithm described in the Appendix performs the spectral correction. Second, two suspensions were labeled with several dyes: The first suspension was labeled with AMCA, FITC, Red613, and APC, and the second suspension was labeled with LY, PE, and PerCP. The two suspensions were then mixed together (Fig. 4B). Signal intensities corresponding to presence or absence of labeling are shown in Table 6. These data show that it is possible to identify multiple-labeled objects of different types on the same field. In addition, the S.D. of emission intensities recorded for negative objects provide a basis for determining the detection limit for each label.

DISCUSSION

This paper describes a methodology that is aimed at optimizing multiple immunophenotyping and applying it to the detection and measurement of seven SA-fluorochrome probes bound to latex microbeads. The main points of the strategy were 1) preliminary selection of fluorochromes and filter/mirror sets based on spectrofluorometric data of streptavidin-fluorochrome solutions, 2) determination of the spectral crosstalk matrix from cytometric measurement of labeled microbeads and reselection of separable probes, 3) modulation of source intensity in order to harmonize the brightness of images, 4) spectral compensation based on a set of linear equations derived from the modified crosstalk matrix, and 5)

Table 5
Digital Fluorescence Imaging of Latex Microbeads Single Labeled With Seven Streptavidin-Conjugated Dyes[a]

	Mean emission intensity (arbitrary units)				
	Positive objects			Negative objects	
Fluorochrome[b]	Mean	Min	Max	Mean	S.D.
AMCA	46.5	22	89	1.0	1.8
LY	59.0	42	95	−0.5	1.8
FITC	123.9	97	178	1.2	2.2
PE	100.9	39	138	0.2	0.8
Red613	120.5	79	153	0.3	2.1
PerCP	126.8	88	189	1.6	2.4
APC	113.1	65	177	1.3	2.9

[a]Data from several fields (n = 87 beads) of the preparation depicted in Figure 4A were listed out in each fluorescence channel after background and spectral overlap correction. Each object was considered to be positive in the fluorescence channel where it had the highest gray level and was considered to be negative in the six others. Statistics of positive and negative beads are indicated for each type of labeling. *P* values for unpaired t tests between positive and negative objects were <0.0001 for all fluorochromes.
[b]For fluorochrome abbreviations, see Materials and Methods.

Table 6
Digital Fluorescence Imaging of Latex Microbeads Multiple Labeled With Seven Streptavidin-Conjugated Dyes[a]

	Mean emission intensity (arbitrary units)				
	Positive objects			Negative objects	
Fluorochrome[b]	Mean	Min	Max	Mean	S.D.
AMCA	34.2	27	50	1.5	0.9
LY	30.0	24	39	1.5	2.3
FITC	59.0	48	73	0.1	0.6
PE	47.6	36	62	1.4	1.6
Red613	56.6	44	78	−1.1	1.4
PerCP	58.5	43	75	3.7	2.2
APC	26.0	19	38	−2.8	1.4

[a]Data from several fields (n = 30) of the preparation illustrated in Figure 4B were listed out in each fluorescence channel. Each object could be attributed to one of two populations: The first one was labeled with AMCA, FITC, Red613, and APC and was negative for LY, PE, and PerCP, and the second one was labeled with LY, PE, and PerCP but was negative for AMCA, FITC, Red613, and APC. Statistics of emission values corresponding to presence or absence of labeling are indicated in each probe channel. *P* values for unpaired t tests between positive and negative objects were <0.0001 for all fluorochromes.
[b]For fluorochrome abbreviations, see Materials and Methods.

evaluation of accuracy and sensitivity of the procedure. The strategy was iterative, because steps 2–5 were repeated until satisfactory discrimination was achieved.

Because, when "n" markers are used simultaneously, the number of potential combinations of positive and negative probe emissions is 2^n, it may be necessary to analyze a few hundred cells to get significant population statistics. The maximum number of analyzable particles in one field is about 50 with the ×40 objective used in this study; therefore, several fields of the same preparation would have to be collected in a seven- parameter phenotyping study. To rapidly analyze larger samples, the wider field of view provided by a reducing camera lens would be required. For instance, a ×0.63 ocular lens could multiply both the light gathering power of the optical system and the viewing area by a factor of about 2.5.

To ensure the stability of spectral compensation, the ISIT camera was used at constant gain, a procedure that considerably limited its interscene dynamic range. Keeping the fluorescence of the seven probes on scale was made possible by tuning the excitation intensity with two polarizers for each dye collection. However, although excitation adjustment can extend the interscene dynamic range of the camera, this procedure does not affect its capacity to record widely variable emission intensities within a given field, i.e., its intrascene dynamic range (38). In cases where, in a given field, strongly labeled cells emit a saturating nonquantifiable signal (whereas some others give a barely detectable one), two methods may be proposed to extend the usable dynamic range available with the ISIT camera, whose range is intrinsically limited by its eight-bit gray level scale. First, two images recorded at low and high illumination may be merged after calculating a corrected intensity on each cell. Second, a double recording can be dispensed with if a camera with a much wider dynamic range, such as a 12–16 bit CCD camera, is used.

Based on the strategy developed in this study and the available equipment, we found that seven SA fluorochromes can be discriminated and measured. However, this is by no means the maximal number of probes that can be used in the context of immunophenotyping applications. For instance, utilization of Cy7 would only require a camera with sufficient sensitivity in the infrared region (31). Detection of propidium iodide-stained cells using a 360/620 filter set may be indispensable to ensure viability of the cells to be immunophenotyped and would be compatible with the dye combination used in this study. Europium chelates also have large Stokes shifts (29) and may have applications in the future.

Previous works have reported successful discrimination of seven probes by combinatorial analysis. These studies used probes labeled with mixtures of three dyes that were combined to provide up to seven color combinations (20,25). Combinatorial analysis is applicable when a given site (for instance, a chromosomal segment) will bind only one specific fluorescent probe. In the techniques described here, each cellular marker has to be labeled with a distinct fluorochrome, because a given cellular target may possibly be occupied by several antigens.

The application of the methodology developed here to cell labeling has several implications. It would be advisable to conjugate the weakest fluorophores to the antibodies that are expected to yield the strongest labeling. The amplification provided by indirect labeling via biotin-streptavidin or antiisotype can also help to increase the detection of these less intense fluorophores. Cellular preparations can also show a higher background in the

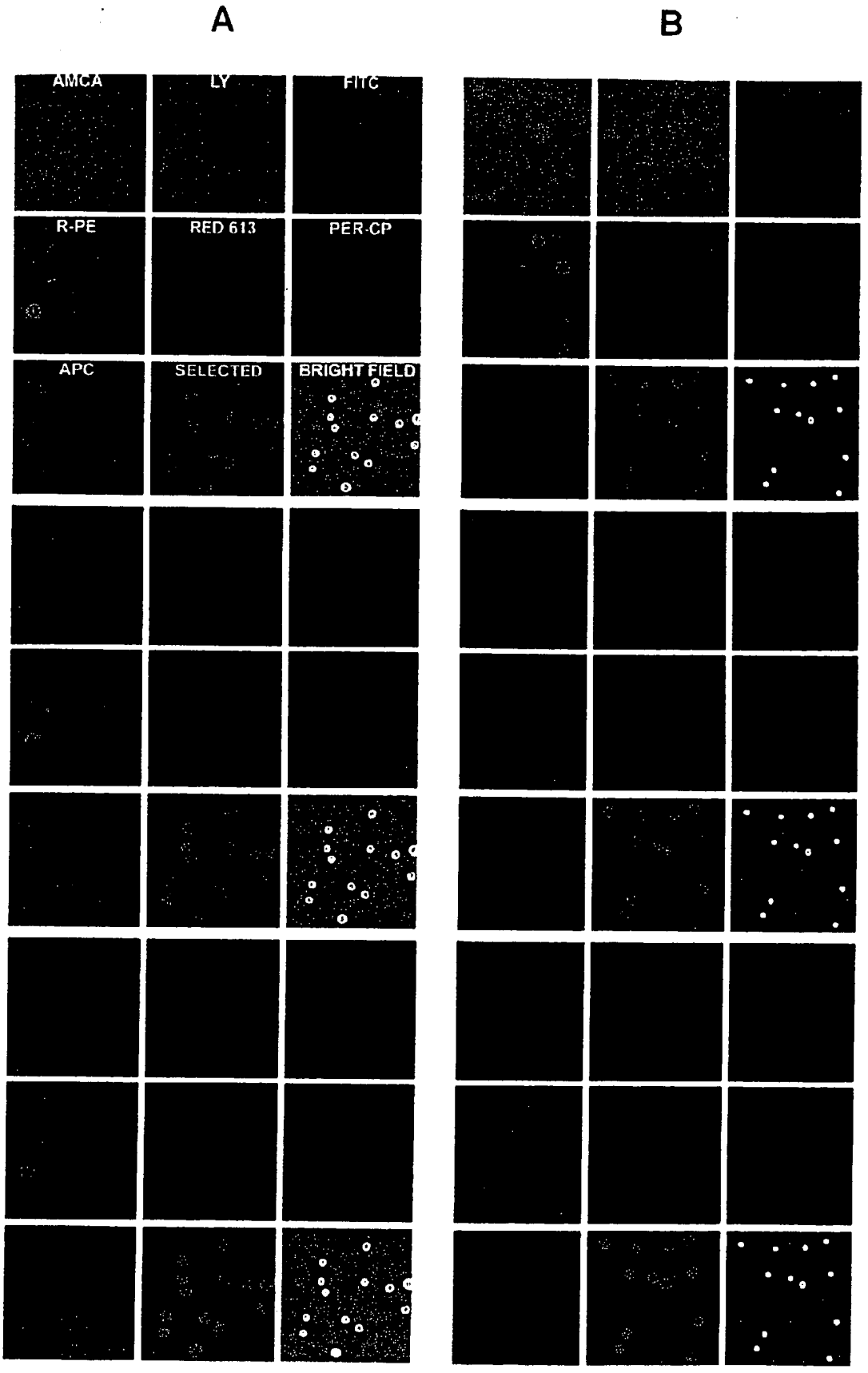

FIG. 4. (Legend on facing page)

AMCA, LY, and FITC channels because of autofluorescence. Unless the latter can be eliminated from the cell preparation, it must be corrected by using digital imaging methods, such as subtracting the mean fluorescence ±3 S.D. determined on a negative control preparation. An additional consideration is the large variability of cellular antigen density, which may span up to four orders of magnitude of fluorescence intensity. Therefore, the wide dynamic range provided by CCD cameras may be required in order to permit accurate quantification and correction of cellular signals.

Multiple parameter phenotyping will certainly help to assess complex phenotypes in a single-labeling procedure, especially when one or several probes are expected to react with a small percentage of the population of interest. In such cases, it may be difficult to find unequivocal relationships from a series of two- or three-color labelings. This technique can also prove to be useful for the phenotyping of small samples, such as hemopoietic colonies in the early stages of their development. In many cases, the need for large cell numbers by flow cytometers may lead to a severe limitation of the numbers of usable probes. Image cytometry, however, requires only a few thousand cells to perform such an analysis.

ACKNOWLEDGMENTS

The authors are grateful to Prof. C. Houssier and his team from the Department of Physical Chemistry, University of Liege, for excellent assistance in spectrofluorometric measurements and M.Y. de Menten (Zeiss, Brussels, Belgium) for help in the development of the IBAS programs.

FIG. 4. Multiparameter fluorescence imaging of seven fluorochromes bound to latex microbeads. Image processing of a relevant field of two distinct preparations are displayed. A: Seven bead suspensions were labeled with aminomethylcoumarin acetate (AMCA), Lucifer yellow (LY), fluorescein isothiocyanate (FITC), PE, Red613, PerCP, or allophycocyanin (APC), and aliquots were mixed in a single suspension. B: Microbeads were stained either with AMCA, FITC, Red613, and APC or with LY, PE, and PerCP and were mixed in a single suspension. For each field, seven fluorescent images were acquired by using the filter sets depicted in Figure 2. They are indicated by their corresponding fluorochromes. The image termed "selected" represents the binary masks of objects to be quantified. The brightfield transmitted image is also displayed. All sets of nine images are displayed in the same order. Image processing is depicted in three steps. Fluorescent images are displayed without image correction (top set of nine squares), after background and shading correction (middle set of nine squares), and after the COMBINE procedures used to correct for spectral overlaps (bottom set of nine squares). To illustrate the algorithm used by the spectral compensation routine, consider the middle and bottom sets in A. The equations for correction of PE, Red613, PerCP, and APC emissions are Equations 4–7 in the Appendix. Note that the three $PE^+/Red613^+$ cells shown in the middle set are found to be $PE^+/Red613^-$ in the corrected bottom set, because Equation 5 for Red613 contains a term (−0.85 Em4) that subtracts a fraction of measured PE emission from measured Red613 emission. Similarly, a $PE^-/Red613^+/PerCP^+$ cell in the middle set is found to be positive for Red613 only after correction (bottom set). Of the several cells in the PerCP and APC images in the middle set, three are $PerCP^+$, and two are APC^+ after correction in the bottom set.

LITERATURE CITED

1. Afar B, Merrill J, Clark EA: Detection of lymphocyte subsets using three-color/single-laser flow cytometry and the fluorescent dye peridinin chlorophyll-a protein. J Clin Immunol 11:254–261, 1991.
2. Aubry JP, Durand I, De Paoli P, Banchereau J: 7-Amino-4-methylcoumarin-3-acetic acid-conjugated streptavidin permits simultaneous flow cytometry analysis of either three cell surface antigens or one cell surface antigen as a function of RNA and DNA content. J Immunol Methods 128:39–49, 1990.
3. Bagwell CB, Adams EG: Fluorescence spectral overlap compensation for any number of flow cytometry parameters. Ann NY Acad Sci 677:167–184, 1993.
4. Beavis AJ, Pennline KJ: Simultaneous measurement of five cell surface antigens by five-colour immunofluorescence. Cytometry 15: 371–376, 1994.
5. Campana D, Pui CH: Detection of minimal residual disease in acute leukemia: Methodologic advances and clinical significance. Blood 85:1416–1434, 1995.
6. Champaneria S, Swenarchuk LE, Anderson MJ: Increases in pericellular proteolysis at developing neuromuscular junctions in culture. Dev Biol 149:261–277, 1992.
7. Civin CI: Human monomyeloid cell membrane antigens. Exp Hematol 18:461–467, 1990.
8. DeBiasio R, Bright GR, Ernst LA, Waggoner AS, Taylor DL: Five-parameter fluorescence imaging: Wound healing of living Swiss 3T3 cells. J Cell Biol 105:1613–1622, 1987.
9. Debili N, Issaad C, Massé JM, Guichard J, Katz A, Breton-Gorius J, Vainchenker W: Expression of CD34 and platelet glycoproteins during human megakaryocytic differentiation. Blood 80:3022–3035, 1992.
10. Glazer AN, Stryer L: Phycofluor probes. Trends Biochem Sci 9:423–427, 1984.
11. Gore SD, Kastan MB, Civin CI: Normal human bone marrow precursors that express terminal deoxynucleotidyl transferase include T-cell precursors and possible lymphoid stem cells. Blood 77:1681–1690, 1991.
12. Greimers R: Contribution à l'analyse multiparamétrique par cytométrie en flux de lymphomes radio-induits chez la souris et de tumeurs solides humaines. Doctoral Thesis, University of Liège. Presses Universitaires, Liège, 1993, pp 1–441.
13. Greimers R, Trebak M, Moutschen M, Jacobs N, Boniver J: Improved four-color flow cytometry method using fluo-3 and a triple immunofluorescence for analysis of intracellular calcium ion ($[Ca^{2+}]i$) fluxes among mice lymph node B and T lymphocyte subsets. Cytometry 23:205–217, 1996.
14. Haugland RP, Larison KD: Handbook of Fluorescent Probes and Research Chemicals. Molecular Probes, Inc., Eugene, OR, 1992, pp 1–421.
15. Inoue S: Imaging of unresolved objects, superresolution, and precision of distance measurements with videomicroscopy. Methods Cell Biol 30:85–112, 1989.
16. Khalfan H, Abuknesha R, Rand-Weaver M, Price RG, Robinson D: Aminomethyl coumarin acetic acid: A new fluorescent labeling agent for proteins. Histochem J 18:497–499, 1986.
17. Loken MR, Shah VO, Dattilio KL, Civin CI: Flow cytometric analysis of human bone marrow. II. Normal B lymphocyte development. Blood 70:1316–1324, 1987.
18. Mayani H, Lansdorp PM: Thy-1 expression is linked to functional properties of primitive hematopoietic progenitor cells from human umbilical cord blood. Blood 83:2410–2417, 1994.
19. Mehrotra B, George TI, Kavanau K, Avet-Loiseau H, Moore D II, Willman CL, Slovak ML, Atwater S, Head DR, Pallavicini MG: Cytogenetically aberrant cells in the stem cell compartment ($CD34^+lin^-$) in acute myeloid leukemia. Blood 86:1139–1147, 1995.
20. Nederlof PM, van der Flier S, Wiegant J, Raap AK, Tanke HJ, Ploem JS, van der Ploeg M: Multiple fluorescence in situ hybridization. Cytometry 11:126–131, 1990.
21. Oi VT, Glazer AN, Stryer L: Fluorescent phycobiliprotein conjugates for analyses of cells and molecules. J Cell Biol 93:981–986, 1982.
22. Olweus J, Lund-Johansen F, Terstappen LWMM: CD64/FcγRI is a

granulo-monocytic lineage marker on CD34+ hematopoietic progenitor cells. Blood 85:2402–2413, 1995.
23. Paulus JM, Grosdent JC, de Menten Y: Four wavelength immunofluorescence using an image analyzer: A preliminary evaluation. Seventh Meeting Belgian Hematol Soc, Brussels, pg. 52, 1992 (abstract).
24. Perkampus HH: UV-VIS Spectroscopy and Its Applications. Springer-Verlag, Berlin, 1992, pp 1–244.
25. Ried T, Baldini A, Rand TC, Ward DC: Simultaneous visualization of seven different DNA probes by in situ hybridization using combinatorial fluorescence and digital imaging microscopy. Proc Natl Acad Sci USA 89:1388–1392, 1992.
26. Riggs JL, Seiwald RJ, Burckhalter JH, Downs CM, Metcalf TG: Isothiocyanate compounds as fluorescent labeling agents for immune serum. Am J Pathol 34:1081–1097, 1958.
27. Roederer M, Bigos M, Nozaki T, Stovel RT, Parks DR, Herzenberg LA: Heterogeneous calcium flux in peripheral T cell subsets revealed by five-color flow cytometry using log-ratio circuitry. Cytometry 21: 187–196, 1995.
28. Schlossman SF, Boumsell L, Gilks W, Harlan JM, Kishimoto T, Morimoto C, Ritz J, Shaw S, Silverstein R, Springer T, Tedder TF, Todd RF: Leucocyte Typing V: White Cell Differentiation Antigens. Oxford University Press, Oxford, 1995, pp 1–2044.
29. Seveus L, Väisälä M, Syrjänen S, Sandberg M, Kuusisto A, Harju R, Salo J, Hemmilä I, Kojola H, Soini E: Time-resolved fluorescence imaging of europium chelate label in immunohistochemistry and in situ hybridization. Cytometry 13:329–338, 1992.
30. Shapiro HM: Practical Flow Cytometry, 3rd Ed. Wiley-Liss, New York, 1995, p 214.
31. Southwick PL, Ernst LA, Tauriello EW, Parker SR, Mujumdar RB, Mujumdar SR, Clever HA, Waggoner AS: Cyanine dye labeling reagents—Carboxymethylindocyanine succinimidyl esters. Cytometry 11:418–430, 1990.
32. Srour EF, Leemhuis T, Jenski L, Redmond R, Jansen J: Cytolytic activity of human natural killer cell subpopulations isolated by four-color immunofluorescence flow cytometric cell sorting. Cytometry 11:442–446, 1990.
33. Srour EF, Leemhuis T, Brandt JE, vanBesien K, Hoffman R: Simultaneous use of rhodamine 123, phycoerythrin, Texas red, and allophycocyanin for the isolation of human hematopoietic progenitor cells. Cytometry 12:179–183, 1991.
34. Steen HB: Characteristics of flow cytometers. In: Flow Cytometry and Sorting, Melamed MR, Lindmo T, Mendelsohn ML (eds). Wiley-Liss, New York, 1990, pp 11–25.
35. Stewart WW: Lucifer dyes—Highly fluorescent dyes for biological tracing. Nature 292:17–21, 1981.
36. Terstappen LWMM, Huang S, Safford M, Lansdorp PM, Loken MR: Sequential generations of hematopoietic colonies derived from single nonlineage-committed CD34+, CD38− progenitor cells. Blood 77:1218–1227, 1991.
37. Titus JA, Haugland RP, Sharrow SO, Segal DM: Texas red, a hydrophilic, red-emitting fluorophore for use with fluorescein in dual parameter flow microfluorometric and fluorescence microscopic studies. J Immunol Methods 50:193–204, 1982.
38. Waggoner A, DeBiasio R, Conrad P, Bright GR, Ernst L, Ryan K, Nederlof M, Taylor D: Multiple spectral parameter imaging. Methods Cell Biol 30:449–478, 1989.
39. Waggoner AS, Ernst LA, Chen CH, Rechtenwald DJ: A new fluorescent antibody label for three-color flow cytometry with a single laser. Ann NY Acad Sci 677:185–193, 1993.
40. Whitaker JE, Haugland RP, Moore PL, Hewitt PC, Reese M, Haugland RP: Cascade blue derivatives: Water soluble, reactive, blue emission dyes evaluated as fluorescent labels and tracers. Ann Biochem 198: 119–130, 1991.

APPENDIX: CALCULATION OF SPECTRAL OVERLAP CORRECTIONS

The determination of the fluorescence intensities of each of the seven dyes requires the resolution of a set of seven linear equations in seven unknowns and is an application of multicomponent analysis (24). The *unknowns* (F1 . . . F7) are the actual emissions of AMCA, LY, FITC, PE, Red613, PerCP, and APC, respectively, when cleared of crosstalk from the others. The *measures* (Em1 . . . Em7) are the total emissions originating from any fluorochrome and detected within each filter set (see Table 4). The system can be written as the following equations:

$$Em1 = F1 + b1\,F2 + c1\,F3 + d1\,F4 + e1\,F5 + f1\,F6 + g1\,F7$$
$$Em2 = a1\,F1 + F2 + c2\,F3 + d2\,F4 + e2\,F5 + f2\,F6 + g2\,F7$$
$$Em3 = a2\,F1 + b2\,F2 + F3 + d3\,F4 + e3\,F5 + f3\,F6 + g3\,F7$$
$$Em4 = a3\,F1 + b3\,F2 + c3\,F3 + F4 + e4\,F5 + f4\,F6 + g4\,F7$$
$$Em5 = a4\,F1 + b4\,F2 + c4\,F3 + d4\,F4 + F5 + f5\,F6 + g5\,F7$$
$$Em6 = a5\,F1 + b5\,F2 + c5\,F3 + d5\,F4 + e5\,F5 + F6 + g6\,F7$$
$$Em7 = a6\,F1 + b6\,F2 + c6\,F3 + d6\,F4 + e6\,F5 + f6\,F6 + F7$$

The coefficients a1–a6 . . . g1–g6 represent the crosstalks of a particular dye in adjacent filter sets. For instance, d3 is the fraction of the fluorescence of FITC at 530 nm that can be detected at 575 nm. These coefficients were measured experimentally under standardized conditions of lamp intensity and exposure times, and many of these were found to be equal to zero (see Table 4). By using percentage crosstalk values, the set of equations can be rewritten in a much simpler way:

$$Em1 = F1 + 0.06\,F2$$
$$Em2 = 0.09\,F1 + F2 + 0.17\,F3$$
$$Em3 = 0.07\,F2 + F3 + 0.08\,F4$$
$$Em4 = 0.03\,F3 + F4 + 0.08\,F5$$
$$Em5 = 0.79\,F4 + F5$$
$$Em6 = 0.23\,F4 + 0.40\,F5 + F6 + 0.01\,F7$$
$$Em7 = 0.32\,F6 + F7$$

or in matrix form:

$$\begin{bmatrix} 1 & 0.06 & 0 & 0 & 0 & 0 & 0 \\ 0.09 & 1 & 0.17 & 0 & 0 & 0 & 0 \\ 0 & 0.07 & 1 & 0.08 & 0 & 0 & 0 \\ 0 & 0 & 0.03 & 1 & 0.08 & 0 & 0 \\ 0 & 0 & 0 & 0.79 & 1 & 0 & 0 \\ 0 & 0 & 0 & 0.23 & 0.40 & 1 & 0.01 \\ 0 & 0 & 0 & 0 & 0 & 0.32 & 1 \end{bmatrix} \cdot \begin{bmatrix} F1 \\ F2 \\ F3 \\ F4 \\ F5 \\ F6 \\ F7 \end{bmatrix} = \begin{bmatrix} Em1 \\ Em2 \\ Em3 \\ Em4 \\ Em5 \\ Em6 \\ Em7 \end{bmatrix}$$

which in simplified form is written:

$$A \cdot X = Y.$$

The unknowns of vector X can be solved by the equation:

$$X = A^{(-1)} \cdot Y,$$

where $A^{(-1)}$ is the following inversed matrix of A.

1.01	−0.06	0.01	0	0	0	0
−0.09	1.02	−0.17	0.01	0	0	0
0	−0.07	1.02	−0.09	0	0	0
0	0	−0.03	1.07	−0.09	0	0
0	0	0.03	−0.85	1.07	0	0
0	0	0	0.10	−0.41	1	−0.01
0	0	0	−0.03	0.13	−0.33	1

The inverse matrix can be written as a set of linear equations, which can be resolved by image processing to yield corrected emission intensity values.

$$F1 = 1.01\,Em1 - 0.06\,Em2 + 0.01\,Em3 \quad (1)$$

$$F2 = -0.09\,Em1 + 1.02\,Em2 - 0.17\,Em3 + 0.01\,Em4 \quad (2)$$

$$F3 = -0.07\,Em2 + 1.02\,Em3 - 0.09\,Em4 \quad (3)$$

$$F4 = -0.03\,Em3 + 1.07\,Em4 - 0.09\,Em5 \quad (4)$$

$$F5 = 0.03\,Em3 - 0.85\,Em4 + 1.07\,Em5 \quad (5)$$

$$F6 = 0.10\,Em4 - 0.41\,Em5 + Em6 - 0.01\,Em7 \quad (6)$$

$$F7 = -0.03\,Em4 + 0.13\,Em5 - 0.33\,Em6 + Em7 \quad (7)$$

Biotechnol. Prog. 2000, 16, 800–802

Using the Microcyte Flow Cytometer To Monitor Cell Number, Viability, and Apoptosis in Mammalian Cell Culture

Claire L. Harding,[†,§] David R. Lloyd,[‡] Caroline M. McFarlane,[‡] and Mohamed Al-Rubeai*[,‡]

Aber Instruments Ltd., Science Park, Aberystwyth, SY23 3AH, U.K., and Centre for Bioprocess Engineering, School of Chemical Engineering, University of Birmingham, Edgbaston, Birmingham, B15 2TT, U.K.

The Microcyte is a novel, portable flow cytometer based on diode laser technology whose use has been established for yeast and bacterial analysis. We present data that demonstrate its suitability for routine mammalian cell counting and viability determination. To extend its range of applications in the field of animal cell culture biotechnology, a test to determine the number of apoptotic cells present has been developed for use with the instrument. Apoptosis was induced in hybridoma cell cultures by treatment with camptothecin. Apoptotic cells were labeled with biotinylated Annexin V and then visualized using a streptavidin−allophycocyanin conjugate. Their numbers were counted, and the cell size of the apoptotic cell population was determined using the Microcyte.

Introduction

Flow cytometry is a valuable research tool but is generally considered unsuitable for routine monitoring of mammalian cell cultures, because until now instrumentation was large and expensive and required considerable operator training. The introduction of the Microcyte, a portable and robust flow cytometer, whose use has been described for monitoring yeast and bacterial cultures (*1*), means that these restrictions can now be overcome. The Microcyte uses a diode laser as the light source, greatly reducing the size and weight of the instrument compared with conventional flow cytometers. Sheath fluid can be recirculated internally and the instrument can be powered by a battery pack, making it fully portable. The Microcyte also possesses a novel optical arrangement, housed within a solid aluminum block for stability, negating the need for laser alignment before use. The red diode laser produces light at 635 nm, and the instrument operates at a constant controlled sample uptake rate, so that absolute counts per volume of sample are obtained.

This work aims to demonstrate the utility of the Microcyte for count and viability determination in mammalian cell cultures and to show that the Microcyte can reliably detect apoptotic cells. Comparison will be made with the traditional mammalian cell analysis method.

Materials and Methods

Cells and Culture Conditions. Stirred batch suspension cultures of a mouse:mouse hybridoma cell line, TB/C3.pEF, producing antibody against human IgG (*2*) were grown at 37 °C in RPMI 1640 (Gibco, U.K.) supplemented with 5% fetal calf serum (Sigma, U.K.). At regular intervals, 2 mL samples were taken off line for cell density and viability determination by flow cytometric and traditional methods. For apoptosis induction, cells were grown as above, and recently passaged cells were redistributed to 2 × 40 mL cultures. Camptothecin (Sigma, U.K.) was then added (3 μM final concentration) to one culture to induce apoptosis while the second remained untreated as a control.

Cell Density and Viability Determination. For manual counting cells were stained with trypan blue (Sigma, U.K.; final concentration 0.25%). Triplicate samples were examined; the number of viable and dead cells were counted using an Improved Neubar counting chamber and binocular microscope at 200× magnification. The total cell density (cells/mL) and viability (number of viable cells as a percentage of the total number of cells) were calculated.

For flow cytometric analysis, cells were stained with the cell membrane impermeable fluorescent nucleic acid stain TO-PRO-3 iodide (Molecular Probes, OR, U.S.; final concentration 0.1 μM). Fluorescent TO-PRO-3 stained cells were defined as dead cells, while the nonfluorescent cells that excluded TO-PRO-3 were deemed viable. Triplicate samples were analyzed using the Microcyte flow cytometer (Aber Instruments Ltd., U.K.). After appropriate gating to exclude culture debris, total cell density (cells/mL) was determined directly by the instrument using the forward scatter light signal. Culture viability (number of dead cells as a percentage of the total number of cells) was calculated from these values. Gating, or selecting the region of interest, is accomplished by using a cursor to define a line representing that region on a single parameter histogram, analogous to setting a linear analysis gate on a Coulter instrument. Gates were set empirically, as would be the case with a conventional cytometer. Redefining regions of interest between samples was possible but was not usually found to be necessary.

Detecting and Analyzing Apoptotic Cells. The Annexin V binding assay (*3*, *4* and reviewed by *5*) was adapted for use with the Microcyte. A TACS Annexin V-biotin apoptosis detection kit (Genzyme, U.K.) was used in accordance with the manufacturer's instructions.

[†] Aber Instruments Ltd.

[‡] University of Birmingham.

[§] Current address; New Product Development Unit, Bio Products Laboratory, Dagger Lane, Elstree, Hertfordshire, WD6 3BX, U.K.

10.1021/bp0000813 CCC: $19.00
Published on Web 08/25/2000

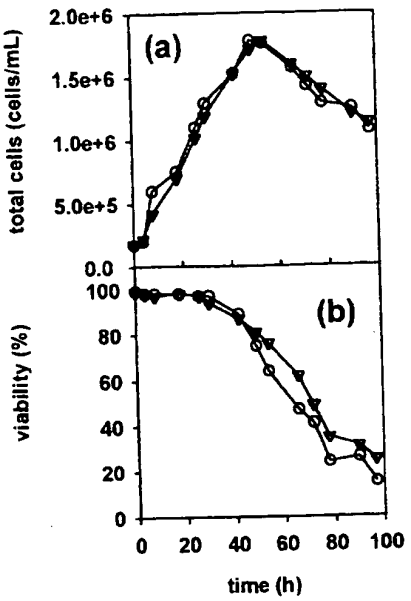

Figure 1. (a) Total cell density and (b) viability measured by traditional microscopic methods (○) and Microcyte (▽) during hybridoma batch culture.

Briefly, cells were harvested by centrifugation (200 × *g*, ambient temperature, 5 min) and washed in 500 μL of cold phosphate buffered saline. The cell pellet was resuspended in 100 μL of incubation reagent containing biotin-conjugated Annexin-V and dark incubated for 15 min. Cells were then recentrifuged and resuspended in 100 μL of binding buffer (10 mM HEPES/NaOH, 150 mM NaCl, 5 mM KCl, 1 mM $MgCl_2$, 1.8 mM $CaCl_2$, pH 7.4) containing 2 μg/mL streptavidin-conjugated allophycocyanin (Molecular Probes, OR). After 15 min of dark incubation, samples were diluted to 500 μL with binding buffer, mixed thoroughly, and analyzed immediately.

Results

Cell Count and Viability. The batch culture growth curves produced by Microcyte and the traditional manual method were essentially identical and are shown in Figure 1a. However, the point to point curve generated from the Microcyte data was smoother than that generated by the manual method, possibly indicating greater error in the manual method. From the same batch culture, the two methods gave viability curves with similar profiles (Figure 1b). However, when viability was below approximately 80% the results obtained by Microcyte were consistently higher than those obtained by microscopy. Measuring cell density and viability, as described in the Methods section, took 15 min, compared with 1−2 min for the Microcyte method.

Detecting Apoptosis. The Microcyte was also used to monitor the onset of apoptosis. In the untreated culture, spontaneous apoptosis occurred at very low levels and barely changed during the experiment (Figure 2 a). However in the camptothecin-treated culture, the proportion of apoptotic cells started to rise dramatically after 4 h, with all cells apoptotic by 9 h (Figure 2b). The Microcyte's speed of analysis allowed cultures to be sampled frequently, thus pinpointing the onset of apoptosis (between 3.5 and 4 h) much more accurately. At the same time the size (as forward scatter) of the apoptotic subpopulation was recorded (Figure 3 a−d), demonstrating that apoptotic cells are smaller than the general cell population.

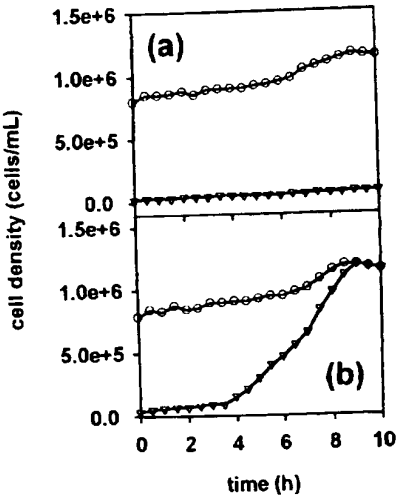

Figure 2. Time course of apoptosis development in (a) untreated control and (b) camptothecin-treated hybridoma cultures, showing total cells (○) and apoptotic cells (▽).

Discussion

The cell density profiles produced by the manual and Microcyte methods were essentially the same. This was also true for the first part of the viability profiles, although after approximately 40 h culture, when viability was below about 80%, that determined by Microcyte was consistently greater than that determined by the traditional manual method. This apparent discrepancy between the two methods may be simply explained by the use of different stains. It is generally accepted that different exclusion stains exhibit different properties; a dying cell membrane may be permeable to one stain but not to another. Fortunately, since this difference only occurs in lower viability samples, it is unlikely to be of any great practical importance for process monitoring applications; production processes are normally terminated before viability drops as low as 80%.

It has already been shown that cell counting and viability determination by flow cytometry (using a Coulter EPICS Elite) can be applied to animal cell production process monitoring. Flow cytometry is more precise, as accurate, less subjective, and much faster than using the traditional manual microscopic method (*6*). One major drawback to routine flow cytometric analysis that was found by the previous work was simply the cost, scale, and complexity of the instrument upon which the measurements were made. This work demonstrates that the smaller, cheaper, simpler, portable Microcyte flow cytometer is able to address these problems. The Microcyte performs as well as the manual method for determining cell density and cell viability, just as did the large research instrument, while maintaining all the inherent advantages of speed, accuracy, precision, and objectivity (no interobserver variation) shown by the research instrument.

Thus the Microcyte is an ideal tool for culture monitoring in a bioprocess production environment, because for this purpose it displays three major practical advantages over a conventional flow cytometer. It is portable and so can be taken to the point of sample. Its robust simplicity means that it can be used by production staff with minimal training or supervision. Its cost is of the same order as a quality microscope that would needed for the alternative traditional method.

Much research has been done in the life sciences to try to understand the mechanisms of apoptotic cell death

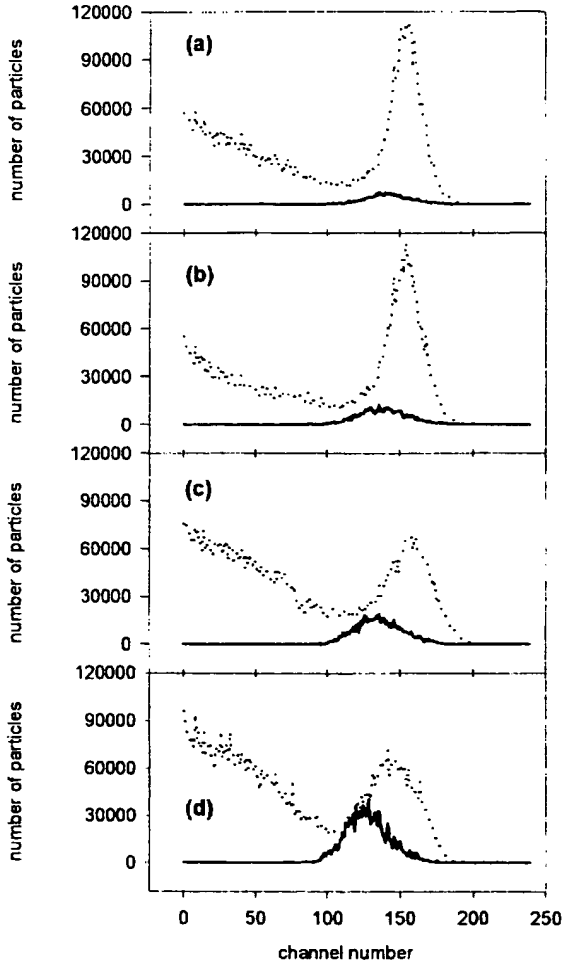

Figure 3. Cell size distribution (as forward scatter) of the total population ····· (dotted upper line) and the apoptotic fraction —— (solid lower line) (a) before induction and (b) 3 h, (c) 6 h, and (d) 9 h after addition of camptothecin to induce apoptosis.

and the signals that trigger apoptosis. In animal cell biotechnology it is accepted that, when subjected to massive stress, cells die by necrosis, although when subjected to less severe but perhaps more sustained stress, cells initiate and ultimately die by the apoptotic pathway. Some of these less severe stresses include accumulation of toxic metabolites, nutrient depletion, hypoxia, and hyperoxia (*7*). Recent work by Pläsier et al. (*8*) has shown that measuring apoptosis in hybridoma cultures using Annexin-V in conjunction with propidium iodide to detect necrosis and followed by flow cytometry, manual microscopy, or image analysis microscopy all give very similar results. Because the Microcyte is only equipped with a single fluorescence detection channel, directly comparable results could not be obtained; there was no means to distinguish between early apoptotic and late apoptotic (necrotic) cells. However, the Microcyte was able to detect apoptotic cells (early and late apoptotic (necrotic) together), and the time course of their appearance was similar to that of previous work (*8*). The size of cells in the apoptotic subpopulation was compared with that of the general population and showed, in agreement with other work (*4, 8*) as well as the general consensus, that the cell size of the apoptotic population is smaller than that of "normal" cells. However, there is marked overlap in the size distribution of the two populations. Having demonstrated the Microcyte's ability to count annexin-V stained cells allows the possibility of using the instrument to monitor cell surface markers or intracellular epitopes during culture processes and correlate these observations with cell size.

Furthermore, there remains the prospect of automated on line process monitoring and control. In 1999, Zhao et al. (*9*) published work demonstrating an on line process monitoring and control system for yeast and bacterial fermentations based upon an Ortho Cytofluorograf flow cytometer. The latter have not been available or even supported by the manufacturers for several years. However, the Microcyte offers an excellent alternative that could easily be incorporated into a similar bioproduction process management system for animal (or yeast) cells.

Conclusions

The Microcyte is an excellent tool for the rapid and accurate enumeration of animal cells in suspension culture. It provides similar results to the established manual counting and staining techniques, with advantages of reduced intra- and inter-observer variation, increased speed of analysis, and the ability to count large numbers of cells, leading to more statistically valid results. The Microcyte can also be used to detect apoptotic cells, using the annexin-V affinity assay, not only at the high levels seen when apoptosis is induced but also when apoptosis is at low background levels in a healthy culture. The Microcyte is an ideal flow cytometer for use in process biotechnology applications and has the potential for inclusion, as the core analytical unit, in an on line process monitoring/control strategy.

Acknowledgment

The authors thank the DTI Teaching Company Scheme (C.L.H.) & BBSRC (D.R.L.) for financial support.

References and Notes

(1) Davey, H. M.; Kell, D. B. Flow cytometry and cell sorting of heterogeneous microbial populations: the importance of single-cell analyses. *Microbiol. Rev.* **1996**, *60*, 641–696.
(2) Simpson, N.; Milner, A. N.; Al-Rubeai, M. Prevention of hybridoma cell death by bcl-2 during sub-optimal culture conditions. *Biotechnol. Bioeng.* **1997**, *54*, 1–16.
(3) Vermes, I.; Haanen, C.; Steffensnakken, H.; Reutelingsperger, C. A novel assay for apoptosis—flow cytometric detection of phosphatidylserine expression on early apoptotic cells using fluorescein-labeled Annexin V. *J. Immunol. Methods* **1995**, *184*, 39–51.
(4) Ishaque, A.; Al-Rubeai, M. Use of intracellular pH and Annexin-V flow cytometric assays to monitor apoptosis and its suppression by *bcl-2* overexpression in hybridoma cell culture. *J. Immunol. Methods* **1998**, *221*, 43–57.
(5) van Engeland, M.; Nieland, L. J. W.; Ramaekers, F. C. S.; Schutte, B.; Reutelingsperger, C. P. M. Annexin V-affinity assay: A review of an apoptosis detection system based on phosphatidylserine exposure. *Cytometry* **1998**, *31*, 1–9.
(6) Al-Rubeai, M.; Welzenbach, K.; Lloyd, D. R.; Emery, A. N. A rapid method for evaluation of cell number and viability by flow cytometry. *Cytotechnology* **1997**, *24*, 161–168.
(7) Singh, R. P.; Finka, G.; Emery, A. N.; Al-Rubeai, M. Apoptosis and its control in cell culture systems. *Cytotechnology* **1997**, *23*, 87–93.
(8) Pläsier, B.; Lloyd, D. R.; Paul, G. C.; Thomas, C. R.; Al-Rubeai, M. Automatic image analysis for quantification of apoptosis in animal cell culture by Annexin-V affinity assay. *J. Immunol. Methods* **1999**, *229*, 81–95.
(9) Zhao, R.; Natarajan, A.; Srienc, F. A flow injection flow cytometry system for on-line monitoring of bioreactors. *Biotechnol. Bioeng.* **1999**, *62*, 609–617.

Accepted for publication July 17, 2000.

BP0000813

Cytometry 29:328–339 (1997)

8 Color, 10-Parameter Flow Cytometry to Elucidate Complex Leukocyte Heterogeneity

Mario Roederer,* Stephen De Rosa, Rachel Gerstein, Michael Anderson, Martin Bigos, Richard Stovel, Thomas Nozaki, David Parks, Leonore Herzenberg, and Leonard Herzenberg

Department of Genetics, Stanford University, Stanford, California

Received 7 April 1997; Accepted 11 July 1997

We developed the chemistry, instrumentation, and software technologies needed to measure, simultaneously and independently, eight different fluorescent molecules on individual cells. Conjugation of these fluorochromes to monoclonal antibodies is straightforward; all immunofluorescence staining is accomplished with direct stains only. We built a hybrid flow cytometer with eight fluorescence detectors and two light scatter channels, with excitation provided by three spatially separated laser beams emitting at 407 nm, 488 nm, and 595 nm. The fluorescence compensation required to make the data orthogonal is of sufficient complexity that it cannot be performed manually; thus, we use software to compensate the data post hoc, based on data collected from singly stained compensation control samples. In this report, we evaluate the 8 color staining technology. Of the seven fluorochromes other than fluorescein, six have a useful brightness at least as great as fluorescein. Three of the fluorochromes (phycoerythrin, allophycocyanin, and the Cy5 resonance energy tandem of phycoerythrin) are considerably brighter than fluorescein and are useful for detecting antigens expressed at low levels. Finally, we show the power and utility of the 8 color, 10-parameter technology using staining experiments on both human and murine immune systems. Cytometry 29:328–339, 1997. © 1997 Wiley-Liss, Inc.

Key terms: resonance energy transfer; spectral compensation; T cell subsets; pre-B cells; pro-B cells; bone marrow leukocytes; GFP (green fluorescent protein)

The advantages of multicolor flow cytometric analysis are well known; over the past 25 years there has been a continuous desire to analyze simultaneously more parameters of each cell. Nonetheless, developments to increase the number of useful parameters has stagnated over the past 15 years—4 color analysis (first performed in the early 1980s) has been supplanted by 5 color analysis in very few laboratories. Three reasons contribute to this relative lack of progress: 1) the low number of available fluorochrome conjugates; 2) the extreme limitations imposed by extant software, which did not allow for the complex types of analyses and postcollection compensation required by high-order multiparameter collections; and 3) the difficulty in adapting commercial flow cytometry platforms to analyze simultaneously more than four or five fluorescences.

The need for more than 5 color analysis has become very clear. The complexity of the immune system is such that identification of phenotypically (and functionally) homogeneous subsets requires the simultaneous measurement of at least six cell surface antigens. Using peripheral human T cells as an example: a minimum of three antigens are required to identify uniquely T cell lineages (i.e., CD3, CD4, and CD8; all three must be present to resolve the $CD4^-CD8^-$ and $CD4^+CD8^+$ from the single positive T cells). In addition, another three colors are required to identify functionally distinct memory lineages (e.g., CD45RA, CD62L, and CD11a). Unique identification of B cell subsets requires at least three measurements and NK subsets require at least four. Unless subsets are uniquely identified by appropriate multiple markers, comparative functional studies between individuals will be artefactually affected by a differential (and unknown) representation of unresolved, functionally distinct subsets.

High-order multiparametric analysis is also required to combine functional and phenotypic analyses. For instance, the assignment of "Th1" or "Th2" to a particular cell (or subset) requires not only the phenotypic markers noted above, but also two additional measurements devoted to

Contract grant sponsor: National Institutes of Health; Contract grant numbers: LM-04836, AI-31770, CA-42509.

Portions of these data were reported in the 1996 ISAC meeting, Rimini, Italy, and the 1997 AAI meeting, San Francisco, CA.

*Correspondence to: Mario Roederer, Beckman B011, Stanford, CA 94305-5125.

E-mail: roederer@darwin.stanford.edu

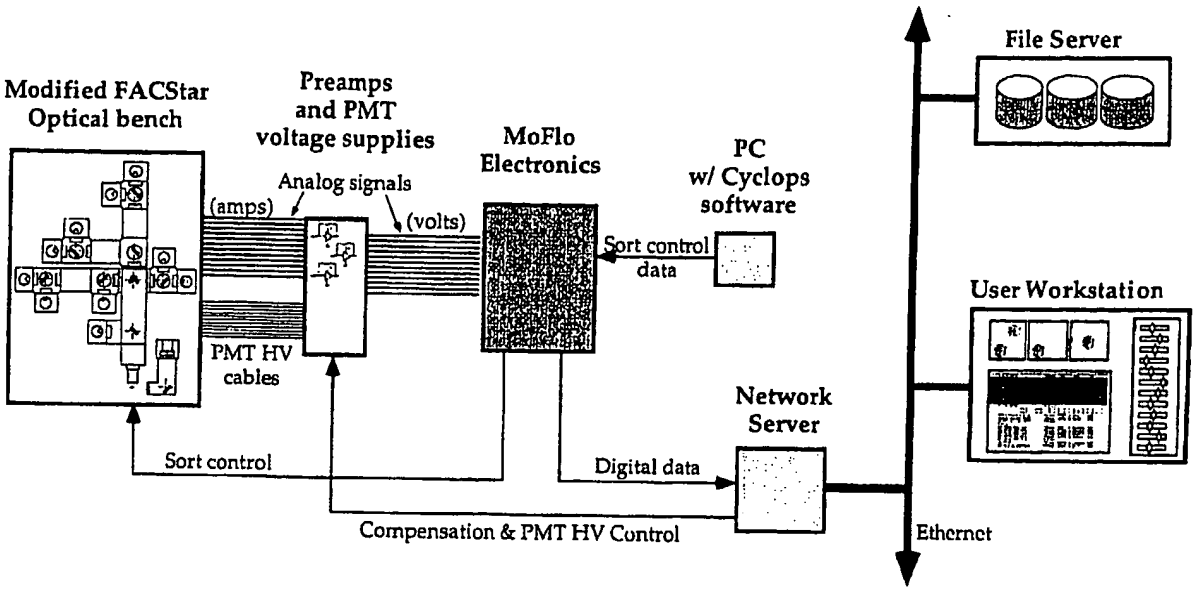

FIG. 1. Diagrammatic layout of the 10-parameter flow cytometer. Our system is a hybrid consisting of a FACStarPlus bench, Cytomation electronics, and our own electronics and computer system. The Cytomation electronics is used to amplify (log or linear mode), evaluate, and digitize the signals from the PMTs. Electronics designed and built in our laboratory allows the computer to set PMT voltages, interface the bench signals to the MoFlo electronics, and handle instrument-to-computer data transfers.

intracellular quantitation of cytokines such as interleukin-4 and γ-interferon. In addition, it is useful to combine other functional measurements such as cell cycle analysis or apoptosis with complete phenotypic identification of cell subsets.

In the past two years, we have made significant advances in the hardware, software, and reagents for flow cytometry analysis. As a result, we have increased our capabilities to the level of seven colors (plus forward and side scatter) with two-laser excitation and eight colors with three-laser excitation. Our reagents include the more commonly-used fluorochromes fluorescein (FITC), phycoerythrin (PE), Cy5PE, Texas Red (TR), allophycocyanin (APC), and Cascade Blue (CB); to this combination we added two relatively new tandem dyes: Cy7PE and Cy7APC. The development and spectral properties of Cy7 tandem dyes for use in immunoglobulin staining experiments has been previously described (23).

Here we describe in detail the development of the 8 color, 10-parameter system. We compare the eight different fluorochrome reagents for use in immunostaining experiments and describe the complex compensation required for analysis. Finally, we show two examples of 8 color staining to demonstrate the power of this approach in dissecting the immune system.

MATERIALS AND METHODS

Antibody Reagents

Unconjugated antibodies were either purified from ascities or tissue culture supernatant or obtained in concentrated form from PharMingen (San Diego, CA). Conjugated antibodies were prepared in our laboratory with the exception of FITC CD8 and Cy5PE RA3-6B2 (PharMingen). Conjugation of all reagents was done as previously described (21).

Cell Staining and Analysis

Human PBMC or mouse bone marrow leukocytes were obtained by standard methods; at least 10^6 cells were used for each stain. Cells were stained on ice for 15 min with fluorescently conjugated antibodies and then washed three times with staining medium (biotin, flavin-deficient RPMI supplemented with 4% newborn calf serum and 0.02% sodium azide). For murine cell analysis, 1 mM EDTA was added to the staining medium to reduce cellular aggregation. Flow cytometry analyses were performed on a hybrid instrument (as described below). Data were collected by FACS-Desk (18) and compensated and analyzed using FlowJo (TreeStar, San Carlos, CA).

Cytometry Hardware

The instrumentation used for this report is a hybrid (Fig. 1). The main optics bench was derived from a FACStarPlus (Becton Dickinson, San Jose, CA). MoFlo electronics (Cytomation, Fort Collins, CO) was used to collect and digitize the data from the ten parameters at 12-bit resolution. Finally, our own electronics was used to control the photomultiplier tube (PMT) voltages, interface the signals from the bench to the MoFlo, and to handle data transfers to the VAX system.

Laser excitation was provided by two primary lasers and a dye head. A 5-watt Innova-90 Argon ion laser (Coherent, Sunnyvale, CA) was run in "all lines" mode; a dichroic mirror near the output of this laser reflected part of the

shorter wavelength light (mostly 488 nm) away from the main beam. This beam was filtered to pass only 488 nm light and was steered into the first laser position below the nozzle. The remainder of the "all lines" beam was directed into a dye head tuned to 595 nm; the output of the dye laser was steered into the third laser position. Finally, the second laser on the bench was a UV-violet-enhanced Innova-300 Krypton laser (Coherent) operating with 407 nm emission steered into the second laser position below the nozzle. Thus, three parallel but non-colinear beams were used for excitation. Appropriate delay timing was set to collect fluorescences arising from each of the three different excitation beams.

The optical layout was an extension of the standard 5 color layout available on the FACStarPlus (Fig. 2). The primary difference is the presence of three separate apertures, two of which are backed by 45° mirrors, at the focus of the fluorescence signals (Fig. 2, inset). This assembly directs each of the three laser emissions to a different set of photomultiplier tubes (PMTs). The dichroic and interference filters used for each channel are shown in Figure 2. Note the presence of additional relay lenses used in the extended optical layout to ensure proper delivery of light onto the detectors. We used standard PMTs for all detectors except the Cy7 channels, for which we used Hamamatsu R3896 (red-sensitive) PMTs. The R3896 PMTs gave an increase in signal-to-noise of approximately two-fold for Cy7 signals; we found no benefit from using an R636 Gallium-arsenide PMT (data not shown).

RESULTS

Fluorochrome Reagents

The ability to measure simultaneously many different fluorescences on individual cells has two requirements: multiple non-colinear excitation beams and a spectral resolution which minimizes emission overlap. We minimized detector cross-talk by appropriate selection of dyes and excitation conditions (including laser wavelength and power). In addition, we selected optimal optical filters to minimize signal overlap without losing too much intensity (Fig. 2).

Fluorochromes chosen for immunophenotyping should be as "bright" as possible in order to achieve the greatest sensitivity. Brightness, as used in this report, is an empirical quantity that relates not only physical properties, including the extinction coefficient, lifetime, and quantum efficiency of a given fluor, but also detector sensitivity, background noise, and autofluorescence contributions from cellular material in that portion of the spectrum. To date, fluorescein (FITC), Texas Red (TR), the phycobiliproteins phycoerythrin (PE) and allophycocyanin (APC), and a resonance energy transfer tandem dye Cy5PE have been commonly used in flow cytometry analyses because they are bright and spectrally well-resolved dyes. To extend the capabilities to 8 color analyses, we chose the new tandems Cy7PE and Cy7APC (23), because these are well resolved spectrally from the others. In addition, we use Cascade Blue (CB) excited by a 407 nm Krypton laser line (manuscript in preparation).

The fluorescence spectra of these eight dyes are shown in Figure 3. For any given excitation beam, the fluorescence emissions are well resolved, such that interference filters that selectively pass the primary fluorescence of interest can be easily chosen.

Useful Brightness of Fluorochromes

In order to assess the brightness (and utility) of these fluorochromes, direct conjugates of anti-human CD8 were conjugated with each. Saturating concentrations of the antibodies were used to stain human PBMC in combination with either FITC CD3 or CB CD3; the histograms corresponding to the $CD3^+$ cells from each of the stained samples are shown in Figure 4. Each of the fluorescent dyes resolves CD8 T cells from other T cells very well; all of the dyes except CB appear to separate these cells from $CD8^-$ T cells as well or better than FITC. Indeed, quantification of the peak positions shows that this is the case, as shown in Table 1.

The useful brightness of a conjugate can be evaluated in several ways. The simplest is the ratio of the median signals of the positive to unstained cells. However, this does not take into account that the distribution of the negative population may be quite different for different spectral regions. Indeed, for the far-red channels there are so few photoelectrons (on the order of 1–10) collected for unstained cells that the absolute signal level of these cells is not necessarily meaningful.

Another measure of useful brightness is the resolution of the two peaks (positive and negative). In Table 1, this value was calculated by normalizing the signal level of the positively stained cells to a measure of the variation in the negative population. This is a value akin to a "t-score"; it is related to how well separated the peaks actually are and makes no assumptions about absolute signal levels for either the stained or unstained populations. For our instrument, the amount of signal in the far-red channels is so low for the APC and Cy7APC channels that the "autofluorescence" peak actually bifurcates—into events with zero or one photoelectrons. This increases the peak width of the autofluorescent cells, thereby significantly reducing this particular brightness estimator for APC and Cy7APC.

A final measure of brightness also takes into account the general "stickiness" of the reagents—the tendency of some fluorochrome conjugates to display increased nonspecific binding to cells (Table 1). To quantify this value, the signal level of the positively stained cells is compared to the signal level of $CD8^-$ cells present in the stained population—cells that have autofluorescence equivalent to the $CD8^+$ lymphocytes (data not shown).

All three measures of brightness give the same general order when comparing reagents (the main difference being the absolute value of the computed brightness). CB is the least bright, being about one-third the brightness of FITC. FITC, Cy7PE, and Cy7APC are roughly equivalent. TR is about threefold brighter than FITC (but suffers from unusually high background binding commonly observed for TR reagents). Finally, PE, Cy5PE, and APC are 5–10 times as bright as FITC. This order is consistent with the

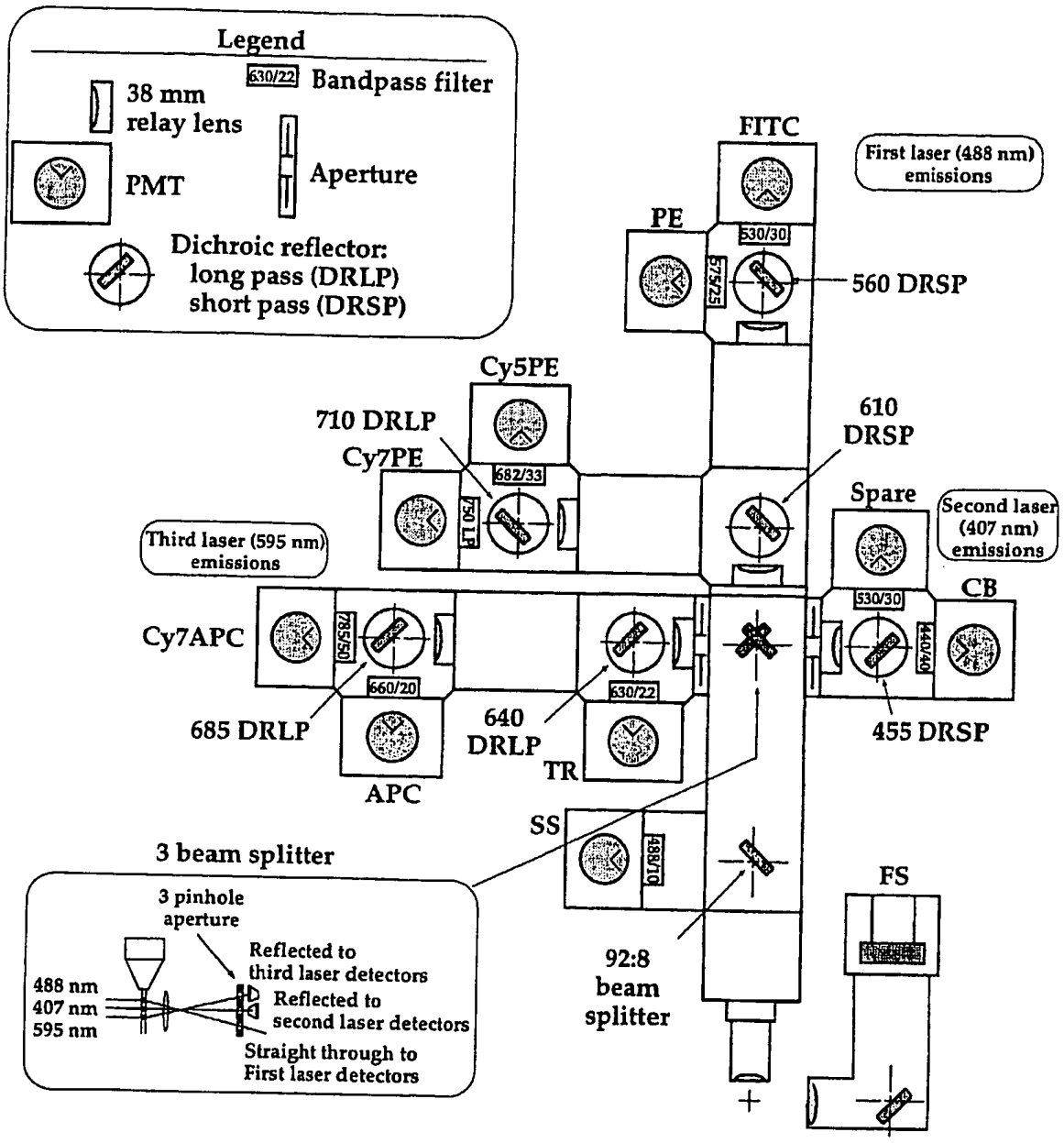

FIG. 2. Diagrammatic layout of the optics. The block diagram shows the layout of the 11 detectors on the modified FACStarPlus bench. For this report, the "UV2" detector was not used. The Cy5PE and Cy7PE detectors are rotated 90 degrees out of the plane of the optics block in order to accommodate the orientation of the beam splitter (all splitter blocks have "left-hand" turns only). Thus, the cable connections for these two PMTs point away (backwards) from the nozzle area, whereas all other PMT connections point up. Note the presence of additional relay lenses in the extended fluorescence pathways in order to refocus the emission on the detectors. The side scatter beam splitter is achromatic, and reflects 8% of incident light. The "three-beam" splitter has two mirrors mounted at right angles to deflect the second and third laser emissions; the first laser emission passes underneath the mirrors.

brightest reagents being farther red in the spectrum; however, for the Cy7 tandems the transfer efficiency as well as the detector efficiency at >750 nm is dropping off sufficiently that their brightness is less than APC or Cy5PE.

Complex Compensation

While the fluorescence emissions are well-resolved, there is still considerable spectral overlap. In other words, most of the fluorochromes show appreciable signal in more than one detector. The exception to this is CB, which has no emission components from the detectors for 488 nm or 595 nm excited dyes; likewise, none of the other fluors is excited by the 407 nm line to emit at 440 nm.

To correct for the spectral overlap, compensation must be performed to make the measured values orthogonal.

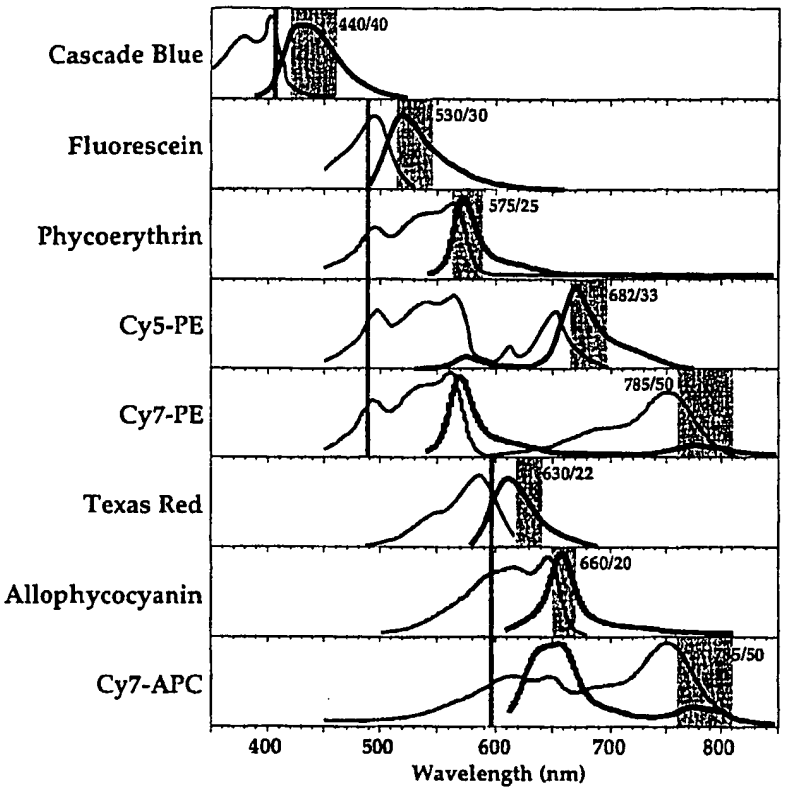

FIG. 3. Fluorescence spectra of the eight fluorochromes used in these studies. Excitation and emission spectra for the fluorochromes are uncorrected for detector sensitivity. Thus, the relatively low peak in the far-red region for the Cy7 emissions is not necessarily reflective of the brightness of Cy7 reagents. In addition, the extremely low autofluorescence of cells in the far red increases the signal-to-noise for these reagents. The wavelengths of the excitation beams are shown by vertical bars; the bandpass region for each detector is shown as a shaded region.

Because of the great number of different corrections required for the 8 color system, compensation cannot be performed manually using pair-wise controls, as are found on commercial flow cytometers; complete compensation requires computer assistance. Because we currently do not have such a system designed into the electronics, we collect uncompensated signal values and use software to compensate the data at the time of analysis (24).

To compensate a sample properly, we singly stain cells with representative reagents for each fluorochrome. These singly stained samples are collected and analyzed; the compensation matrix can be computed from the resulting fluorescence measured in all of the channels. A typical spillover (spectral overlap) matrix is given in Table 2. The values in this table directly show the amount of fluorescence from any given fluorochrome detected in the other channels.

In order to perform the compensation, this matrix must be inverted to generate the compensation coefficient matrix (24). The matrix resulting from this operation in Table 2 is shown in Table 3; the values in Table 3 are those that correspond most closely to the compensation values that are set on typical instruments performing pair-wise compensation between two fluorescence channels.

Application to Murine Leukocyte Staining

We explored the utility of using eight colors for flow cytometric phenotyping of mouse bone marrow cells. In this case, in place of FITC-conjugated monoclonal antibodies we used the FITC detector to detect BEX GFP (blue-excited Green Fluorescent Protein) expression (2). Unlike other GFPs which lack the S65T mutation, BEX is primarily excited at 488 nm, with little excitation at 407 nm. Thus, the krypton laser can be used for the excitation of CB without significant compensation with BEX (manuscript in preparation). The mice from which we obtained bone marrow expresses BEX as a transgene driven by an H2-K (class I MHC) promoter; expression of the BEX GFP is closely correlated with H2-K expression in individual cells (manuscript in preparation). The transgenic mice used in these experiments have detectable BEX expression in 20–40% of hematopoietic cells. As transgenic mice derived from a separate founder exhibit GFP transgene expression in almost all bone marrow cells (RG, unpublished results), the lower frequency of BEX expression in these animals is most likely due to a position effect at the transgene insertion site.

In order to investigate transgene expression within the B cell lineage, we stained cells with the panel of seven monoclonals indicated in Figure 5 (IgM, CD22, IgD, B220, Gr-1, AA4.1, and HSA). In addition, the dye propidium iodide was used to detect and exclude dead cells (6) in the Cy5PE channel, without significant overlap with B220-Cy5PE-positive cells. Figure 5 shows that a significant fraction of Gr-1$^+$ cells (a marker of the myeloid/granulocyte lineage (8)) express GFP. Smaller fractions of B220-

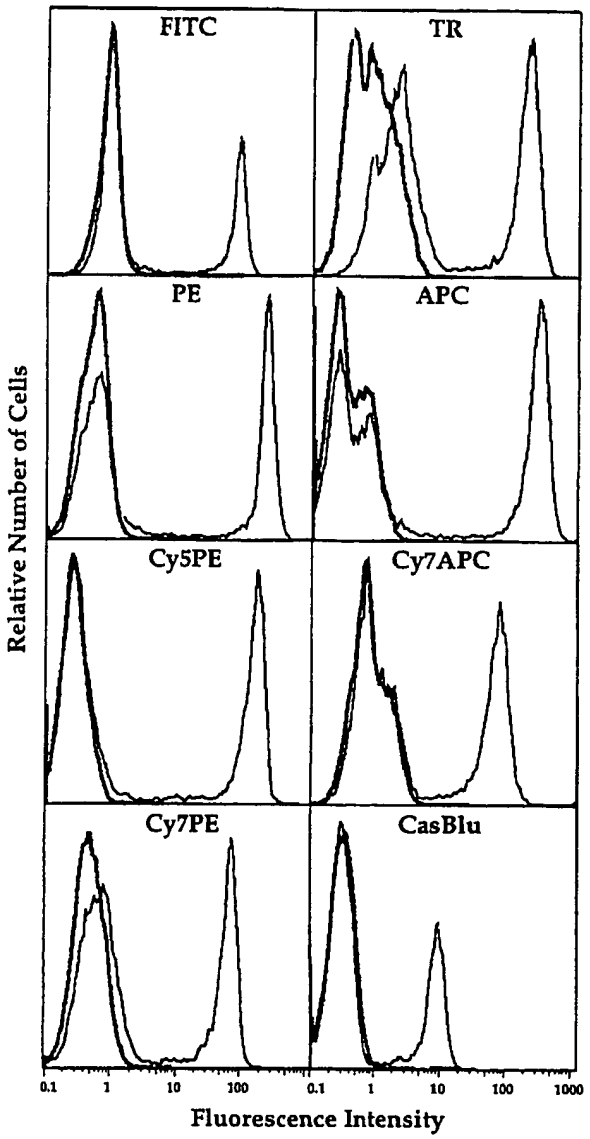

FIG. 4. Comparison of the staining properties of anti-CD8 conjugated to each of the eight fluorochromes. Anti-CD8 was conjugated to each of the fluorochromes; the reagent was used in saturating titers to stain human peripheral blood mononuclear cells. In addition, CD3 was used as a counterstain in each sample; for CB CD8, FITC CD3 was used; for all others, CB CD3 was used. Histograms of unstained lymphocytes and the stained CD3$^+$ T cells are overlaid for each detector. The relative brightness of each of these reagents, computed in various ways, is shown in Table 1.

Table 1
Relative Brightness of the Eight Probes in Immunofluorescence Staining

		Relative brightness,[2] with respect to:		
Fluor	%CD8+[1]	AF[3]	Background[4]	AF width[5]
CB	36.0	0.3	0.3	0.2
FITC	37.1	1.0	1.0	1.0
PE	37.0	4.6	4.5	3.0
Cy5PE	36.3	6.2	6.2	4.3
Cy7PE	36.0	1.4	1.1	0.8
TR	38.1	2.8	1.2	0.8
APC	36.5	9.2	8.7	2.2
Cy7APC	35.2	0.9	0.9	0.4

[1]Cells were stained with saturating concentrations of CD8 conjugated to the listed fluorescent probes. The value is the percent of lymphocytes staining brightly for CD8 (CD8 T cells).

[2]Brightness values are normalized separately for each column, such that FITC = 1.0.

[3]Median fluorescence of CD8+ cells divided by the median of unstained lymphocytes (i.e., autofluorescence, or AF).

[4]Median fluorescence of CD8+ cells divided by the median of CD8− lymphocytes in the same tube (NK cells, dimly staining for CD8, were excluded).

[5]Median fluorescence of CD8+ cells divided by twice the difference of the 67th and 50th percentiles of the unstained population (i.e., normalizing by the approximate standard deviation of the autofluorescence of unstained cells).

positive cells (a B lineage marker in most cases (3, 25)) and Gr-1-negative, B220-negative cells express BEX. Gr-1$^+$ cells were excluded from further analyses; this gating eliminates not only Gr-1$^+$ cells but also the most autofluorescent cells as well as cells that express Fc receptors. Examination of all B220$^+$ Gr-1-negative cells for the expression of IgD and IgM (data not shown) revealed three distinct populations of cells. For convenience, we define IgD$^+$ IgM$^{lo/+}$ cells as Population I, IgM$^+$ IgD$^{-/lo}$ (i.e., IgM$^+$, IgD non- or low-expressing cells) as Population II, and IgD$^-$ IgM$^-$ as Population III. Pop. I cells, expected to be composed predominantly of mature, recirculating B cells (1, 9) have the largest percent of GFP-positive cells. Pop. II, with fewer GFP$^+$ cells, contains immature IgM$^+$ cells (10). Pop. III, which includes mostly pro- and pre-B cells, has the least proportion of GFP$^+$ cells.

These B220$^+$ Gr-1$^-$ populations can be defined more specifically using the monoclonal AA4.1 (Fig. 5). AA4.1 has been used previously to isolate stem cells (11), B cell precursors (5, 14-17), and "bi-potent" progenitors that can differentiate along myeloid or B cell pathways (4, 12). It has also been noted that approximately 50% of cells with surface Ig in bone marrow were AA4.1$^+$ (15). Using a bright APC conjugate of AA4.1, it is evident that most B220-positive bone marrow cells express AA4.1. Figure 5 further shows that Populations I, II, and III are differentially represented among AA4.1$^+$ and AA4.1$^-$ cells; most notably, Pop. I is significantly underrepresented in AA4.1$^+$ cells. Finally, for each of the fine subsets plots of CD22 expression (a mature B cell marker) versus GFP expression and CD22 versus HSA expression (mature B cells are HSA intermediate, low, or null) are shown.

In AA4.1$^+$ cells, Pop. I is comprised mostly of CD22$^+$ HSA ^{lo} cells (in agreement with (7)). Pop. II is uniformly CD22$^{-/lo}$ and HSA$^+$. Pop. III, which includes mostly pro- and pre-B cells is CD22$^{-/lo}$ and is mostly HSA$^+$ (Fr. B,C,D using Hardy's criteria (10)). Pop. III includes some HSA$^{-/lo}$ cells (predominantly Fr. A (10, 14)).

In contrast, AA4.1$^-$ cells have a striking increase in the fraction of IgD$^+$ cells. Note that Pop. II is reduced among

Table 2
Spillover Matrix for 8 Color Flow Cytometry[a]

	Emission detector						
	First laser (488 nm)				Second laser (595 nm)		
Fluor	FITC	PE	Cy5PE	Cy7PE	TR	APC	Cy7APC
FITC	100	20	1.6	0.26	0.00	0.00	0.24
PE	1.6	100	8.8	1.1	0.60	0.02	0.28
Cy5PE	0.59	8.4	100	16	0.61	5.3	7.8
Cy7PE	1.4	25	3.8	100	0.22	0.03	12
TR	0.08	0.13	1.3	0.19	100	6.1	6.6
APC	0.11	0.06	6.6	1.1	28	100	76
Cy7APC	0.20	0.10	0.33	1.6	2.9	3.5	100

[a]Cascade Blue is not in the table since there is no spillover between its detector and any other detector. Each value is the percentage of a fluor's signal measured in each of the seven detectors (normalized to 100% for the fluor's cognate detector). Thus, each row is related to the emission spectrum of the fluor named in the first column—given the particular combination of lasers, filters, detectors, and PMT voltages used in our instrument. For instance, the measured signal voltage of FITC in the PE channel is 20.2% of that in the FITC channel. Since FITC is not excited by the dye laser, there is essentially no contribution of FITC fluorescence into the second laser channels. The top left and bottom right quadrants of the matrix represent intra-laser spillovers; the other two quadrants are inter-laser spillovers.

Table 3
Compensation Matrix for 8 Color Flow Cytometry[a]

	Emission channel						
	First laser (488 nm)				Second laser (595 nm)		
Fluor	FITC	PE	Cy5PE	Cy7PE	TR	APC	Cy7APC
FITC		20	−0.14	0.07	−0.13	0.00	0.19
PE	1.6		8.8	−0.39	0.69	−0.49	−0.03
Cy5PE	0.28	4.2		16	−1.0	5.3	1.8
Cy7PE	0.97	25	1.6		−0.16	−0.47	12
TR	0.06	0.05	0.85	−0.05		6.0	2.0
APC	−0.08	−0.25	6.1	−1.2	26		74
Cy7APC	0.18	−0.35	0.05	1.6	2.0	3.4	

[a]Each value represents the compensation percentage value that needs to be applied to the original signals in order to achieve orthogonality. These values are equivalent to the compensation that would be selected on an instrument capable of performing the pairwise compensations on all parameters (i.e., the FITC − %PE compensation value is 20.%). Those values greater (in absolute magnitude) than 0.4% can be considered significant compensations; all others are shaded. These values were obtained by inverting, normalizing, and negating the spillover coefficient matrix in Table 2; the diagonal elements were removed for clarity.

$AA4.1^-$ cells and the distribution of IgM of this population is quite different from that of $AA4.1^+$ cells. For example, in the $AA4.1^-$ compartment, Pop. III includes significantly more $CD22^+$, GFP^+, and HSA^- cells than are found among $AA4.1^+$ Pop. III cells. $AA4.1^+B220^+$ IgM^-IgD^- cells are almost exclusively pro- and pre-B cells (data not shown). The corresponding $AA4.1^-B220^+IgM^-IgD^-$ population may contain mature B cells, as suggested by the presence of $CD22^+$ GFP^+ HSA^- cells. We have yet to examine these cells for surface IgG. It will be interesting to determine if memory or antibody secreting cells reside within this population.

Application to Human Leukocyte Staining

Peripheral T cells in the human can be divided into a number of subsets. These divisions can be classified as lineages (e.g., CD4 versus CD8 T cells) and as differentiation stages (e.g., naive versus memory). Based on functional and phenotypic studies, naive T cells have been defined as those T cells expressing CD45RA and CD62L (19, 20, 22); memory cells lack one or both of these markers. We explored the phenotypic heterogeneity of naive and memory T cells within several T cell lineages in human peripheral blood.

To divide the T cells into lineages, we used antibodies to CD3 (to define T cells), CD4, CD8, and the γδ-T cell receptor. To define differentiation stages, we used antibodies to CD45RA and CD62L. Finally, to explore the heterogeneity of these subsets we examined the expression of CD11a and CD57.

Figure 6 shows the progressive gating to define six T cell lineages. We can identify two lineages of γδ T cells ($CD4^+$ and $CD4^-$; the latter express zero to low levels of CD8). Of the αβ T cells, we identify four distinct lineages: the CD4 helper cells ($CD4^+CD8^-$), the CD8 cytotoxic/suppressor cells ($CD4^-CD8^+$), the double-negative cells (DN, $CD4^-CD8^-$), and cells which express CD4 and dimly express CD8 ($CD8^{dim}$). The $CD8^{dim}$ T cells are phenotypically and functionally distinct from the other subsets (27);

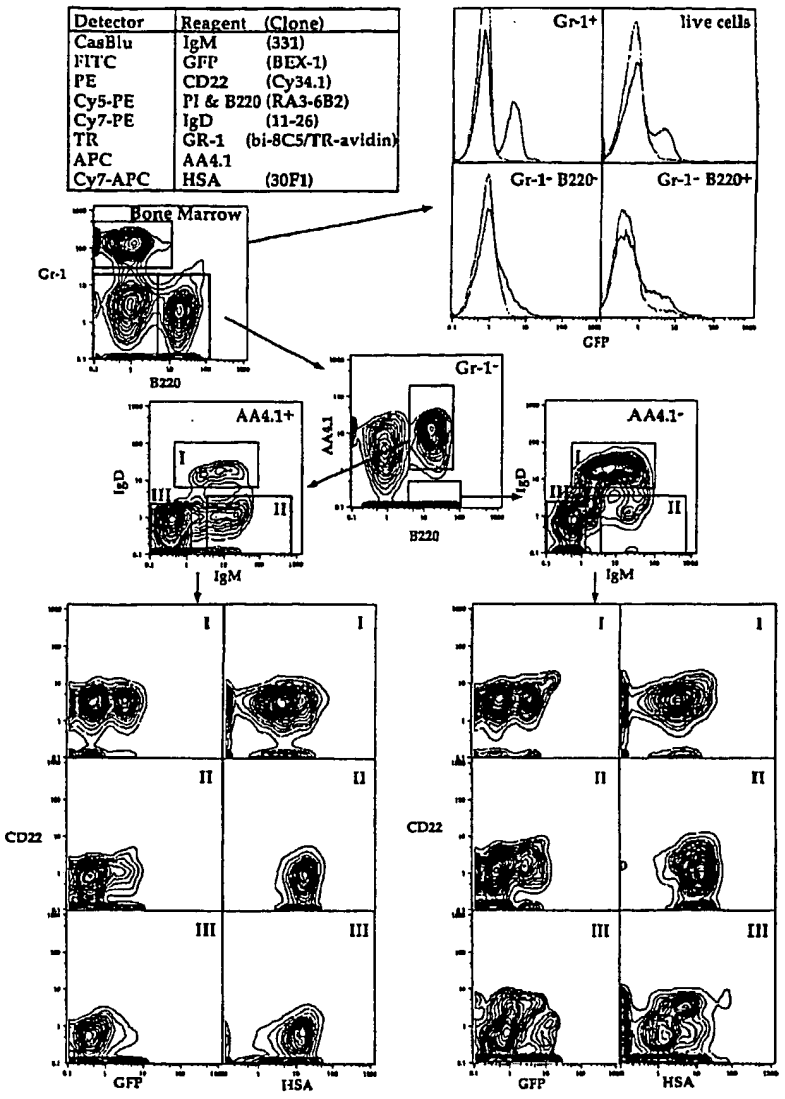

FIG. 5. 8 color flow cytometric analysis of murine bone marrow cells. These plots are all derived from the same single-tube collection of 1×10^5 cells. Bone marrow cells were isolated from a 3-month-old mouse transgenic for BEX-1 GFP driven by a H-2K (murine Class I MHC) promoter. Similar results (except for GFP expression) were obtained with nontransgenic mice of comparable genetic background (data not shown). Ungated data were collected for 100,000 cells. In order to establish a compensation matrix, data were also recorded from separate samples of cells that were singly stained with bright reagents. For compensation of the GFP signal, transgenic spleen cells were analyzed and used in the compensation matrix in the "FITC" channel. Dead cells (defined as propidium iodide-bright cells in the Cy5-PE channel) were excluded from post hoc analyses (8% of cells). All two-dimensional plots are 5% probability contour plots. Boxes indicate software gates drawn for analysis of data. The combination of reagents used to stain bone marrow cells simultaneously and the detector used for each reagent is indicated in the box. The upper left panel depicts Gr-1 (8C5) (a marker of the myeloid/granulocyte lineage) expression versus B220 (expressed predominantly by B lineage cells). In the top right, histograms showing GFP expression in all live cells, $8C5^+$, $8C5^-B220^-$, and $8C5^-B220^+$ cells are shown. The lighter histogram indicates fluorescence from nontransgenic mouse bone marrow using equivalent staining and gating. The center panel shows the expression of AA4.1 and B220 on $Gr\text{-}1^-$ cells. These cells are divided into AA4.1+ or AA4.1− cells; the expression of IgD and IgM is then used to further subdivide these cells into three classes each (population I, IgD^+, $IgM^{lo/+}$; II, IgD^-IgM^+; and III, IgD^-IgM^-). Data from each of these 12 populations is displayed in the panels, as CD22 (a marker of mature B cells) vs. GFP expression, and CD22 vs. HSA expression are shown. HSA is expressed on immature and germinal center B cells. (See text for a description of the subsets.)

in particular, they express the CD8αα homodimer rather than the CD8αβ heterodimer. Finally, within the αβ T cells we can identify, in general, at least four subsets based on the differentiation markers CD45RA and CD62L (Fig. 6).

CD57 and CD11a have been used previously to distinguish differentiated subsets of T cells. CD11a is expressed on all T cells, but occurs at higher levels on memory subsets (26). The expression of CD57 is reciprocal to CD28; its expression has been thought to mark terminally differentiated T cells (13).

Examination of the T cell subsets for CD57 and CD11a reveals several features that are consistent across all lineages. First, naive T cells, as expected, express lower levels of CD11a and essentially no CD57. Memory T cells that express CD62L (and are $CD45RA^-$) can be divided into cells which express low or high levels of CD11a—although this distinction is often lost in the smear of the distribution. In addition, there is a subset which dimly expresses CD57 (and, perhaps surprisingly, relatively low CD11a). The $CD45RA^-CD62L^-$ subset has a greater frequency of cells which express CD57; the highest frequency of CD57 expression (and brightest expression) is found on the $CD45RA^+$ $CD62L^-$ subset. It is remarkable that lineages which are functionally so distinct as CD4 and CD8 T cells have differentiation stages with such highly conserved phenotypic properties.

DISCUSSION

We report here some of the first experiments performed using 8 color, 10-parameter flow cytometry analysis. While at first this technology may seem esoteric, it has become apparent that this degree of resolution is necessary for identifying unique cell populations within the immune system. Based on functional studies, we believe that, using

8 color phenotyping, we are beginning to identify phenotypically and functionally homogeneous subsets—a primary goal of flow cytometric analysis.

The power of the 8 color analysis is readily apparent by the complex data presented in Figures 5 and 6. These two figures represent analysis of a single tube (each); data for 1–3 × 10^5 cells was collected. From this data, we are able to resolve dozens of phenotypically distinct T cell subsets in human peripheral blood.

In addition to the ability to finely subset lymphocytes, the 8 color technology gives us the ability to combine phenotypic and functional analysis to a degree previously unattainable. For instance, we can subset T cells using five different antibodies (CD3, CD4, CD8, CD45RA, and CD62L), and then use two antibodies to measure cytokine profile (e.g., IL4 and γ-IFN) and one color to measure apoptosis (annexin V). Thus, we can quantify several functional capacities of fine T cell subsets. This will be crucial to understanding whether phenotypic heterogeneities such as that seen in Figure 6 are meaningful or not.

The murine staining example demonstrates the power of 8 color flow cytometry analysis for immunophenotyping as well as detection of a GFP reporter gene. Based on this figure alone, we can divide murine bone marrow B lineage cells into at least six subsets. In addition, we show that several of these subsets display further heterogeneity and exhibit unique features compared to other populations. Our general strategy is to select reagents such that the gating uses both exclusion and inclusion criteria, i.e., Gr-1 expression as an exclusion criterion and B220 expression as an inclusion criterion. The lineage-defined cells are then examined for markers of interest, e.g., AA4.1—for which there is little information about expression during differentiation. Correlating expression of this marker with other well-defined cell surface proteins (e.g., IgM, IgD, CD22, HSA), as well as a BEX reporter of the H2K promoter, can be used to make inferences about B cell maturation in bone marrow. Finally, we demonstrated that BEX transgenic mice can be evaluated for GFP expression simultaneously with the expression of seven distinct cell surface antigens. This lays the foundation for exploiting the power of 8 color flow cytometry for evaluation of GFP reporter genes within defined immune system subsets.

There were a number of obstacles to achieving 8 color analysis. First was the development of appropriate reagents (some of which are described in detail elsewhere (2, 23)). Antibodies conjugated to most of these reagents are commercially available; at this time, the Cy7 tandem and CB conjugates must be synthesized in the laboratory (21).

The second obstacle was the electronics. Currently, only the Cytomation MoFlo electronics module is able to collect ten measurable parameters and use three different delay timers (for three-laser excitation); thus, we built a hybrid instrument using these electronics. The extended optical layout has been somewhat problematic; the emission paths are very long and it is critical to maintain proper beam path alignment at every juncture.

Finally, we found it necessary to develop an entirely new software package capable of performing the multidimensional compensation (24), plus organizing and presenting the complex datasets that arise from multiparameter analyses.

Compensation has become one of the most critical aspects of the analysis. Whereas in 2 color staining compensation is easy to assess at the time of collection, the multiple interactions make it impossible to do so with 8 color staining. In addition, it is important to remember that each lot of a tandem dye (Cy5PE, Cy7PE, Cy7APC) will have different spectral characteristics—as will APC reagents obtained from different manufacturers. In general, compensation will be different for two different Cy5PE reagents. We collect data for a single-stained sample for each different lot of each of the tandems used in an experiment. In a typical four-tube experiment (using as many as 32 different reagents), we would have approximately a dozen different compensation samples. The software selectively applies the appropriate compensation matrices to each of these analyses.

It is important to note that many of the values in a typical compensation matrix (such as shown in Table 3) are negative. This is because of the interaction between different compensation values. For instance, FITC has a significant contribution of fluorescence to the Cy5PE channel. A pair-wise compensation between FITC and CY5PE would require about 1.6% compensation. However, the PE to Cy5PE compensation already removes a contribution of the FITC (because of the contribution of FITC into the PE channel). Indeed, this second compensation removes too much of the FITC signal (because the spectral overlap of PE into the Cy5PE channel compared to the PE channel is more than that of the FITC into the Cy5PE channel compared to FITC in the PE channel). The net result is that some of the FITC signal must actually be added back into the Cy5PE channel—i.e., a negative compensation value. In addition to the sheer number of compensations required, the interaction between the values makes it essentially impossible to set the compensation values manually.

An unfortunate disadvantage to the large number of compensations is the concomitant loss in dynamic range. Part of this loss results from often having to subtract several significant signal components from other dyes before evaluating the residual signal due to the dye of

FIG. 6. An example of 8-color staining of human lymphocytes. These plots are all derived from the same single-tube collection of 3 × 10^5 cells. Peripheral blood mononuclear cells were stained with FITC CD11a, PE TcR γδ, Cy5PE CD45RA, Cy7PE CD62L, TR CD4, APC CD57, Cy7APC CD8, and CB CD3. Progressive gating is shown for lymphocytes (top left, based on forward and side scatter), and αβ or γδ T cells. The γδ T cells are further divided based on expression of CD4. The αβ T cells are divided on the basis of CD4 and CD8 expression into four lineages. Each of the lineages is further subdivided into differentiation stages based on CD45RA and CD62L expression. Finally, the expression of CD11a and CD57 is compared for the two γδ lineages, and the four subsets of each of the four αβ lineages. On these plots, boxes and lines are positioned identically within each lineage to allow for comparison of the relative expression of these markers. All two-dimensional graphs are 5% probability contour plots; some have outlier events marked.

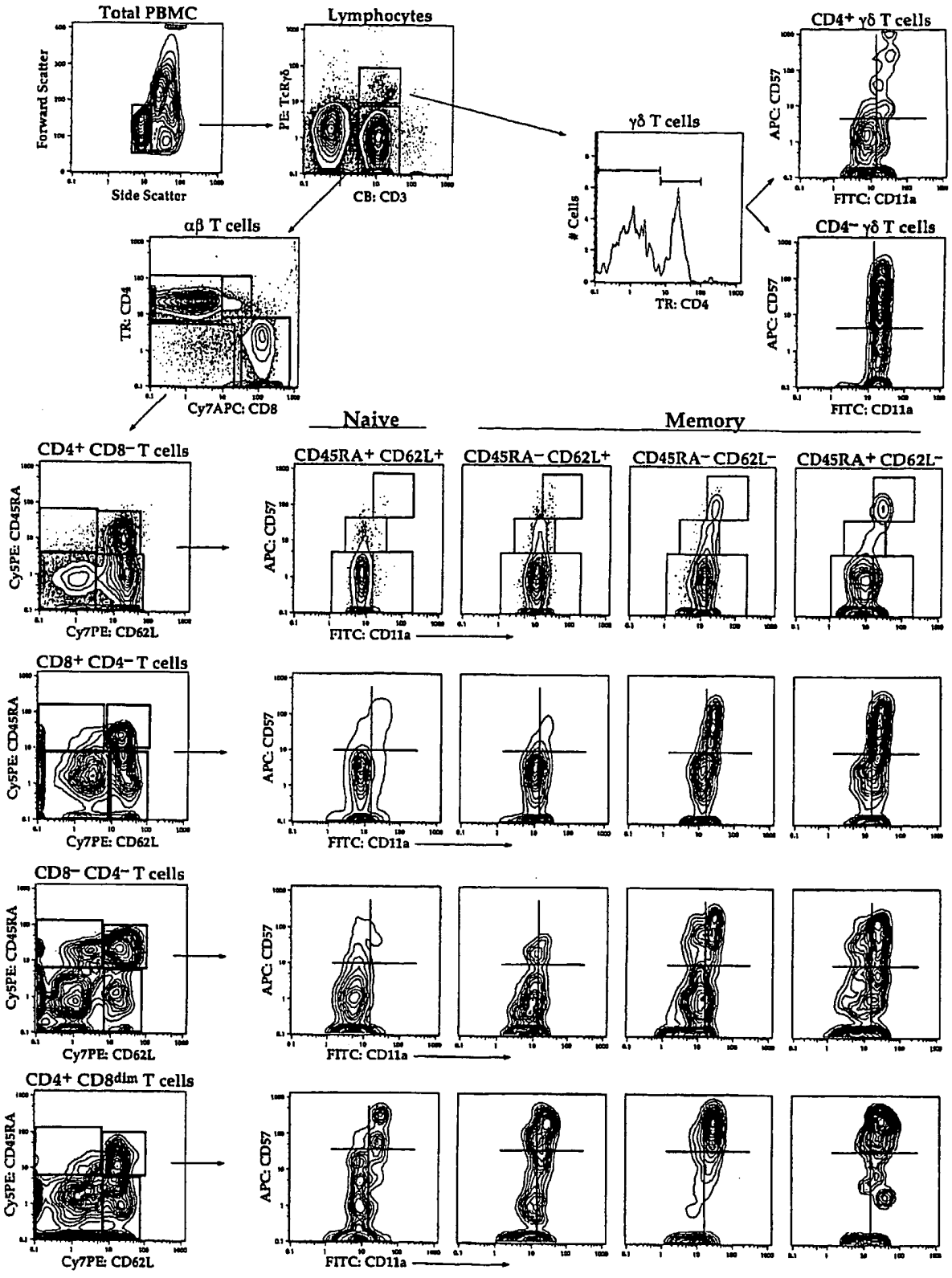

Roederer et al., Figure 6

FIG. 6.

interest on that measurement channel. Additional losses are introduced into the compensation calculations because of imperfect logarithmic conversion of the signals. Our logarithmic amplifiers show as great as 5% deviation across the four-decade range of signals. The deviation leads to inaccuracies in computing the absolute signal intensity from the digitized log data. The absolute signal intensity is required for the linear transformation used in compensation; for some channels, this error is introduced several times as multiple parameters have significant compensations into that channel. The net result is a broadening of all distributions (and especially the "negative" populations with the lowest signal levels); a broader distribution means less resolution of positive and negative populations and is mathematically equivalent to a loss in dynamic range.

Future instrumentation developments should focus on performing the compensation "live"—i.e., before conversion to log data. Alternatively, collection of very high resolution linear values (at least 16 bit data) allows for accurate compensation during the analysis stage (software logarithmic conversion would then be used to present the data in the desired format).

Perhaps one of the most important lessons that we have learned in the application of 8 color flow cytometry is that there is a great need for new software analysis tools. Some of these tools, such as compensation and log-conversion of linear data, are currently available in only a few software packages. More importantly, however, is the requirement for software which allows for logical analysis of the highly complex datasets generated by >5 parameter collections. New paradigms for the analysis as well as presentation of data are needed. For example, in both Figures 5 and 6 there is much more complexity within the datasets than we are able to show here—indeed, it is nearly impossible to present raw data from these analyses in a way which can be quickly grasped by even experienced persons.

Our 8 color studies have demonstrated that this technology is not only powerful, it has quickly become requisite for understanding the complexity of the immune system. Before this technology can be used by a wide variety of researchers, however, there are still several obstacles that must be overcome: Manufacturers must start making instrument benches that can be extended to more than seven or eight parameters. These instruments need to have computer-assisted instrument set-up, calibration, and data collection. Software developers have to give us new and powerful tools, and the reagent manufacturers have to start supplying many more fluorochrome-conjugated versions of their monoclonal antibodies.

What is the future for increasing the number of colors? At this time, there is only a single color from the Krypton 407 nm laser line; there are additional fluorochromes which can be excited efficiently by this laser line and have emissions that are spectrally resolved from CB (manuscript in preparation). In addition, there is a mutant of GFP, VEX, which is efficiently detected using this system (2). These have already provided us with a ninth color; it is certainly conceivable that there are tandem dyes that can be specifically excited at 407 nm and emit in the orange or red region of the spectrum that will provide even more independent colors. It may also be possible to squeeze more colors out of the 488 nm line—for example, by using Cy5.5-PE tandems—however, there is already so much spectral overlap that these may be of little value. The increases in colors will more likely come from the use of additional excitation beams in the far red, using infra-red fluorescent dyes. In any case, it is clear that we have not yet reached the limit on the number of available colors and will, over the next decade, probably achieve nearly a dozen useful fluorescence parameters.

ACKNOWLEDGMENTS

We thank Becton Dickinson for the generous donation of the FACStarPlus optical bench. We are grateful to Drs. Chris Klug and Irving Weissman for collaborating with us on analysis of their GFP transgenic mouse. We thank Gina Jager for excellent technical assistance, Ometa Herman for animal husbandry and technical support, Dr. Nicole Baumgarth and other members of the Herzenberg laboratory for helpful advice, and Drs. Aaron Kantor and Masahiko Amano for the preparation of some murine reagents and helpful advice.

LITERATURE CITED

1. Allman DM, Ferguson SE, Lentz VM, Cancro MP: Peripheral B cell maturation. II. Heat-stable antigen(hi) splenic B cells are an immature developmental intermediate in the production of long-lived marrow-derived B cells. J Immunol 151:4431–4444, 1993.
2. Anderson MT, Tjioe IM, Lorincz MC, Parks DR, Herzenberg LA, Nolan GP, Herzenberg LA: Simultaneous fluorescence-activated cell sorter analysis of two distinct transcriptional elements within a single cell using engineered green fluorescent proteins. Proc Natl Acad Sci USA 93:8508–8511, 1996.
3. Coffman RL: Surface antigen expression and immunoglobulin gene rearrangement during mouse pre-B cell development. Immunol Rev 69:5–23, 1982.
4. Cumano A, Paige CJ: Enrichment and characterization of uncommitted B-cell precursors from fetal liver at day 12 of gestation. Embo J 11:593–601, 1992.
5. Cumano A, Paige CJ, Iscove NN, Brady G: Bipotential precursors of B cells and macrophages in murine fetal liver. Nature 356:612–615, 1992.
6. Dangl JL, Parks DR, Oi VT, Herzenberg LA: Rapid isolation of cloned isotype switch variants using fluorescence activated cell sorting. Cytometry 2:395–401, 1982.
7. Erickson LD, Tygrett LT, Bhatia SK, Grabstein KH, Waldschmidt TJ: Differential expression of CD22 (Lyb8) on murine B cells. Int Immunol 8:1121–1129, 1996.
8. Fleming TJ, Fleming ML, Malek TR: Selective expression of Ly-6G on myeloid lineage cells in mouse bone marrow. RB6-8C5 mAb to granulocyte-differentiation antigen (Gr-1) detects members of the Ly-6 family. J Immunol 151:2399–2408, 1993.
9. Forster I, Vieira P, Rajewsky K: Flow cytometric analysis of cell proliferation dynamics in the B cell compartment of the mouse. Int Immunol 1:321–331, 1989.
10. Hardy RR, Carmack CE, Shinton SA, Kemp JD, Hayakawa K: Resolution and characterization of pro-B and pre-pro-B cell stages in normal mouse bone marrow. J Exp Med 173:1213–1225, 1991.
11. Jordan CT, McKearn JP, Lemischka IR: Cellular and developmental properties of fetal hematopoietic stem cells. Cell 61:953–963, 1990.
12. Kee BL, Paige CJ: In vitro tracking of IL-7 responsiveness and gene expression during commitment of bipotent B-cell/macrophage progenitors. Curr Biol 6:1159–1169, 1996.
13. Kern F, Ode-Hakim S, Vogt K, Hoflich C, Reinke P, Volk HD: The enigma of CD57+CD28− T cell expansion—anergy or activation? Clin Exp Immunol 104:180–184, 1996.
14. Li YS, Wasserman R, Hayakawa K, Hardy RR: Identification of the earliest B lineage stage in mouse bone marrow. Immunity 5:527–535, 1996.
15. McKearn JP, Baum C, Davie JM: Cell surface antigens expressed by subsets of pre-B cells and B cells. J Immunol 132:332–339, 1984.

16. McKearn JP, McCubrey J, Fagg B: Enrichment of hematopoietic precursor cells and cloning of multipotential B-lymphocyte precursors. Proc Natl Acad Sci USA 82:7414–7418, 1985.
17. McKearn JP, Rosenberg N: Mapping cell surface antigens on mouse pre-B cell lines. Eur J Immunol 15:295–298, 1985.
18. Moore WA, Kautz RA: Data analysis in flow cytometry. In: Handbook of Experimental Immunology, 4th ed., Weir DM, Herzenberg LA, Blackwell CM, Herzenberg LA (eds). Blackwell Scientific Publications, Edinburgh, 1986, 30.1–30.11.
19. Picker L, Treer J, Ferguson D, Collins P, Buck D, Terstappen L: Control of lymphocyte recirculation in man. I. Differential regulation of the peripheral lymph node homing receptor L-selectin on T cells during the virgin to memory cell transition. J Immunol 150:1105–1121, 1993.
20. Rabin RL, Roederer M, Maldonado Y, Petru A, Herzenberg LA, Herzenberg LA: Altered representation of naive and memory CD8 T cell subsets in HIV-infected children. J Clin Invest 95:2054–2060, 1995.
21. Roederer M: Conjugation of monoclonal antibodies. http://cmgm.stanford.edu/~roederer/abcon/ (1996).
22. Roederer M, Bigos M, Nozaki T, Stovel RT, Parks DR, Herzenberg LA: Heterogeneous calcium flux in peripheral T cell subsets revealed by five-color flow cytometry using log-ratio circuitry. Cytometry 21:187–196, 1995.
23. Roederer M, Kantor AB, Parks DR, Herzenberg LA: Cy7PE and Cy7APC: Bright new probes for immunofluorescence. Cytometry 24:191–197, 1996.
24. Roederer M, Murphy RF: Cell-by-cell autofluorescence correction for low signal-to-noise systems: Application to epidermal growth factor endocytosis by 3T3 fibroblasts. Cytometry 7:558–565, 1986.
25. Rolink A, ten Boekel E, Melchers F, Fearon DT, Krop I, Andersson J: A subpopulation of B220+ cells in murine bone marrow does not express CD19 and contains natural killer cell progenitors. J Exp Med 183:187–194, 1996.
26. Sanders ME, Makgoba MW, Shaw S: Human naive and memory T cells. Immunol Today 9:195–199, 1988.
27. Watanabe N, Rosa SCD, Cmelak A, Hoppe R, Herzenberg LA, Herzenberg LA, Roederer M: Long-term depletion of naive T cells in patients treated for Hodgkin's disease. Blood, in press (1997).

ELSEVIER

Journal of Immunological Methods 235 (2000) 121–131

JOURNAL OF IMMUNOLOGICAL METHODS

www.elsevier.nl/locate/jim

Measurement of lymphocyte subset proliferation by three-color immunofluorescence and DNA flow cytometry [1]

Ingrid Schmid *, Steve W. Cole, Jerome A. Zack, Janis V. Giorgi

UCLA School of Medicine, Department of Hematology / Oncology, 12-236 Factor Building, Los Angeles, CA 90095, USA

Received 29 September 1999; received in revised form 9 November 1999; accepted 9 November 1999

Abstract

We developed a method for simultaneous flow cytometric analysis of three-color immunofluorescence and DNA content. We show here that staining with 7-amino-actinomycin D (7-AAD) at 10 μg/ml using a phosphate–citrate buffer at low pH containing saponin for cell membrane permeabilization yields good resolution DNA histograms with low coefficients of variation. Furthermore, light scatter properties of cells are preserved after permeabilization; this permits gating on cell populations that differ in scatter signals on the flow cytometer. Because of the low pH of the phosphate–citrate staining buffer, Alexa™488, a pH-independent green-fluorescent fluorochrome is used instead of fluorescein–isothiocyanate (FITC) for cell surface staining in combination with phycoerythrin (PE) and with allophycocyanin (APC) which are both pH insensitive. Removal of 7-AAD after staining and replacing it with non-fluorescent actinomycin D (AD) retains DNA staining and allows detection of Alexa™488, PE and APC cell surface immunofluorescence without interference from fluorescent 7-AAD in solution for clear identification of cell subpopulations even after prolonged stimulation in culture. Thus, using a four-color benchtop flow cytometer, measurement of Alexa™488, PE and APC three-color immunofluorescence can be combined with 7-AAD DNA content analysis. Furthermore, we demonstrate that sample storage overnight without fixation for later analysis on the flow cytometer is possible without compromising results. Application of the method to the assessment of the differential proliferative responses of lymphocyte subsets of human peripheral blood mononuclear cells (PBMC) that were costimulated with CD3 and with CD28.2 is presented.

Keywords: Flow cytometry; DNA content; Proliferation; 7-Aminoactinomycin D; CD3/CD28 stimulation; CD71; CD56

Abbreviations: 7-AAD, 7-aminoactinomycin D; AD, actinomycin D; APC, allophycocyanin; BP, band pass filter; CV, coefficient of variation; FITC, fluorescein–isothiocyanate; mAb, monoclonal antibody; NCS, newborn calf serum; PBMC, peripheral blood mononuclear cells; PCB, phosphate–citrate buffer; PE, phycoerythrin; PI, propidium iodide; RNAse, ribonuclease A

* Corresponding author. Tel.: +1-310-206-7289; fax: +1-310-794-2145; e-mail: schmid@mednet.ucla.edu

[1] This work was performed in the UCLA Jonsson Comprehensive Cancer Center and Center for AIDS Research Flow Cytometry Core Facility and was supported by National Institutes of Health awards CA-16042, AI-28697 and AI-36059.

0022-1759/00/$ - see front matter
PII: S0022-1759(99)00225-2

1. Introduction

Assessment of cell proliferation by combined flow cytometric measurement of cell surface antigen expression and DNA content is an alternate method to measuring bulk cellular responses to stimulation by thymidin incorporation. This technique can also be used to assess cell cycle progression in studies of cellular differentiation and arrest. Advantages of the flow cytometry technique are that it does not require work with radioactivity and that it allows study of responses of cellular subpopulations in mixed cell preparations to various stimuli without the need for cell separation (Loken, 1980; Kruth et al., 1981; Rabinovitch et al., 1986; Schmid et al., 1991; Storek et al., 1992). Commercial availability of monoclonal antibodies targeted to various cell surface antigens, fluorochromes suitable for multi-color flow cytometric assays, and benchtop dual-laser flow cytometers equipped with an argon laser emitting at 488 nm and a 635-nm red diode laser for excitation of allophycocyanin (APC) has made four-color flow cytometry more widely accessible, making it desirable to utilize the enhanced analytical potential of multiparameter assays. In addition to providing a more in-depth analysis of cell populations, simultaneous staining with multiple probes reduces the number of cells needed for each experiment and the quantity of tubes that have to be handled in the laboratory.

However, flow cytometric multi-color experiments are potentially complex. When stained cells are analyzed on dual-laser flow cytometers, fluorochromes with broad excitation curves can be sequentially excited by both lasers requiring fluorescence compensation among laser beams. In addition, interactions and spectral emission overlaps of fluorochromes must be considered. For instance, propidium iodide (PI), the most commonly used fluorescent dye for flow cytometric DNA content analysis, has a broad emission spectrum in the orange–red range. PI, therefore, can only be combined with other fluorescent probes that emit fluorescence in the green range of the spectrum (Kruth et al., 1981; Storek et al., 1992). By contrast, the DNA dye 7-aminoactinomycin D (7-AAD) is suitable for cells that have also been cell-surface stained with phycoerythrin (PE)-conjugated antibodies, because its emission in the far red can be effectively separated from the orange PE emission and from the emission of green-fluorescent probes, respectively (Rabinovitch et al., 1986; Schmid et al., 1991). Despite its utility in multicolor flow cytometric assays, nevertheless 7-AAD has a broad excitation curve and has been noted for its high coefficients of variation (CV) of the $G_{0/1}$ peaks on DNA histograms (Darzynkiewicz et al., 1984) due to its binding characteristics and its large size (Mueller and Crothers, 1968; Gill et al., 1975; Zelenin et al., 1984). Furthermore, it has been noted that 7-AAD in solution can affect other fluorochromes through dye–fluorochrome interactions (Telford et al., 1994; Schmid, 1999). Therefore, we sought to develop a method that would optimize simultaneous cell surface antigen and DNA analysis.

In this report we present a method for measuring cell cycle progression and cell proliferation by DNA content analysis in cell subpopulations that are identified by three-color immunofluorescent staining. Cells are cell surface-stained with Alexa™488, a green-fluorescent fluorochrome that tolerates acidity down to pH 4.0 (Panchuck-Voloshina et al., 1999) and has an emission spectrum that can be effectively separated from the emissions of PE, APC and 7-AAD; DNA staining is performed with 7-AAD in low concentration. Application of the staining protocol to the detailed flow cytometric analysis of the proliferative responses of lymphocyte subsets as characterized by their differential expression of cell surface antigens to a T cell stimulus is shown.

2. Materials and methods

2.1. Cells and culture conditions

CEM, a T cell leukemia line, was maintained in continuous culture in RPMI 1640 (Mediatech, Herndon, VA) supplemented with 10% fetal bovine serum (Summit Biotechnology, Boulder, CO), 100 U/ml penicillin, 100 μg/ml of streptomycin, and 2 mM glutamine (all from Life Technologies, Rockville, MD). CEM cells were washed once in PBS.

Healthy donor peripheral blood mononuclear cells (PBMC) were obtained from commercial leukopaks and separated by Ficoll density gradient essentially as described by Böyum (1968). PBMC were washed

twice with PBS and were stained immediately or were cultured for 1, 2 or 3 days either in medium alone (RPMI 1640, supplemented with 10% (v/v) human AB serum (Omega Scientific, Tarzana, CA), 100 U/ml penicillin, 100 μg/ml of streptomycin, and 2 mM glutamine) or in this medium containing 100 ng/ml of soluble CD28.2 (Biodesign, Kennebumkport, ME) in the presence of 100 ng/ml of plate-bound OKT3 (Ortho Diagnostics, Raritan, NJ). Cultured PBMC were washed once in PBS.

2.2. Reagents and monoclonal antibodies

Phosphate buffered saline (PBS without Ca^{++} and Mg^{++}) and newborn calf serum (NCS) were purchased from Irvine Scientific (Irvine, CA). Sodium azide (NaAz), phosphate–citrate buffer (PCB) tablets, sodium chloride, sodium EDTA, bovine serum albumin, ribonuclease A (RNAse), and saponin were from Sigma (St. Louis, MO). Biotinylated CD8 (Leu™-2a), PE-labeled CD56, APC-labeled CD4 (Leu™-3a), PE-labeled and APC-labeled mouse IgG_1 isotypic controls were obtained from Becton Dickinson Biosciences (BD Biosciences) (San Jose, CA). CD71 PE, biotinylated CD5, CD8 APC, and biotinylated isotypic controls were from Pharmingen (San Diego, CA). Streptavidin Alexa™488 was from Molecular Probes (Eugene, OR). PI and 7-AAD were purchased from Calbiochem (San Diego, CA). Actinomycin D (C_1) (AD) was obtained from Roche Molecular Biosystems (Indianapolis, IN).

2.3. Staining of cell surface antigens

1×10^6 PBS-washed cells were placed into a 12×75 mm tube and resuspended in 100 μl of PBS supplemented with 2% NCS and 0.1% NaAz (PBSAz). Then, 20 μl of biotinylated monoclonal antibody (mAb), 20 μl of PE-labeled mAb, and 20 μl of APC-labeled mAb or 20 μl each of isotypic control antibody were added and cells were incubated for 20 min at 4°C. Next, cells were washed once with 2 ml of PBSAz by centrifugation at $250 \times g$ for 5 min. The supernatant was removed and 100 μl of PBSAz containing 2 μg of streptavidin Alexa™488 was added followed by incubation for 20 min at 4°C. Cells were washed once with 2 ml of PBSAz by centrifugation at $250 \times g$ for 5 min at 4°C.

2.4. DNA staining using 7-AAD

1×10^6 PBS-washed cells or cells stained for cell surface antigens were resuspended in 0.5 ml of PCB solution (0.1 M phosphate–citrate, 0.15 M of NaCl, 5 mM sodium EDTA, 0.5% BSA, pH 4.8) containing 0.02% of saponin (PCBS) and 10 μg/ml of 7-AAD followed by incubation for 20 min at room temperature. For experiments that investigated DNA staining using different cell concentrations, cell numbers as indicated were used. For experiments that tested DNA staining using different 7-AAD concentrations, the amount of 7-AAD as indicated in the text was added. Then, cells were spun down by centrifugation at $250 \times g$ for 5 min. The cell pellet was resuspended in 0.5 ml of PCBS containing 10 μg/ml of AD and was placed on ice protected from light for at least 10 min before analysis on the flow cytometer to permit stabilization of 7-AAD fluorescence intensity after the addition of non-fluorescent AD. On occasion cells were kept for a maximum of 3 days protected from light at 4°C in the staining solution before sample acquisition on the flow cytometer without adverse effects.

2.5. DNA staining using PI

For experiments that involved PI DNA staining, 1×10^6 PBS-washed cells were resuspended in PBS containing 0.3% of saponin essentially as described previously (Jacob et al., 1989). 10 μg/ml of PI and 200 μg/ml of RNAse were added followed by incubation for 20 min at room temperature. Samples were then acquired on the flow cytometer in their staining solution.

2.6. Flow cytometry

Samples were analyzed on a FACSCalibur flow cytometer (BD Biosciences) equipped with a 15 mW air-cooled 488 nm argon-ion laser for excitation of Alexa™488, PE, and 7-AAD and a 635-nm red diode laser for excitation of APC. Green Alexa™488 fluorescence was collected after a 530/30 nm band pass

(BP) filter. Orange emission from PE and from PI were filtered through a 585/42 nm BP filter. Red APC emission was collected through a 661/16 BP filter and far red 7-AAD emission through a 670 longpass filter. Electronic compensation was used among the fluorescence channels to remove residual spectral overlap. Photomultiplier tube voltage and spectral compensation were set using cells single-stained with streptavidin Alexa™488 alone, with PE alone, with APC alone, or with 7-AAD alone. Alexa™488, PE and APC fluorescence data were all displayed on 4-decade log scales. PI and 7-AAD fluorescence were both collected using linear amplification. For 7-AAD staining experiments that did not include cell surface antigen staining and for experiments that compared exclusion of clumps by light scatter gating with doublet discrimination, FL-3 (7-AAD fluorescence) height (H), FL-3 area (A) and width (W) were measured. For acquisition of four-color stained samples, only FL-3 H and FL-3 A could be collected due to limited availability of parameters on the flow cytometer. For acquisition of PI-stained samples, FL-2 (PI fluorescence) H, FL-2 A and FL-2 W were collected for doublet discrimination. The low flow rate setting (12 μl/min) was used for sample acquisition to improve the CV on DNA histograms. A minimum of 10,000 events was collected on each sample. Analysis of the multivariate data was performed with CELLQuest™ software (BDIS). Cell cycle analysis of DNA histograms was performed with ModFit LT™ software (Verity Software House, Topsham, ME).

3. Results and discussion

3.1. Optimization of DNA staining

7-AAD has been shown to be compatible with dual-color immunofluorescent staining using FITC and PE (Rabinovitch et al., 1986; Schmid et al., 1991). However, with various cell permeabilization methods (Rabinovitch et al., 1986; Stokke et al., 1988; Schmid et al., 1991) it yielded DNA histograms with considerably higher CV than the CVs that are obtainable with PI DNA staining. By contrast, using a PCB supplemented with saponin, it has been demonstrated that 7-AAD can produce DNA distributions with low CVs (Toba et al., 1995). We modified the published protocol (Toba et al., 1995) for reliable cell permeabilization and nucleic acid staining with the saponin preparations available to us and conducted initial experiments on cells that were triple-stained with Alexa™488, PE and APC. We observed that staining for DNA content with 7-AAD at a concentration of 25 μg/ml as published previously (Rabinovitch et al., 1986; Schmid et al., 1991; Toba et al., 1995) leads to the appearance of excessive amounts of 7-AAD (FL-3) fluorescence in the channel for APC detection (FL-4), requiring approximately 90% cross-beam subtraction of FL-3 fluorescence out of the FL-4 detector. Furthermore, the resolution of PE and APC fluorescence from background was decreased when 7-AAD was added to the cell suspension (data not shown). Interactions of dyes with other fluorochromes conjugated to probes have been noted previously (Shapiro, 1981; Telford et al., 1994; Schmid, 1999; Schmid et al., 1999) and may be caused either by energy transfer due to fluorochrome proximity or by fluorescence quenching (Stokke et al., 1998).

Therefore, we investigated the possibility of lowering the concentration of 7-AAD in the staining solution to decrease its interference with the detection of APC fluorescence. Table 1 shows one representative of four individual experiments where cell cycle distributions were obtained by staining CEM cells with decreasing concentrations of 7-AAD. As expected, fluorescence intensity of the staining distributions decreased with lower dye concentrations, however, DNA content data obtained with all the dye concentrations we tested were similar. These data indicate that 7-AAD at lower concentration produces reliable cell cycle data using the current method of cell permeabilization with PCB containing saponin. Furthermore, to eliminate the influence of 7-AAD in solution on the other fluorochromes present on the cell surface (Telford et al., 1994), we replaced the DNA dye after staining with an equal amount of its non-fluorescent analogue AD. Replacement with AD has been previously shown to retain 7-AAD fluorescence after cell fixation/permeabilization in cell preparations where dead cells were identified by 7-AAD up-take (Fetterhoff et al., 1993; Schmid and Giorgi, 1995; Schmid et al., 1999). Addition of AD

Table 1
Effects on DNA content analysis of 7-AAD staining concentration and addition of AD

Dye (concentration)	Cell cycle distribution				
	$\%G_1$	%S	$\%G_{2+M}$	%CV G_1	G_1 peak position
7-AAD (25 μg/ml)	51	43	5	3.8	117
7-AAD (20 μg/ml)	51	44	5	3.8	105
7-AAD (15 μg/ml)	49	45	6	4.6	89
7-AAD (10 μg/ml)	51	44	5	5.6	68
7-AAD (5 μg/ml)	49	44	6	7.2	44
7-AAD (2 μg/ml)	49	45	6	6.9	22
7-AAD (25 μg/ml) + AD[a]	49	45	6	3.8	
7-AAD (20 μg/ml) + AD[a]	50	43	7	4.0	
7-AAD (15 μg/ml) + AD[a]	51	42	7	3.8	
7-AAD (10 μg/ml) + AD[a]	50	43	7	4.0	
7-AAD (5 μg/ml) + AD[a]	50	42	8	5.2	
7-AAD (2 μg/ml) + AD[a]	51	42	8	5.9	

[a]In each sample, after DNA staining with 7-AAD, CEM cells were spun down, then AD was added at the same concentration as 7-AAD.

did not affect cell cycle data (Table 1), and the CVs of the G_1 peaks remained low down to a 7-AAD concentration of 10 μg/ml. Table 2 shows one of two experiments where we examined the effect of cell concentration on cell cycle data using 7-AAD at a staining concentration of 10 μg/ml followed by replacement with AD. Data on CEM cells as presented in Table 2 indicates that DNA staining with 7-AAD under these conditions is effective over a wide range of cell concentrations.

3.2. Single cell DNA analysis comparing two different concentrations of 7-AAD with PI

Although the cell cycle data we obtained with CEM cells indicated that it was feasible to lower the staining concentration of 7-AAD to 10 μg/ml, we wanted to test if we would be able to reliably measure proliferating cells in in vitro stimulated PBMC. Furthermore, we wanted to compare DNA content data obtained with doublet discrimination with data obtained by excluding cell clumps by light scatter gating, because due to the limited availability of parameters, doublet discrimination is not possible on our flow cytometer in the four-color acquisition set-up that is necessary for samples stained for three-color immunofluorescence and DNA. Doublet discrimination is a fluorescence gating procedure commonly used in DNA flow cytometry to distinguish two cells with single DNA content that are clumped together from single cells with double DNA content; this strategy serves to prevent a false high frequency of cells to be assigned to the G_{2+M} phase of the cell cycle. Alternatively, current DNA analysis softwares can provide aggregate modeling algorithms to compensate for cell clumps during DNA histogram deconvolution. To investigate the effect of different gating approaches, we stained PBMC that were cultured in the presence of CD3 and CD28.2 with 25 μg/ml of 7-AAD, 10 μg/ml of 7-AAD followed by addition of AD, or with PI. Then, cells

Table 2
Effect of cell concentration on DNA content analysis using 7-AAD staining followed by AD. In each sample, after DNA staining with 7-AAD, CEM cells were spun down, then AD was added at the same concentration as 7-AAD

Cell numbers ($\times 10^6$)	Cell cycle distribution				
	$\%G_1$	%S	$\%G_{2+M}$	%CV G_1	G_1 peak position
0.1	43	43	13	5.6	60
0.5	42	46	12	5.7	52
1	41	45	13	4.8	53
1.5	43	44	13	5.5	53
2	42	44	14	5.8	49
2.5	45	44	11	6.7	46
3	40	45	15	7.3	43
3.5	45	43	12	6.7	53
4	43	45	12	6.4	48

stained with either 25 μg/ml of 7-AAD or with PI were acquired with doublet discrimination and cells stained with 10 μg/ml of 7-AAD followed by addition of AD were run on the instrument without doublet discrimination.

After gating on single cells either by fluorescence or by light scatter, we did not observe any differences in cell cycle data among staining conditions obtained from cells after 24 h of culture (Fig. 1). However, interestingly, when we compared the same staining conditions on cells that were stimulated for 48 h with CD3/CD28.2, we noted that the DNA distribution obtained with 25 μg/ml of 7-AAD showed a bimodal $G_{0/1}$ peak, and it was difficult to deconvolute the DNA histogram for estimation of cell frequencies in the $G_{0/1}$, S and G_{2+M} cell cycle phases. When we set two separate light scatter gates on the sample stained with 25 μg/ml of 7-AAD, one on smaller, less stimulated cells, the second one on larger cells with more forward and side scatter that had proliferated in response to the T cell stimulus, we obtained two DNA distributions that differed in their fluorescence intensity (data not shown). At the same timepoint, cells stained with 10 μg/ml of 7-AAD followed by addition of AD and cells stained with PI, respectively, did not show a bimodal $G_{0/1}$ peak and their DNA content data compared well. It has been demonstrated previously that the level of 7-AAD binding is dependent on chromatin structure (Shapiro, 1995) and is affected by transcriptional activity of the cells (Stokke et al., 1988) which may influence low and high affinity 7-AAD DNA binding differently (Yu, 1983). Consequently, our results suggest that at lower dye concentration, the DNA staining properties of 7-AAD may be unaffected by the proliferative state of the cells while higher concentrations are problematic; thus, using 7-AAD at a concentration of 10 μg/ml may be more suitable for

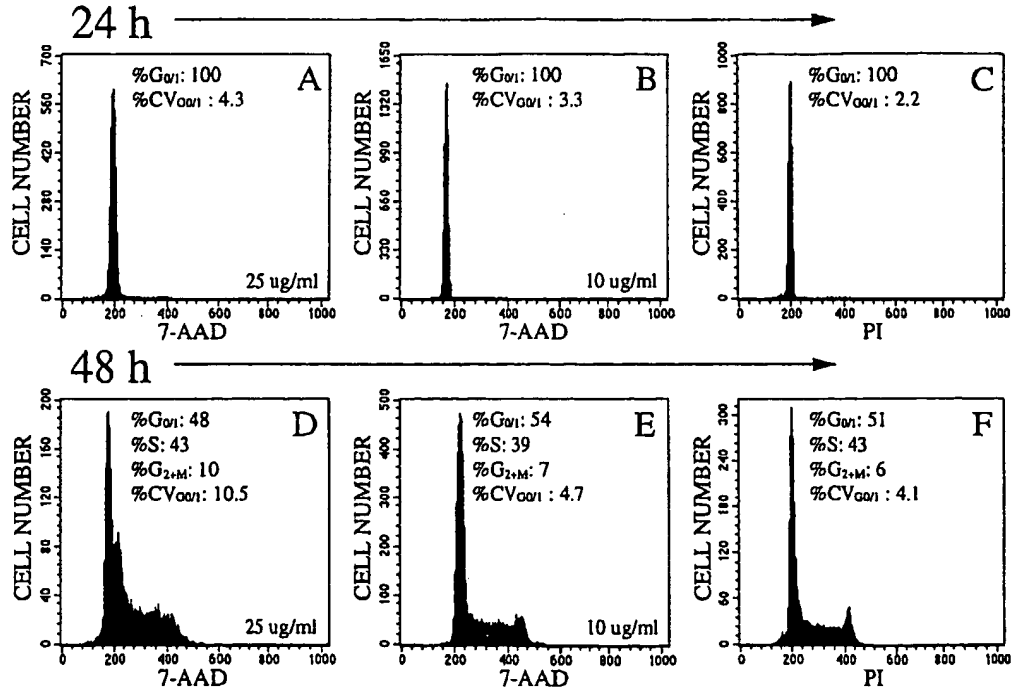

Fig. 1. Human PBMC were cultured in the presence of CD3 and CD28.2 as described in Section 2, either for 24 h (A, B, C), or for 48 h (D, E, F). (A, D) Histogram of 7-AAD fluorescence of cells stained with 25 μg/ml of 7-AAD, gated on FL-3 (7-AAD fluorescence) width (*W*) vs. FL-3 area (*A*) for doublet discrimination; (B, E) histogram of 7-AAD fluorescence of cells stained with 10 μg/ml of 7-AAD followed by addition of AD, gated on forward vs. side scatter to exclude clumps and debris; (C, F) histogram of PI-stained cells, gated on FL-2 W vs. FL-2 *A* for doublet discrimination.

the analysis of cell populations which are stimulated in an in vitro culture system. Results as shown in Fig. 1 also demonstrate that 7-AAD DNA distributions and cell cycle data that match PI DNA data obtained with doublet discrimination can be obtained by gating single cells on forward vs. side scatter. Therefore, we chose 10 μg/ml of 7-AAD as the dye concentration for DNA staining, replaced 7-AAD with AD, and performed the procedure as outlined in Section 2 for subsequent experiments on quadruple-stained cells.

3.3. Correlation of DNA content and transferrin receptor expression on lymphocyte subsets during CD3 / CD28 costimulation

Fig. 2 shows one representative of three individual experiments where PBMC were stimulated for

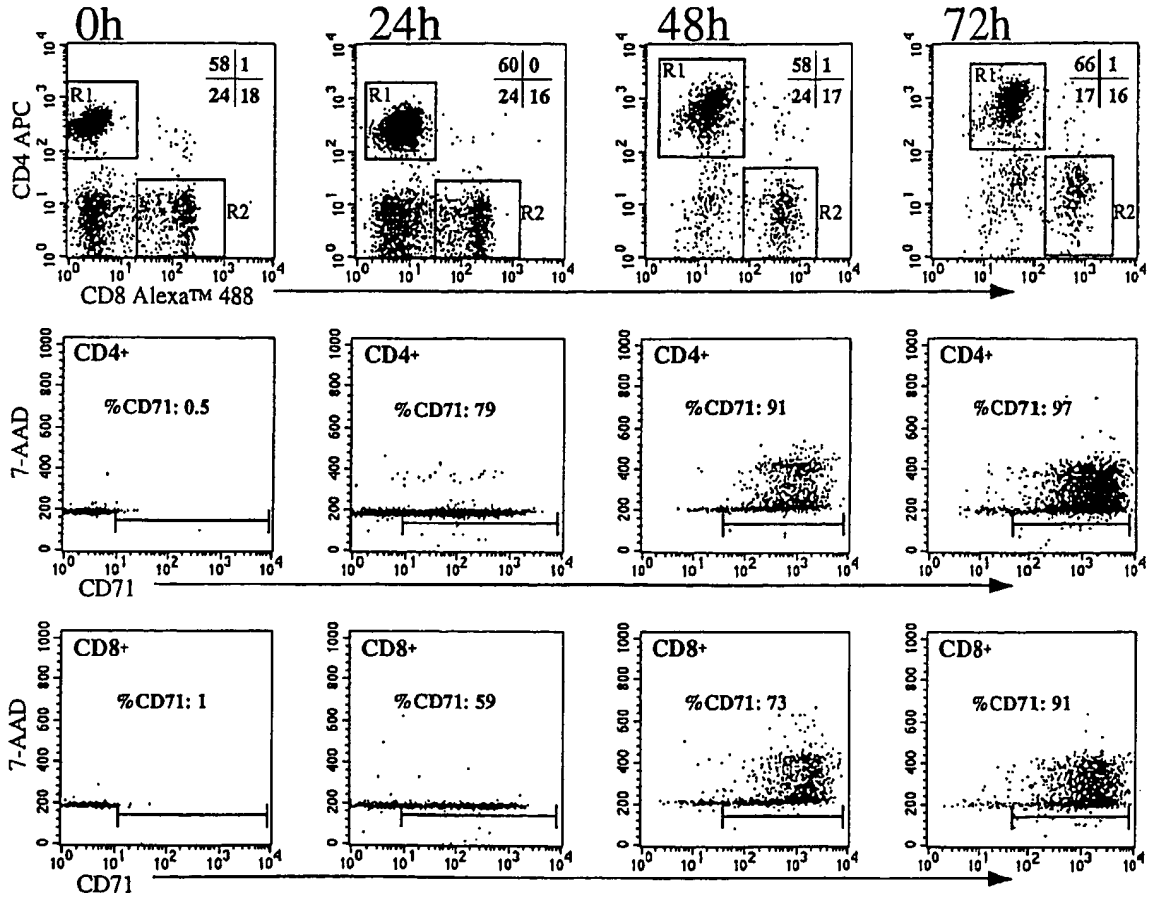

Fig. 2. Fresh human PBMC or PBMC cultured in the presence of CD3 and CD28.2 for 24, 48 or 72 h were stained with biotinylated CD8 plus streptavidin Alexa™488, CD71 PE, CD4 APC and 10 μg/ml of 7-AAD followed by the addition of AD as described in Section 2. The 0 h timepoint dotplot in row 1 was gated on lymphocytes; all other dotplots shown in row 1 were gated on forward vs. side scatter to exclude debris and clumps. All CD71 vs. 7-AAD fluorescence dotplots of $CD4^+$ cells were gated on R1 as shown on the CD8/CD4 dotplot for each timepoint. All CD71 vs. 7-AAD fluorescence dotplots of $CD8^+$ cells were gated on R2 as shown on the CD8/CD4 dotplot for each timepoint. Frequencies of lymphocyte subsets as shown in row 1 for each CD8/CD4 dotplot have been determined by setting quadrant cursors according to isotype control background levels. Cursor positions for determination of frequencies of $CD71^+$ cells for each timepoint were set according to appropriate isotype control background levels. Cell cycle distributions of $CD4^+$ cells were as follows: 0 h: $\%G_{1/0} = 100$; 24 h: $\%G_{1/0} = 100$; 48 h: $\%G_{1/0} = 54$, $\%S = 35$, $\%G_{2+M} = 11$; 72 h: $\%G_{1/0} = 37$, $\%S = 62$, $\%G_{2+M} = 2$. Cell cycle distributions of $CD8^+$ cells were as follows: 0 h: $\%G_{1/0} = 100$; 24 h: $\%G_{1/0} = 100$; 48 h: $\%G_{1/0} = 61$, $\%S = 33$, $\%G_{2+M} = 6$; 72 h: $\%G_{1/0} = 37$, $\%S = 59$, $\%G_{2+M} = 4$.

24, 48 and 72 h, and then stained simultaneously with CD4, CD8, CD71 (transferrin receptor) mAbs and 7-AAD. Using 7-AAD at low concentration, fluorescence compensation settings among FL-3 and FL-4 for sample acquisition were now reduced to approximately 20% subtraction of FL-3 out of FL-4. The frequency of CD71 positive cells was very low at the 0 h timepoint within the $CD4^+$ and $CD8^+$ lymphocyte subset, respectively; however, after 24 h of culture, although $CD4^+$ and $CD8^+$ cells remained in the $G_{0/1}$ phase of the cell cycle, considerable proportions of both these lymphocyte subsets expressed CD71 with higher frequencies of $CD71^+$ cells within the $CD4^+$ subset. After 48 h, cells in both subsets had progressed to the S and G_{2+M} phases; again, more $CD4^+$ cells than $CD8^+$ lymphocytes co-expressed CD71 and also slightly more $CD4^+$ cells were in the proliferative state. At the 72 h timepoint, most of $CD4^+$ and $CD8^+$ lymphocytes, respectively, expressed CD71 and both had similar frequencies of proliferating cells. As shown in Fig. 2, during proliferation, cells with the highest level of CD71 expression were the ones that were actively synthesizing DNA. These data indicate that the appearance of the CD71 activation antigen precedes entry of cells into S phase and that CD71 expression levels correlate with cell proliferation. Furthermore, our data show that both the $CD4^+$ and the $CD8^+$ cell subset respond to the T cell stimulus with the $CD4^+$ cells reacting somewhat more rapidly compared to the $CD8^+$ cells. $CD8^+$ cell proliferation may depend on activation through cytokines that are released by $CD4^+$ T cells during CD3/CD28 stimulation leading to a time-delayed reaction (Cole et al., 1998). Data as shown in Fig. 2 compare well with published results on CD3/CD28 co-stimulation of human PBMC that showed that this T stimulation system allows cells to progress through the G_{1b} phase of the cell cycle within 24 h, and through the S and G_{2+M} phases by 48 h (June et al., 1990; Cole et al., 1998; Korin and Zack, 1998). Our data on CD71 expression is in accordance with published results that show that transferrin receptors are expressed in late G_1 phase before the initiation of DNA synthesis (Toba et al., 1995) and that activation antigen expression can be induced in the absence of cell proliferation (Caruso et al., 1997). $CD4^+$ and $CD8^+$ lymphocytes in PBMC cultured in parallel without CD3/CD28.2 remained in $G_{0/1}$ during the whole culture period and also did not co-express CD71 (data not shown).

3.4. Analysis of $CD8^+$ lymphocyte subset proliferation

Fig. 3a shows one experiment of three individual experiments where we studied the differential proliferation of $CD8^+$ lymphocyte subsets in response to CD3/CD28.2 stimulation. As expected with this T cell stimulatory system, $CD8^+$ T cells which co-expressed the T lymphocyte antigen CD5 had responded strongly to stimulation by 48 h of culture. In contrast, $CD8^+CD56^+$ (NK) cells (Lanier et al., 1989) did not enter the proliferative phases of the cell cycle. These results confirm the potential of the method to provide reliable cell cycle data on immunophenotypically defined subsets within mixed cell populations.

3.5. Sample storage

It is not always possible to acquire samples on the flow cytometer on the same day they were stained. Therefore, we investigated if cells could be stored until the next day without detrimental effects. Towards this end we kept cells collected for Fig. 3a in

Fig. 3. Human PBMC were cultured in the presence of CD3/CD28.2 for 48 h, then stained with biotinylated CD5 plus streptavidin Alexa™488, CD56 PE, CD8 APC and 10 μg/ml of 7-AAD followed by the addition of AD as described in Section 2. Samples were either acquired on the flow cytometer immediately (a) or kept overnight protected from light at 4°C and then run through the instrument (b). A: Forward vs. side scatter dotplot of all cells, ungated; B: CD5 fluorescence vs. CD56 fluorescence dotplot, gated on R1 to exclude cell clumps with high forward and high side scatter as shown in A and on R2 as shown in the insert of the CD8 fluorescence histogram; C: histogram of 7-AAD fluorescence, gated on R1, R2, and on R3 as shown in B; D: histogram of 7-AAD fluorescence, gated on R1, R2, and on R4 as shown in B. Note that the peak positions of the $G_{0/1}$ peaks as indicated in the histograms C and D as shown in (a) and (b), respectively, are derived from histograms and data generated by Modfit *LT*™ DNA analysis software.

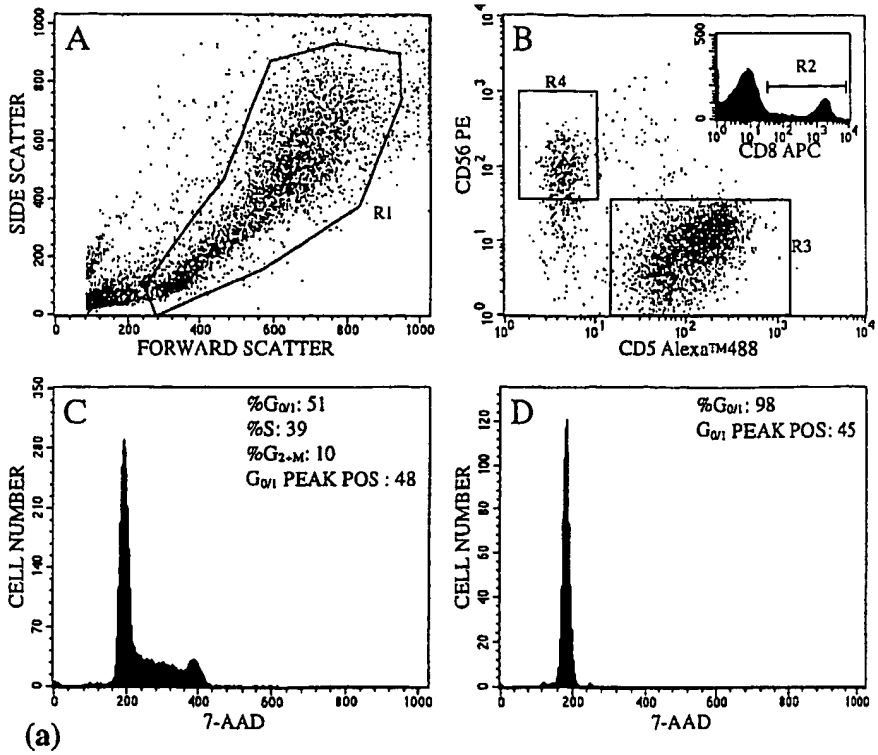
A
SIDE SCATTER
FORWARD SCATTER
R1
B
CD56 PE
CD5 Alexa™488
R4
R3
R2
CD8 APC
C
%G0/1: 51
%S: 39
%G2+M: 10
G0/1 PEAK POS : 48
CELL NUMBER
7-AAD
D
%G0/1: 98
G0/1 PEAK POS: 45
CELL NUMBER
7-AAD

(a)

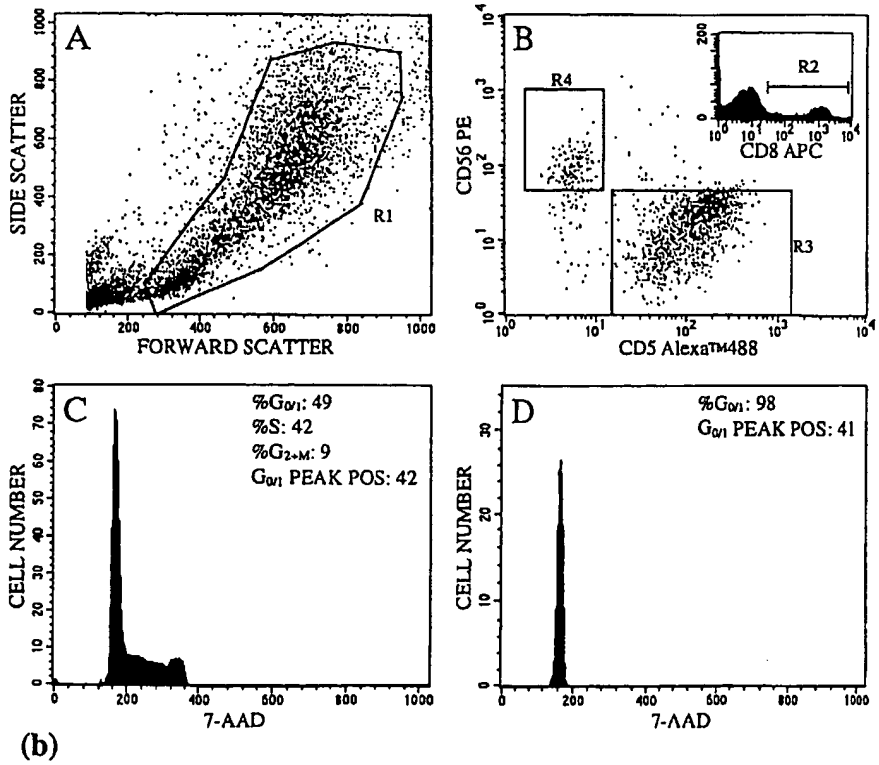
A
SIDE SCATTER
FORWARD SCATTER
R1
B
CD56 PE
CD5 Alexa™488
R4
R3
R2
CD8 APC
C
%G0/1: 49
%S: 42
%G2+M: 9
G0/1 PEAK POS: 42
CELL NUMBER
7-AAD
D
%G0/1: 98
G0/1 PEAK POS: 41
CELL NUMBER
7-AAD

(b)

their staining solution overnight protected from light at 4°C and compared data from samples that were run immediately to results from samples that were stored and run 24 h later. Fig. 3b shows one representative of five experiments where light scatter and fluorescence parameters remained stable during storage and where data analysis yielded very similar results. Generally, there was a slight decrease (on average 15%) in the fluorescence intensity of 7-AAD staining in the samples that were kept overnight, but cell cycle data were not altered. It is somewhat surprising that samples can be stored in the PCB at pH 4.8 without fixation with a standard preservative such as formaldehyde. However, the stabilizing effect of low pH on the preservation of cellular cytoplasm (Shapiro, 1995) may contribute to sample stability. On occasion, cells were kept for a maximum of 3 days without notable alterations in the parameters we measured. The fact that stained samples can be readily stored facilitates flow cytometric analysis at a more convenient time and provides the opportunity for sample shipping.

4. Summary

We present here a staining protocol for three-color immunofluorescence using Alexa™488, PE and APC in combination with DNA content. We have applied the method to the analysis of coordinate expression of an activation antigen across the cell cycle and distinct cell cycle profiles in cellular subpopulations identified by multiple cell surface markers. Our data indicate that reliable cell cycle measurements with a low CV can be obtained by using 7-AAD at a low concentration with replacement of 7-AAD with AD. Our method provides clear resolution of positively stained cells from background and has also been successfully applied to cell cycle analysis of cellular subsets of in vitro cultured human thymocytes. Potential extension of this method to the study of other cell types obtained from immune organs and its application to the in-depth proliferation analysis by flow cytometry of mixed cell preparations will aid in the collection of biological relevant information on differential activation of cellular subpopulations by various stimuli.

Acknowledgements

The authors thank Mary Ann Hausner for her expertise and excellent assistance with cell cultures and Nathan J. Regimbal and Laura Ortaliza for help with the preparation of the manuscript.

References

Böyum, A., 1968. Isolation of mononuclear cells and granulocytes from human blood. Scand. J. Clin. Invest. 97, 77, Suppl. 21.

Caruso, A., Licenziati, S., Corulli, M., Canaris, A.D., De Francesco, M.A., Fiorentini, S., Peroni, L., Fallacara, F., Dima, F., Balsari, A., Turano, A., 1997. Flow cytometric analysis of activation markers on stimulated T cells and their correlation with cell proliferation. Cytometry 27, 71.

Cole, S.W., Korin, Y.D., Fahey, J.L., Zack, J.A., 1998. Norepinephrine accelerates HIV replication via protein kinase a-dependent effects on cytokine production. J. Immunol. 161, 610.

Darzynkiewicz, Z., Traganos, F., Kapuscinski, J., Staiano-Coico, L., Melamed, M.R., 1984. Accessibility of DNA in situ to various fluorochromes: relationship to chromatin changes during erythroid differentiation of Friend leukemia cells. Cytometry 5, 355.

Fetterhoff, T.J., Holland, S.P., Wile, K.J., 1993. Fluorescent detection of non-viable cells in fixed cell preparations. Cytometry Suppl. 6, (Abstract).

Gill, J.E., Jotz, M.M., Young, S.G., Modest, E.J., Sengupta, S.K., 1975. 7-Amino-actinomycin D as a cytochemical probe: I. Spectral properties. J. Histochem. Cytochem. 23, 793.

Jacob, M.C., Favre, M., Bensa, J.-C., 1989. Membrane cell permeabilisation with saponin and multiparametric analysis by flow cytometry. Cytometry 12, 550.

June, C.H., Ledbetter, J.A., Linsley, P.S., Thompson, C.B., 1990. Role of the CD28 receptor in T-cell activation. Immunol. Today 11, 211.

Korin, Y.D., Zack, J.A., 1998. Progression to the G_1b phase of the cell cycle is required for completion of human immunodeficiency virus type 1 reverse transcription in T cells. J. Virol. 72, 3161.

Kruth, H.S., Braylan, R.C., Benson, N.A., Nourse, V.A., 1981. Simultaneous analysis of DNA and cell surface immunoglobulin in human B-cell lymphomas by flow cytometry. Cancer Res. 412, 4895.

Lanier, L.L., Testi, R., Bindl, J., Phillips, J., 1989. Identity of the Leu-19 (CD56) leucocyte differentiation antigen and neural-cell adhesion molecule. J. Exp. Med. 169, 2233.

Loken, M.R., 1980. Simultaneous quantitation of Hoechst 33342 and immunofluorescence on viable cells using a fluorescence activated cell sorter. Cytometry 1, 136.

Mueller, W., Crothers, D.M., 1968. Studies of the binding of actinomycin and related compounds to DNA. J. Mol. Biol. 35, 251.

Panchuck-Voloshina, N., Haugland, R., Bishop-Stewart, J., Bhalgat, M., Millard, P., Mao, F., Leung, W., 1999. Alexa dyes, a series of new fluorescent dyes that yield exceptionally bright, photostable conjugates. J. Histochem. Cytochem. 47, 1179.

Rabinovitch, P.S., Torres, R.M., Engel, D., 1986. Simultaneous cell cycle analysis and two-color surface immunofluorescence using 7-amino-actinomycin D and single laser excitation: applications to study of cell activation and the cell cycle of murine LY-1 B cells. J. Immunol. 136, 2769.

Schmid, I., 1999. Assessment of viability, immunofluorescence, and DNA content. In: Robinson, J.P., Darzynkiewicz, Z., Dean, P.N., Dressler, L.G., Tanke, H.J., Rabinovitch, P.S., Stewart, C.C., Wheeless, L.L. (Eds.), Current Protocols in Cytometry. Wiley, New York, p. Unit 7.11.1.

Schmid, I., Ferbas, J., Uittenbogaart, C.H., Giorgi, J.V., 1999. Flow cytometric analysis of live cell proliferation and phenotype in populations with low viability. Cytometry 35, 64.

Schmid, I., Giorgi, J.V., 1995. Preparation of cells and reagents for flow cytometry, intracellular staining. In: Coligan, J.E., Kruisbeek, A.M., Margulies, D.H., Shevach, E.M., Strober, W. (Eds.), Current Protocols in Immunology. Wiley, New York, p. 5.3.1.

Schmid, I., Uittenbogaart, C.H., Giorgi, J.V., 1991. A gentle fixation and permeabilization method for combined cell surface and intracellular staining with improved precision in DNA quantification. Cytometry 12, 279.

Shapiro, H.M., 1981. Flow cytometric estimation of DNA and RNA content in intact cells stained with Hoechst 33342 and Pyronin Y. Cytometry 2, 143.

Shapiro, H.M., 1995. Parameters and probes; chromatin structure; identifying cells in mitosis. In: Practical Flow Cytometry, p. 265.

Stokke, T., Holte, H., Steen, H.B., 1988. In vitro and in vivo activation of B-lymphocytes: a flow cytometric study of chromatin structure employing 7-actinomycin D. Cancer Res. 48, 6708.

Stokke, T., Solberg, K., DeAngelis, P., Steen, H.B., 1998. Propidium iodide quenches the fluorescence of TdT-incorporated FITC-labeled dUTP in apopotic cells. Cytometry 33, 428.

Storek, J., Schmid, I., Ferrara, S., Saxon, A., 1992. A novel B cell stimulation/proliferation assay using simultaneous flow cytometric detection of cell surface markers and DNA content. J. Immunol. Methods 151, 261.

Telford, W.G., King, L.E., Fraker, P.J., 1994. Rapid quantitation of apoptosis in pure and heterogeneous cell populations using flow cytometry. J. Immunol. Methods 172, 1.

Toba, K., Winton, E.F., Koike, T., Shibata, A., 1995. Simultaneous three-color analysis of the surface phenotype and DNA–RNA quantitation using 7-amino-actinomycin D and pyronin Y. J. Immunol. Methods 182, 193.

Yu, F.-L., 1983. Actinomycin D-binding in vivo: active chromatin preferred. FEBS Lett. 156, 83.

Zelenin, A.V., Poletaev, A.I., Stepanova, N.G., Barksky, V.E., Kolesnikov, V.A., Nikitin, S.M., Zhuze, A.L., Gnutchev, N.V., 1984. 7-amino-actinomycin D as a specific fluorophore for DNA content analysis by laser flow cytometry. Cytometry 5, 348.